



HAL
open science

Nanostructured carbons from cellulose-derivative-based aerogels for electrochemical energy storage and conversion: evaluation as EDLC electrode material

Claudia Hildenbrand

► **To cite this version:**

Claudia Hildenbrand. Nanostructured carbons from cellulose-derivative-based aerogels for electrochemical energy storage and conversion: evaluation as EDLC electrode material. Other. École Nationale Supérieure des Mines de Paris, 2010. English. NNT : 2010ENMP0022 . pastel-00547497

HAL Id: pastel-00547497

<https://pastel.hal.science/pastel-00547497>

Submitted on 16 Dec 2010

HAL is a multi-disciplinary open access archive for the deposit and dissemination of scientific research documents, whether they are published or not. The documents may come from teaching and research institutions in France or abroad, or from public or private research centers.

L'archive ouverte pluridisciplinaire **HAL**, est destinée au dépôt et à la diffusion de documents scientifiques de niveau recherche, publiés ou non, émanant des établissements d'enseignement et de recherche français ou étrangers, des laboratoires publics ou privés.

École doctorale n° 432 : SMI - Sciences des Métiers de l'Ingénieur

Doctorat ParisTech

THÈSE

pour obtenir le grade de docteur délivré par

l'École nationale supérieure des mines de Paris

Spécialité " Énergétique "

présentée et soutenue publiquement par

Claudia HILDENBRAND

le 9 Septembre 2010

Nanostructured carbons from cellulose-derivative-based aerogels for electrochemical energy storage and conversion: evaluation as EDLC electrode material

Carbones nanostructurés à base d'aérogels d'acétate de cellulose pour la conversion et le stockage électrochimique d'énergie: évaluation en tant que matériau d'électrode de supercondensateur

Directeurs de thèse : **Sandrine Berthon-Fabry & Arnaud Rigacci**

Jury

Mme Cathie VIX , DR, IS2M Institut de Sciences des Matériaux de Mulhouse	Président
M. Angel LINARES-SOLANO , Prof., Departamento de química inorgánica, Universidad de Alicante, Espagne	Rapporteur
M. Jean-Paul PIRARD , Professeur, Département de chimie appliquée, Université de Liège, Belgique	Rapporteur
M. Philippe AZAÏS , Docteur, BATSCAP	Examineur
Mme Sandrine BERTHON-FABRY , Docteur HDR, Centre Énergétique et Procédés, MINES Paristech	Examineur
M. Arnaud RIGACCI , Docteur HDR, Centre Énergétique et Procédés, MINES Paristech	Examineur

Remerciements

Je tiens à remercier ici toutes les personnes qui m'ont aidée à réaliser ce travail de thèse.

Je pense bien sûr dans un premier temps à Sandrine et Arnaud, qui ont suivi ce travail de très près, et qui se sont toujours rendus très disponibles tout au long de ces trois ans. Leur gentillesse et la pertinence de leurs conseils ont eu une influence très positive sur la qualité de ce travail.

Je pense ensuite à Pierre Ilbizian, Patrick Leroux, Suzanne Jacomet et Monique Repoux, qui m'ont beaucoup aidée avec mes travaux expérimentaux et les caractérisations.

Je pense aussi à Bartosz Grzyb, Nathalie Job, Bernard Simon, Christophe Fargeau, Romain Sescousse, Tania Budtova, Philippe Azaïs et tous les membres du projet CARBOCELL, avec lesquels j'ai eu de nombreuses collaborations fructueuses.

De manière plus générale, je pense au groupe EM&P et à sa bonne humeur, ainsi qu'à tous les membres du CEP et du centre de l'Ecole des Mines de Paris de Sophia-Antipolis grâce à qui j'ai pu passer trois années très agréables dans un cadre propice à un travail scientifique de qualité.

Je remercie finalement l'ANR/Capenergies ainsi que l'association Armines pour leur soutien financier.

GENERAL INTRODUCTION	11
CHAPTER I: STATE OF THE ART	15
1. CARBON IN ELECTROCHEMICAL ENERGY STORAGE, CONVERSION, AND ENVIRONMENTAL PROTECTION	17
1.1. INTRODUCTION	17
1.2. ELECTROCHEMICAL ENERGY STORAGE AND CONVERSION	20
1.2.1. ELECTROCHEMICAL CAPACITORS: ELECTROCHEMICAL DOUBLE LAYER CAPACITOR (EDLC) AND PSEUDOCAPACITOR	20
1.2.2. BATTERY	20
1.2.3. ELECTROCHEMICAL H ₂ STORAGE	22
1.2.4. PROTON EXCHANGE MEMBRANE FUEL CELLS (PEMFC)	22
1.3. ENVIRONMENTAL PROTECTION	24
1.3.1. ADSORPTION	24
1.3.1.1. Chemical Energy Storage	24
1.3.1.2. Gas Separation and Adsorption of Pollutants	24
1.3.2. CATALYSIS	25
1.4. CONCLUSION	26
2. STATE OF THE ART: NANOSTRUCTURED CARBONS	26
2.1. OVER VIEW: ENGINEERED CARBON MATERIALS	26
2.2. OVER VIEW: CARBON MATERIAL	27
2.2.1. ACTIVATED CARBONS (AC)	28
2.2.2. CARBON AEROGELS (CA)	29
2.2.3. CARBON BLACKS (CB)	30
2.2.4. CARBON NANOSTRUCTURES (CN) – CARBON NANOTUBES (CNTs)	31
2.2.5. TEMPLATED CARBONS (TC)	32
2.2.6. FURTHER PROCESSES FOR SYNTHESIZING NANOSTRUCTURED CARBON MATERIAL	33
2.2.6.1. Defluorination of Polytetrafluoroethylene	34
2.2.6.2. Polymer Blend Process	34
2.2.6.3. Selection of specific Precursors	34
2.3. NANOSTRUCTURED CARBON MATERIAL DERIVED FROM BIOMASS	35
2.3.1. PYROLYSIS OF SPECIFIC BIOMASS-BASED PRECURSORS	35
2.3.2. BIOMASS-BASED ACTIVATED CARBONS	35
2.3.3. BIOMASS-BASED CARBON AEROGELS	36
3. CARBON AEROGELS	36
3.1. GEL SYNTHESIS	36
3.2. DRYING	38
3.2.1. EVAPORATIVE DRYING	38
3.2.2. SUPERCRITICAL DRYING	39
3.2.3. FREEZE DRYING	40
3.3. CARBONIZATION	40
3.3.1. GENERAL DESCRIPTION	40
3.3.2. PYROLYSIS PARAMETERS	41

4. BIOMASS-BASED CARBON AEROGELS	43
4.1. BIOMASS-BASED PHYSICAL GELS AND WET REGENERATED COMPOUNDS	43
4.2. BIOMASS-BASED CHEMICAL GELS	44
4.3. SUMMARY AND SELECTION OF SYNTHESIS METHOD	49

CHAPTER II: CELLULOSE-ACETATE BASED ORGANIC AEROGELS **51**

1. INTRODUCTION	53
2. EXPERIMENTAL	55
2.1. SOL-GEL SYNTHESIS	55
2.2. SUPERCRITICAL DRYING	57
2.3. ANALYSIS METHODS	57
2.3.1. MICROGRAPHY	57
2.3.2. ANALYSIS OF POROUS CHARACTERISTICS	57
2.3.2.1. Density, Porous Volume and Porosity	58
2.3.2.2. Specific Surface Area	59
2.3.2.3. Pore Size Distribution and Mean Pore Size	59
2.3.2.4. Specific Porous and Microporous Volume	61
2.3.3. ELEMENTAL ANALYSIS	62
2.4. INFLUENCE OF CATALYST MECHANISMS	62
3. RESULTS	68
3.1. INFLUENCE OF SOL-GEL PARAMETERS ON GELATION TIME AND SHRINKAGE	68
3.1.1. INTRODUCTION TO SOL-GEL CHARACTERISTICS	68
3.1.1.1. Gelation Time	68
3.1.1.2. Shrinkage due to Syneresis	68
3.1.2. INFLUENCE OF SOL-GEL SYNTHESIS PARAMETERS ON GELATION TIME AND SHRINKAGE	69
3.1.2.1. Cellulose Acetate Concentration %CA	69
3.1.2.2. Cross-linking Ratio I/CA	72
3.1.2.3. Catalyst Ratio I/Cat and Type	73
3.2. INFLUENCE OF SOL-GEL PARAMETERS AND DRYING ON THE ORGANIC AEROGEL STRUCTURE	76
3.2.1. INFLUENCE OF SOL-GEL SYNTHESIS PARAMETERS	76
3.2.1.1. Macro- and Microscopic Observation	76
3.2.1.2. Organic Aerogel Structure	80
3.2.2. INFLUENCE OF THE DRYING PROCESS ON THE ORGANIC AEROGEL STRUCTURE	88
3.2.3. ORGANIC AEROGEL ELEMENTAL COMPOSITION	90
4. CONCLUSION	91

CHAPTER III: CELLULOSE-ACETATE-BASED CARBON AEROGELS **93**

1. INTRODUCTION	95
------------------------	-----------

2. EXPERIMENTAL	95
3. RESULTS AND DISCUSSION	97
3.1. EVOLUTION OF CELLULOSE-ACETATE-BASED AEROGELS DURING PYROLYSIS	97
3.1.1. MACROSCOPIC OBSERVATION	97
3.1.2. MICROGRAPHIC OBSERVATION	98
3.1.3. EVOLUTION OF CELLULOSE-ACETATE-BASED AEROGELS DURING PYROLYSIS	102
3.1.4. EVOLUTION OF THE SURFACE CHEMISTRY DURING PYROLYSIS	106
3.1.5. SKELETAL DENSITY	108
3.1.6. REPRODUCIBILITY OF THE CARBON AEROGEL PREPARATION	108
3.2. INFLUENCE OF THE PRISTINE ORGANIC AEROGEL	108
3.2.1. INFLUENCE OF ORGANIC AEROGEL STRUCTURE ON THE CARBON AEROGEL STRUCTURE	109
3.2.2. INFLUENCE OF ORGANIC AEROGEL COMPOSITION ON CARBON AEROGEL COMPOSITION	117
3.3. INFLUENCE OF PYROLYSIS PARAMETERS	117
3.3.1. INFLUENCE ON CARBON AEROGEL STRUCTURE	118
3.3.2. INFLUENCE ON CARBON AEROGEL COMPOSITION	121
4. CONCLUSION	124

CHAPTER IV: MODIFICATION OF THE CELLULOSE-ACETATE BASED CARBON AEROGELS - STRUCTURE AND SURFACE CHEMISTRY **125**

1. INTRODUCTION	127
2. MODIFICATION OF THE CARBON AEROGEL STRUCTURE	127
2.1. PHYSICAL ACTIVATION	127
2.1.1. EXPERIMENTAL	128
2.1.1.1. Carbon aerogel synthesis	128
2.1.1.2. Activation	128
2.1.1.3. Structural and Chemical Analysis	128
2.1.2. RESULTS AND DISCUSSION	129
2.1.2.1. Structure	129
2.1.2.2. Elemental Composition	132
2.1.3. CONCLUSION ON ACTIVATION	132
2.2. CELLULOSE-ACETATE-BASED AEROGEL/CELLULOSE POWDER COMPOSITES	132
2.2.1. EXPERIMENTAL	133
2.2.2. RESULTS AND DISCUSSION	133
2.2.2.1. Macro- and Microscopic Observation	133
2.2.2.2. Structural Analysis of Organic Composites	137
2.2.2.3. Structural Analysis of Carbonized Composites	138
2.2.3. CONCLUSION ON CELLULOSE-ACETATE-BASED AEROGEL/CELLULOSE POWDER COMPOSITES	140
3. MODIFICATION OF THE CARBON AEROGEL SURFACE CHEMISTRY	140
3.1. EXPERIMENTAL	141
3.1.1. CARBON AEROGEL SYNTHESIS	141

3.1.2.	CHEMICAL MODIFICATION OF THE CARBON AEROGEL	141
3.1.3.	STRUCTURAL ANALYSIS	142
3.1.4.	ANALYSIS OF CHEMICAL PROPERTIES	143
3.2.	RESULTS AND DISCUSSION	143
3.2.1.	STRUCTURE	143
3.2.2.	ELEMENTAL COMPOSITION	145
3.2.3.	EVOLUTION OF THE SURFACE CHEMISTRY ON THE CHEMICAL TREATMENT OF THE CARBON AEROGELS	146
3.2.4.	HETEROGENEITY OF CARBON AEROGELS	161
3.3.	CONCLUSION ON THE MODIFICATION OF THE CARBON AEROGEL SURFACE CHEMISTRY	162
4.	CONCLUSION	162

CHAPTER V: ELECTROCHEMICAL ANALYSIS OF CELLULOSE-ACETATE-BASED CARBON AEROGELS ON THE EXAMPLE OF AN EDLC **165**

1.	INTRODUCTION	167
2.	STATE OF THE ART: EDLC	169
2.1.	EDLC DESIGN	169
2.1.1.	CONVENTIONAL CAPACITOR	169
2.1.2.	EDLC ASSEMBLY	170
2.2.	IMPORTANCE OF THE EDLC ELECTRODE	171
2.3.	POTENTIAL IMPROVEMENT OF EDLC ASSEMBLY	172
2.3.1.	IMPROVEMENT OF ENERGY AND POWER CAPABILITIES	172
2.3.2.	ELECTRODE STRUCTURE	173
2.3.3.	ORGANIC ELECTROLYTES	174
2.3.4.	PSEUDOCAPACITANCE	174
2.3.5.	HYBRID CAPACITOR	175
2.4.	TARGETED PERFORMANCE	176
3.	EXPERIMENTAL SECTION	176
3.1.	EDLC TEST BENCH ASSEMBLY	176
3.2.	ANALYSIS METHODS	178
3.2.1.	ANALYSIS OF EDLC PERFORMANCE	178
3.2.2.	CYCLIC VOLTAMMETRY	179
3.3.	CARBON SAMPLES	187
4.	RESULTS AND DISCUSSION	189
4.1.	INFLUENCE OF TEST CELL	189
4.2.	INFLUENCE OF STRUCTURE	191
4.2.1.	INTEREST OF SYNTHESIZING CARBON AEROGELS	191
4.2.2.	XEROGEL PERFORMANCE	194
4.2.3.	INTEREST OF ACTIVATION	197
4.2.4.	PERFORMANCE OF CELLULOSE-ACETATE-BASED AEROGEL/CELLULOSE POWDER COMPOSITES	201
4.3.	INFLUENCE OF SURFACE CHEMISTRY	205

4.3.1. INFLUENCE OF OXIDATION	205
4.3.2. INFLUENCE OF NITROGEN INTRODUCTION	209
4.4. COMPARISON WITH OTHER NANOSTRUCTURED CARBONS	213
4.4.1. COMPARISON OF DIFFERENT CELLULOSE-BASED CARBON AEROGELS	213
4.4.2. COMPARISON WITH A COMMERCIALY AVAILABLE ACTIVATED CARBON	216
<u>5. CONCLUSION</u>	<u>218</u>
<u>GENERAL CONCLUSION</u>	<u>221</u>
<u>RESUME EN LANGUE FRANÇAISE</u>	<u>227</u>
<u>REFERENCES</u>	<u>229</u>
<u>PERSONAL REFERENCES</u>	<u>250</u>

General Introduction

The ever-increasing utilization of fossil energy sources aggravates environmental pollution and the depletion of these energy carriers. Enhancement of energy efficiency and the valorisation of renewable resources are only two of several approaches to counteract these effects. Energy efficiency can be drastically improved by efficient energy conversion and storage of surplus or intermittent energy.

Electrochemical energy storage and conversion, as well as several devices used in environmental protection, depend amongst others on the use of suitable nanostructured carbonaceous material. Nanostructured carbon is thus used in electrochemical energy storage and conversion devices, *e.g.* as electrode material for fuel cells, batteries, or still EDLCs (Electric Double Layer Capacitors). Further, nanostructured carbon is employed in environmental protection, *e.g.* in gas separation and adsorption applications for pollution control, but also for fuel storage and as catalyst support. Carbon used in all these applications has to feature a particular structure adapted to each specific application. The structure needs to be adapted, for example in terms of high available specific surface area and pore size distribution. Being such a crucial parameter, the carbon structure has to be adjusted to each application's requirements.

Carbon aerogels are considered to be a very promising solution for creating carbon material adjusted to the particular requirements of any of the above-mentioned applications. As aerogels are synthesized by soft chemistry, their structural properties, such as pore size and shape, density, or particle size, can be tailored simply by varying the parameters of the synthesis process [Pan 2006]. Carbon aerogels are obtained by the pyrolysis of organic aerogels. Organic aerogels are synthesized *via* sol-gel process allowing the use of a wide variety of precursors including renewable resources, such as biomass-derived products. This has been shown *e.g.* by Tan *et al.* [Tan 2001] who have synthesized organic aerogels based on cellulose acetate. Fischer *et al.* [FIR 2006] have then refined this type of aerogel synthesis using only non-toxic and non-corrosive chemical products. In addition, they have demonstrated that carbon aerogels with interesting structural features can be prepared from these biomass-based products [Gui 2007].

This PhD thesis aimed at developing a family of novel nanostructured carbons from renewable organic sol-gel precursors, *i.e.* cellulose-acetate-based aerogels. The underlying objective has been to create the possibility of tuning the carbon aerogels' characteristics to the properties required for the use in different applications, by predicting the influence of the synthesis and pyrolysis parameters. Therefore, my work has been based on an experimental approach focused at creating a set of correlations between the carbon synthesis parameters and the carbons' structure.

Even though being a crucial parameter, the carbon structure is not the only influential parameter determining the performance of a carbon used in electrochemical energy storage and conversion and environmental protection devices. The carbon surface chemistry also plays a very important role, due to inevitable interactions at the solid/fluid interphase at the carbon surface. Surface functional groups influence the carbons' behaviour, *e.g.* in terms of wettability, charge transfer, blocking of reactive sites, possible redox reactions, etc. A variety of heteroatoms and therefore functional groups can be present in a carbon, depending on the precursor and on the method of preparation. In addition, heteroatoms can be added by a variety of different post-treatments. Thus, I have additionally focused on at understanding the influence of different post-treatments of the cellulose-acetate-based carbon aerogel on its chemical and physical properties through an experimental study.

This document is organized into five chapters as follows:

- The first chapter presents the state of the art of nanostructured carbons conventionally used in electrochemical energy storage and conversion devices, particularly of those derived from biomass.
- The second chapter examines the results of my experimental studies on creating a broad range of structurally different organic aerogels and on establishing correlations between the organic aerogel synthesis parameters (*i.e.* precursor and catalyst concentration and catalyst nature) and the organic aerogels' structure.
- The third chapter describes the results of my experimental work on establishing correlations between the pyrolysis parameters (maximum pyrolysis temperature and pyrolysis atmosphere) and the resulting carbon material characteristics, in terms of structure and composition.
- The fourth chapter provides the results of different experimental studies aiming at modifying the carbon aerogels in terms of structure and surface chemistry. In order to modify the structure carbon aerogels have been activated in CO₂ and cellulose-acetate-based aerogels containing cellulose powder have been prepared. Additionally, the surface chemistry of one representative carbon sample has been modified by oxidation and/or nitrogen enrichment methods.
- The fifth chapter finally focuses on evaluating the electrochemical performance of different cellulose-acetate-based carbon aerogels synthesized during my PhD thesis. The carbon aerogels performance if being used as EDLC electrode material has been examined. The performance of cellulose-acetate-based carbon aerogels of different structures and surface chemistries has been analyzed and compared to other cellulose-based and conventional carbon material.

The works for present PhD thesis have been carried out within the “Energy, Materials, and Processes” group of the Center for Energy and Processes (EM&P, CEP, site of Sophia Antipolis) of the Ecole Nationale Supérieure des Mines de Paris (ENSMP)/Mines ParisTech. Work on this PhD thesis has contributed to the project CARBOCELL. CARBOCELL is partly financed by the French research agency ANR and brings together experts working in academic and industrial research on carbon material and electrochemical energy storage and conversion (CEP/MinesParisTech, CEMEF/Mines ParisTech, LEPMI/INPG, batScap, PaxiTech, SAFT Batteries, and Timcal). The project CARBOCELL focuses on synthesizing cellulose-based carbon aerogels and evaluating them in devices for electrochemical energy storage and conversion. Therefore, cellulose-acetate-based carbon aerogels, synthesized for and studied in this PhD thesis, have also been evaluated if used in other electrochemical applications, such as in proton exchange membrane fuel cells [Roo 2009] and Li/SOCl₂ primary batteries. The study on the evolution of the surface chemistry of cellulose-acetate-based carbon aerogels (presented in chapter IV.3) has been carried out in collaboration with Dr. Bartosz Grzyb and partially been financed by Carnot MINES (project Nanomines “Nanocarbone”).

Chapter I: **State of the Art**

State of the Art

1. Carbon in electrochemical Energy Storage, Conversion, and Environmental Protection

1.1. Introduction

The element carbon in its solid state can be found in the form of different allotropes, *i.e.* multi-atomic structures with different molecular configurations in terms of hybridisation. Figure I-1 presents the naturally occurring carbon allotropes diamond (sp^3 -bonding) and graphite (sp^2 -bonding). Another non-naturally occurring carbon allotrope is carbyne (sp^1 -bonding) [StG 2006]. Although other carbon structures, like fullerenes, are oftentimes thought to be further allotropes of carbon, specialists like Marsh and Rodríguez-Reinoso maintain that all carbon forms are related to the graphite lattice in some way [Mar 2006]. Graphite consists of layers of fused hexagonal arrangements of carbon atoms (*i.e.* graphene layers). Other graphite-based carbon forms are considered to be different assemblies of defective graphene layers (see figure I-2 for a two-dimensional model of the macromolecular structure of coal [Shi 1984]), with different degrees of order (which is highest for the single-crystal hexagonal graphite).

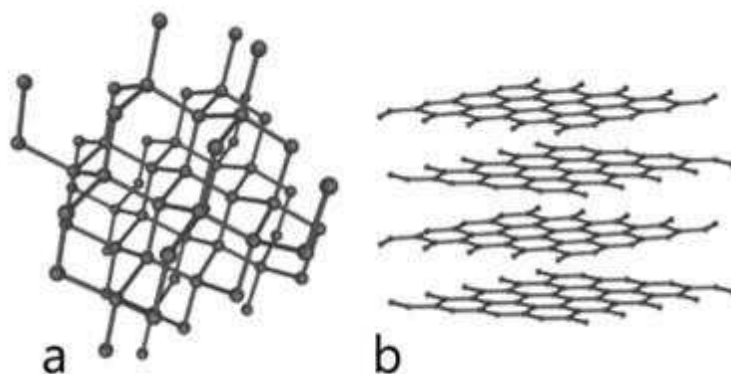


Figure I-1: Schematic illustration of carbon allotropes: a) diamond, b) graphite (based on [Str 2006])

The physical and chemical properties of carbon material, such as mechanical strength and conductivity, vary significantly with the allotropic form as well as with the arrangement of graphene layers and the degree of order for graphite-related carbons. Graphite, for example, is electrically conductive due to the electron delocalization within the graphene layers.

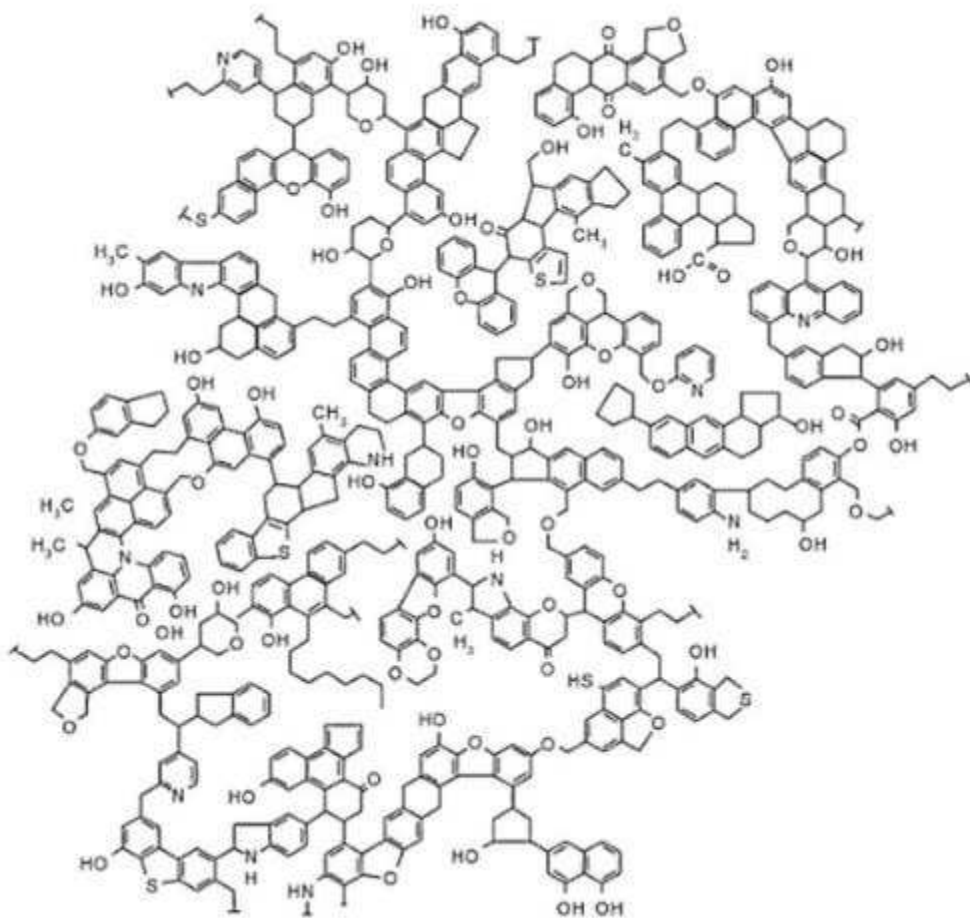


Figure I-2: Two-dimensional model for the macromolecular structure of coal illustrating (i) the network, (ii) the surface functionality, and (iii) the porosity [Shi 1984]

Disordered carbon also contains graphitic regions. Defective graphene layers in disordered carbons, however, are not stacked parallel to one another, as opposed to the organization of graphene in hexagonal graphite.

The carbon form obtained depends particularly on the carbon manufacturing process (including precursor), pressure and temperature conditions. A broad variety of carbon materials lying in between the extremes of graphite and very disordered carbon is known, such as activated carbons, carbon aerogels, carbon blacks, carbon fibers, carbon nanostructures, and glass-like carbons.

Carbon used in all devices for electrochemical energy storage and conversion and environmental protection has to feature particular characteristics adapted to the specific application. Composition (*e.g.* surface functionalities and impurities) as well as structure¹, in terms of specific surface area/porous volumes and pore size distributions, often need to be adjusted. Pores can be classified based on their origin, size, state, or strength, as proposed by [Ina 2009] and shown in Table I-1.

¹ Throughout this PhD thesis, the term structure does not refer to the crystallography of the carbon material, but to the organization of carbon enclosing pores.

Table I-1: Classification of pores in porous solid materials (based on [Ina 2009])

Based on		
Origin	Intraparticle pores	Intrinsic intraparticle pores
		Extrinsic intraparticle pores
Size	Interparticle pores	
	Micropores < 2 nm	Ultramicropores < 0.7 nm
		Supermicropores 0.7-2 nm
	Mesopores 2-50 nm	
State	Macropores > 50 nm	
	Open pores	Bottleneck pores
		Blind pores
		Through pores
		Interconnected pores
		Closed pores
Strength	rigid	
	flexible	

Figure I-3 illustrates the difference of pores according to their state, as mentioned in table I-1. Closed pores are pores within the material and without an opening onto the surface. Open pores comprehend bottleneck pores (narrow pore entrance), blind pores (pores with a single connection to the surface), through pores (pores open on both sides of the particle), and interconnected pores (pores communicating with other pores) [Gre 1976].

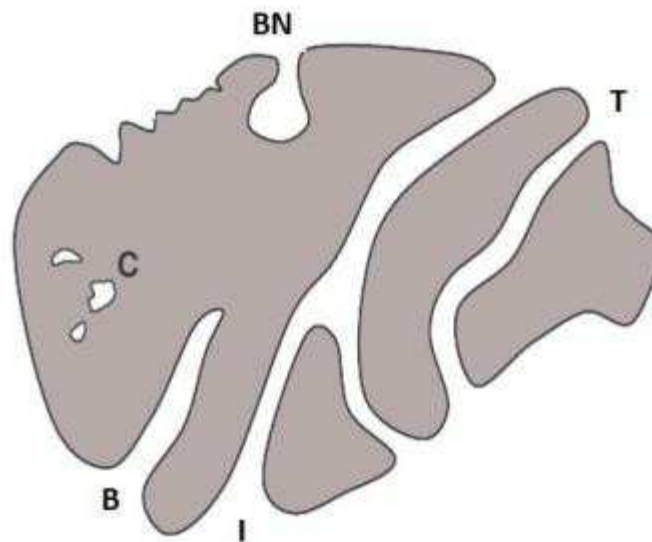


Figure I-3: Cross-section of a hypothetical porous grain showing pores of various states: C – closed pores, B – blind pores, BN – bottleneck pores, T – through pores, and I – interconnected pores (based on [Gre 1976])

Nanostructured carbon material is used in many electrochemical energy storage and conversion and pollution control devices, with the performance of these devices depending on the use of suitable carbon material. Devices containing nanostructured carbon material include:

- Electrochemical energy storage and conversion devices: electrochemical capacitors [Con 1999, Pan 2006], batteries (*i.e.* lithium storage [Fra 2001]), electrochemical hydrogen (H₂) storage [Ble 2008], proton exchange membrane fuel cells (PEMFC) [Dic 2006, Ant 2009], etc...
- Environmental protection: H₂ and methane (CH₄) storage [Kun 2010, LoQ 2002, Alc 2009, Loz 2002], carbon dioxide (CO₂) adsorption [Ina 2009], separation of CH₄/CO₂ [Loz 2002], adsorption of heavy oils and volatile organic compounds (VOC) [Ina 2009, Loz 2002, Lil 2005], removal of gaseous pollutants such as ammonia (NH₃) and sulfur dioxide (SO₂) [Lee 2005, Loz 2002], capacitive deionization [Pek 1998], as catalyst and catalyst support [Fra 2001], etc...

1.2. Electrochemical Energy Storage and Conversion

Carbon material is often employed in electrodes of electrochemical energy storage and conversion devices, due to its interesting electrochemical behavior. Although the properties of a carbon material depend particularly on its degree of crystallinity, structure, and chemistry (*e.g.* content and disposition of heteroatom), graphite-based carbon is, in general, electrically conductive and can donate as well as accept electrons. Additionally, carbon possesses a high chemical stability and is, in general, of relatively low cost.

Below, requirements of carbon material used in electrochemical capacitors, batteries, electrochemical H₂ storage, and PEMFC are presented. The performance of all these devices depends significantly on the carbon structure and on their surface chemistry.

1.2.1. Electrochemical Capacitors: Electrochemical Double Layer Capacitor (EDLC) and Pseudocapacitor

Electrochemical capacitors like, Electrochemical Double Layer Capacitors (EDLC) and pseudocapacitors, store electrical energy electrochemically. While EDLC ideally store electrical energy through electrostatic phenomena only, pseudocapacitors store energy also partly through pseudocapacitive phenomena based on quick faradaic reactions. The capacity of EDLC depends strictly on the surface area accessible to the electrolyte ions. The total capacitance of an EDLC can be maximized if carbons with a high micropore volume made up of pores of 0.7-0.8 nm (depending on the electrolyte) are employed [Vix 2005, RaK 2006]. For quick charge propagation, however, small mesopores seem to be required [Pan 2006]. While carbon material for EDLC only contains a minimum of functional surface groups to ensure chemical stability, a pseudocapacitor's specific capacitance is increased by introducing certain surface functional groups (*e.g.* nitrogen [Jur 2006] or oxygen [RaL 2006]) or by doping the porous carbon material (*e.g.* with ruthenium particles [Pek 1998]). These functional groups and dopants may store energy by undergoing redox reactions with the electrolyte, depending on the electrolyte nature. Currently, commercially available EDLC often contain a blend of activated carbon with a more conductive carbon material (such as carbon black or graphite) [Pan 2006]. See chapter V for further information EDLC and carbon material used in this application.

1.2.2. Battery

Batteries are electrochemical cells for electricity storage. A broad variety of primary and secondary battery types (non-rechargeable and rechargeable batteries, respectively) are known today. Quite a

number of batteries employ some kind of carbon as electrode material. One of the best known types of batteries, also oftentimes featuring carbon electrodes, is lithium-based batteries: primary lithium batteries, rechargeable lithium-ion batteries, or still lithium-air batteries.

Primary lithium batteries, such as Li/SO₂, Li/SOCl₂, Li/MnO₂, Li/FeS₂, and Li/(CF)_x, usually possess a lithium metal or compound electrode and often a cathodic current collector made up of porous carbon material. Preferential characteristics for carbon to be used as cathode material depend on the exact type of primary lithium battery. The capacity of Li/SOCl₂ batteries, for example, depends significantly on the cathode's pore volume provided by pores with a diameter of more than 80 nm. Pores which are smaller than about 80 nm may be clogged by the creation of a passivation layer which builds up on the carbon surface after first utilization. Specific surface for a given pore volume of pores with a size superior to 80 nm are preferably high, but range generally between 30-100 m²/g due to the constraint on pore sizes [Sim 2005, Car 2001, Car 2002].

Rechargeable lithium batteries, so-called lithium-ion batteries, generally possess metal oxide cathodes and carbon anodes. Carbon anodes are usually made from graphitic carbon with controlled active surface area and oxygen-containing functional groups. Oxygen containing-functional groups facilitate the formation of the passivation or SEI (solid electrolyte interphase) layer [NgV 2009]. Even though graphitic carbons are commercially used for this application, the use of less dense and more porous nanostructured carbons remains interesting in order to obtain fast kinetics. Higher surface areas are also interesting in view of the carbon's lithium storage capacity, as lithium is stored in 3D defects of disordered carbons and at the interfaces/surface. Nonetheless, for lithium-ion batteries as well, the necessary and unavoidable formation of the SEI layer may lead to a high loss of specific surface in the smaller pores of nanostructured carbons, and therefore to a consequential irreversible capacity upon use [Kas 2009].

Lithium-air (Li/O₂) batteries, a type of secondary battery being currently developed, contain lithium-based anodes and porous carbon cathodes. The cathode, also called oxygen electrode, consists generally of a porous carbon matrix doped with a catalyst (see figure I-4). Within the porous carbon matrix, lithium ions from the electrolyte and electrons from the external circuit combine reversibly with oxygen from air during discharge according to $2Li^+ + 2e^- + O_2 \rightleftharpoons Li_2O_2$ (for non-aqueous media and if a catalyst is used) [Déb 2007, Déb 2008]. The structure of carbon matrix is therefore required to allow the circulation of the reactants in the porosity. High porous volumes and wide pore sizes (≥ 14 nm) are therefore beneficial for achieving high capacities [Mir 2009].

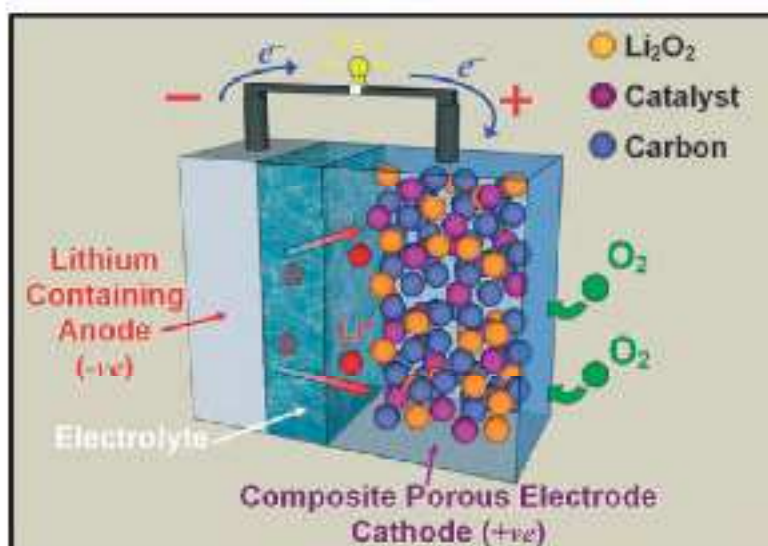


Figure I-4: Schematic representation of a Li/O₂ battery [Déb 2008]

1.2.3. Electrochemical H₂ Storage

Energy may be stored chemically in the form of H₂ (*i.e.* as a fuel). Hydrogen can be stored in nanostructured carbons by electrodecomposition of water and subsequent electrosorption of the hydrogen into the carbon material. The capacity of carbon to electrosorb H₂ increases with the ultramicropore volume. However, a part of this porous volume seems to be irreversibly trap H₂, hinting at an importance of surface functional groups in electrochemical H₂ storage [BeF 2006, BeK 2006]. Higher storage capacities have been found, *e.g.* for carbons with a low content of oxygen-containing surface functionalities [Ble 2008].

1.2.4. Proton Exchange Membrane Fuel Cells (PEMFC)

In fuel cells, chemical energy is converted into electrical energy. The requirements for the anode and the cathode electrocatalysts depend on the type of cell and the nature of the fuel. In PEMFC, a catalyst (*e.g.* platinum) is needed to activate the reduction of oxygen at the cathode and the oxidation of the fuel at the anode. Generally, carbon is used as support for this catalyst (see also paragraph on **1.3.2 Catalysis** in the section **1.3 Environmental protection** for more information on carbon as metal catalyst support in general).

The electrodes of PEMFC need to comply to different technical specifications. The electrodes are made up of different solid components: an electrically conductive catalyst support (*e.g.* carbon), a catalyst dispersed on the support, and an ionically conductive ionomer network (see figure I-5) which need to be in contact. The carbon support has to possess a high accessible surface area allowing i) for a fine dispersion of the catalyst nanoparticles (see figure I-6) and ii) for the maximization of the interface between electrode and fuel [Dic 2006, Job 2009]. A pore size distribution in the mesopore range (*i.e.* 20-40 nm) contributes particularly to the creation of a high electrode surface accessible to the fuel and therefore lowering the diffusional limitations [Mar 2009]. Therefore, materials exhibiting only moderate porosity and specific surface area (*e.g.* commercial carbon material Vulcan with a specific surface area of about 250 m²/g) are commonly applied for PEMFC carbonaceous catalyst support [Ant 2009]. Current research on PEMFC electrode material is therefore focused on the

synthesis of carbons with a controllable and tuneable structure, such as carbon aerogels and xerogels based on different organic gels [Glo 2001, Pet 2001, Mar 2004, Gui 2007, Gui 2008, Job 2009].

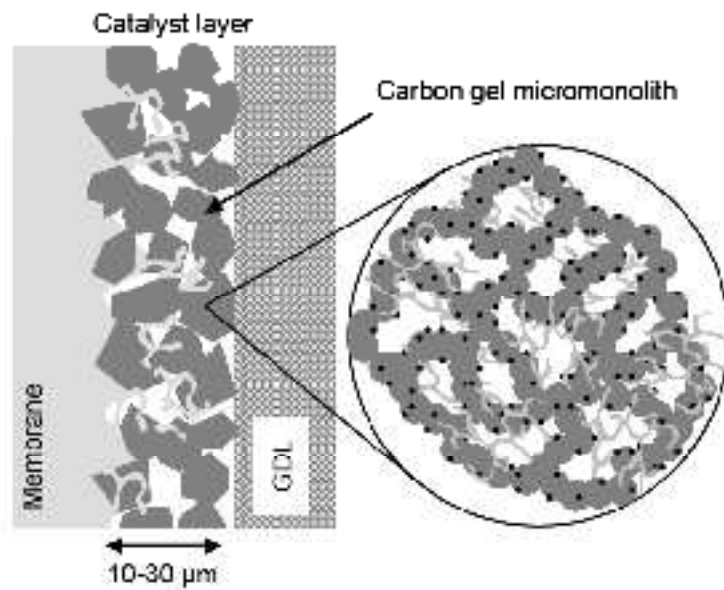


Figure I-5: Structure of a PEMFC electrode: membrane, catalyst layer, and gas diffusion layer (GDL): in the illustration, the catalytic layer is composed of carbon aerogel micromonoliths made of a rigid 3D structure, Nafion® network and Pt catalyst particles are represented in light grey and black, respectively [Job 2009]

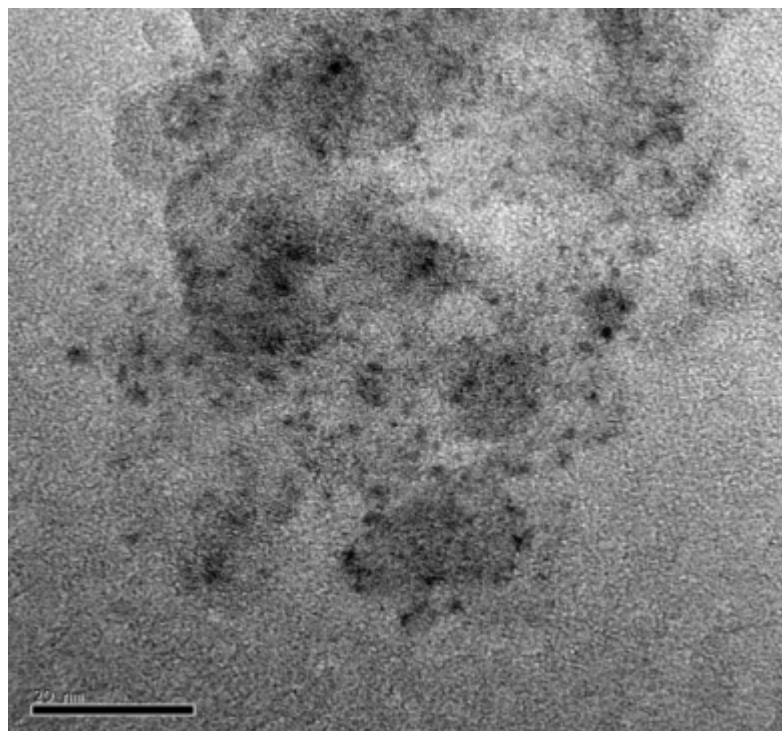


Figure I-6: TEM micrograph (20 nm scale) of carbon aerogel support with Pt particles deposited through impregnation of carbon in $H_2Cl_6Pt_5H_2O$ (courtesy of Dr. Joanna Rooke)

1.3 Environmental Protection

Carbon is often chosen in devices for environmental protection or pollution control, *i.e.* in adsorption and catalysis, for its large choice of porous structures and the carbon atoms' interactions with different liquid or gas molecules.

1.3.1. Adsorption

Adsorption is a process frequently applied in environmental protection, *e.g.* in (gaseous) fuel storage and in the capture of pollutants. The adsorption process depends significantly on carbon structure and surface chemistry. At low pressures, the surface chemistry dominates the adsorption process, while at high pressures the structure is responsible for controlling the adsorption process through pore filling [Lee 2005].

The adsorption of gases and liquids plays an important role in chemical energy storage as well as in gas separation and adsorption of pollutants.

1.3.1.1. Chemical Energy Storage

Energy may be stored in its chemical form, for example as hydrogen H_2 or methane CH_4 (*i.e.* natural gas). Adsorbed onto carbon in their gaseous phase, these energy carriers may be used as gaseous fuel upon their release.

The carbon's capacity for adsorbing H_2 or CH_4 depends particularly on its structure (*e.g.* accessible surface area, pore size and pore size distribution) and surface chemistry, along with pressure and temperature.

H_2 adsorption: Nanostructured carbon material may physisorb and/or chemisorb H_2 . Generally, H_2 is first adsorbed onto the outer surface of the porous carbon and subsequently transferred to and retained within the internal spaces of the adsorbent [Kun 2010]. A high accessible surface area, a high microporous volume made up of narrow pores in the supermicropore range (and a narrow pore size distribution) together with a high bulk density lead to high H_2 storage capacities [Tex 2004, Jor 2008, Yür 2009, Zub 2009]. Additionally, the carbon's surface chemistry may improve the interaction between carbon and H_2 [Zub 2009].

CH_4 adsorption: In terms of structure, CH_4 adsorption is most effective in carbons with a high micropore volume, a uniform pore size distribution of pores of the size of 0.8 nm or smaller [LoQ 2002, Wan 2004, Alc 2009] and a high bulk density. Wider micropores, however, have been shown to yield increased storage capacities at elevated pressures [Wan 2004]. In terms of surface chemistry, the carbon material should be hydrophobic [Wan 2004, Alc 2009], *i.e.* contain a minimum of heteroatoms so as to avoid the presence of polar molecules.

1.3.1.2. Gas Separation and Adsorption of Pollutants

CO_2 adsorption: CO_2 capture may participate in the reduction of the quantity of green house gases in the atmosphere and is frequently used in the gas processing industry as a part of air separation processes. CO_2 can be adsorbed reversibly or irreversibly onto carbons, *e.g.* carbons with a controlled

pore size distribution in the micropore range, a specific surface of around 800 m²/g, and containing basic nitrogen-containing functional groups (if CO₂ is adsorbed at lower partial pressures) [Mar 2005, Pev 2008, Pla 2009, Ina 2009].

NH₃ adsorption: Ammonia NH₃ is a gaseous chemical compound, which, in high concentrations, is toxic, corrosive, and dangerous for the environment and needs therefore often to be removed from gaseous streams. Carbons with a high surface area and a high pore volume, especially micropore volume, generally show good NH₃ adsorption capacity [Sha 2008]. In very low relative pressure ranges, however, the surface chemistry has been found to show particularly dominant effects on the adsorption process. The carbon's capacity to adsorb NH₃ may increase with an increasing number of oxygen-containing surface functional groups, seemingly due to the adsorption of NH₃ onto active adsorption sites provided by oxygen functional groups *via* hydrogen bonding [Guo 2005, Lee 2005, Sha 2008].

VOC adsorption: Volatile organic compounds, VOC, are air pollutants and their adsorption may avoid contamination of the air. Some of the most common VOCs are benzene, toluene, but also gasoline. In addition to avoiding air contamination, the adsorption and subsequent desorption of gasoline may also help to recover gasoline to be used as fuel. VOC-containing gaseous streams can also be treated by absorption, condensation, thermal oxidation and catalytic oxidation, but adsorption remains the most preferable choice for diluted streams [Lil 2005]. Structure, particularly porosity, and the content of oxygen- and nitrogen-containing surface function groups have a strong influence on the carbon's capacity to adsorb VOCs. While pore sizes of 2-5 nm seem most suitable for the adsorption of gasoline vapor [Ina 2009], ultramicropores seem to have the greatest effect on the adsorption of toluene and benzene [Lil 2005]. Carbon surfaces with a small number of oxygen-containing functional groups have higher adsorption capacities, due to their hydrophobic character [Lil 2005]. Carbons containing basic nitrogen, on the other hand, have been found to be particularly interesting for adsorbing weakly acidic compounds (such as dichloromethane CH₂Cl₂) [Sta 2006]. In addition to gaseous VOCs, porous carbons may also adsorb heavy oils (*i.e.* organics with large molecules), for example in order to recover and/or recycle them. A carbon material containing macropores with sizes in the range of 1-600 μm seem to be most efficient in the sorption of heavy oils [Ina 2009].

1.3.2. Catalysis

Nanostructured carbon material may be used as catalyst or as catalyst supports.

Catalysis: Catalysis plays an important role, for example, in pollution control. Gaseous pollutants as sulphur dioxide (SO₂), hydrogen sulphide (H₂S), and nitrogen oxides (NO_x) have to be removed from off-gases quite frequently, for example by carbonaceous catalysts. Along adsorption of gaseous pollutants, the catalytic splitting of these compounds is a widely used method [Ric 1990]. Required structure and surface chemistry depend on the application. The oxidation of SO₂, for example, is optimized by using carbon material with narrow micropores (around 0.7 nm) and free of oxygen-containing surface groups [Ray 2000].

Catalyst support: Further, nanoporous carbon may be used as support material for precious metal powder catalysts (such as palladium, platinum, ruthenium, or rhodium). A fine dispersion of small metallic particles on chemically stable supports may be obtained by depositing the metal on carbon

supports [Kal 2001, Mon 2002, Zhe 2002, JoH 2005, Roo 2009, Job 2009, FuL 2010, Job 2010]. Also, the precious metal can be recovered easily by burning off the carbon support. Precious metal powder catalysts on carbon supports are mainly used in liquid phase hydrogenation, dehydrogenation or oxidation reactions. The most important parameters for carbon material used as support material are the carbon porosity and the pore size distribution. Often, activated carbon is used for its high porosity and the pore and particle size distribution (usually with surface areas of 800-1200 m²/g). Still, other carbon material with much lower specific surface areas and different porosities may be used, depending on the type of catalyst and its function. The fractions of micro-, meso-, and macropores have to be balanced to reach an optimal performance for each reaction. Heteroatoms on the carbon surface (particularly oxygen-containing groups) influence the metal deposition [Aue 1998].

1.4. Conclusion

Based on the information given for the applications above, structure (*i.e.* specific surface areas, accessible surface areas, porous volumes, pore sizes, pore size distributions, etc.) and surface chemistry are obviously crucial characteristics for carbon material used in electrochemical energy storage and conversion as well as in pollution control. As a wide variety of carbon species, fabricated from different materials and in different conditions, are known, carbon material of almost all configurations required can be found or created. However, many of these carbon materials are on the basis of fossil sources. As carbon material to be used in applications beneficial for the environment, the use of materials based on renewable resources would be most coherent. Therefore, in section 2 of this chapter I shall first present the state-of-the-art of nanostructured carbon material, before discussing the possibility of producing biomass-based nanostructured carbon material.

2. State of the Art: Nanostructured Carbons

2.1. Overview: Engineered Carbon Materials

The majority of porous carbons are engineered carbons, *i.e.* carbon having been manufactured in order to display a structure of more or less disordered graphitic microcrystallites [Pan 2006]. Engineered carbons are frequently based on carbon-rich organic precursors having undergone carbonization. Carbonization is the process in which carbon-containing organic compounds are heat-treated in an inert atmosphere in order to manufacture solid residues with high carbon content. During carbonization, the precursor undergoes thermal decomposition (pyrolysis), resulting amongst others in the volatilization of volatile matter including heteroatoms and leaving behind a carbon-rich residue. Further, high temperatures often trigger condensation reactions leading to a growth of localized graphitic units (resulting in the creation of graphitic microcrystallites). Carbonization, however, is a complex process involving different types of reactions (such as dehydrogenation, condensation, hydrogen transfer and isomerisation) and the occurrence of reactions as well as the properties of the final carbon material are subject to diverse factors. The precursor is a crucial factor (particularly its composition, aggregation state during carbonization, and structure) as are processing conditions [Fit 1995]. Table I-2 offers an overview of different widely distributed carbon materials,

their phase during aggregation, common precursors used and the structural features generally obtained.

As can be seen from table I-2, carbon material can be engineered to possess structures or pores in the nanometer range. According to Inagaki, Kaneko, and Ishizawa [InK 2004], carbons whose size or structure has been controlled during production can be called “nanocarbons”. Further, they distinguish “nano-sized” carbons from “nano-structured” carbons. Nano-sized carbons are considered to be carbon material with a size on the nanometer scale (*e.g.* carbon material of small size produced using the template method or a polymer blend process, etc.). Nano-structured carbon, on the other hand, designates carbon material whose structure has been controlled on a nanometer scale. Several methods allow controlling the structure at least to some extent, for example by creating nano-sized pores (*e.g.* activated carbons), by designing the structure of the organic precursor before carbonization (*e.g.* carbon aerogels), or by controlling preparation conditions (*e.g.* templating technique).

Table I-2: Common precursors and structural features for different carbon material (based on [Pan 2006] and [Ina 2002])

Phase during aggregation	Carbon material	Common precursors	Structural features
Gas phase	Carbon blacks	Hydrocarbon gas or liquid	Nanosized
	Pyrolytic carbons	Hydrocarbon gas	Preferred orientation
	Vapour-grown carbon fibres	Hydrocarbon gas	Catalyst particle size/shape dependent
	Fullerenes	Graphite rod	Nanosize molecule
Liquid phase	Nanotubes	Hydrocarbon vapour	Nanosize molecule
	Cokes	Coals, petroleum pitch	Mesophase formation and growth
	Graphite Carbon fibres (pitch derived)	Petroleum coke	Mesophase formation and growth
Solid phase	Carbon fibres (pitch derived)	Coal pitch, petroleum pitch	Mesophase formation and growth
	Activated carbons	Biomass, coals, petroleum cokes, selected polymers	Nanosize pores
	Carbon aerogels	Organic aerogels	Nanosized/ nanosize pores (nm - μm)
	Molecular sieve carbons	Selected biomass, coals, polymers	Nanosized
	Glass-like carbons	Thermosetting polymers	Random crystallites, impervious
	Carbon fibres (polymer derived)	Selected polymers	Random crystallites, non-porous
	Highly oriented graphites	Pyrolytic carbon, poly-imide film	Highly oriented crystallites

Most applications in electrochemical energy storage and conversion and pollution control require nano-structured carbon material. A non-comprehensive overview of the most widely known nano-structured and/or nano-sized carbon species and synthesis methods is given below.

2.2.Overview: Carbon Material

Carbons can, amongst others, be synthesized as activated carbons, carbon aerogels, carbon blacks, carbon nanostructures, template carbons, and using several other methods. Above mentioned carbon types are briefly presented below.

2.2.1. Activated Carbons (AC)

Activated carbons are a group of carbon materials having undergone a process known as activation. Activation aims at increasing the carbon's specific surface area and porosity [Fit 1995, Pan 2006, Mar 2006].

Two activation methods can be distinguished: thermal (or physical) and chemical activation. Physical activation can be defined as the partial oxidation of carbon material leading to the gasification of a selected amount of carbon atoms on the material's surface. The removal of carbon atoms through gasification on the surface of a carbonaceous material creates porosity. During physical activation, the carbon is partially oxidized by exposure to an oxygen-containing gas at elevated temperatures, generally between 700 and 1100 °C. The mechanisms of chemical activation depend on the activating agent and may be complex. They may also include the partial gasification of carbon atoms. During chemical activation, the carbon is impregnated with a chemical agent (in general an acid, a strong base, or a salt, such as sulfuric or phosphoric acid, sodium hydroxide, or zinc chloride respectively) usually between 200 to 700 °C [Kin 1988, Pan 2006]. In the activation step, carbon structure and surface chemistry are modified simultaneously. Oxygen-containing functional groups are created during physical as well as chemical activation. In chemical activation, however, the chemical activating agent may remain in the carbon even after washing [Pra 2008, Guo 2003].

The porosity of activated carbon is conditioned by the carbonaceous precursor and the activation method, *i.e.* the activation agent and activation profile in terms of temperature, activation duration, and concentration of activation agent (*i.e.* gas flow for physical activation).

The structure, the composition (*i.e.* impurities), and other properties of the final activated carbon thus depend largely on the source material and on carbonization and activation conditions. By choosing a certain precursor (such as renewable resources in the form of wood, other biomass, waste, etc., but also coals, cokes, or synthetic polymers) and controlling carbonization and activation (*e.g.* in terms of temperature, heating rate, activation duration, atmosphere, concentration of activating agent etc.), a broad variety of active carbons with different characteristics can be produced [Has 1963, Fit 1995].

Activation of carbon-rich material is the classic method in order to engineer porous carbons. The first recorded example of activation dates back to 1822 (Bussy A., 1822, Journal of the American Pharmaceutical Association 8, 257) [Has 1963]. Activated carbons have long since been commercially available (since 1909). This group of economically viable porous carbon material features a broad variety of carbons with different structures, for example with controlled distribution of pores and specific surface areas of up to 3000 m²/g [Tak 1999]. Most activation methods, however, result in the widening of micropores [Loz 2002]. Also, as the creation of porosity in activated carbons is achieved through the gasification of a part of the materials' carbon atoms, the final carbon yield after activation is relatively low [Ina 2009].

The advantage of activation is that it can be applied to virtually any carbon-rich material. A series of non-porous carbon materials such as glass-like carbons and carbon fibers can thus be engineered by activation to possess a fair porosity whilst maintaining their innate characteristics.

Activated Glass-like Carbon

Glass-like carbon, often also called glassy or vitreous carbon, is produced by pyrolysis of a selection of polymers (typically phenolic resins or furfuryl alcohol). The glass-like carbons' characteristics depend chiefly on the pyrolysis maximum temperature. Glass-like carbons have generally a relatively low accessible surface area and low density (around 1.5 gcm^{-3}), high mechanical strength and very low electrical resistances. Due to these characteristics, their permeability for liquids and gases is very low. Through activation however, high surface areas of up to $1800 \text{ m}^2/\text{g}$ can be reached [Pan 2006, Fit 1995].

Activated Carbon Fibers

Carbon fibers are produced either by pyrolysis of organic fibers (such as cellulose or rayon, phenolic resins, polyacrylonitrile, and pitch-based materials) or by growth from gaseous hydrocarbons. The carbon fibers' characteristics depend on the precursor and production method. Generally carbon fibers possess low electrical resistances and good electrical conductivities. The raw fiber can be activated, resulting in activated carbon fibers with surface areas of up to $2500 \text{ m}^2/\text{g}$ [Pan 2006, Fit 1995].

2.2.2. Carbon Aerogels (CA)

Carbon aerogels are produced by pyrolysis of organic aerogels [Pek 1989, Bri 1990]. Initially, organic aerogels have been obtained by synthesis of organic gels *via* sol-gel method and subsequent supercritical drying of the gel. Nowadays, however, materials resulting from any drying process of a gel synthesized by any method may be called aerogel, if the organic gel's structure is maintained throughout the drying process. The carbon aerogel, resulting from gel synthesis, gel drying, and pyrolysis of the organic aerogel, is a three-dimensional network of interconnected nanometer-sized and usually colloidal-like carbon particles. Carbon aerogels have been synthesized based on various precursors such as resorcinol-formaldehyde (RF), phenol-resorcinol-formaldehyde, phenolic-furfural, melamine-formaldehyde, polyurethanes, and polyureas [Pek 1998]. A carbon aerogel's structure and other characteristics depend naturally on the organic precursor, the drying method, and the pyrolysis process. The chemistry and the structure of the organic precursor, which in this case is the organic aerogel (OA) have an influence on the resulting carbon aerogel. Conveniently, the OA structure depends on the synthesis conditions, *i.e.* on the sol-gel synthesis parameters. An OAs structure can, therefore, be tailored by adapting synthesis conditions (*e.g.* by precursor ratios and drying method). Characteristics such as density, mean pore size and mean pore size distribution, specific surface area, and particle size can be tuned [Sch 1995, LuC 1995]. Also, particle size and pore size can be changed independently by the variation of sol-gel synthesis parameters [Mar 2009], for example by varying the pH of RF-based gels (see figure I-7). In addition, micropores and mesopores have different origins and can thus be tailored independently. While micropores in aerogels are related to the intra-particle structure, meso- and macropores depend on the inter-particle structure [Mor 2005].

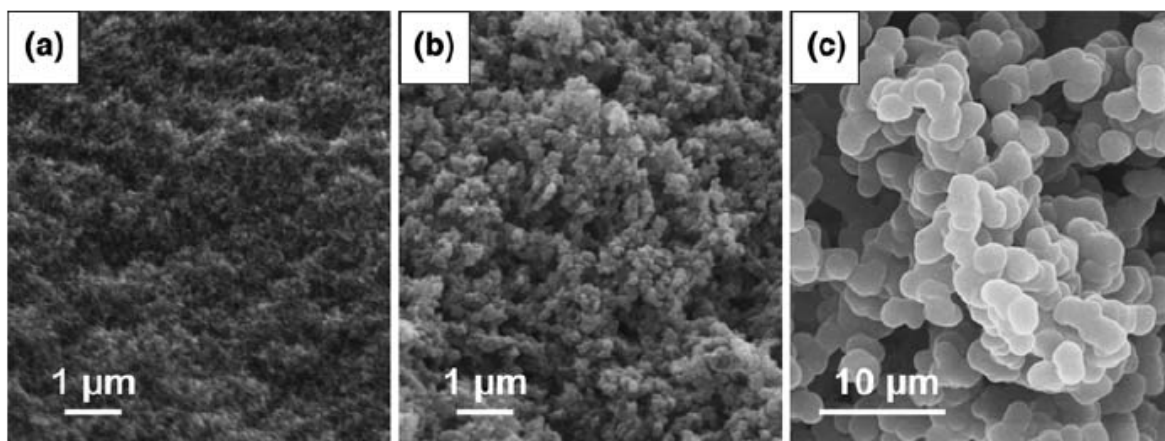


Figure I-7: Morphology of RF-based carbon xerogels prepared at various pH a) pH 6.50, b) pH 6.00, c) pH 4.00 [Job 2009]

Resorcinol-formaldehyde based carbon aerogels, which are the most widely known type of carbon aerogels, display high porous volumes and surface areas (up to 1100 m²/g), uniform mesopores sizes, and high electrical conductivity (25-100 S/cm), *i.e.* low electrical resistivity [Pan 2006, Lee 2010, LiW 2008]. Further, they can be produced as monoliths, composites, thin films, etc. As for any other carbon material, a CA's surface and porosity can additionally still be augmented by activation.

2.2.3. Carbon Blacks (CB)

Carbon blacks are commercially available and economically viable carbon materials (with a production of roughly 8 million tons per year [Mor 2006]) in the form of carbon spheres and their aggregates of colloidal size (*i.e.* with sizes below 1000 nm). Carbon blacks are fabricated by thermal decomposition or partial combustion usually of gaseous hydrocarbons (such as gases, oils, or distillates) [Fit 1995, Pan 2006]. Typically, carbon blacks are characterized by small carbon particle and also aggregate sizes, relatively high porosity, high conductivity, and a chemically clean oxygen free surface. Specific surface areas can be as low as 10 m²/g, but are usually around 100 – 150 m²/g and may become as high as 1500 m²/g upon thermal activation [Pan 2006]. CB's of high surface areas (> 500 m²/g) contain of a high quantity of interparticle meso- and micropores. These are interparticle pores of small carbon particles (10-15 nm), which by covalent linking make up aggregates, which, in return, agglomerate by van der Waals forces (see figure I-8) [Mor 2006, Mar 2009].

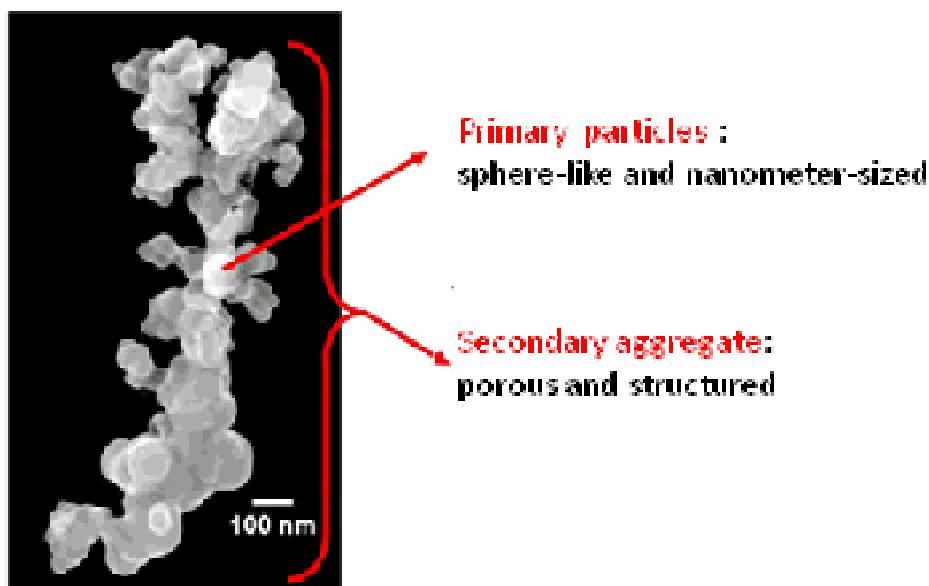


Figure I-8: Carbon black microstructure (based on [Mor 2006])

Evidently, the porous properties of carbon blacks are governed by the carbon aggregates and their agglomeration. As the formation of aggregates and their subsequent agglomeration can hardly be controlled, particle sizes (*i.e.* specific surface area) and porous properties are closely linked.

2.2.4. Carbon Nanostructures (CN) – Carbon Nanotubes (CNTs)

Carbon nanostructures (*e.g.* carbon nanotubes, nano-fibers, fullerenes, etc.) are produced by catalytic decomposition of a selection of hydrocarbons or by high temperature processes aimed at vaporizing a certain carbon composite. The type of nanostructure (*e.g.* nanotubes, buckyballs, nanohorns, nanobuds, etc.) and corresponding characteristics can be controlled by the choice of precursor and production parameters. However, some types of carbon nanostructures (such as the different fullerenes, *e.g.* the buckminsterfullerene C_{60}) are used to design a specific molecular form of carbon only, while others (*e.g.* carbon nanotubes) are used to design a whole group of different molecular forms and compounds. Carbon nanotubes (CNTs), for example, are usually produced by catalytic decomposition of hydrocarbons on small metal particles (see figure I-9), but may also be produced by electric arc growth [ViD 2001] and plasma processes [Oku 2004, Mor 2006]. Their compounds feature high accessible porosities (typically made up of mesopores), low electrical resistance, high thermal conductivity, and high mechanical strength, depending on the molecular form of the nanotube. Porosities in carbon nanostructures are commonly based on interstitial spaces in the entangled nanostructure network and therefore easily accessible. Due to the nature of the specific surface in carbon nanostructures, surface areas are limited, but may be increased by activation [Pan 2006].



Figure I-9: TEM images of carbon nanotubes obtained over Fe,Co/zeolite catalyst aligned into bundle-like structure [Her 2004]

2.2.5. Templated Carbons (TC)

Templated carbons are strictly speaking not a type of carbon material, but rather different carbon materials engineered to be porous by using the template method. In the template method, a gaseous or liquid carbon-rich precursor is introduced into the pores of a template (such as ordered silica, or zeolites). After introduction of the precursor inside the template, the template/precursor composite is heat-treated and the carbon-rich precursor, therefore, pyrolyzed. Subsequently, the template is removed from the composite by acid treatment (usually in hydrofluoric acid). The carbon remaining after acid treatment is thus the negative replica of the template (see figure I-10) [Joo 2001, Vix 2004, InK 2004, Vix 2005, Fra 2007, Ina 2009].

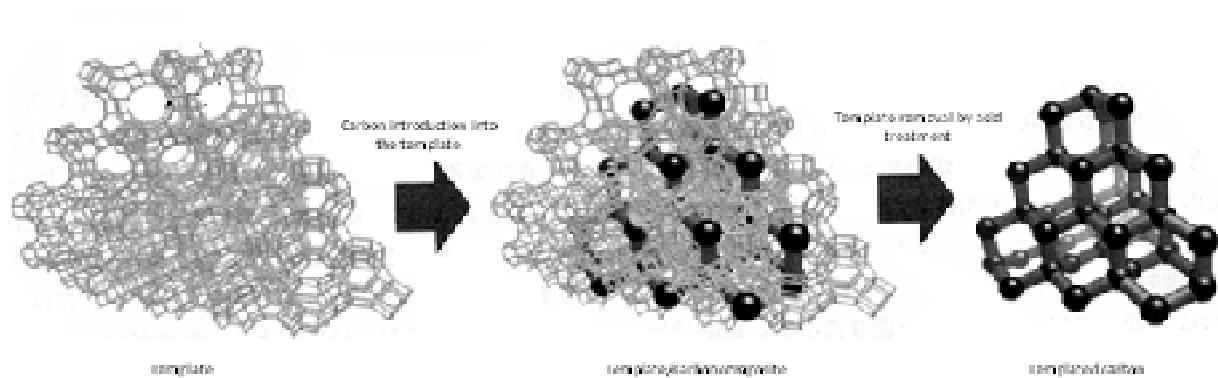


Figure I-10: Schematic illustration of the formation of a templated carbon (based on [Ina 2009])

The structure of the template carbon depends on the template and type of precursor. Different templates of different structures and porous characteristics have been investigated, particularly meso- and microstructured silica (see figure I-11) [Joo 2001, Vix 2004, Vix 2005, Fra 2007, Ina 2009] and zeolites [InK 2004, Ina 2009]. The carbon-rich precursor may either be a liquid or a gas and the

template carbon synthesis is carried out either *via* liquid impregnation (e.g. of a sucrose solution, pitch, furfuryl alcohol) or by chemical vapor infiltration (e.g. of propylene) or introduction through vapor (e.g. acrylonitrile) [Joo 2001, Vix 2004, InK 2004, Vix 2005, Fra 2007].

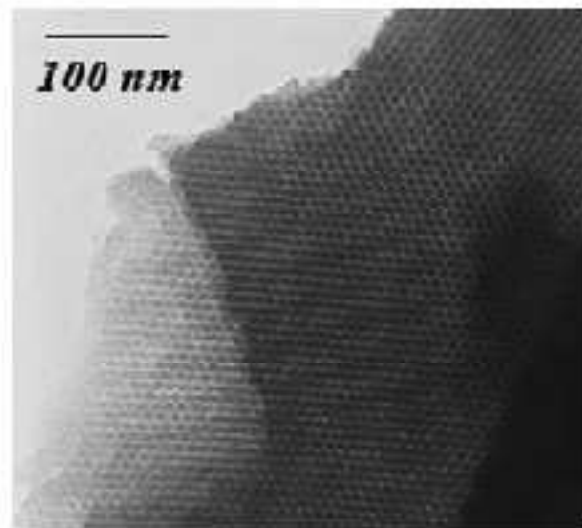


Figure I-11: TEM image of a template carbon using silica as template and pitch as carbon source [Vix 2005]

General characteristics of template carbons include that their structure in terms of pore sizes, pore size distributions, pore shapes, and interconnectivity of pores may be perfectly controlled. The micro- and mesoporosity may be varied by using different templates, precursor types and precursor quantity [Gad 2005]. Templated carbons can display very high microporous volumes and surface areas, depending on the template used. Surface areas and micropore volumes of up to 4000 m²/g and 1.8 cm³/g respectively have been reported for the use of a zeolite template [Ina 2009]. Nonetheless, the template method also has some disadvantages mainly due to the complicated carbon preparation process for example generating high costs and the use of oftentimes toxic and/or corrosive acids for the template dissolution. Also, for the time being, only a limited choice of template structures has been investigated, although research on templates continues (such as metal oxide templates MgO and NiO) [Ina 2009]. Therefore, an industrial production of templated carbon has not been envisioned.

Additional porosity, *i.e.* porosity not induced by the template, may be created by using specific carbon-rich precursors. At using a sucrose aqueous solution as precursor, for example, the formation of additional microporosity has been observed (due to the elimination of water and to the extensive thermal decomposition of sucrose) [Vix 2005]. Therefore, it has to be taken into account, that depending on the carbon-rich precursor, the final template carbon's structure may or may not be the exact negative replica of the template.

2.2.6. Further Processes for synthesizing Nanostructured Carbon Material

Still other methods also allow engineering porous carbons; amongst them defluorination of polytetrafluoroethylene, polymer blend process, and selection of specific precursors.

2.2.6.1. Defluorination of Polytetrafluoroethylene

Porous carbons may be produced by defluorinating polytetrafluoroethylene PTFE with alkali compounds (such as lithium fluoride, sodium, potassium, and rubidium) at elevated temperatures and sometimes pressures and subsequent washing (to remove excess alkali metals) and carbonization. The resulting carbons structure depends chiefly on the alkali metal used for defluorination. Using this method, porous carbons with specific surface areas as high as 2225 m²/g can be generated. However, this process is quite expensive due to the precursors and the treatment of the oftentimes toxic and/or corrosive by-products [InK 2004, Ina 2009].

2.2.6.2. Polymer Blend Process

In the polymer blend process, two different types of polymers are mixed. One of the polymers is supposed to have a high carbon yield upon carbonization (such as phenol-formaldehyde resin or polyacrylonitrile), while the second polymer is wanted to have a low carbon yield if pyrolyzed (such as polyethylene or polymethylmethacrylate). Generally the precursor yielding much carbon (also called carbon precursor polymer) is enveloped by the precursor yielding less carbon (also called pore former polymer), as can be seen schematically in figure I-12. In the course of the pyrolysis, the pore forming polymer in the polymer composite's core is gasified nearly completely. In the meantime, the carbon precursor polymer results in a solid carbon material enveloping the porous spaces created by the pyrolysis of the pore forming polymer [InK 2004, Ina 2009]. Thus, pore-containing carbons may be generated by using the polymer blend process.

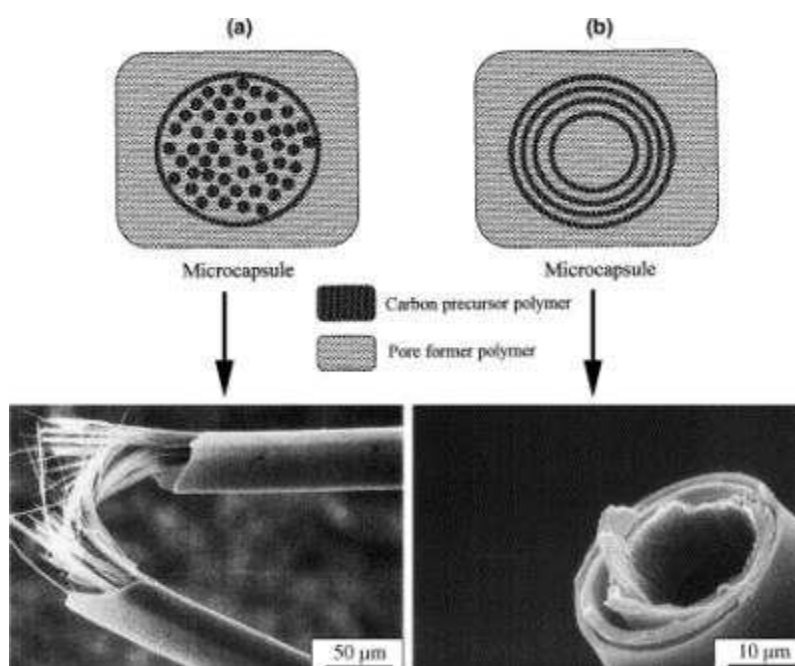


Figure I-12: Polymer blend process used for producing a) carbon tube containing thin carbon fibers b) multi-walled carbon tube [InK 2004]

2.2.6.3. Selection of specific Precursors

One of the simplest methods of producing porous carbon material is the choice of specific organic precursors which give porous carbons upon pyrolysis. Such specific precursors may be polyimides, metal carbides, biomass products, etc. In the case of carbon based on polyimide precursors, for

example, the polyimide's structure is retained throughout carbonization. As for biomasses, for example, carbonization of the kenaf plant without any kind of activation treatment involved, leads to carbons with specific surface areas as high as 2700 m²/g [InK 2004, InN 2004, Ina 2009]. Nonetheless, this method of creating porous carbons is hardly flexible; porosity characteristics cannot be adjusted. In addition, carbon characteristics, costs, and availability depend obviously foremost on the organic precursor.

2.3.Nanostructured Carbon Material derived from Biomass

As seen above, nanostructured, porous carbons can be synthesized from manifold precursors through a variety of methods. Most combinations of precursors and synthesis methods resulting in porous carbon material, however, do not include biomass-based carbons. Nonetheless, some methods may employ biomass or biomass derivatives to produce nanostructured carbons, such as the selection of specific precursors, activation, or carbon aerogel synthesis.

2.3.1. Pyrolysis of specific biomass-based Precursors

By selection of specific biomass-based precursors and corresponding carbonization conditions, nanostructured carbons can be produced. Carbonizing biomass, like other non-graphitizing carbons, can result in the creation of porous carbons, due to the retention of a rigid and complex molecular structure in addition to a loss of volatile matter during pyrolysis [Pan 2006]. Carbons resulting from the pyrolysis of biomass products such as coconut shells and wood chips may possess high macroporous volumes, due to the memory of the original biomass' cell structure. Carbonization of organic material like the cores of the kenaf plant or sucrose solutions may even lead to microporous carbons with high specific surface areas [InK 2004, InN 2004, Vix 2005]. This porosity seems to be created by the elimination of metallic impurities or of water combined with an extensive thermal decomposition, for the cores of kenaf plants [InN 2004] and sucrose solutions [Vix 2005], respectively. The cost for these biomass precursors is variable, but oftentimes still economical. The availability of large amounts of certain precursors, on the other hand, might be difficult. A still larger drawback of choosing this method in order to synthesize nanostructured, porous carbons, is that porous characteristics (*i.e.* pore sizes and pore size distributions) can hardly be controlled.

An attempt to control porous characteristics while using specific biomass precursors has been made, for example, using the template method with a sucrose solution [Vix 2005]. Nonetheless, in this case the porous characteristics can also be controlled only partly, *i.e.* the part of porosity created by dissolving the template. Also, even though the precursor for carbonization may be chosen to be on the basis of biomass for environmental concerns, a harmful acid treatment is still required to separate the carbon from the template.

2.3.2. Biomass-based Activated Carbons

As activation can be used on all types of carbon-rich material to introduce porosity into these, all types of biomass material having undergone pyrolysis can be activated. Activation has been investigated, for example, for fruit stones (*e.g.* olive, peach, and cherry stones), cellulose fibers (*e.g.* jute and coconut fibers), wood (*e.g.* teak sawdust) and other biomass (*e.g.* almond shells), as well as for other organic waste material (*e.g.* textile waste) [Rod 1995, Mol 1996, Rod 1992, Oli 2009, Pha

2006, Ism 2005, Guo 2003, Pra 2008, Sch 2007, Wil 2006, Tay 2009]. Even for biomass already containing macropores after carbonization, such as coconut shells and wood chips [Ina 2009], activation can be used to introduce microporosity. Although the porous characteristics (*i.e.* porous volumes and mean pore sizes) can essentially be controlled by the choice of activating agent and the process parameters, the carbon structure cannot (*i.e.* the carbon forming the pore walls). Also, narrow pore size distributions are difficult to obtain [Loz 2002]. In addition, activating agents for chemical activation are often harmful to the environment and may leave residues.

2.3.3. Biomass-based Carbon Aerogels

As mentioned before, carbon aerogels are obtained from the pyrolysis of organic aerogels. Even though a variety of biomass derivative-based gels have been investigated (*e.g.* cellulose-, lignin-, or xylane-based [Jin 2004, Aal 2009]), only very few have been synthesized by sol-gel method. Reports on biomass-based or biomass-derivative-based gels synthesized by sol-gel method are usually constricted to gels on the basis of chemically modified cellulose (such as cellulose acetate [Tan 2001, FiR 2006]), with some exceptions such as a recent report on the synthesis of chitin-based organic aerogels [Tsi 2009]. By synthesizing gels *via* sol-gel method, the gels structure and therefore the aerogels structure can be controlled.

3. Carbon Aerogels

Aerogels have first been synthesized, studied, and also named by S. Kistler in the 1930s [Kis 1931]. Carbon aerogels, however, have only been developed and studied thoroughly much later by Pekala in the 1980s [Pek 1989].

The preparation of a carbon aerogel consists of three main steps (see figure I-13): i) synthesis of an organic gel by sol-gel method, ii) drying of the wet gel, and iii) carbonization of the aerogel. Drying of the wet gel needs to be carried out in conditions which allow to maintaining the three-dimensional structure and open porosity of the initial gel.

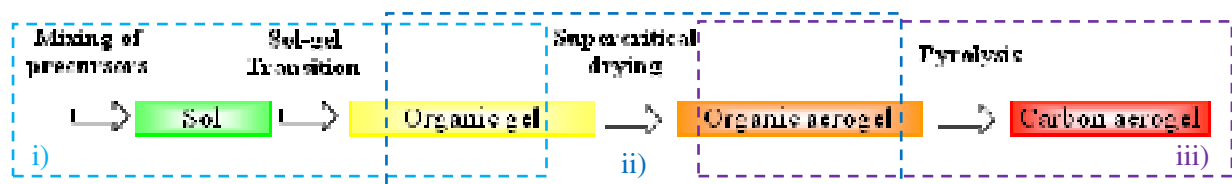


Figure I-13: Schematic illustration of carbon aerogel synthesis

3.1. Gel Synthesis

Aerogels are prepared on the basis of a gel, typically having been synthesized by sol-gel method. A gel is, according to [Pha 2004], a thermodynamically stable solid-liquid biphasic system consisting of two interpenetrated three-dimensional networks: a solid one and a liquid one.

The preparation of gels by sol-gel process can be divided in three main stages: i) preparation of the sol, ii) sol evolution and sol-gel aggregation resulting finally in the transition from sol to gel, and iii)

gel ageing (see figure I-14). A sol is defined as a colloidal suspension of solid particles in a liquid [Bri 1990].

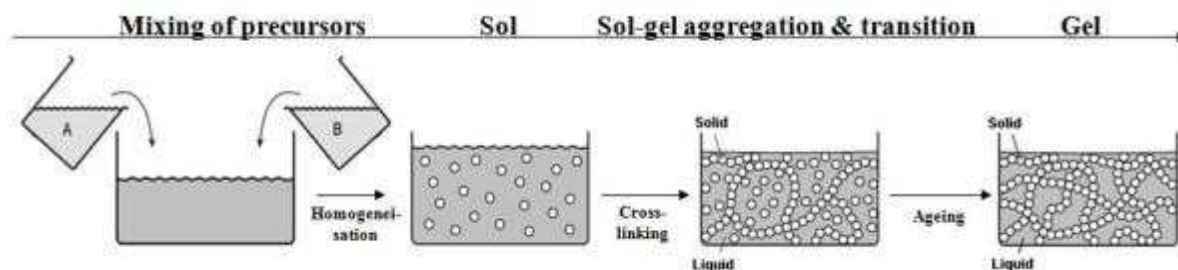


Figure I-14: Schema of sol-gel process (based on [Hüs 1998])

Sol Preparation and Evolution: The sol in the sol-gel method is the dispersion of precursors (*i.e.* starting compounds) in a solvent and the subsequent addition of a catalyst. The precursors' solvent provides also the reaction media for the sol-gel process. Upon the addition of catalyst into the precursor solution, reactions between precursors are triggered. The application of a catalyst is not always required, but oftentimes useful to increase the reaction kinetics.

Sol-gel Transition: Within the sol, chemical reactions (mainly hydrolysis and condensation for mineral gels and addition and condensation for organic gels) lead to the reaction between the precursors. The reactions advance towards forming a single three-dimensional polymer. As the evolution of the sol progresses (simultaneous aggregation of numerous macromolecules and eventual cross-linking between these macromolecules), the sol's viscosity increases incessantly until it tends suddenly to infinity, *i.e.* forming a gel. The moment the sol changes to a gel, is called the sol-gel transition.

Ageing: Even though the sol's viscosity tends towards infinity at some point of time, resulting in a gel, the cross-linking reactions may continue as long as functional groups involved in the cross-linking process remain un-reacted and accessible. In the process of ageing, mechanically weak gels usually become stronger, as more bonds are formed. Usually, the gel shrinks as more bonds are formed and the liquid solvent network contained in the pores is partly expelled. This phenomenon is referred to as syneresis.

The structure of gels obtained by sol-gel synthesis is known to depend on:

- intrinsic parameters, *i.e.* the choice of precursors and thus nature of atoms, groups, and molecular complexity,
- extrinsic parameters, *i.e.* processing conditions, such as the choice of catalyst, solvent, concentration of precursors, and pH.

All these parameters influence the kinetics of several reactions potentially involved in a sol-gel process and therefore the structure of the resulting gel [Bri 1990]. The sol-gel synthesis thus allows controlling the solid network's structure through a adaptation of the synthesis parameters.

3.2. Drying

During the drying process, basically, the liquid network of the gel is replaced by air. Thus the liquid network of the gel is transformed into a network of pores [Pha 2004] and a porous material is created. If the structure of the gel having been tailored by the sol-gel process can be maintained during the drying step, the resulting porous material may be called an aerogel.

As drying of the liquid network by simple evaporation in air often results in the collapse of the gel, special drying methods, such as supercritical drying and freeze drying have been investigated. Supercritical and freeze drying eliminate the liquid network through by-passing the liquid's critical and triple point respectively (see figure I-15). Of course, the behavior of the gels during drying depends significantly on the type of gel and also on the solvent to be extracted.

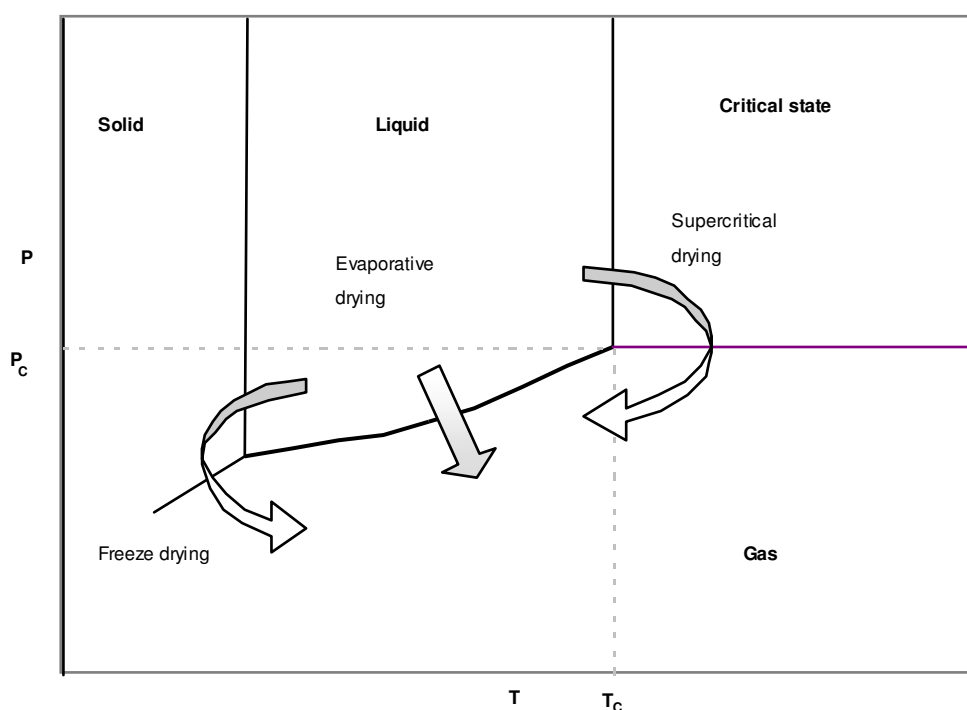


Figure I-15: State diagram illustrating different drying methods [Bis 2003]

3.2.1. Evaporative Drying

Drying a gel by evaporation of the liquid phase in air, results in the creation of a so-called xerogel. Evaporation may be carried out in ambient conditions or at elevated temperatures, in natural or forced convection.

As a gel can be considered to consist of a solid network enclosing a liquid phase in small porosities (or capillaries), gas-liquid interfaces in capillaries are formed if the gel is exposed to air. Due to the liquid's surface tension, capillary tensions arise and often force the gel to collapse. This collapse results in significantly modified structures for the xerogel as compared to the initial gel's structure and normally in shrinkage of the gel [Bis 2003, Mor 2005]. Nonetheless, by adjusting the chemical synthesis parameters the shrinkage of certain gels may be mastered [JoT 2005]. Shrinkage of RF-based gels during evaporative drying decreases if the gels are made up of sufficiently big particles,

which in return increase the mean pore size as well as the mechanical resistance of the solid network to capillary pressures and compression. Although these xerogels undergo shrinking, the shrinking rate and therefore the structure obtained after drying may be mastered. Job et al. have thus been able to synthesize RF-based carbon xerogels with pore volumes inferior to $1.5 \text{ cm}^3/\text{g}$ and pore sizes superior to 30 nm [Job 2009].

However, if the formation of capillary tensions can be avoided during the removal of the solvent, the gel's initial structure should be maintained. For example, capillary tensions do not occur if the liquid-gas phase boundary is avoided, *i.e.* for sublimation or the change from supercritical fluid to gas.

3.2.2. Supercritical Drying

In order to avoid capillary tensions due to gas-liquid interfaces, the liquid network of the gel may be transferred to its supercritical state before drying. A supercritical fluid does not feature a surface tension, so that no capillary tensions at interfaces between gas and supercritical fluid exist. Therefore, using supercritical drying, the gel's initial structure is mostly maintained and gels only shrink little during the drying process (see figure I-16 for a schematic comparison between the impact of supercritical and evaporative drying).

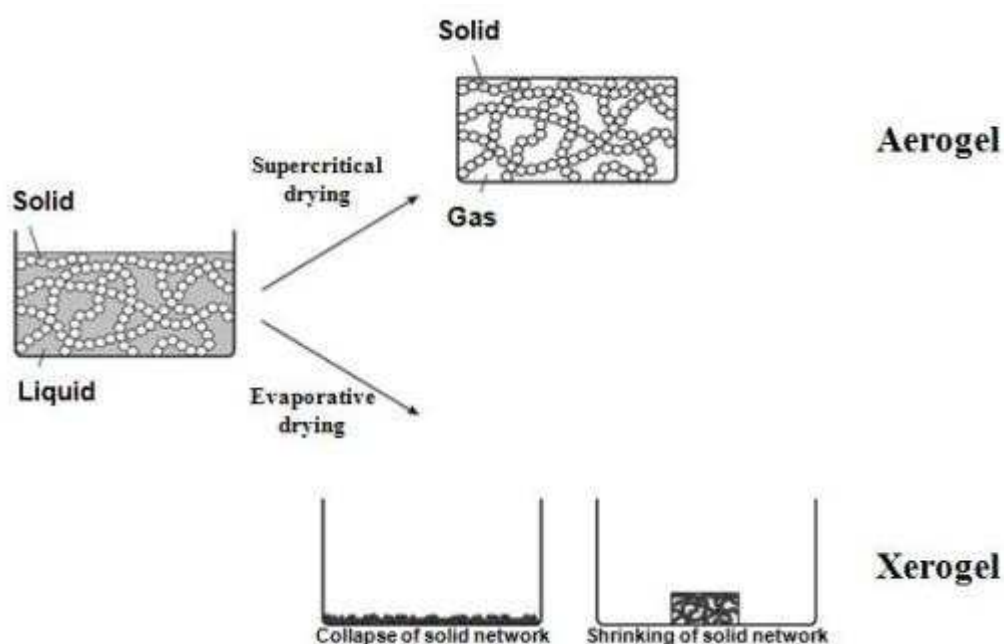


Figure I-16: Schematic comparison between the impacts of supercritical and evaporative drying (based on [Hüs 1998])

For supercritical drying, as can be seen in figure I-15, first the liquid to be extracted is heated past its critical temperature and the pressure is raised past the critical pressure. Subsequently, the fluid is slowly released, *i.e.* slow isothermal depressurization (*i.e.* $T > T_c$) allows avoiding condensation of the fluid initially trapped within the capillaries. The fluid released is first supercritical fluid and changes at a lower pressure (*i.e.* for $P < P_c$) to gaseous fluid.

A disadvantage of this process is related to the position of the critical point for many liquids. The critical point of most organic solvents used as reaction media (such as alcohol), for example, requires operation at high temperatures and high pressures, which in return may be dangerous due to the

high flammability and harmfulness (at times toxicity) of a great part of organic solvents. Therefore, Tewari, Hunt, and Lofftus [Tew 1985] proposed to replace the liquid solvent network trapped in the gel by liquid CO₂ first. After having replaced all the initial solvent within the gel's pores by liquid CO₂, temperature and then pressure are raised to reach the supercritical state of CO₂. The advantage of this method is that the supercritical point of CO₂ is reached at almost ambient temperature and rather reasonable pressure ($T_c \approx 31^\circ\text{C}$, $p_c \approx 7.4\text{ MPa}$). In addition, CO₂ is non-toxic and non-flammable.

Further, van Bommel and de Haan [Bom 1995] proposed replacing the liquid solvent directly by supercritical CO₂ instead of liquid CO₂. This development allowed accelerating the drying process notably, as the diffusion of supercritical fluids into the nanoporous gels is much faster than the diffusion of liquids [Bri 1990, Bis 2003, Mas 2006].

Although supercritical drying directly in supercritical CO₂ is very advantageous in order to more or less preserve a gel's structure, the process itself presents several disadvantages including relatively high equipment and operating costs and time-consuming washing and depressurization steps. Nonetheless, supercritical drying directly in supercritical CO₂ remains the reference drying method for synthesizing aerogels, as it remains the most efficient method to prepare crack-free monoliths even of very high porous volumes, very low densities, and large dimensions.

3.2.3. Freeze Drying

A wet gel having been dried by freeze drying (also known as lyophilisation or cryodesiccation) [Mar 2000] may be called a cryogel [Paj 1989].

Freeze drying proceeds, theoretically, in two steps. First, the liquid solvent network of the gel gets frozen by lowering the temperature below the temperature of the solvent's triple point. Second, the pressure is decreased in order to pass directly from the solid frozen phase of the solvent to the gaseous phase by sublimation. In practice, however, the solvent often needs first to be replaced by another liquid with a low expansion coefficient and a relatively high pressure of sublimation [Hüs 1998]. Additionally, the liquid used to replace the solvent should present a relatively high (equilibrium) vapour pressure in order to be able to work at reasonable sublimation kinetics. Sublimation is used so as to avoid the appearance of a liquid-gas interface and accompanying capillary tensions in the gel's pores. Theoretically, the solid network's structure may thus be preserved during drying. In practice, however, crystal growth in the frozen liquid phase, destroys the solid network. Therefore, cryogel monoliths are difficult to obtain [Bis 2003, Mor 2005] and could only have been generated on rare occasions [Rig 2004].

3.3. Carbonization

3.3.1. General Description

Organic aerogels may be transformed into carbon aerogels through carbonization.

Carbonization describes the process in which carbon-containing organic compounds are heat-treated in an inert atmosphere in order to produce carbon material. During carbonization, the precursor undergoes pyrolysis. Pyrolysis can be defined as the thermal decomposition of materials in the

absence of oxygen [Moh 2006]. Organics are converted to solid, liquid, and gas fractions in the process of pyrolysis. The amount and composition of the solid, liquid and gaseous fractions formed depends on the process variables. Generally, pyrolysis is carried out in inert atmosphere (most often in N₂ or Ar) at temperatures above 600 °C, which is the temperature at which carbonization begins [Koc 2005].

The organic precursors generally undergo following steps in the course of pyrolysis [Moh 2006]:

1. heat transfer from heat source to the precursor increases the temperature inside precursor
2. primary pyrolysis reactions release volatiles and form char (elevated but not final temperature yet)
3. heat transfer between hot volatiles and cooler un-pyrolyzed precursor takes place due to the flow of hot volatiles toward cooler solids
4. a part of the volatiles condenses in the cooler part of the precursor which can result in secondary reactions, *e.g.* producing tar
5. autocatalytic secondary pyrolysis reactions proceed while primary pyrolytic reactions continue
6. further thermal decomposition may occur, depending on the pyrolysis profile (activation duration, temperature, pressure), *e.g.* reforming, water gas shift reactions, radicals recombination, dehydration, etc.

Obviously, the precursor material, but also the pyrolysis process variables have a considerable influence on the amount and composition of the solid, liquid and gaseous fractions formed, as well as the type of thermal decomposition reactions occurring. Carbon structure, surface chemistry and the material's transport properties also depend on the process variables of the pyrolysis process.

Pyrolysis is typically accompanied by mass loss, structural modifications, and an evolution of the microstructure often in terms geometrical shrinking of the material. The structural characteristics of aerogels (*e.g.* in terms of specific surface area, micropore diameter and volume, etc.), for example, vary during the pyrolysis process [Koc 2005]. A multitude of variables may possibly have an influence on the pyrolysis process [Ste 2005, Koc 2005, Moh 2006, Mer 2006, SuL 2007, Cou 2007, Ona 2003], namely:

- material-related influences: precursor material, particle size, humidity, etc...
- pyrolysis process-related influences: pyrolysis atmosphere and pressure, rate of sweeping gas, heating rate, pyrolysis profile (*i.e.* non-linear heating), final temperature, etc...

3.3.2. Pyrolysis Parameters

Material-related Influence

The *nature of the precursor material* clearly has a very pronounced effect on the resulting carbon material's structure, yield, and chemistry [Koc 2005, Ish 2004, Las 1999, Cou 2007].

Precursor particle size and humidity (along with activation duration and heating rate within slow pyrolysis conditions) have been found to have little influence on the amount of gas produced during

the pyrolysis of ligno-cellulosic material [Cou 2007]. Nonetheless, the particle size, and probably also humidity, may have an influence at high heating rates [Ona 2003].

Process-related Influence

Pyrolysis atmosphere has a significant influence on structure, composition and surface chemistry of a carbon material resulting from pyrolysis [Ste 2005, SuL 2007, Kim 2002]. Organic material can be carbonized in vacuum, in inert gases (such as nitrogen, argon, or helium), or in oxidative atmospheres (like carbon dioxide or oxygen/nitrogen mixtures). Pyrolysis in vacuum demands a higher activation energy (because of the smaller thermal conductivity compared to inert gases), but results in higher residues with a higher density [SuL 2007]. Pyrolysis in oxidative atmospheres involves physical activation. Further, organic material can be pyrolyzed in different chemical agents, such as gaseous hydrochloric acid and sulphuric acid [Ish 2004] enhancing carbon yield or catalyzing carbonisation reactions respectively. The pyrolysis atmosphere may thus have an influence on the evolution of porosity and pore characteristics as on structural changes in general (*e.g.* specific surface area, pore size distribution, and micropore volume). In addition, the atmosphere can influence the purity of the material or change its' surface chemistry. Also, specific gas molecules may possibly adsorbed onto the surface of a porous carbon material [Fey 2002].

Pyrolysis under pressure has an influence on the temperature dependence of the yield of the solid fraction [Ari 2007]. Under pressure, the solid yield differs more for different temperatures.

The *rate of sweeping gas* determines the delay of removal of volatile products from the hot zone. If the volatiles are quickly removed from the hot zone, secondary reactions breaking down weighty molecules into gaseous species (such as thermal cracking, repolymerization, and condensation) are minimized; liquid yield is maximized. Volatile residence time is understandably a very important factor affecting gas and liquid yield, but does not have an obvious influence in the solid yield [Bri 1990, Ona 2003].

Heating rate may have an influence on the yield of the different fractions (*i.e.* gaseous, liquid, and solid fraction being generated in the pyrolysis process) and accompanying on chemical composition and structural properties [Bri 1990]. To perceive an influence of the heating rate, slow, fast, and flash pyrolysis (*i.e.* heating in some hours or even days, some minutes, or only some seconds respectively) need to be distinguished [Ona 2003]. Low heating rates are known to yield less volatiles and more of a solid fraction [Mer 2006]. For this reason, slow pyrolysis is generally used to produce char, while fast pyrolysis produces a rather large fraction of liquid hydrocarbons. In slow pyrolysis, the heating period is sufficiently slow to allow equilibration even at reaching the final temperature but not residing at it. The yield of char is maximized *via* secondary coking and repolymerization of the volatiles inside the solid [Bri 1990, Mer 2006]. Whether the products residence time in the reactor is important depends therefore on the heating rate [Ona 2003]. Non-linear heating *i.e.* residence times at intermediary temperatures, does thus also only have an influence if the heating rate is too high and pyrolysis reactions cannot reach their equilibrium state.

Another major influence on the slow pyrolysis process affecting product yield is the *pyrolysis' final temperature* [Wil 1996]. The char yield generally decreases with temperature, while the gas yield increases [Ona 2003]. Final, or maximum, pyrolysis temperature further influences the carbon's composition and surface chemistry and its structure [Ari 2007, Fey 2002].

4. Biomass-based Carbon Aerogels

Knowing that the organic precursor for pyrolysis has a fundamental influence on the resulting carbon, the most important step in order to synthesize a carbon aerogel is the choice of the type of organic aerogel which will act as precursor. As mentioned in section 2.3.3, the biomass derivative used to produce most known biomass-based organic aerogels is cellulose or one of its derivatives.

Even though aerogels are typically prepared from gels synthesized by sol-gel method, any type of gel with open porosity which does not undergo fundamental structural damages upon drying can be transformed into an aerogel-like material. Therefore, I have investigated different methods of preparing cellulose-based gels. Two types of gels can be distinguished: i) chemical gels, *i.e.* gels based on covalent bonding, and ii) physical gels, *i.e.* gels based on physical aggregations (*e.g.* by van der Waals or hydrogen bonding, dipole-dipole interactions, or electrostatic interactions) [Kav 1998]. Further, gels based on cellulose can be distinguished from gels based on cellulose derivatives. Overviews of different methods leading to cellulose-based gels are presented in tables I-3 to I-6. Physical gels based on cellulose and on cellulose derivatives are shown in tables I-3 and I-4, respectively. Chemical gels based on cellulose and on cellulose derivatives can be seen in tables I-5 and I-6, respectively.

4.1. Biomass-based Physical Gels and wet regenerated Compounds

As explained above, physical gels are gels made-up of physical aggregations. They are synthesized by the dissolution of the precursor (in this work cellulose or a cellulose derivative) in a solvent and subsequent gelation due to a change in solution conditions. Gelation may be initiated *e.g.* by a modification of the solution temperature, pH, or the solvent composition. Numerous physical gels are thermodynamically reversible; *i.e.* they are stable in a given range of thermodynamic conditions, but may be destroyed by a change in temperature [DeG 1979, Kav 1998]. Dissolution and gelation depend both on temperature and precursor concentration, not only for physical gels. Additionally, cellulose solutions, in the form of liquids and also gels, may be regenerated (precipitated) by adding a non-solvent of cellulose. In a so-called regenerating bath, the cellulose solution coagulates and the cellulose precursor is regenerated, *i.e.* desolvation occurs. The properties of the regenerated compound depend importantly on the composition of the regeneration bath. The regenerated cellulose fibers are wet after regeneration and need to be dried prior to other treatments. The structure of the regenerated fiber differs usually from the structure of the cellulose precursor having been dissolved previously and depends particularly on the nature of the solvent.

Physical gels are oftentimes stable only under certain conditions and may not possess a mechanical strength high enough to resist to structural modifications induced by the drying process. However, the feasibility of supercritically drying (in CO₂) of wet regenerated cellulose compounds has been demonstrated previously [Gav 2007].

A broad variety of biopolymer physical gels has been investigated, including gelatin, seaweed, plant polysaccharides such as agarose and pectin, starches and of course cellulose and its derivatives [Kav 1998]. An overview of physical cellulose(-derivative) based gels and/or wet regenerated cellulose-based compounds can be found below:

1. Physical cellulose-based gels and/or wet regenerated cellulose compounds
 - a. Dissolution of cellulose in *aqueous alkali hydroxides* [Lan 1999, Roy 2002, YaX 2002, Zho 2002, Ega 2006, Mao 2006, Gav 2007, Cai 2008]
 - b. Dissolution of cellulose in *N-methylmorpholine N-oxide (NMMO)* [Hin 1993, Fin 2001, Inn 2006, Gav 2007, Lie 2009]
 - c. Dissolution of cellulose in *aqueous solutions of inorganic salts* [Hat 1998, Jin 2004, Kug 1980, Hoe 2008]
 - d. Dissolution of cellulose in *organic solutions of inorganic salts* [Cuc 1983, Fre 1996, Yan 2000, Yan 1999, Yan 1996]
 - e. Dissolution of cellulose in *ionic liquids* [Kos 2008, Don 2009, Aal 2009, Bud 2010]
2. Physical cellulose-derivative based gels and/or wet regenerated cellulose compounds
 - a. Dissolution of cellulose acetate [Alt 1986, Reu 1986, Pim 2003]
 - b. Dissolution of methyl cellulose [Haq 1993, Sar 1995, Des 1998, Kun 2001, LiT 2001, Tak 2001]
 - c. Dissolution of hydroxypropyl cellulose [Wer 1980, Gao 2001]

4.2. Biomass-based Chemical Gels

Chemical gels are based on strong molecular cohesion due to covalent bonding. Due to the type of bonding, gelation is never reversible. Chemical gels are basically macromolecules synthesized by cross-linking of the polymeric precursor or by polymerization of a monomeric precursor. One possible method of synthesizing chemical gels is the sol-gel method [Tan 1981, Kav 1998].

Generally, chemical gels possess a higher mechanical stability than physical gels. Therefore, they are better suited to resist to structural modifications induced by the drying process.

Various methods of cross-linking cellulose have been investigated; although they have not been used to prepared cellulose-based gels (see table I-5). Synthesis of chemical gels on the basis of cellulose-derivatives, however, has been studied widely (see table I-6). An overview of methods for cross-linking cellulose and cellulose-derivatives may be found seen below:

1. Chemical cross-linking of cellulose
 - a. Cellulose cross-linking by *formaldehyde* [Row 1966, Pie 1967, Wea 1978]
 - b. Cellulose cross-linking by *polycarboxylic acids* [YaC 1991, YaC 1993, Zho 1995, YaC 2002, Che 2006]
 - c. Cellulose cross-linking by *epichlorohydrin* [Lub 1976, Che 1998]
2. Chemical cellulose-derivative based gels
 - a. Cross-linking of cellulosic polymers by *polyisocyanates* [Kam 1996, Tan 2001, Riv 2004, Fis 2006]
 - b. Cross-linking of cellulosic polymers by *divinylsulphone* [Anb 1990, Esp 1996, Kat 2004, San 2005]
 - c. Cross-linking of cellulosic polymers by *epichlorohydrin* [Bai 2006]
 - d. Cross-linking of cellulosic polymers *phosphoric acids* [Bie 1987, Dul 2006]

Table I-3: Physical cellulose-based gels and wet regenerated cellulose compounds

	Chemical products	Classification	Conditions			References
			Dissolution temperature	Gelation temperature	Reversibility	
Precursor	cellulose powder		-60 to < 20 °C	no gelation	irreversible	¹⁾ [Roy 2002] ¹⁾ [Lan 1999] ¹⁾ [YaX 2002] ¹⁾ [Zho 2002] ¹⁾ [Mao 2006] ¹⁾ [Ega 2006] ¹⁾ [Gav 2007] ^{1&2)} [Cai 2008]
Solvent	sodium hydroxide ¹⁾ or lithium hydroxide ²⁾	X_n, C C				
Regenerating bath	example: water					
Optional additives (examples)	(thio)urea zincates (e.g. ZnO)	X_n, N (thiourea) N (zinc oxide)				
Precursor	cellulose powder			no gelation		[Hn 1993] [Fn 2001] [hn 2006] [Gav 2007] [Lie 2009]
Solvent	aqueous solution of N-methylmorpholine N-oxide	X_i				
Regenerating bath	example: water					
Optional additives (examples)	hydrogen peroxide	X_n, C				
Precursor	cellulose powder		> 100 °C	below dissolution temperature	thermoreversible (80 °C)	[Hat 1998] [Jin 2004] [Kug 1980] [He 2008]
Solvent	calcium thiocyanate tetrahydrate	X_i				
Regenerating bath	example: methanol	T, F (methanol)				
Optional additives (examples)						
Precursor	cellulose powder			15 °C to 30 °C ¹⁾	thermoreversible (30 °C) ¹⁾	¹⁾ [Cuc 1983] ¹⁾ [Fre 1996] ²⁾ [Yan 2000] ²⁾ [Yan 1999] ²⁾ [Yan 1996]
Solvent	ammonium / ammonium thiocyanate solution ¹⁾ or cuprammonium complexes ²⁾	T, N, C (ammonia)				
Regenerating bath	example: aqueous solution of acetic acid	C				
Optional additives (examples)	example: pyridine	F, X_n				
Precursor	cellulose powder		T_{amb}	no gelation		¹⁾ [Den 2009] ¹⁾ [Al 2009] ²⁾ [Kos 2008] ²⁾ [Bud 2010]
Solvent	1-butyl-3-methyl-imidazolium chloride ¹⁾ or 1-ethyl-3-methyl-imidazolium acetate ²⁾	T, N				
Regenerating bath	example: water					
Optional additives (examples)	example: dimethyl sulfoxide					

C	-	corrosive substances	F	-	flammable substances	N	-	substances dangerous for the environment
T	-	toxic substances	X_i	-	irritants	X_n	-	harmful substances

Table I-4: Physical cellulose-derivative based gels and wet regenerated compounds

	Chemical Products	Classification	Conditions			References	
			Dissolution temperature	Gelation temperature	Reversibility		
2a)	Precursor	cellulose acetate	90 °C hot	quenched to 20°C 0 - 25 °C	ther moreversible ther moreversible	¹⁾ [Alt 1986] ¹⁾ [Reu 1986] ²⁾ [Pm 2003]	
	Solvent	solution aqueuse de dioxane ¹⁾ ou chbroforme ²⁾					<i>T, F, X_n</i> <i>T, N</i>
	Regenerating bath						
	Optional additives (examples)	Méthanol <i>T, F</i>					
2b)	Precursor	methyl cellulose	5 °C	> 40-50 °C	ther moreversible	[Tak 2001] [Des 1998] [Haq 1993] [Sar 1995] [LiT 2001] [Kun 2001]	
	Solvent	w ater					
	Regenerating bath						
	Optional additives (examples)						
2c)	Precursor	hydroxypropyl cellulose	cold	phase separation > 40°C coagulation of the polymer-rich phase	metastable	[Wer 1980] [Gao 2001]	
	Solvent	w ater					
	Regenerating bath						
	Optional additives (examples)	sodium hydroxide divinylsulphone (chemical cross-linking) <i>X_n, C</i> <i>T, C</i>					

<i>C</i>	-	corrosive substances	<i>F</i>	-	fl ammable substances	<i>N</i>	-	substances dangerous for the environment
<i>T</i>	-	toxic substances	<i>X_i</i>	-	irritants	<i>X_n</i>	-	harm ful substances

Table I-5: Chemical cross-linking of cellulose

	Chemical products		Classification	Conditions		References
				Dis solution temperature	Cross-linking temperature	
3a)	Precursor	cellulosic material				[Row 1966]
	Solvent	none: reaction in heterogeneous environment			T_{amb}	[Fle 1967]
	Cross-linker	formaldehyde	T, C			[Wea 1978]
	Catalyst					
3b)	Precursor	cellulosic material				[Zho 1995]
	Solvent	none: reaction in heterogeneous environment				[YaC 2002]
	Cross-linker	polycarboxylic acids example: aqueous solution of succinic acid	X_n, C			[YaC 1993] [YaC 1991]
	Catalyst	example: phosphoric acids				[Che 2006]
3c)	Precursor	cellulose powder				[Lub 1979]
	Solvent	sodium hydroxide	X_i	$> 5^{\circ}C$	60-65 $^{\circ}C$	[Che 1998]
	Cross-linker	epichlorohydrine	T			
	Catalyst					

C	-	corrosive substances	F	-	flammable substances	N	-	substances dangerous for the environment
T	-	toxic substances	X_i	-	irritants	X_n	-	harmful substances

Table I-6: Chemical cellulose-derivative based gels

	Chemical Products	Classification	Conditions		Sources	
			Dissolution temperature	Cross-linking temperature		
4a)	Precursor	example: cellulose acetate	T_{amb}	T_{amb}	¹⁾ [Fis 2006] ²⁾ [Tan 2001] [Riv 2004] [Kam 1996]	
	Solvent	example: acetone				X_i, F
	Cross-linker	diisocyanates example: diphenylmethane 4,4-diisocyanate ¹⁾				X_n
	Catalyst	dibutyltin dilaurate ¹⁾ pyridine ²⁾				T F, X_n
4b)	Precursor	example: hydroxyethyl cellulose	T_{amb}	T_{amb}	[Anb 1990] [Esp 1996] [San 2005] [Kat 2004]	
	Solvent	alkaline solution example: sodium hydroxide				X_n, C
	Cross-linker	divinyl sulphone				T, C
	Catalyst					
4c)	Precursor	cellulose acetate	T_{amb}	40 °C	[Bai 2006]	
	Solvent	dimethyl sulfoxide				X_i
	Cross-linker	epichlorohydrin				T
	Catalyst					
4d)	Precursor	example: cellulose acetate	T_{amb}	T_{amb}	[Bie 1987] [Dul 2006]	
	Solvent	example: sodium hydroxide				X_n, C
	Cross-linker	phosphoric acids example: phosphoric pentoxide				C
	Catalyst					

C	-	corrosive substances	F	-	flammable substances	N	-	substances dangerous for the environment
T	-	toxic substances	X_i	-	irritants	X_n	-	harmful substances

4.3 Summary and Selection of Synthesis Method

In order to be able to generate an aerogel on the basis of a cellulosic gel or wet regenerated compound, following criteria need to be taken into account:

- Gels need to be non-thermoreversible in ambient conditions and conditions of supercritical CO₂
- Gels need to feature an open porosity

According to these criteria, some of the physical gels might not be used such as, but would need to be regenerated prior to supercritical drying. Nonetheless, most cellulosic physical gels have been shown to possess an open porosity, at least after regeneration. Contrary to chemical gels, however, the pore sizes in physical gels may be less easily to adjust (*e.g.* by varying the regeneration agent for physical gels, as compared to adjusting for example the sol-gel conditions for chemical gels).

Further, to be coherent with the use of the final material in an application beneficial for the environment, following criteria may also be considered:

- Easy accessibility of precursor material
- Utilization of non-toxic, non-corrosive precursors and cross-linkers and substances dangerous for the environment

Even after application of these criteria, several methods for synthesizing cellulose-based gels remain eligible. Cellulose dissolved in NMMO or calcium thiocyanate or ionic liquids like 1-ethyl-3-methylimidazolium acetate (EMIMAc) and subsequently regenerated, for example, seem like interesting synthesis methods. Nonetheless, these methods are still subject to environmental concerns (*e.g.* due to the use of harmful solvents, recycling issues, etc.) and do not offer the same possibilities of adjusting the gel/composite structure as chemical gels do. The only method of synthesizing a cellulosic chemical gel corresponding to above-mentioned criteria is the cross-linking of cellulosic polymers by polyisocyanates (method 4a in table I-6). Even though most types of polyisocyanates are also considered to be toxic, F. Fischer [Fis 2006] has developed a method of cross-linking cellulose acetate by non-toxic (although still harmful) methylene diphenyl diisocyanate (MDI), based on works of Tan et al. [Tan 2001]. Therefore, I have chosen to examine nanostructured carbon synthesized by pyrolyzing cellulose-acetate-based organic aerogels (cellulose acetate cross-linked using MDI, as described by F. Fischer [Fis 2006]) during my PhD thesis.

Chapter II: Cellulose-acetate based Organic Aerogels

Cellulose-acetate-based Organic Aerogels

1. Introduction

This chapter focuses on the synthesis of cellulose-acetate-based (CAB) aerogels which will act as precursor for carbon aerogels investigated in chapters III (Cellulose-acetate-based Carbon Aerogels), IV (Modification of the Cellulose-acetate-based Carbon Aerogels: Structure and Surface Chemistry), and V (Electrochemical Analysis of Cellulose-acetate-based Carbon Aerogels as Electrochemical Double Layer Capacitor Electrode Material).

First, the reference process for synthesizing cellulose-acetate-based organic aerogels, consisting of *i*) sol-gel synthesis and *ii*) drying in supercritical CO₂, is described. The influence of different fundamental synthesis parameters on the sol-gel process and the resulting organic aerogels is analyzed. Several fundamental synthesis parameters have been varied to create a broad range of structurally different organic aerogels. In addition, the influence of different drying processes on the resulting organic aerogel is examined.

CAB gels are synthesized by sol-gel method, based on a protocol established by Fischer [Fis 2006]. Supercritical drying in CO₂ is carried out following a protocol developed by Y. Masmoudi [Mas 2006].

A sol-gel synthesis, in general, involves different chemical species: different precursors, a solvent for the precursors simultaneously acting as reaction media, and a catalyst.

Gels for this study have been prepared using

- ⇒ cellulose acetate as cellulosic precursor,
- ⇒ a polyfunctional isocyanate as second precursor,
- ⇒ acetone as solvent for the precursors, and
- ⇒ one of three different polyurethane catalysts (a metallic salt, a tertiary amine, or a heterocyclic compound).

The sol-gel synthesis of CAB gels as developed by Tan and further explored and optimized by Fischer [Tan 2001, Fis 2006] proceeds in three main steps:

- (i) First cellulose acetate is dispersed in acetone (simultaneously acting as reaction media).
- (ii) A catalyst is added, to activate the sol-gel process and to accelerate the kinetics of the condensation reaction between the precursors.
- (iii) Upon the addition of a polyisocyanate compound, the cross-linking process is triggered: covalent bonds in the form of urethane links (–NH(CO)O–) form between the isocyanate groups (–N=C=O) of the polyisocyanate compound and the hydroxyl functional groups of the cellulose acetate (–O–H) (see figure II-1).

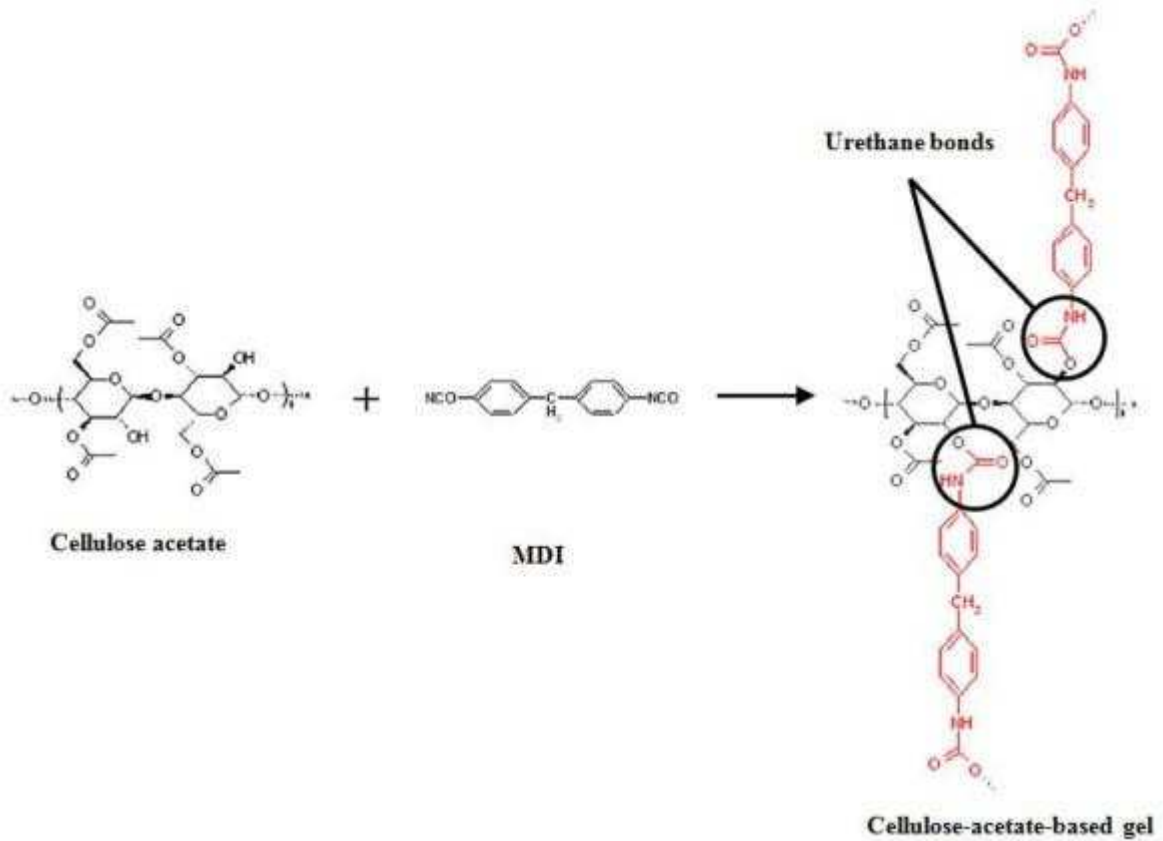


Figure II-1: Schematic representation of the sol-gel reaction cross-linking acetate cellulose and the polyisocyanate MDI through urethane bonds

In the present work, several fundamental sol-gel parameters have been modified systematically in order to create differently structured gel networks and to analyze the parameters' influence on the wet gels' structure. We have maintained the nature of the two precursors, and the solvent, as well as the synthesis protocol throughout the work. Below-mentioned parameters have been modified:

- ⇒ Precursor concentration **% CA** (*i.e.* mass percentage of cellulose acetate dissolved in acetone):

$$\%CA = 100 \cdot \frac{m_{CA}}{m_{acetone}} \quad \text{Equation II-1}$$

- ⇒ Cross-linking ratio **I/CA** (*i.e.* isocyanate mass in relation to cellulose acetate mass):

$$I/CA = \frac{m_I}{m_{CA}} \quad \text{Equation II-2}$$

- ⇒ Catalyst concentration (*i.e.* catalyst mass per liter of solvent):

$$[Catalyst] = \frac{m_{Catalyst}}{V_{sol}} \quad \text{Equation II-3}$$

⇒ or the ratio of isocyanate precursor to catalyst **I/Cat** (i.e. isocyanate mass in relation to catalyst mass):

$$I / Cat = \frac{m_I}{m_{Cat}} \quad \text{Equation II-4}$$

(Note that the parameter **I/Cat** changes with the **%CA**, if the catalyst quantity is fixed).

⇒ Catalyst nature

The concentration of each precursor is known to have a considerable impact on particle size, porosity, mean pore size, and specific surface area resorcinol-formaldehyde (RF) based organic and carbon aerogels. A change of precursor concentration influences directly the RF-based aerogel's final density and mean pore size [Boc 1998, Pek 1998]. Similarly, precursor concentration seems to influence the density and pore size of cellulose-acetate-based aerogels [Fis 2006]. The ratio of reactive precursor to catalyst (I/Cat) has also been proven to be significant for RF-based aerogels, influencing not only reaction kinetics but more importantly density, particle and pore size [ScP 1995, Boc 1998, Pek 1998]. Moreover, it has been found that high catalyst quantities yielded small particles, low porous volumes and mean pore sizes in RF-aerogels [Sal 1998]. Although catalyst quantity has also been found to exert an influence on the structure of polyurethane-based aerogels, higher catalyst concentrations have resulted in lower densities for this type of gels [Rig 2007]. Catalyst quantity and nature may also influence the network density controlling both the size and the skeletal density, for example for RF-based aerogels as shown by Schaefer et al. [ScP 1995]. Catalyst nature, finally, determines reaction kinetics. As mentioned above, in sol-gel synthesis different reactions may generally take place simultaneously. Different types of catalysts favor different reactions and might therefore have an impact on the resulting gel structure. Therefore, we have decided to initiate a comprehensive study on the influence of precursor concentrations and ratio as well as on catalyst concentration and nature on CAB gels and aerogels.

2. Experimental

2.1 Sol-gel Synthesis

Cellulose acetate (CAS [9004-35-7], with an acetyl content of 39.8 wt. % and a number-average molecular weight M_n of 30 000, Sigma-Aldrich) and PMDI (CAS [101-68-8], polymethylene polyphenylpolyisocyanate, 31.8 wt% NCO content, Lupranat® M20S, BASF, Dangerous Substances Directive: X_n) react in extra-dry acetone (CAS number [67-64-1], purity of 99.8 %, Sigma-Aldrich, Dangerous Substances Directive: F, X_n) having been selected to be the reaction medium. See figure II-2 for the structural formula of the two precursors. Three different kinds of catalysts have been employed alternatively to activate the step-growth polymerisation. Firstly, the tin-based organometallic complex dibutyltin dilaurate (CAS number [77-58-7], purity of 95 %, Aldrich, Dangerous Substances Directive: T) has been used. Secondly, the amino compound DABCO TMR® (CAS number [280-57-9], 1,4-diazabicyclo[2.2.2]octane, DABCO TMR®, Air Products, Dangerous Substances Directive: F, X_n) and, thirdly, the heterocyclic compound Pyridine (CAS number [110-86-

1], purity of at least 99 %, Aldrich, Dangerous Substances Directive F, X_n) have been employed. Dibutyltin dilaurate, DABCO TMR[®], and pyridine will be referred to as DD, DA, and P, respectively.

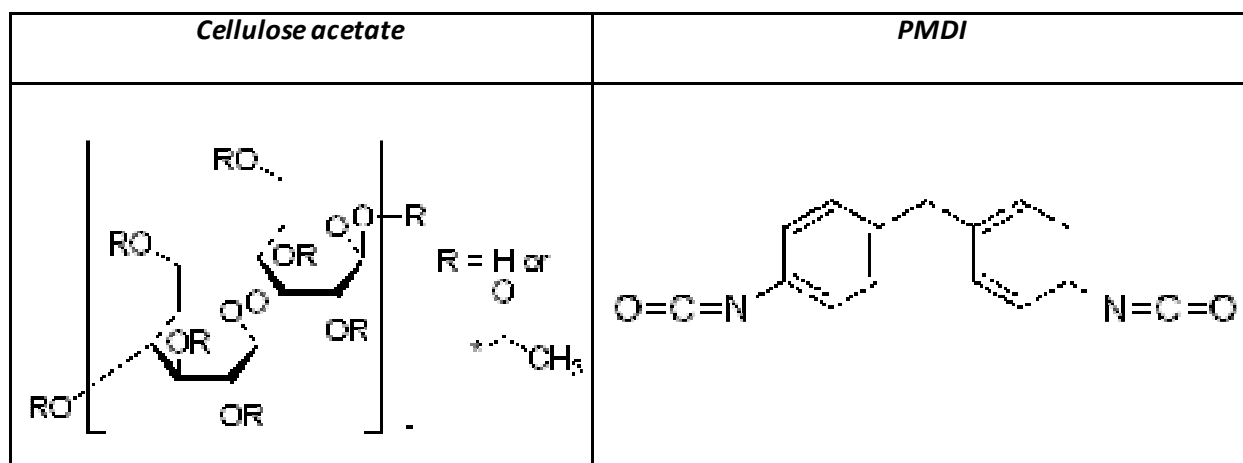


Figure II-2: Structural formula of cellulose acetate and MDI [Sig 2010]

For the sol-gel synthesis, cellulose acetate has first been dried 24 h at 100 °C to ensure that all water potentially adsorbed beforehand has been eliminated in order to avoid isocyanate/water reactions (refer to section 2.4 on catalyst mechanisms). Cellulose acetate has then been introduced into acetone at room temperature under mechanical stirring for 24 h to obtain a translucent homogeneous polymer solution (*i.e.* a colloidal dispersion of cellulose acetate in acetone). Catalyst and isocyanate precursor have also each been dissolved separately in acetone under mechanical stirring for 10 minutes. First the catalyst solution has been added to the cellulose acetate solution and stirred for 10 min, before the isocyanate-solution has been added. The solution resulting from mixing solvent, both precursors, and catalyst is called the sol. The sol has been stirred mechanically for a duration adjusted to the catalyst type and quantity used (*i.e.* gels gelling at 30 min or more have been stirred for 30 minutes, for gels gelling in less than 30 minutes, the agitator has been removed shortly before gelation). Gels have been left to age for 7 days at room temperature in closed recipients in order to avoid evaporation of the solvent.

The cellulose acetate concentration **%CA** used has been equal either to 3, 5, 10, or 15. The cross-linking ratio **I/CA** has been chosen to be equal to 0.1, 0.2, or 1. Different quantities of each of the three catalysts **I/Cat** have been investigated. Stoichiometry between the functional groups of the two precursors is reached at an **I/CA** of around 0.3. An **I/CA** of less than 0.3 indicates substoichiometric concentration of the isocyanate functionalities; an **I/CA** of more than 0.3 indicates a hyperstoichiometric concentration of MDI in view of urethane reactions [Fis 2006].

Sample Nomenclature: The nomenclature of our samples consists of four obligatory parts (see figure II-3): three numbers (in the form of x-y-z) and one or two majuscule letters: x indicates the degree of cellulose acetate concentration **% CA**, y stands for the cross-linking ratio **I/CA**, z indicates the catalyst concentration in grams per litre of solvent. The majuscule letter(s) denominate the type of catalyst employed: DD stands for dibutyltin dilaurate, DA for DABCO TMR[®], P for pyridine.

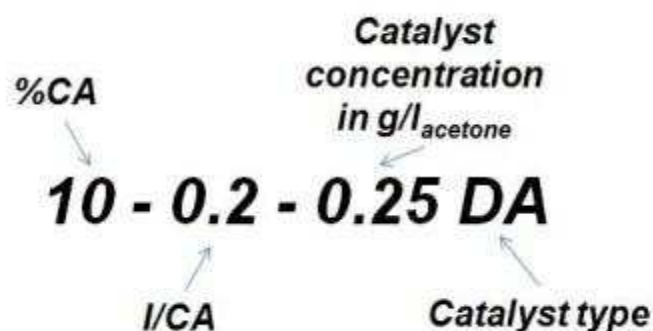


Figure II-3: Nomenclature of CAB gels on the example of a sample with 10 %CA, I/CA=0.2, and 0.25 g/l_{acetone} of DABCO TMR® catalyst

2.2 Supercritical Drying

Indirect supercritical drying in CO₂ has been determined as the standard drying process for this study. Supercritical drying of the acetate cellulose based gels has been performed according to the protocol established by Y. Masmoudi et al. [Mas 2006]. The drying procedure has been carried out in a 1-litre autoclave. After ageing for 7 days, the gels are impregnated in acetone and are first washed dynamically by a flow of supercritical carbon dioxide (5 kg_{CO2}/h) at 8.5 MPa and 40 °C for 2 h. They have then been left to dwell in the same static conditions for 2 h (solvent exchange governed by molecular diffusion), before again being washed dynamically for another 2 h. Subsequent to the recovery of the whole interstitial liquid phase, CO₂ has been vented out isothermally (0.01 MPa/min, 40 °C), thus preventing any tensile stress due to the occurrence of CO₂ condensation phenomena [Sch 1994, Woi 1994].

2.3 Analysis Methods

Below, analysis instruments, methods and models used for effecting analyses on this chapter's materials are given.

2.3.1. Micrography

The structure has been observed by scanning electron microscopy (SEM) with a FEI XL 30 ESEM (S. Jacomet/CEMEF/MINES ParisTech) and by field emission gun (FEG) SEM with a MEB CARL ZEISS/ULTRA 55 (F. Charlot/CMTC/INPG). Samples have not been treated (*i.e.* metallized) prior to micrography.

2.3.2. Analysis of porous Characteristics

Porous properties of cellulose-acetate based aerogels have been obtained by nitrogen sorption, mercury (Hg) porosimetry and pycnometry, and helium (He) pycnometry. Nitrogen (N₂) sorption isotherms have been measured at -196 °C with a BellSorb Mini II after outgassing at 10⁻³ Pa for 24 h at ambient temperature (by B. Simon/SAFT Batteries). Hg porosimetry and pycnometry have been carried out on a Micromeritics AutoSorb IV for a pressure range of 0.1 to 200 MPa (by B. Simon/SAFT Batteries). He pycnometry, has been carried out on a Micromeritics Accupyc 1330 pycnometer (by N. Job/Laboratoire de Génie Chimique/ULg).

Following parameters have been analyzed in the course of this work to depict the aerogels' structure:

- apparent or bulk density ρ_b (from Hg pycnometry)
- skeletal density ρ_s (from He pycnometry),
- specific porous volume V_{SP} ,
- porosity ϵ ,
- specific porous volumes V_{Hg} and V_{BJH} (according to the model by Barret, Joyner, and Halenda) as determined by Hg pycnometry and N_2 sorption respectively,
- the fraction of porous volume characterized by Hg pycnometry $\%V_{Hg}$ and by N_2 adsorption $\%V_{BJH}$,
- specific surface area s_{BET} according to the model by Brunauer, Emmett and Teller (from N_2 sorption),
- mean pore size estimated by Hg porosimetry L_{Hg} and by N_2 adsorption L_{BJH} (according to the model by Barret, Joyner, and Halenda),

Because CAB organic aerogels undergo compression during Hg porosimetry, **PSD** based on mercury porosimetry have been determined according to the buckling theory [Pir 2000] with a buckling constant of $28 \text{ nm}\cdot\text{MPa}^{0.25}$ (buckling constant having been determined for polyurethane-based aerogels by R. Pirard et al. [Pir 2003] and having been confirmed as viable mean value by F. Fischer for CAB aerogels [Fis 2006]).

2.3.2.1. Density, Porous Volume and Porosity

Apparent density or bulk density ρ_b refers to the density of a material including the pores [Rou 1994]. The bulk density can either be estimated for samples of regular geometric shapes, or more precisely be derived from Hg pycnometry measurements, as has been done in this work.

The *specific porous volume of an aerogel characterized by Hg pycnometry* V_{Hg} (in cm^3/g) is therefore:

$$V_{Hg} = 1/\rho_b \quad \text{Equation II-5}$$

The *skeletal density* ρ_s , which is the density of the solid network of the porous material only (*i.e.* without the pores), is generally determined by helium pycnometry.

The *specific porous volume* V_{SP} (in cm^3/g) refers to the difference between specific porous volume V_{Hg} and skeletal specific volume (*i.e.* the reciprocal value of the skeletal density):

$$V_{SP} = 1/\rho_b - 1/\rho_s \quad \text{Equation II-6}$$

The *porosity* ϵ , finally, is the ratio of the volume of the pores of a material to the total volume of the material including pores.

$$\epsilon = 1 - \rho_b/\rho_s \quad \text{Equation II-7}$$

2.3.2.2. *Specific Surface Area*

The *specific surface area* s designates a material's total surface per unit of bulk volume. The specific surface area can be estimated on the basis of the N_2 volume adsorbed on the material's surface [Sin 1982] at an isotherm temperature of 77 K as a function of the relative N_2 pressure (P/P_0). In this work, the classical model to determine the specific surface area s_{BET} from the nitrogen volume adsorbed on the material's surface developed by Brunauer, Emmett and Teller [Bru 1938] has been used.

2.3.2.3. *Pore Size Distribution and Mean Pore Size*

Pores are generally classified in three categories according to their size, *i.e.* diameter, as defined by the IUPAC [IUP 1997]:

- Macropores: pores with width exceeding 50 nm
- Mesopores: pores with width between 2 and 50 nm
- Micropores: pores with width not exceeding 2 nm

The *pore size distribution PSD* gives information, in particular, on the mean pore size and the homogeneity of the pore sizes.

Classically, a porous material's **PSD** can be determined either by Hg porosimetry or by N_2 adsorption and desorption, by relating the porous volume measured to a mean pore diameter under certain assumptions. In this work, both methods have been used, as neither one of these two different techniques allows to evaluate the total porous volume, and thus correct **PSD**, of materials displaying large ranges of pore size (from micro- to macropores). Nevertheless, Hg porosimetry and N_2 adsorption may complement each other as their operation ranges partly overlap. Mercury porosimetry is generally used to obtain porosity information of meso- to macroporous materials, whereas physical adsorption techniques can evaluate pore volumes of micro- and mesoporous materials not attainable by mercury porosimetry [Rig 1998].

Determination of PSD by Mercury Porosimetry

Mercury porosimetry can not only be used to determine the total pore volume of a porous material, its surface area, bulk and absolute densities, but also to calculate the **PSD**. As mercury is a non-reactive, non-wetting liquid, pressure has to be applied for the mercury to enter the pores of a material. The porous sample is immersed in mercury, after evacuating the gas from the sample. Isostatic pressure is then applied to force the mercury into the pores. The smaller the pores, the higher the pressure has to be for the non-wetting mercury to penetrate them. The Washburn equation [Was 1921, Bra 1981] links mercury intrusion pressure to the corresponding pore size:

$$P_{Hg} = - \frac{2\gamma \cos\theta}{r_p}$$

Equation II-8

P_{Hg} : mercury pressure (MPa)

γ : surface tension of mercury (0,485 N·m⁻¹)

θ : contact angle between mercury meniscus and pore surface (rad)

r_p : pore radius (m)

Determination of **PSD** using the Washburn equation relies on the presumption that mercury is non-reactive and non-wetting, but also that the porous solid network is stable and inelastic. Aerogels, however, are often subject to a volumetric contraction [Duf 1996], rather than being penetrated by the mercury. **PSD** for aerogels undergoing irreversible volume shrinkage during analysis can thus generally not be determined *via* the Washburn equation. A method to calculate the **PSD** from Hg porosity for aerogels which collapse due to the application of pressure (*i.e.* decreasing pore sizes are eliminated completely and consecutively at increasing mercury pressure) has been developed by R. Pirard [Pir 2000]. Pirard's buckling theory directly links pore size L_{Hg} to the pressure, using a constant k_f to be experimentally identified for each material type:

$$L_{Hg} = \frac{k_f}{P^{1/4}}$$

Equation II-9

L_{Hg} : pore diameter (nm)

P : mercury pressure (MPa)

k_f : experimentally determined buckling strength constant (nm·MPa^{1/4})

In theory, pores of sizes between 3 nm and 400 μm can be detected by measuring devices applying pressure in the range of 0.003-414 MPa, according to equation II-8. However, minimum pore sizes taken into account for measurements of up to 200 MPa (*e.g.* carried out on the samples featured in this work) are rather as large as 7.5 nm. Also, if equation II-9 is used to estimate the **PSD**, that is if the material undergoes compression during Hg porosimetry, maximum pore sizes taken into account are of 85 nm (for pressures of 0.01 MPa carried out in this work). Accordingly, mercury porosimetry is completely inadequate in order to detect microporous volumes. Even small mesopores are not detected well by mercury porosimetry. High pressures, being exerted to force mercury to penetrate smaller mesopores (especially below 20 nm) [Pol 2002], risk the compression of the sample. Therefore, mercury porosimetry rarely takes into consideration the totality of the porous volume of aerogels. The determination of **PSD** through Hg porosimetry is thus, in general, considered more suitable for pore sizes above 30 nm [Pol 2002]. Another drawback of the determination of **PSD** through Hg porosimetry is that the volume of the smallest pores measured is overestimated if a part of the pores is ink-bottle shaped, *i.e.* characterized by small openings.

Determination of PSD by Nitrogen Adsorption

A porous material's **PSD** can also be determined *via* N₂ adsorption, *i.e.* a gas adsorption technique. The gas adsorption techniques are based on physisorption of the gas on the pore walls. In a typical sorption measurement, the uptake (or release in the case of desorption) of the gas is measured as a function of the gas pressure applied. Gas adsorption is generally carried out at a constant cryogenic

temperature, 77 K for nitrogen adsorption: $V_{\text{gas}}=f(p)_{T=\text{const}}$. The **PSD** can thus be calculated *via* methods based on the law of Kelvin [Gre 1982], linking relative gas pressure to pore radius. The porous volume and the **PSD** of mesoporous materials is most commonly estimated by the BJH method, developed by Barret, Joyner, and Halenda in 1951 [Bar 1951, Pol 2002] based on the law of Kelvin.

Micropore diameters, however, inferior to 2 nm, are often of the same dimension as nitrogen molecules. In this case, the law of Kelvin based on multi-layer filling cannot be applied. Therefore, methods based on the Kelvin equation, like the BJH method, are inadequate for microporous material. Microporous volumes and the **PSD** of microporous material can be estimated using other types of models, like the model proposed by Dubinin and Radushkevich [Dub 1960] based on the micropore volume filling theory. Another method often used to determine microporous volume and **PSD** for completely microporous materials is the t-plot method. The t-plot method compares the amount of nitrogen adsorbed on the sample to be studied to an ideally nonporous reference solid with similar surface characteristics [Boe 1966].

Despite the possibility of accessing micro- and mesoporous volumes, porous measurements by N₂ are not precise for pores bigger than 50 nm [Job 2006]. Any existent macroporous volume is thus left out in the evaluation of porous volumes and **PSD**. Further, it has been observed that the total adsorbed nitrogen volume by aerogels is oftentimes considerably inferior to porous volumes calculated from bulk densities or skeletal densities. The explication of this phenomenon probably lies in the aerogels' elasticity. Scherer, Smith, and Stein suggest that the aerogels contract themselves as a reaction to capillary condensation of nitrogen within the pores [ScS 1995]. This contraction results in an underestimation of the total porous volume and may thus also significantly falsify the **PSD** estimated for aerogels.

2.3.2.4. Specific Porous and Microporous Volume

The specific porous volume has been determined by Hg porosimetry as well as by N₂ adsorption.

The total volume V_{Hg} obtained by Hg porosimetry for CAB OA in this work, corresponds to the total volume of pores between 7,5 nm and 85 nm. Because only relatively large mesopores and small macropores are taken into account in this case, it can be interesting to calculate the proportion of the overall porous volume having been characterized by mercury porosimetry. This *proportion* $\%V_{\text{Hg}}$, being the ratio between V_{Hg} (in cm³/g) and specific porous volume V_{sp} (in cm³/g), may be calculated as follows:

$$\%V_{\text{Hg}}=100 \cdot \frac{V_{\text{Hg}}}{V_{\text{SP}}} \quad \text{Equation II-10.}$$

Specific porous volumes determined by nitrogen adsorption are limited to the porous volumes of all big micro-, meso-, and small macropores (< 50 nm), neglecting any contribution to the porous volume from macropores. The proportion of the overall porous volume having been characterized by nitrogen adsorption $\%V_{\text{BJH}}$ can be calculated similar to $\%V_{\text{Hg}}$. The *proportion* $\%V_{\text{BJH}}$, being the ratio between V_{BJH} (in cm³/g) and specific porous volume V_{sp} (in cm³/g), may be calculated according to:

$$\%V_{BJH} = 100 \cdot \frac{V_{BJH}}{V_{SP}} \quad \text{Equation II-11.}$$

By comparing %V_{Hg} and %V_{BJH} a quite representative overview of the aerogels' porous network may be obtained.

2.3.3. Elemental Analysis

Elemental analysis has been carried out at the Central Analysis Service of the CNRS (Vernaison, France). Prior to the analysis, all the samples have been dried for 1 h in air at 130 °C. Carbon, hydrogen, and nitrogen are detected by a total combustion of the sample at 1050 °C in an oxygen/helium atmosphere. Oxygen is detected by total pyrolysis of the sample at 1080 °C in nitrogen atmosphere. The combustion products are quantified by catharometry or infrared sensors (nitrogen oxides after reduction to molecular nitrogen and carbon after transformation into carbon monoxide). For perfectly homogeneous samples, the error of elemental analysis is given to be inferior to 0.3% (for contents superior to 10%).

2.4. Influence of Catalyst Mechanisms

The use of a catalyst affects a reaction's kinetics. Kinetics, *i.e.* the reaction rate, depends on various parameters (*e.g.* nature, physical state, and concentration of the reactants) including the presence of a catalyst. A catalyst accelerates the reaction rate by providing an alternative reaction mechanism requiring a lower activation energy. In theory, catalysts participate in the series of reactions forming the final product, but emerge unaltered.² Otherwise, reactions involving a catalyst behave like any other typical chemical reaction. Their reaction rate is, therefore, also subject to the precursors' concentration. In conclusion, how much kinetics are accelerated by using a catalyst depends on (i) the catalysts' concentration, (ii) the reaction mechanism provided by the catalyst and (iii) the degree of the catalyst's catalytic characteristic (the more pronounced the catalysts catalytic characteristic, the more efficient the reaction mechanism, the higher the reaction rate). The efficiency of a catalyst in general depends thus on the type of reaction mechanism it proposes and the degree of its' catalytic characteristic, but also on the selectivity of the catalyst for the targeted reaction.

In this work on CAB aerogels, the reaction we intend to accelerate by catalysis is the formation of urethane bonds between cellulose acetate chains (see Figure II-1). Urethane bonds form between the functional groups of cellulose acetate, hydroxyl groups –OH, and the functional groups of the polyisocyanate (with isocyanate groups –N=C=O), carbonyl groups =C=O. Urethane formation takes place as the carbonyl's electrophilic carbon reacts with the nucleophilic oxygen of the nucleophilic reactant alcohol [Thi 1993]. The greater either the electrophilicity or the nucleophilicity of the two reacting centres, the higher is the "carbonyl reaction's" rate. Consequently, urethane bonding (*i.e.* the reaction between the carbonyl's carbon and the alcohol's oxygen) can be accelerated – or catalyzed – by a chemical agent increasing either the nucleophilic properties of nucleophilic reactants or the electrophilic properties of electrophilic reactants. Lewis acids and bases are such chemical agents. Lewis bases increase the nucleophilic properties of nucleophilic reactants, *i.e.* they raise the

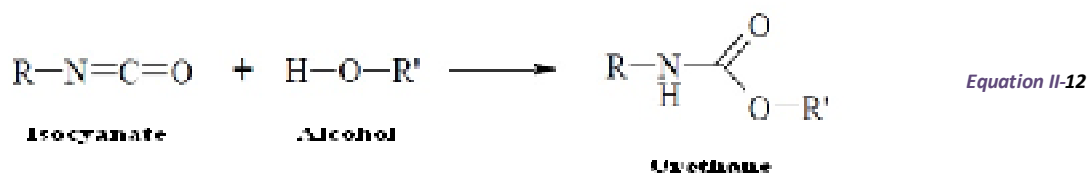
² In reality, catalysts sometimes become inactive in the course of the reaction due to substrate binding or product dissociation.

partial negative charge of the alcohol oxygen. Lewis acids, on the contrary, raise the electrophilic properties of the carbonyl carbon, *i.e.* raise its partial positive charge [Thi 1993].

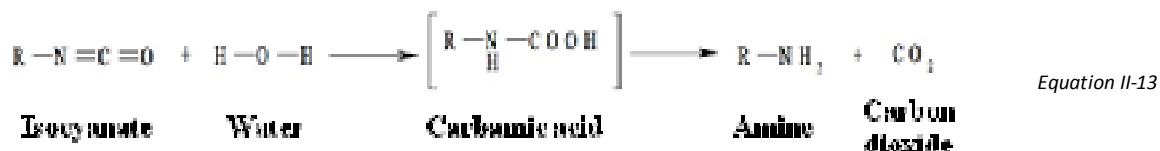
Lewis bases and acids are both commonly used to catalyze urethane formation [Thi 1993, Hou 1996]. Catalysts conventionally used in the commercial synthesis of urethane polymers are generally either (i) organometallic compounds, *e.g.* tin compounds, acting as Lewis acids, or (ii) tertiary amines, acting as Lewis bases. Common examples are the organotin compound dibutyltin dilaurate for (i) and the tertiary amine DABCO TMR[®] for (ii) [Weg 2001, Sil 2004, Bla 1999, Thi 1993].

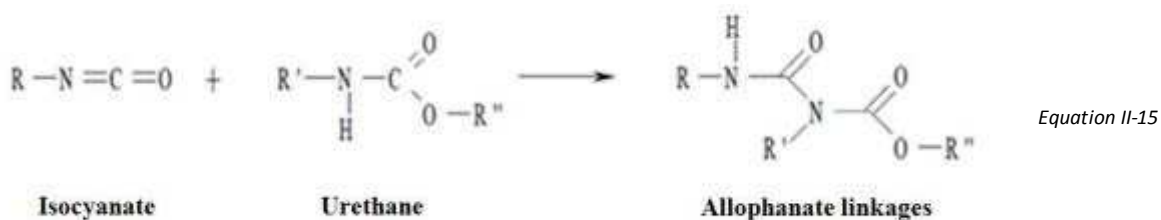
The importance of the choice of catalyst is well recognized in commercial polyurethane production. For the choice of catalyst the catalyst's selectivity towards possible isocyanate reactions [Sil 2004, Bla 1999] is even more important than reaction kinetics.

Possible isocyanate reactions include reactions of the electrophilic carbonyl carbon with labile hydrogen containing compounds, such as alcohol, but also such as water or amines. Typically selectivity toward the isocyanate/hydroxyl reaction forming urethane bonds is preferred [Sil 2004, Weg 2001]:&é



Reactions with water and also with amines result in gassing and blister formation in the gel due to the formation of CO₂ (equations II-13 and II-14). Isocyanate groups also react with urethane and urea, resulting in an increased cross-linking of the structure (equations II-15 and II-16). Lastly, isocyanate compounds may react between themselves, for example forming dimers, trimers, carbodiimides and uretmines [Sil 2004, Weg 2001]. Evidently, the choice of catalyst, due to each catalyst's special selectivity towards isocyanate reactions, partly determines the properties of the resulting polymer.





In conclusion, the choice of catalyst determines:

- (i) the reaction mechanism: as a result of Lewis acids and Lewis bases proposing different reaction mechanisms
- (ii) the reaction rate due to an enhancement of the functional groups' electro- or nucleophilicity
- (iii) the resulting polymer's properties *via* the catalytic selectivity toward certain isocyanate reactions.

In this study we have experimentally compared the influence of three different catalysts on the sol-gel process and resulting organic aerogels (see also figure II-4), namely:

- dibutyltin dilaurate (DD)
- DABCO TMR® (DA)
- Pyridine (P).

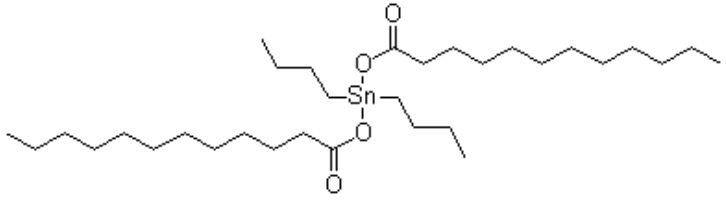
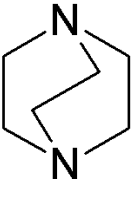
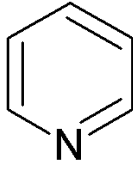
<i>Dibutyltin dilaurate</i>	<i>DABCO TMR®</i>	<i>Pyridine</i>
$\text{C}_{32}\text{H}_{64}\text{O}_4\text{Sn}$	$\text{C}_6\text{H}_{12}\text{N}_2$	$\text{C}_5\text{H}_5\text{N}$
		

Figure II-4: Chemical and structural formulas: Dibutyltin dilaurate, DABCO TMR®, and Pyridine

For a better understanding of the differences we have observed (see section 3. Results and Discussion), the three catalysts' particularities and reaction mechanisms are briefly presented below.

- *Dibutyltin dilaurate* is an organometallic compound, more specifically a(n) (di)organotin(IV)ester) compound [Sil 2004, Weg 2001, Hou 1996, Sub 2000] (see also figure II-4). Organometallic catalysts act as Lewis acids. They feature a good selectivity towards the isocyanate/hydroxyl reaction and are more effective in the isocyanate/alcohol reaction of aliphatic isocyanates than amines. These characteristics result in a strong gelation activity in the urethane forming reaction, which is particularly pronounced for diorganotin (IV) compounds such as DD. For this reason, organometallic catalysts are often referred to as “gel catalysts”. In spite of their selectivity towards the “carbonyl reaction”, organometallic catalysts also catalyze isocyanate/water reactions. Consequently, humid working conditions as well as water content in precursors has to be minimized. Additionally, many organometallic catalysts are highly (aquatic) toxic or at least harmful [Bla 1999].

The reaction mechanism proposed by Lewis-acid catalysts in general and DD (as diorganotin-IV-ester compound) in particular proceeds *via* the activation of the isocyanate by the Lewis-acid catalyst. The reaction proceeds as follows [Hou 1996]: The starting tin compound (a type of diorganotin-IV-ester, here simplified Bu_2SnX_2) is alcoholized (see Figure II-5) at contact with the polyol, *i.e.* cellulose acetate (here simplified ROH), resulting in a so-called tin alkoxide ($\text{X-Bu}_2\text{Sn-OR}$).

- A complex between the tin alkoxide and the isocyanate (here simplified Y-N=C=O) forms, in which the alkoxide anion is transferred onto the isocyanate (see Figure II-6).
- The catalyst/isocyanate complex undergoes alcoholysis to give the urethane and the original tin alkoxide.

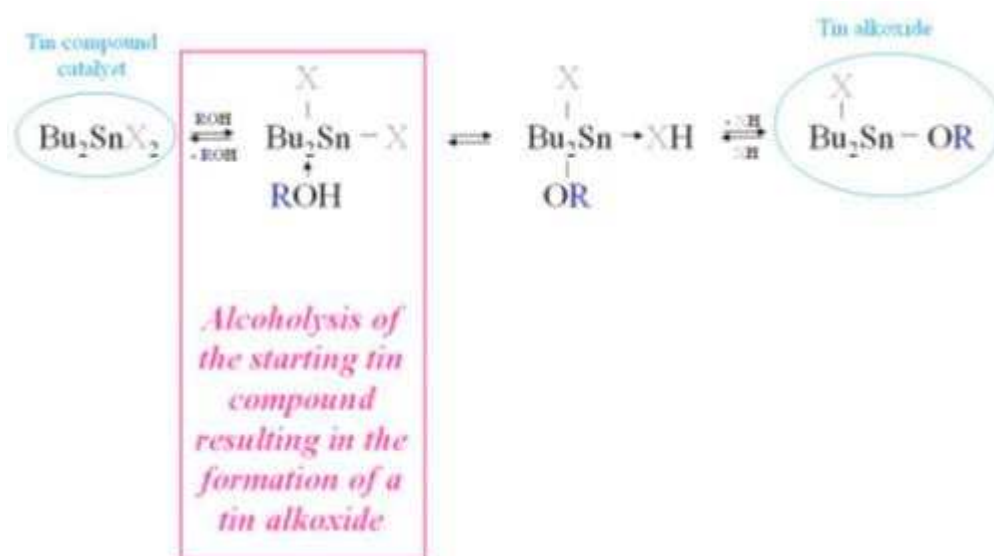


Figure II-5: Alcoholysis of tin-based catalyst for urethane formation (based on [Hou 1996])

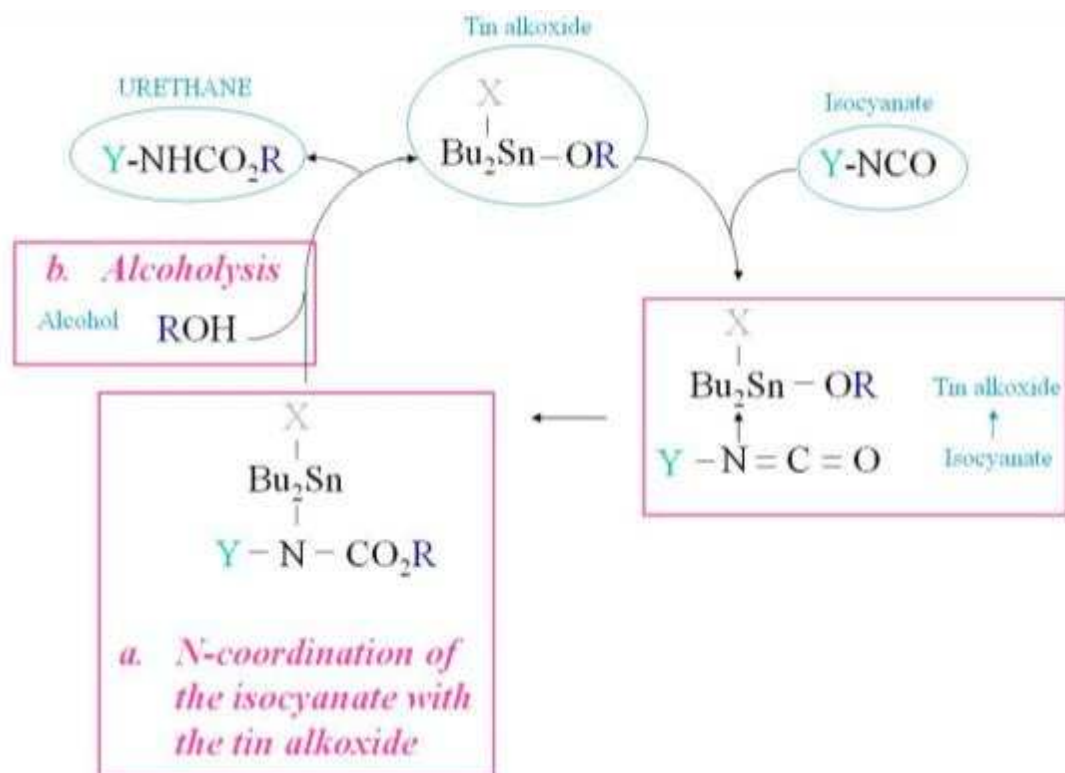


Figure II-6: Schematic representation of the catalysis of urethane bonds by a tin alkoxide (based on [Hou 1996])

- **DABCO TMR®** is a tertiary amine (see also figure II-4) acting as Lewis base catalyst. Tertiary amines are commonly used to catalyze the reaction of aromatic isocyanates with hydroxyl groups (for which it is better suited than organometallic salts). Nevertheless, tertiary amines are not selective and catalyze all reactions between isocyanates and active hydrogen compounds (including the reaction with hydroxyl groups, but also water, amines, and isocyanate trimerization reactions). The reaction of isocyanate with water produces gaseous carbon dioxide, which is why tertiary amine catalysts are often referred to as “blowing catalysts”.

The reaction mechanism proposed by the Lewis-base catalyst DA is still a matter of discussion. I shall present here the most widely accepted reaction [Kra 2000, Sil 2004, Thi 1993]. However, Schwetlick, Noack, and Stebner [ScN 1994], for example, have proposed distinct mechanisms depending on the electrophilicity of the isocyanate, the acidity and nucleophilicity of the hydrogen active compound and the basicity of the catalyst. The catalysis of urethane formation using DA is based on the activation of the alcohol and proceeds as follows:

- The nucleophilic tertiary amine DA undergoes hydrogen bonding with the positively charged hydrogen atom of an alcohol's (*i.e.* cellulose acetate) hydroxyl group (see Figure II-7). This formation of a catalyst/alcohol associate results in a charge transfer. The complex's polarity increases due to a transfer of the positive charge to the catalyst's nitrogen. The alcohol's oxygen atom becomes more nucleophilic and thus more reactive.

- b) The catalyst/alcohol associate reacts with the isocyanate. The hydroxyl's negatively charged electron reacts with the electrophilic carbonyl carbon. The hydroxyl's oxygen becomes positively charged, the isocyanate's nitrogen negatively.
- c) A urethane/catalyst complex is formed.
- d) The charges in the complex are compensated by a proton transfer from the hydroxyl's hydrogen to the isocyanate nitrogen. The hydrogen bond with the catalyst is annihilated and a urethane bonding is formed.

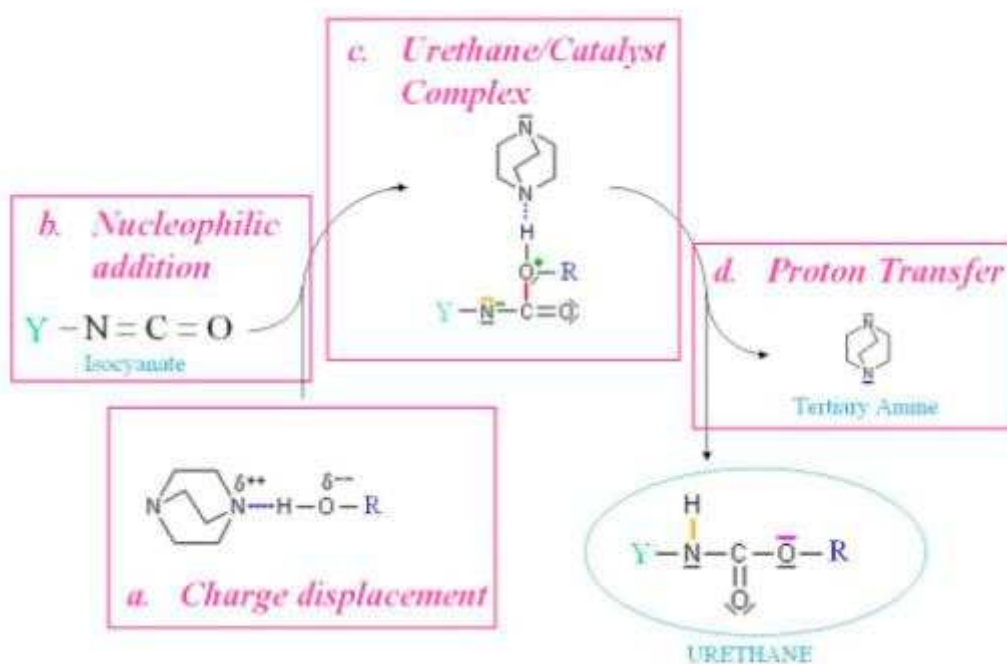


Figure II-7: Catalysis of urethane bonds through tertiary amine ([based on [Sil 2004])

- *Pyridine* is an aromatic heterocyclic organic compound (see also figure II-4). An important solvent and reagent in organic synthesis, P is much less known as catalyst. Nonetheless, its use as catalyst in urethane formation has been recognized by R. Mosher [Mos 1963], whose object it was to have a polyurethane reaction of slow setting. Pyridine is a harmful chemical product.

As P is not a commercially applied catalyst of polyurethane reactions, sources on the reaction mechanism it triggers in polyurethane formation are not readily available. Still, in organic reactions, P may behave as tertiary amine undergoing amongst others protonation. In general, P is basic and its chemical properties are similar to those of tertiary amines. Therefore, it can be assumed that the reaction mechanism proposed by P resembles the reaction mechanism introduced by DA, although its' catalytic characteristic seems to be much less pronounced.

3. Results

3.1. Influence of Sol-Gel Parameters on Gelation Time and Shrinkage

3.1.1. Introduction to Sol-Gel Characteristics

3.1.1.1. Gelation Time

Gelation is the term commonly used to describe the process which leads to the formation of a gel. If a gel is formed by intermolecular reactions, which is the case for chemical gels (refer to chapter I.4), the gel point can be defined according to Kavanagh and Ross-Murphy [Kav 1998] as the moment at which all initial monomers and/or polymers are cross-linked to form one macromolecule. In this case, the sample does not flow anymore in contrast to the initial polymer sol. Gelation time, therefore, is the time taken to achieve the gel point conversion. Gelation time can be determined by rheological characterization methods such as oscillatory strain experiments [Kav 1998]. Nevertheless, determination of the gel point remains difficult and the methods controversial. For CAB aerogels, the nature of the solvent (and reaction media) acetone remains a major problem in the determination of the gelation time. Acetone, quite volatile, might evaporate during the rheological analysis being carried out in air and thus falsify analysis results or even render the analysis impracticable.

Therefore, in this work, gelation time t_g has been defined as the time span between the moment the two reactive sol-gel precursors (here cellulose acetate and MDI) are put into contact and the moment no flowing can be observed anymore. The moment at which the sol stops flowing has been determined by agitating and turning over the sol's container. Evidently, this method of measuring gelation time is only an estimative method and not a precise measurement. The estimation of gelation time through observation has been used for all samples and can consequently be considered useful for comparison between different gels. We have checked that results obtained according to this method have been reproducible within an acceptable error range ($t_g \pm 10\%$).

3.1.1.2. Shrinkage due to Syneresis

Syneresis is the continuation of reactions between the precursors after the sol-gel transition. During syneresis, the gel undergoes irreversible volumetric shrinkage due to the creation of an increasing number of bonds. As these additional urethane bonds take up space previously occupied by the solvent and contribute to a contraction of the gel, resulting in the expulsion of a part of the liquid network, which in this case is acetone, from the gel. In this work, syneresis has been quantified by measuring the volume of acetone ejected by the gel after one week of ageing at ambient temperature. We have verified that no perceptible syneresis occurred anymore after the aging period of 7 days. The gel volume V_{gel} corresponds to the difference between the sol's initial volume and the volume of acetone ejected during syneresis:

$$V_{gel} = V_{sol} - V_{expulsed\ liquid} \quad \text{Equation II-17}$$

Knowing the gel volume after syneresis we have been able to calculate the shrinkage ratio due to syneresis (Equation II-18). The shrinkage ratio due to syneresis τ_{syn} characterizes the volumetric

variation occurring after sol-gel transition. Variations in syneresis due to the variation of sol-gel parameters can be compared using τ_{syn} :

$$\tau_{syn} = \frac{V_{sol} - V_{gel}}{V_{sol}} \quad \text{Equation II-18}$$

3.1.2. Influence of Sol-Gel Synthesis Parameters on Gelation Time and Shrinkage

The influence of different sol-gel parameters (**%CA**, **I/CA**, **I/Cat**, and catalyst type) on the gelation process has been examined (see tables II-1 and II-2). Note that isocyanate concentration is related to the cellulose quantity by **I/CA**. Thus, at constant **I/CA**, the isocyanate precursor quantity increases with the quantity of cellulose acetate introduced into the solvent, whereas the catalyst quantity used does not depend on the cellulose precursor concentration. Therefore, **I/Cat** changes with **%CA** (is not maintained constant), unless stated otherwise.

Through the systematic variation of the sol-gel parameters, we have been able (i) to bear out Fischer's first experimental results on cellulose-acetate based aerogels [Fis 2006], (ii) to complete and significantly extend the range of aerogels studied, and (iii) to initiate an investigation on the influence of the isocyanate precursor/catalyst ratio **I/Cat** and the catalyst type.

3.1.2.1. Cellulose Acetate Concentration %CA

Cellulose acetate concentration has a remarkable impact on the gelation process, as can be seen in tables II-1 and II-2.

Gelation times t_g are shorter for a higher concentration of cellulose acetate if dibutyltin dilaurate and pyridine are used as catalysts (see figures II-8 and II-9). If DABCO TMR® is employed, however, the gelation process takes generally more time for higher cellulose acetate concentrations (see figure II-10). Differences in gelation time due to the use of different catalysts are discussed further below in section 3.1.2.3 on the influence of catalyst concentration and type.

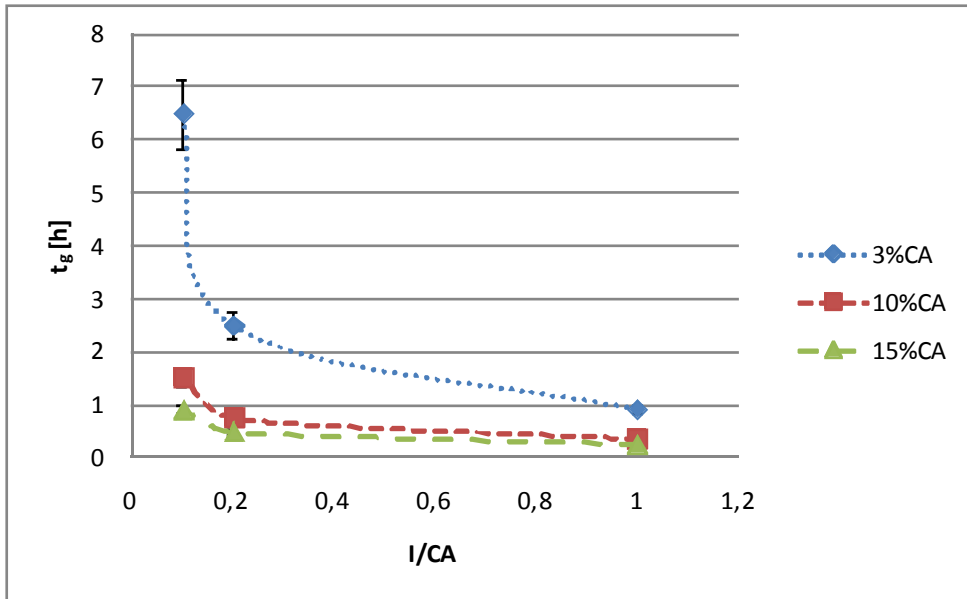


Figure II-8: Gelation times of DD-catalyzed CAB gels (DD concentration of 5 g/l_{acetone})

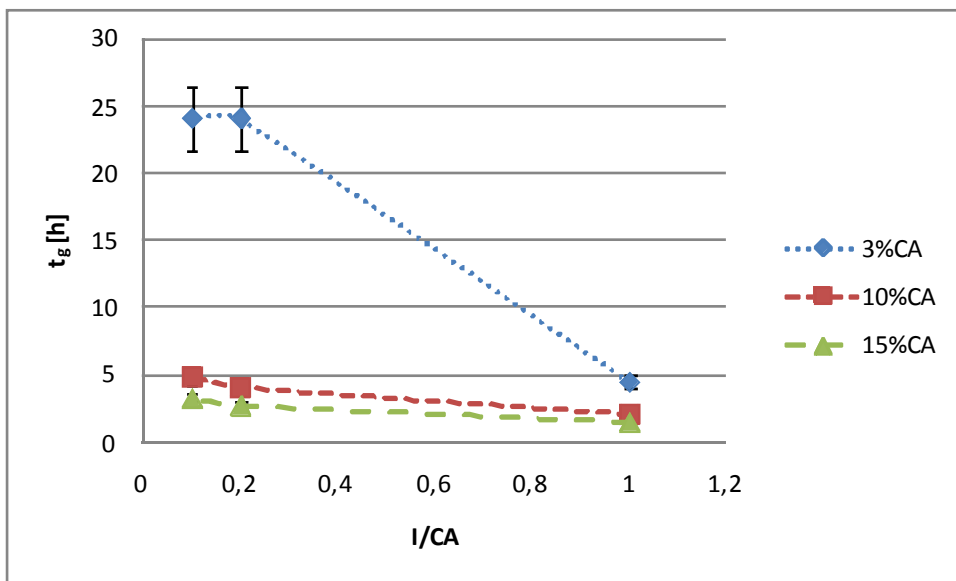


Figure II-9: Gelation times of P-catalyzed CAB gels (P concentration of 25 g/l_{acetone})

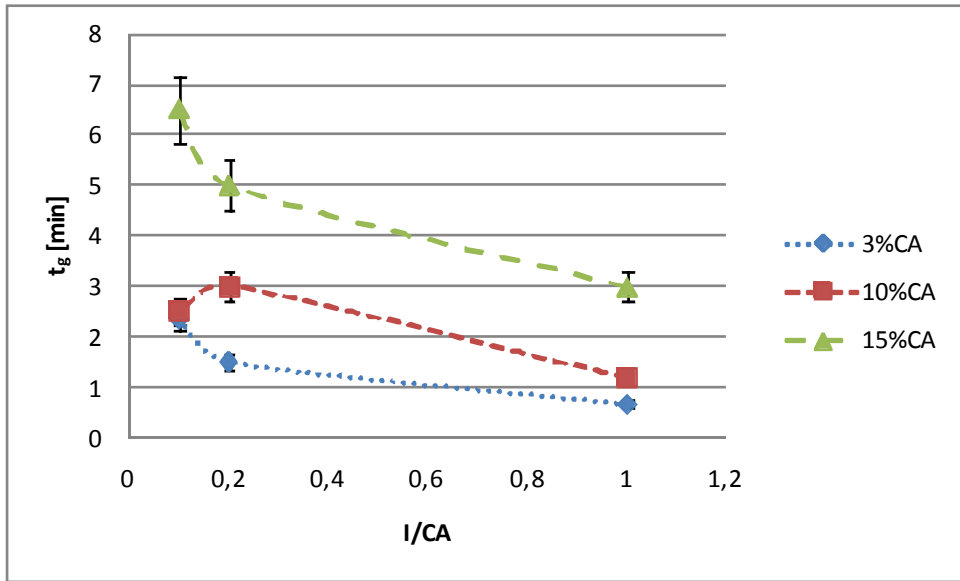


Figure II-10: Gelation times of DA-catalyzed CAB gels (DA concentration of 1 g/ l_{acetone})

Volumetric shrinkage due to syneresis τ_{syn} has a tendency to decrease with an increasing concentration of cellulose acetate for all catalysts (see figures II-11, II-12, and II-13). This tendency seems to hint at a denser solid network at high %CA, possibly more resistant to volumetric shrinkage.

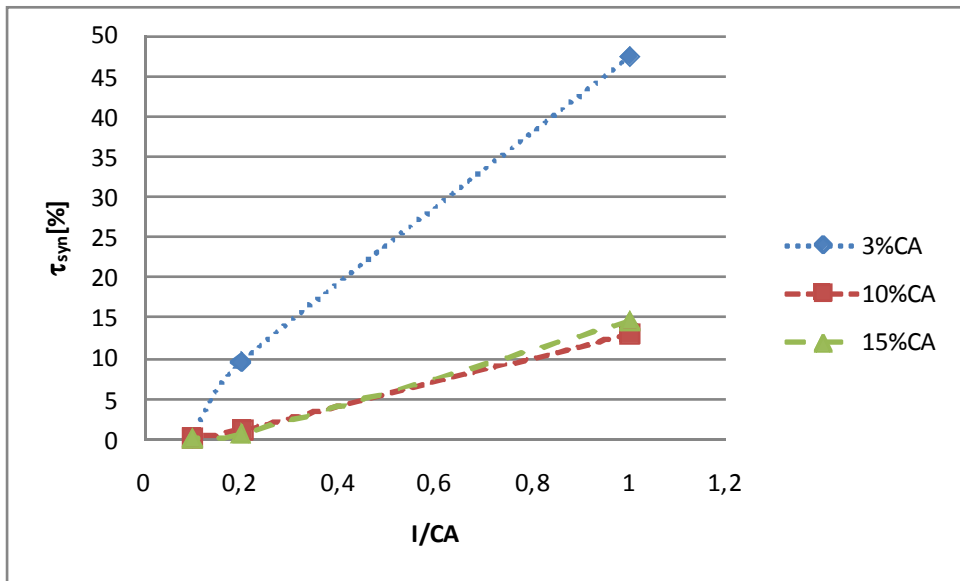


Figure II-11: Syneresis of DD-catalyzed CAB gels (DD concentration of 5 g/ l_{acetone})

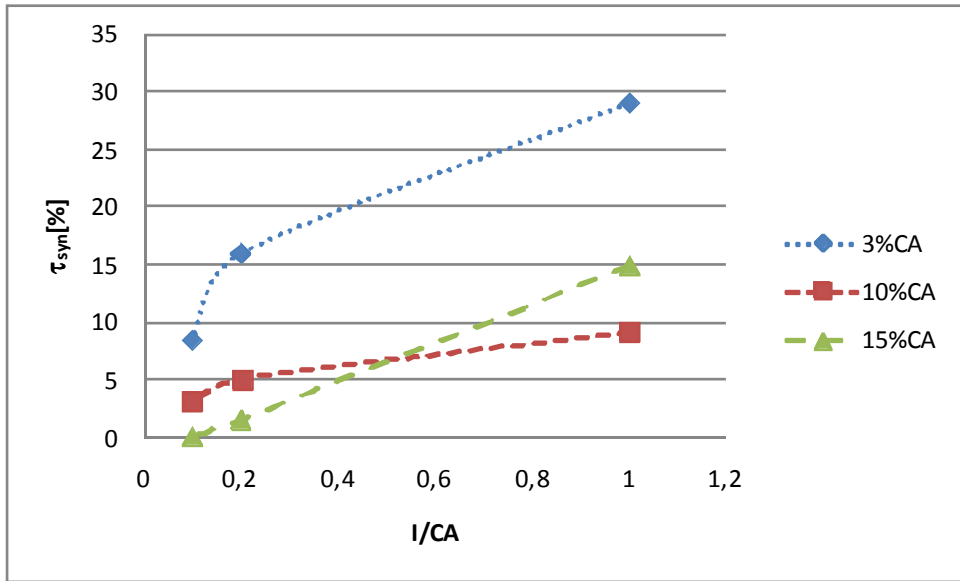


Figure II-12: Syneresis of DA-catalyzed CAB gels (DA concentration of 1 g/l_{acetone})

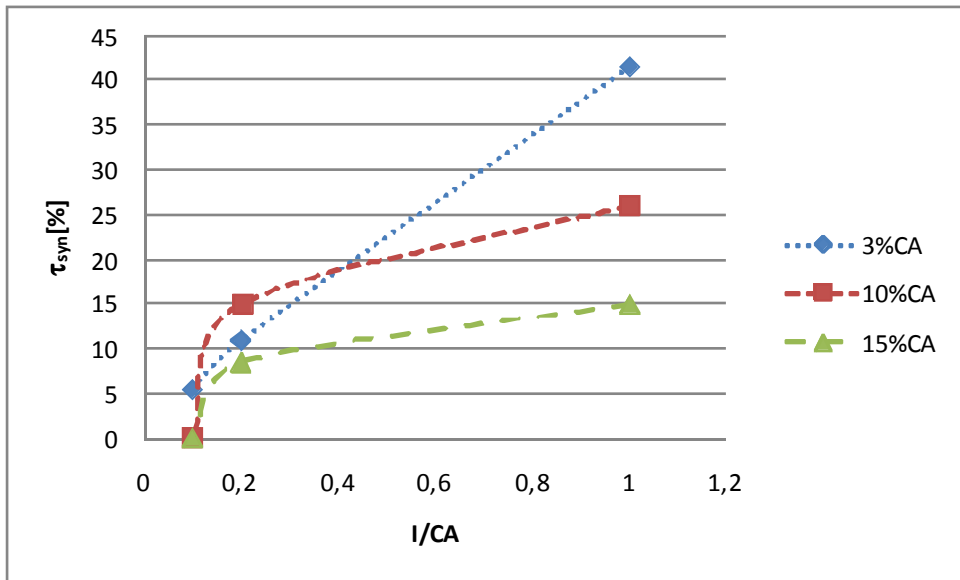


Figure II-13: Gelation times of P-catalyzed CAB gels (P concentration of 25 g/l_{acetone})

3.1.2.2. Cross-linking Ratio I/CA

Cross-linking ratio also has a notable influence on the gelation process (see tables II-1 and II-2).

Gelation times t_g are usually shorter for higher I/CA for all catalyst types (see figures II-8, II-9, and II-10).

Syneresis τ_{syn} is higher for more densely cross-linked gels, for all catalysts (see figures II-11, II-12, and II-13). For DD-catalyzed gels, Fischer has observed that volumetric shrinkage due to syneresis only took place, if the cross-linking ratio has been at least at about 50% of the stoichiometric ratio (*i.e.* $I/CA \geq 0.15$) [Fis 2006]. Regarding gels catalyzed by DD, our study seems to confirm Fischer's results. Using DD syneresis can be detected at an I/CA of 0.2 but not at 0.1. P-catalyzed gels also show syneresis rates of greater than 0% only at an I/CA of about 0.2. DA-catalyzed gels, however, may

feature volumetric shrinkage even at an I/CA of about 0.1 for low cellulose acetate concentrations %CA. At high cellulose acetate concentrations, however, syneresis cannot be detected even for gels catalyzed by 1 g DA per liter of acetone. For networks not very densely cross-linked, the use of DA as catalyst seems to promote reactions between the two precursors to an even higher extent than DD or P, resulting in a higher syneresis and volumetric shrinkage.

3.1.2.3. Catalyst Ratio I/Cat and Type

Obviously, catalyst concentration determines the reaction kinetics as illustrated by the results in table II-2.

Kinetics are evidently accelerated by higher catalyst concentrations, *i.e.* lower **I/Cat**, and gelation times t_g therefore shorter. Results for DA and P can be found in table II-2. For DD the same effect has already been demonstrated previously [Fis 2006]. Results for P and DA confirm that the catalyst is evidently involved in the step determining the reaction rate. For a constant **I/Cat** (**I/Cat** = 50 for DA and **I/Cat** = 0.15 for P, to be found in table II-2), t_g decrease slightly for DA-catalyzed gels and clearly for P-catalyzed gels with increasing %CA. Syneresis τ_{syn} seems to be more pronounced for lower catalyst concentrations. For a constant **I/Cat**, τ_{syn} decrease for P-catalyzed gels (**I/Cat** = 0.15 for P) and most likely also for DA-catalyzed gels (**I/Cat** = 50 for DA) with increasing %CA, assuming that syneresis values for 15-0.2-0.47 DA may be erroneous (see table II-2).

For results on gelation time and syneresis found in table II-1, one might be tempted to associate higher syneresis with lower gelation times. However, this does not seem to be true if gelation times together with syneresis rates are compared for gels having been synthesized using only different catalysts (table II-1). For gels synthesized with a %CA of 3 cross-linked at an I/CA of 1, for example, P-catalyzed gels feature the longest t_g (more than four times as high as those of the DD-catalyzed gel), although the DD-catalyzed gel has the highest τ_{syn} in this case. Nonetheless, DA-catalyzed gel 3-1-1DA possess shorter t_g and lower τ_{syn} than the DD- and P-catalyzed corresponding samples.

In general, gelation takes place quickest for DA, in few minutes (tables II-1 and II-2). P-catalyzed gels feature the longest gelation times out of the three catalyst types investigated in this study, of up to over 24 h (tables II-1 and II-2). DD-catalyzed gels present gelation times in the range of some dozens of minutes up to some hours for the catalyst concentrations used in this work (table II-1). This effect cannot be explained by different molecular weights alone, as the catalysts concentration in order to reach similar gelation times for different catalysts vary significantly. For example, 400 times as much P had to be used as DA (*i.e.* 100 g/l_{acetone} P instead of 0.25 g/l_{acetone} DA) in order to reach shorter gelation times for P-catalyzed gels than for DA-catalyzed gels (note that additionally, this phenomenon could only be observed for elevated cellulose acetate concentration, *i.e.* 15 %CA). While gelation times decrease with increasing %CA (at **I/Cat** not kept constant and therefore decreasing with increasing %CA) for gels catalyzed by DD and P, they increase for gels catalyzed by DA (see table II-1). A decreasing gelation time with increasing precursor concentration (while keeping **I/CA** constant) originates clearly from the fact that the number of possible collisions between reactants is increased by increasing a reactant's concentration.

In the case of DA, the lower reaction rate at high precursor concentrations is not likely to result from a diminished diffusion of the catalyst, seeing that the DD molecule is by far more cumbersome than the DA molecule (figure II-4). A different explanation to this phenomena might be the possibility of substrate binding or product dissociation and thereby a diminished reactivity. In addition, DA has been used in very small quantities in this work, so that any substrate binding or product dissociation would influence the overall catalyst reactivity considerably. An effect comparable to substrate binding is encountered while the catalytic site is saturated.

Table II-1: Gelation time and gel shrinkage due to syneresis depending on cellulose acetate concentration %CA and cross-linking ratio I/CA for a) DD-catalyzed gels, b) DA-catalyzed gels, c) P-catalyzed gels

a) DD-catalyzed gels			3-1-5DD	3-0.2-5DD	3-0.1-5DD	10-1-5DD	10-0.2-5DD	10-0.1-5DD	15-1-5DD	15-0.2-5DD	15-0.1-5DD
t_g	Approximate gelation time		0.9 hours	2.5 hours	6.5 hours	0.35 hours	0.75 hours	1.5 hours	0.25 hours	0.5 hours	0.9 hours
τ_{syn}	[%]	Syneresis	47.5	9.5	0	13	1	0	14.5	0.5	0
b) DA-catalyzed gels			3-1-1DA	3-0.2-1DA	3-0.1-1DA	10-1-1DA	10-0.2-1DA	10-0.1-1DA	15-1-1DA	15-0.2-1DA	15-0.1-1DA
t_g	Approximate gelation time		0.65 minutes	1.5 minutes	2.35 minutes	1.15 minutes	3 minutes	2.5 minutes	3 minutes	5 minutes	6.5 minutes
τ_{syn}	[%]	Syneresis	29	16	8.5	9	5	3	15	1.5	0
c) P-catalyzed gels			3-1-25P	3-0.2-25P	3-0.1-25P	10-1-25P	10-0.2-25P	10-0.1-25P	15-1-25P	15-0.2-25P	15-0.1-25P
t_g	Approximate gelation time		4.5 hours	24 hours	24 hours	2 hours	4 hours	4.75 hours	1.5 hours	2.75 hours	3.25 hours
τ_{syn}	[%]	Syneresis	41.5	11	5.5	26	15	0	15	8.5	0

Table II-2: Gelation time and gel shrinkage due to syneresis depending on cellulose acetate concentration %CA and catalyst quantity or concentration I/Cat for a) DA-catalyzed gels, b) P-catalyzed gels

a) DA-catalyzed gels			3-0.2-1DA	3-0.2-0.25DA	3-0.2-0.01DA	10-0.2-1DA	10-0.2-0.32DA	10-0.2-0.25DA	15-0.2-1DA	15-0.2-0.47DA	15-0.2-0.25DA
I/Cat			5	19	50	16	50	63	24	50	95
t_g	Approximate gelation time		1.5 minutes	5 minutes	19 minutes	3 minutes	12.5 minutes	18.5 minutes	5 minutes	12 minutes	45 minutes
τ_{syn}	[%]	Syneresis	16	27	30	5	12	17	1.5	18.5	12
b) P-catalyzed gels			3-0.2-100P	3-0.2-32P	3-0.2-25P	10-0.2-105P	10-0.2-100P	10-0.2-25P	15-0.2-158P	15-0.2-100P	15-0.2-25P
I/Cat			0.05	0.15	0.19	0.15	0.16	0.63	0.15	0.24	0.95
t_g	Approximate gelation time		3.6 hours	16 hours	24 hours	1 hour	1.25 hours	4 hours	0.5 hours	0.65 hours	2.75 hours
τ_{syn}	[%]	Syneresis	5.5	32.5	11	2.5	8.5	15	0	0	8.5

3.2. Influence of Sol-Gel Parameters and Drying on the Organic Aerogel Structure

3.2.1. Influence of Sol-Gel Synthesis Parameters

3.2.1.1. Macro- and Microscopic Observation

The influence of the different sol-gel parameters (%CA, I/CA, I/Cat, and catalyst type) on the resulting organic cellulose-acetate based aerogels, in terms of structure, has been investigated in several experiments. First macroscopic and microscopic perceivable characteristics are discussed, before the structure is analyzed.

Shrinkage due to Drying in supercritical CO₂

A comparison of the visible aspect of the gels before and after supercritical drying has revealed that CAB gels shrink significantly and systematically during drying in supercritical CO₂ (see figure II-14). These observations bear out findings by Fischer [Fis 2006], who observed the same phenomenon of seemingly identical volumetric shrinkage of about 75-85% for all CAB gels when dried in supercritical CO₂.



Figure II-14: Cellulose-acetate based gel and aerogel (after drying in supercritical CO₂) 10-0.2-0.25DA

As known, a modification of the solid network by capillary forces is theoretically avoided completely by the supercritical drying process. Fischer therefore concludes that volumetric shrinkage is a consequence of chemical interactions between the solid polymer network of the gel and the solvent (first acetone, then supercritical CO₂). This assumption is based on works by Tanaka et al. [Tan 1981], who identified two main forces which govern the equilibrium of cross-linked polymer gels (*i.e.* between the gel's solid network of cross-linked polymers and the liquid network which is the solvent). These two forces are (i) the polymer network's elasticity and (ii) the chemical affinity between the polymer network and the solvent. Together they govern the equilibrium of a gel made

from cross-linked polymers. The equilibrium of such a system can be characterized by the distance between the polymer chains for which elasticity and chemical affinity are in equilibrium. By replacing the gel's liquid network through another solvent, the gel is forced to reach a new equilibrium state. Chemical affinity between the polymer and the solvent can simply be expressed by the Hildebrand parameter. Fischer has examined Hildebrand parameters for cellulose-acetate based gels in various solvents through a screening procedure and has shown a poor chemical affinity for cellulose-acetate based gels in CO₂. Evidently, the CAB gel thus takes on a new equilibrium if the initial solvent acetone is replaced by supercritical CO₂ during the drying step. In this case the gel undergoes a contraction due a poorer chemical affinity with CO₂ in comparison to acetone. This new "physico-chemical" equilibrium after solvent exchange is maintained even upon replacing the supercritical CO₂ by gaseous CO₂ and finally by air. Nevertheless, shrinkage (or expansion) due to different chemical affinities is reversible upon replacing the gel or the dry organic aerogel in the initial solvent [Fis 2006]. This finding tends to confirm that shrinkage due to supercritical drying does not lead to a plastic deformation of gels.

Macroscopic Aspect

Cellulose-acetate-based gels may have very different appearances and be of different brittleness, as do their organic aerogel counterparts (figure II-15).



Figure II-15: Cellulose-acetate based aerogels displaying the results of different synthesis parameters: 3-0.2-100P (left) and 10-1-5DD (right)

The gels' and aerogels' aspect depends strongly on the precursor concentrations and ratios (see figure II-16).



Figure II-16: CAB aerogels having been synthesized %CA and I/CA: 3-0.1-5DD, 10-0.1-5DD, 15-0.1-5DD, 3-0.2-5DD, 10-0.2-5DD, 15-0.2-5DD, 3-1-5DD, 10-1-5DD, 15-1-5DD (from left to right and top to bottom)

The aerogels' aspect, for example in terms of final aerogel size (*i.e.* syneresis), seems also to depend on catalyst concentration and catalyst type (Figure II-17).



Figure II-17: CAB aerogels having been synthesized using different catalysts: 15-0.1-5DD (left), 15-0.1-1DA (middle), 15-0.1-25P (right)

Micrography

The microstructure of the organic aerogels have been analyzed by SEM/FEG SEM. An example of a series of aerogels featuring an increasing cellulose acetate concentration can be seen in figure II-18. Although macropores can be recognized in all samples, pores in the lower nanometer range – small meso- to micropores – are not discernible. However, the aerogel with the lowest cellulose acetate precursor concentration (3 %CA – on the left) seems to possess the lowest density (*i.e.* appears to be

most porous), while that of the highest %CA in this series (15 %CA – on the right) seems to feature the highest density (*i.e.* appears to be least porous) according to the micrographs featured in figure II-18. The orientation on the surface for samples 10-0.2-1DA and 15-0.2-1DA might be a consequence of SEM analysis.

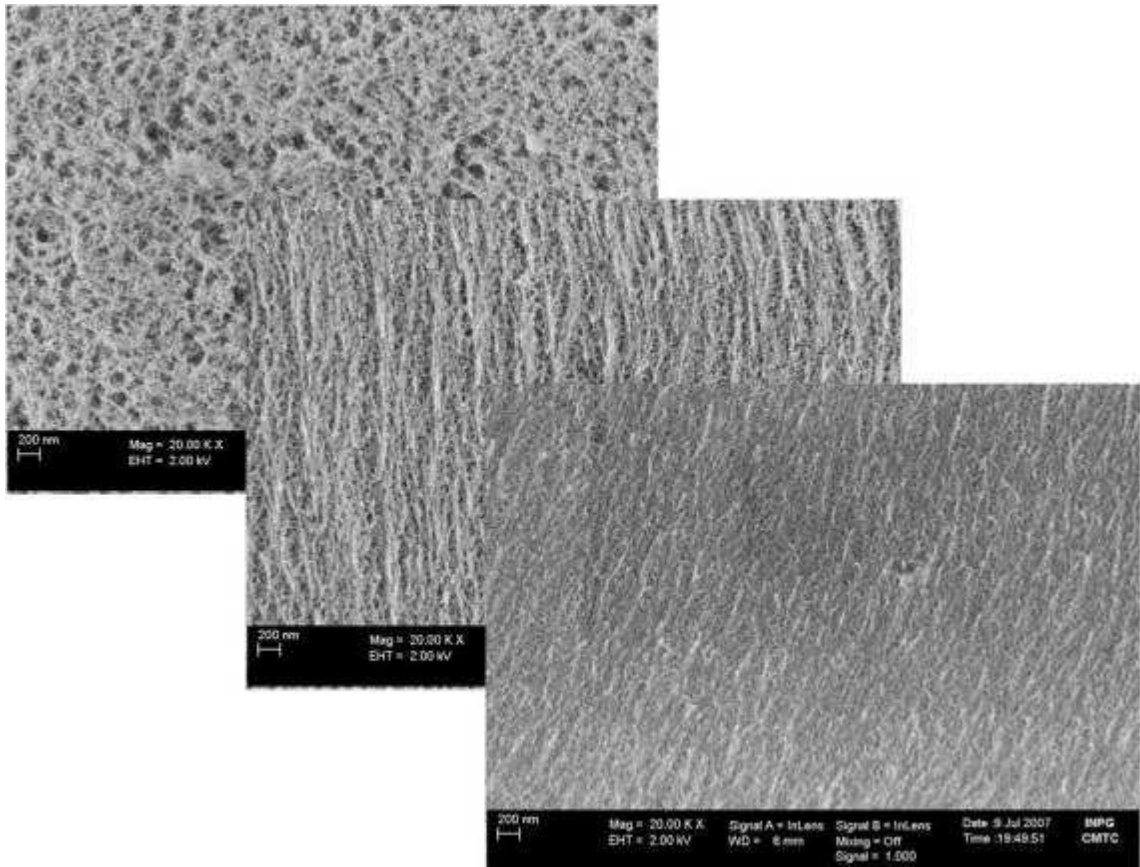


Figure II-18: SEM-FEG of CAB aerogels synthesized using different cellulose acetate concentrations: 3-0.2-1DA (top left), 10-0.2-1DA (middle), 15-0.2-1DA (bottom right)

An example of two aerogels featuring a different I/CA can also be seen in figure II-19. On the densely cross-linked sample (I/CA of 1 – on the left), no big macropores are visible, in contrast to the less densely cross-linked aerogel (I/CA of 0.1).

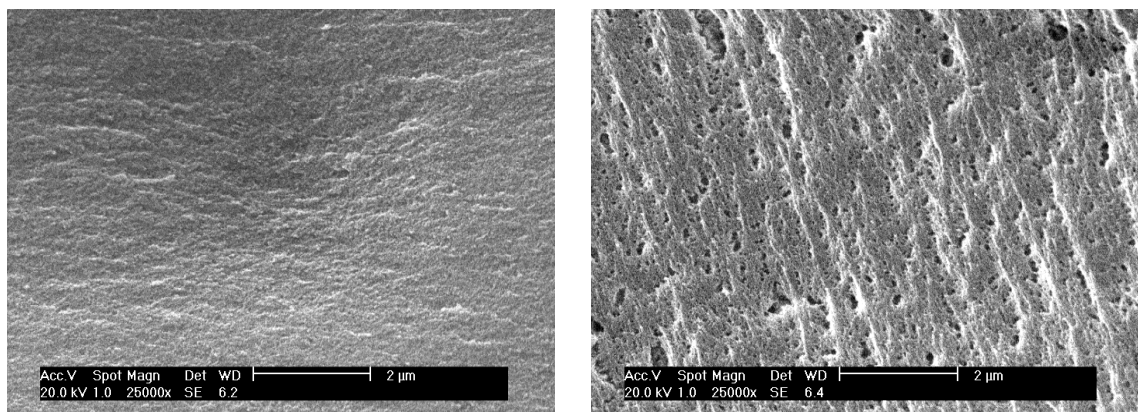


Figure II-19: SEM of CAB aerogels synthesized using different cross-linking ratios: 10-1-1DA (left), 10-0.1-1DA (right)

Skeletal Density

Skeletal densities have been determined by He pycnometry for aerogel samples prepared using different catalysts (table II-3). Modified precursor quantities are assumed to have no clear effect on the skeletal density, as has been postulated by F. Fischer [Fis 2006]. Results of He pycnometry show that the catalyst type does not have a noticeable influence on skeletal density either. Skeletal density is about 1.28 g/cm³ for all three samples, in spite of having used different catalysts. These values bear out previous findings [Fis 2006] of skeletal densities of about 1.4 g/cm³ for different aerogel formulations catalyzed by DD.

Table II-3: Skeletal density determined as determined by helium pycnometry

	5-0.1-5DD	10-0.2-0.25DA	10-0.2-100P	Mean value	
Skeletal density [g/cm ³]	±0.02	1.29	1.30	1.26	1.28

The mean value of the skeletal density of these three samples (*i.e.* 1.28 g/cm³) will further be used for calculating ϵ and V_{sp} of all CAB OA throughout this work.

3.2.1.2. Organic Aerogel Structure

Mercury porosimetry and pycnometry in combination with N₂ adsorption enabled us to identify the influence of the synthesis parameters %CA, I/CA, I/Cat, and catalyst type on the organic aerogel structure (see tables II-4, II-5, and II-6 for the influence of %CA, I/CA for DD-, DA, and P-catalyzed aerogels, respectively and tables II-7 and II-8 for the influence of I/Cat on DA- and P-catalyzed aerogels, respectively).

Table II-4: Structure of organic aerogels depending on cellulose acetate concentration %CA and cross-linking ratio I/CA for DD-catalyzed gels

DD-catalyzed aerogels		3-1-5DD	3-0.2-5DD	3-0.1-5DD	10-1-5DD	10-0.2-5DD	10-0.1-5DD	15-1-5DD	15-0.2-5DD	15-0.1-5DD
ρ_b	[g/cm ³] ± 0,02	0,28	0,18	0,27	1,13	0,38	0,20	0,88	0,56	0,37
ϵ	± 0,05	0,78	0,86	0,79	0,12	0,71	0,85	0,31	0,56	0,71
V_{SP}	[cm ³ /g] ± 0,05	2,84	4,87	2,99	0,10	1,87	4,32	0,35	1,01	1,95
V_{Hg}	[cm ³ /g] ± 0,02	0,94	4,04	2,96	0,14	1,92	4,15	0,36	1,00	1,94
% V_{Hg}	[%] ± 1	33%	83%	99%	130%	102%	96%	103%	99%	99%
V_{BJH}	[cm ³ /g] ± 0,02	0,85	1,65	0,35	0,07	1,85	0,81	0,33	0,87	1,37
% V_{BJH}	[%] ± 1	30%	34%	12%	67%	99%	19%	94%	86%	70%
S_{BET}	[m ² /g] ± 10	220	242	140	43	353	250	182	249	215
L_{Hg}	[nm] ± 1	13	34	19	9	23	30	11	13	22
L_{BJH}	[nm] ± 1	5	4	4	5	28	5	7	18	52

Table II-5: Structure of organic aerogels depending on cellulose acetate concentration %CA and cross-linking ratio I/CA for DA catalyzed gels

DA-catalyzed aerogels		3-1-1DA	3-0.2-1DA	3-0.1-1DA	10-1-1DA	10-0.2-1DA	10-0.1-1DA	15-1-1DA	15-0.2-1DA	15-0.1-1DA
ρ_b	[g/cm ³] ± 0,02	0,50	0,39	0,38	1,04	0,73	0,47	1,14	0,82	0,68
ϵ	± 0,05	0,61	0,70	0,71	0,18	0,43	0,63	0,11	0,36	0,47
V_{SP}	[cm ³ /g] ± 0,05	1,22	1,79	1,88	0,18	0,59	1,33	0,10	0,44	0,69
V_{Hg}	[cm ³ /g] ± 0,02	1,24	1,92	1,89	0,19	0,61	1,35	0,12	0,44	0,75
% V_{Hg}	[%] ± 1	102%	107%	101%	109%	103%	101%	121%	99%	109%
V_{BJH}	[cm ³ /g] ± 0,02	1,13	1,66	0,69	0,16	0,62	0,87	0,03	0,33	0,50
% V_{BJH}	[%] ± 1	92%	93%	37%	91%	105%	65%	27%	74%	72%
S_{BET}	[m ² /g] ± 10	290	257	113	137	217	225	- ^{a)}	146	173
L_{Hg}	[nm] ± 1	16	15	13	9	13	19	9	13	16
L_{BJH}	[nm] ± 1	4	-	50	5	11	16	38	7	12

^{a)} Active surface values below detection limits

Table II-6: Structure of organic aerogels depending on cellulose acetate concentration %CA and cross-linking ratio I/CA for P-catalyzed gels

P-catalyzed aerogels			3-1-25P	3-0.2-25P	3-0.1-25P	10-1-25P	10-0.2-25P	10-0.1-25P	15-1-25P	15-0.2-25P	15-0.1-25P
ρ_b	[g/cm ³]	± 0,02	0,45	0,16	0,14	1,17	0,62	0,35	1,21	0,87	0,56
ϵ		± 0,05	0,65	0,88	0,89	0,09	0,51	0,73	0,06	0,32	0,57
V_{SP}	[cm ³ /g]	± 0,05	1,42	5,67	6,31	0,07	0,83	2,08	0,05	0,37	1,02
V_{Hg}	[cm ³ /g]	± 0,02	1,42	5,20	6,04	0,11	0,85	2,03	0,08	0,39	1,06
% V_{Hg}	[%]	± 1	100%	92%	96%	148%	102%	98%	154%	107%	104%
V_{BJH}	[cm ³ /g]	± 0,02	1,31	0,99	1,36	0,03	1,04	1,36	0,04	0,34	0,81
% V_{BJH}	[%]	± 1	92%	17%	22%	45%	126%	66%	78%	93%	79%
S_{BET}	[m ² /g]	± 10	264	204	200	- ^{a)}	346	272	- ^{a)}	162	260
L_{Hg}	[nm]	± 1	17	34	37	9	17	22	7.5	12	18
L_{BJH}	[nm]	± 1	28	3	28	4	12	32	4	7	14

^{a)} Active surface values below detection limits

Table II-7: Structure of organic aerogels depending on cellulose acetate concentration %CA and catalyst quantity or ratio I/Cat for DA-catalyzed aerogels

DA-catalyzed aerogels			3-0.2-1DA	3-0.2-0.25DA	3-0.2-0.01DA	10-0.2-1DA	10-0.2-0.32DA	10-0.2-0.25DA	15-0.2-1DA	15-0.2-0.47DA	15-0.2-0.25DA
I/Cat			5	19	50	16	50	63	24	50	95
ρ_b	[g/cm ³]	± 0,02	0,39	0,49	0,35	0,73	0,92	0,80	0,82	0,84	0,89
ϵ		± 0,05	0,70	0,62	0,73	0,43	0,28	0,37	0,36	0,34	0,31
V_{SP}	[cm ³ /g]	± 0,05	1,79	1,26	2,09	0,59	0,31	0,47	0,44	0,41	0,35
V_{Hg}	[cm ³ /g]	± 0,02	1,92	1,20	1,98	0,61	0,32	0,51	0,44	0,41	0,25
% V_{Hg}	[%]	± 1	107%	96%	95%	103%	105%	109%	99%	100%	73%
V_{BJH}	[cm ³ /g]	± 0,02	1,66	0,77	1,14	0,62	0,29	0,39	0,33	0,35	0,19
% V_{BJH}	[%]	± 1	93%	61%	54%	105%	95%	83%	74%	85%	54%
S_{BET}	[m ² /g]	± 10	257	179	220	217	129	171	146	171	100
L_{Hg}	[nm]	± 1	15	12	19	13	11	13	13	13	9
L_{BJH}	[nm]	± 1	-	5	24	11	8	11	7	9	6

Table II-8: Structure of organic aerogels depending on cellulose acetate concentration %CA catalyst quantity or ratio I/Cat for P-catalyzed aerogels

P-catalyzed aerogels			3-0.2-100P	3-0.2-32P	3-0.2-25P	10-0.2-105P	10-0.2-100P	10-0.2-25P	15-0.2-158P	15-0.2-100P	15-0.2-25P
I/Cat			0.05	0.15	0.19	0.15	0.16	0.63	0.15	0.24	0.95
ρ_b	[g/cm ³]	± 0,02	0,16	0,33	0,16	0,59	0,54	0,62	0,74	0,85	0,87
ϵ		± 0,05	0,88	0,74	0,88	0,54	0,58	0,51	0,42	0,34	0,32
V_{SP}	[cm ³ /g]	± 0,05	5,63	2,26	5,67	0,91	1,07	0,83	0,57	0,40	0,37
V_{Hg}	[cm ³ /g]	± 0,02	5,27	2,56	5,20	0,96	1,03	0,85	0,62	0,41	0,39
% V_{Hg}	[%]	± 1	94%	113%	92%	106%	96%	102%	108%	104%	107%
V_{BJH}	[cm ³ /g]	± 0,02	0,99	0,27	0,99	0,70	0,76	1,04	0,33	0,34	0,34
% V_{BJH}	[%]	± 1	18%	12%	17%	77%	71%	126%	57%	85%	93%
S_{BET}	[m ² /g]	± 10	224	107	204	212	235	346	125	148	162
L_{Hg}	[nm]	± 1	33	-	34	15	16	17	14	13	12
L_{BJH}	[nm]	± 1	4	4	3	18	16	12	11	11	7

Bulk densities ρ_b generally lie between 0.16 and 1.21 g/cm³ and porosities range from at least 0.15 up to around 0.9. Specific porous volumes differ considerably with the sol-gel synthesis parameters, but depend as well on analysis method and model used. Lowest specific porous volumes approach 0 cm³/g, while highest specific porous volumes tend to 6 cm³/g. Specific surface areas s_{BET} range from 40 to 350 m²/g. Mean pore sizes are as small as 3 nm (L_{BJH}) and as big as 60 nm (L_{BJH}). The porous characteristics seem to be influenced by %CA, I/CA, I/Cat, and the nature of catalyst at the same time. Because of the sensitivity of the sol-gel processes to a relatively high number of parameters and the error range of the analysis methods used, few clear tendencies stand out. However, below an overview of probable tendencies is given.

Cellulose Acetate Concentration %CA

Cellulose acetate concentration has a notable influence on the organicaerogels' structure.

Bulk densities ρ_b feature a tendency to increase with an increasing cellulose acetate concentration (see figures II-20, II-21, and II-22 for DD-, DA-, and P-catalyzed aerogels, respectively), lying between 0.16 and 1.21 g/cm³. Logically, porosity ϵ decreases with increasing density and thus with increasing %CA. Also, with increasing ρ_b *i.e.* increasing %CA, total specific volume V_{Hg} and specific porous volume V_{sp} decrease (equations II-5 and II-6).

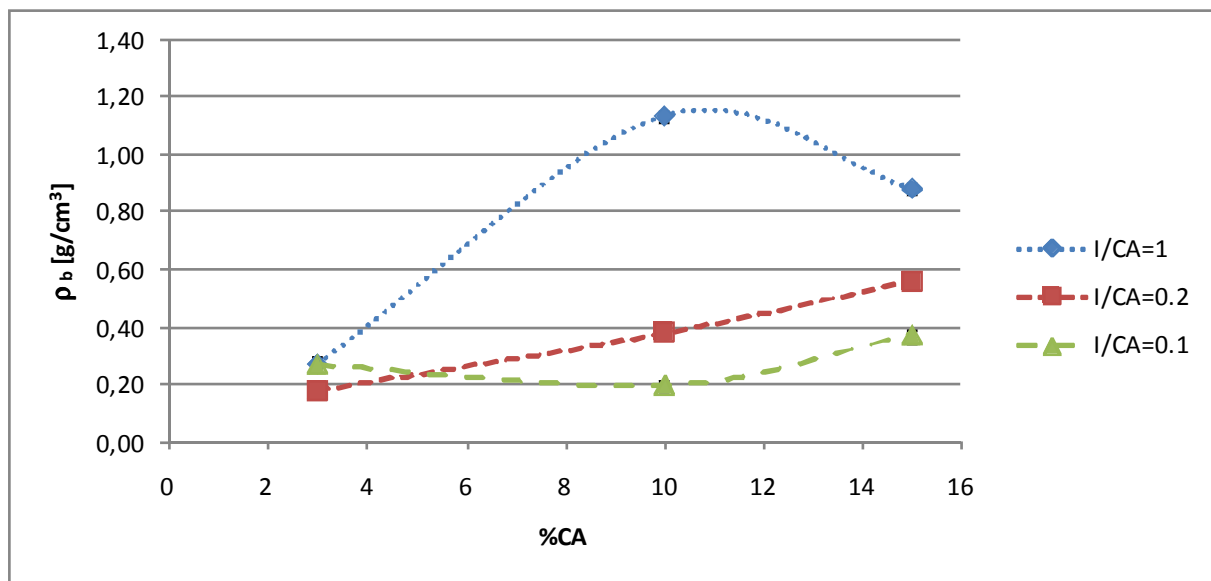


Figure II-20: Evolution of ρ_b with %CA for DD-catalyzed aerogels

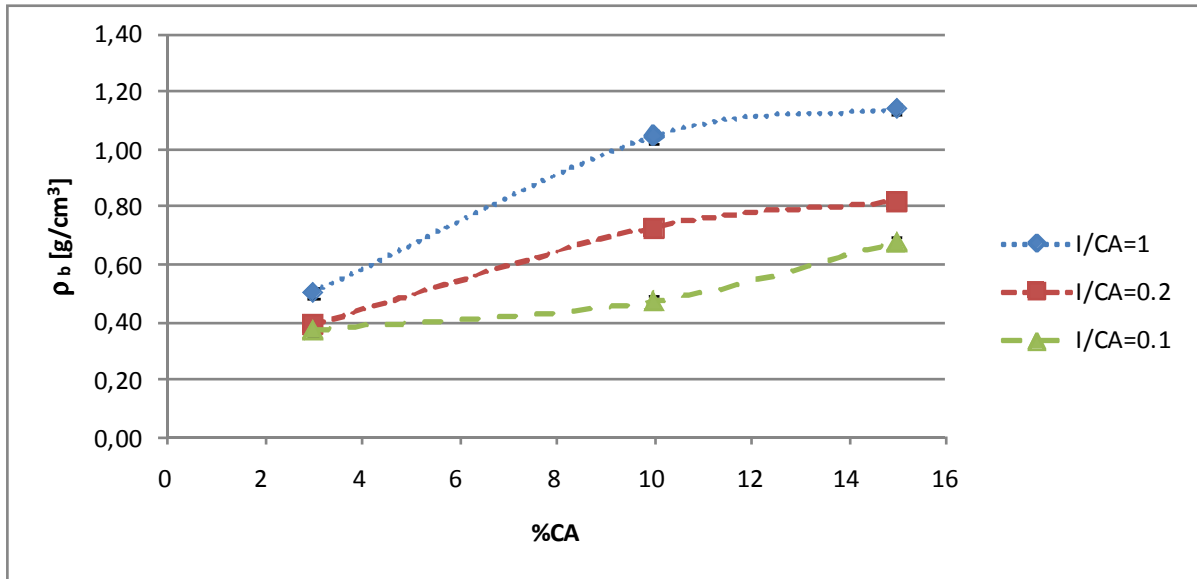


Figure II-21: Evolution of ρ_b with %CA for DA-catalyzed aerogels

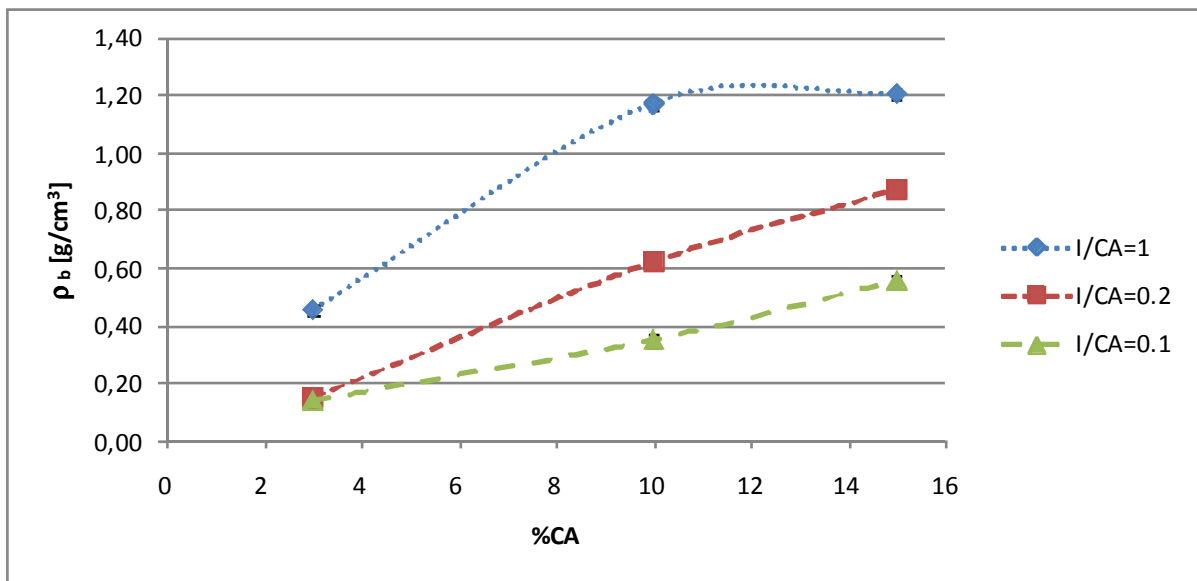


Figure II-22: Evolution of ρ_b with %CA for P-catalyzed aerogels

The ratio of porous volume detected by N_2 adsorption $\%V_{BJH}$ seems to be lowest for aerogels containing only 3 %CA. This result may be explained by lower densities and bigger mean pore sizes not being detected by N_2 adsorption, as well as by a low mechanical resistance to compression due to capillary condensation by N_2 .

According to Fischer, L_{Hg} diminishes significantly with increasing % (between 5 and 10 %CA) for DD-catalyzed CAB OA [Fis 2006]. Although quite a number of our results from Hg porosimetry is in line with this finding, L_{BJH} often do not reflect the same tendencies (see for example figure II-23).

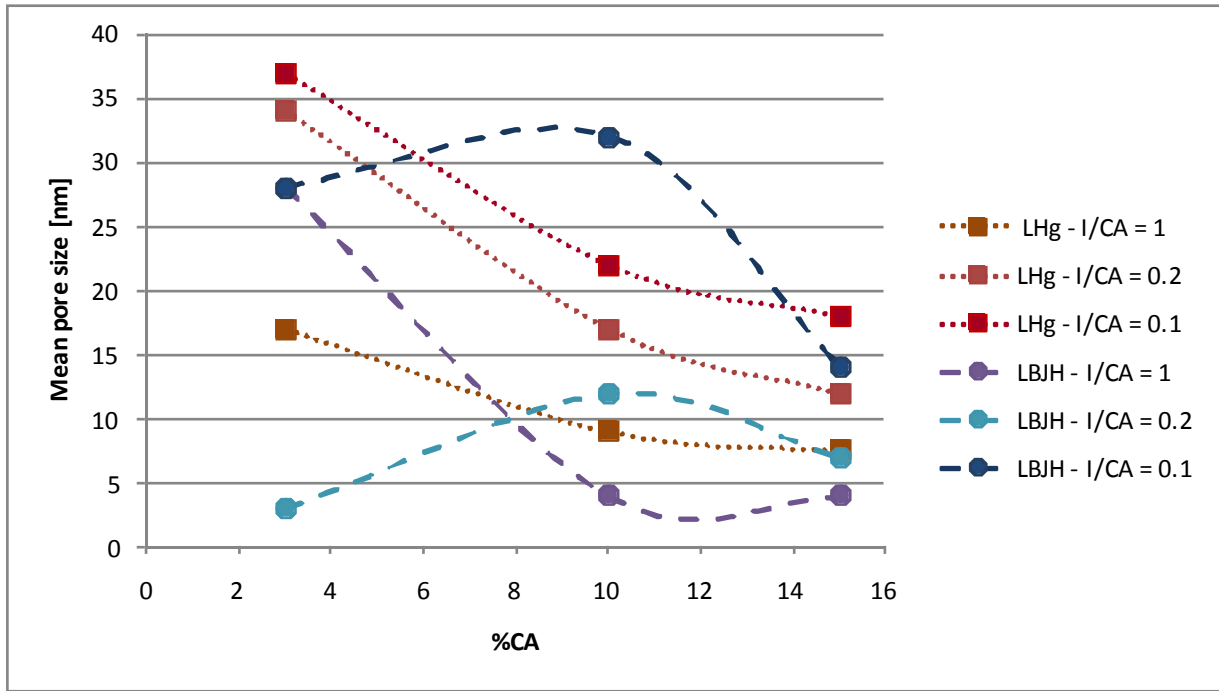


Figure II-23: Evolution of mean pore sizes with %CA for different I/CA, obtained by mercury porosimetry (reddish colours) and by nitrogen adsorption (blueish colours)

Note that the minimum and maximum pore sizes detected depend on the analysis method (N_2 adsorption or Hg porosimetry) and are restricted in both cases. Nitrogen adsorption might thus not be able to detect macroporous mean pore sizes. Also, rather bi-modal pore size distributions or distributions without a distinct peak in the mesopore range, like the pore size distribution for sample 3-0.2-32P to be seen in figure II-24, are susceptible to be found.

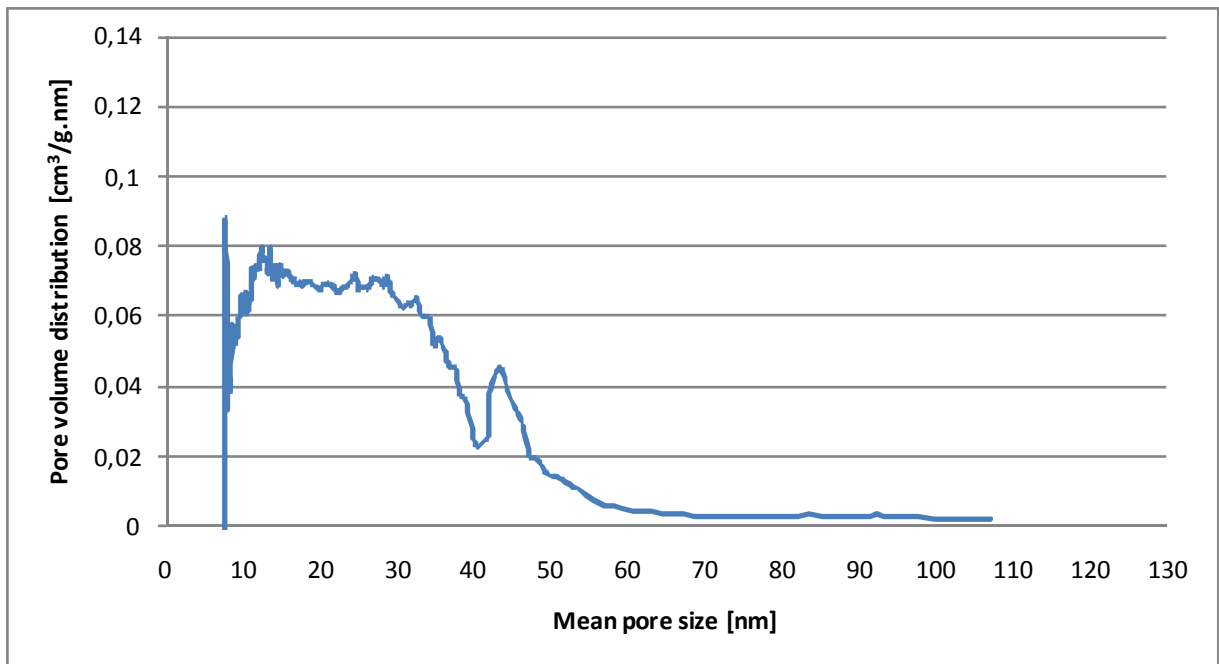


Figure II-24: PSD of sample 3-0.2-32P obtained by mercury porosimetry

Cross-linking Ratio I/CA

Cross-linking has a significant influence on the organic aerogels' structure.

Bulk densities ρ_b generally increase for an increasing I/CA for all catalysts (see figures II-20, II-21, and II-22 for DD-, DA-, and P-catalyzed aerogels, respectively). Consequently, porosity ϵ , specific porous volume V_{Hg} , and specific porous volume V_{SP} decrease with an increasing I/CA .

Experimentally identified mesoporous volumes V_{BJH} may have a tendency to decrease with an increasing I/CA , which would be in line with findings on V_{Hg} and V_{SP} .

The porous volume detected using Hg porosimetry $\%V_{Hg}$ is in many cases relatively close to 100% (particularly for I/CA of 0.2 according to tables II-7 and II-8), although often a bit or even much above this value. Very high $\%V_{Hg}$ (e.g. up to 154%) are often to be found for I/CA of 1, i.e. for gels with a hyperstoichiometric content of MDI, whereas $\%V_{BJH}$ in these cases tend to be low. Values for $\%V_{Hg}$ above 100% are most likely due to a heterogeneous character of CAB aerogels, whereas values approaching 100% may indicate that few pores smaller than 7.5 or bigger than 85 nm are contained in the material and that all of the porous volume may be characterized using Hg porosimetry.

Mean pore sizes L_{Hg} , but also L_{BJH} , are frequently identified to increase with a decreasing I/CA (see for example figure II-25). However, the influence of I/CA on the specific surface area s_{BET} is not clear.

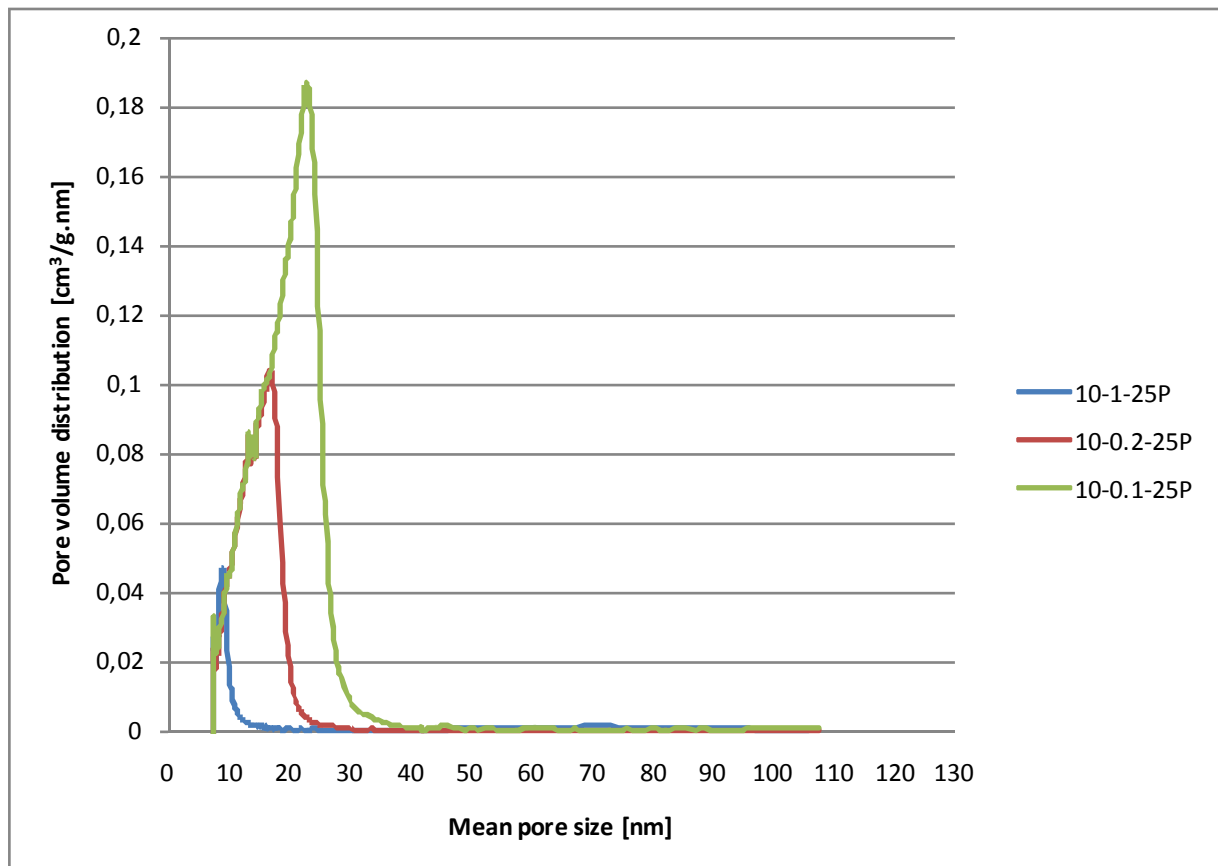


Figure II-25: Influence of I/CA on PSDs obtained by mercury porosimetry for P-catalyzed samples containing 10 %CA

Catalyst Concentration I/Cat and Type

Even for different catalyst concentrations (for catalysts DA and P, see tables II-7 and II-8 respectively), bulk densities ρ_b tend to increase while porosity and specific volumes seem rather to decrease for an increasing %CA. Therefore, catalyst concentration may have an influence on the CAB aerogels porous characteristics, but the influence of %CA must be much more pronounced. However, the range of ρ_b , ϵ , specific porous volumes, and mean pore sizes seems to be generally rather stable, *i.e.* remains in the same range of values, for different catalyst concentrations at the same %CA.

In the range of catalyst concentrations studied in this work, bulk densities ρ_b appear to be generally higher for DA-catalyzed organic aerogels than for DD-catalyzed aerogels. Therefore total specific volumes V_{Hg} and specific porous volumes V_{sp} are higher for DD-catalyzed gels than for DA-catalyzed gels. Pyridine-catalyzed gels, on the contrary, cover the broadest range of values for ρ_b , V_{Hg} , and V_{sp} .

As results on the structure of P-catalyzed gels are comparable to those of DA-catalyzed gels, the difference in porous characteristics does not seem to be a product of different gelation times. Structural differences between gels catalyzed using different agents are most likely a product of different catalyst mechanisms.

3.2.2. Influence of the Drying Process on the Organic Aerogel Structure

Although drying in supercritical CO₂ is known to be able to best preserve a gel's structure (apart from shrinkage due to the networks compatibility with CO₂), it is nonetheless a complicated and costly step in the synthesis of an aerogel. Therefore, we have examined the effects of different drying methods. Two samples of different %CA, I/CA, and catalyst concentration (samples 10-0.1-8DD and 5-1-1 DD) have been dried by evaporation in air (ambient conditions), lyophilisation (in cyclohexane, at -20 °C and 100 Pa for 2 h), and supercritical drying in CO₂. The influence of the drying method on the gel may be seen in figure II-26.



Figure II-26: Comparison of the effects of drying by evaporation in air (left), lyophilisation (middle), and supercritical drying in CO₂ (right) on samples a) 10-0.1-8DD and b) 5-1-1DD

Evidently, the drying method has a major influence on the resulting dry network. Xerogels have not only shrunk notably but have also been deformed. For xerogel 10-0.1-8DD with a relatively low I/CA, only a coronary with a thin and transparent film spanning between the edges remains. More densely cross-linked xerogel 5-1-1DD also shrinks perceptibly and features a large crack on the bottom. Although cryogel 10-0.1-8DD seems to shrink a little less than the xerogel, it features numerous small cracks and did not remain a monolith. Cryogel 5-1-1DD even burst apart during lyophilisation. Both aerogels, however, have maintained their form best and shrunk least in the drying process, apart from shrinkage due to the solvent exchange (*i.e.* from acetone to CO₂).

Concerning subcritical drying, Job et al. have advanced the idea of producing RF xerogel monoliths by optimizing the conditions of convective drying [Job 2006]. Contrary to Job et al., who have investigated the effect of different drying velocities by forced convection, we have chosen to investigate the influence of evaporation kinetics for CAB gels by limiting the natural convection. Gels 3-0.2-0.25DA and 10-0.2-0.25DA have been dried in three different time spans (see figure II-27 for an example). For simplification, xerogels dried in ambient conditions in air (natural convection) are referred to as XS, gels dried in air by limited natural convection XM, and those dried by severely limited natural convection XL.

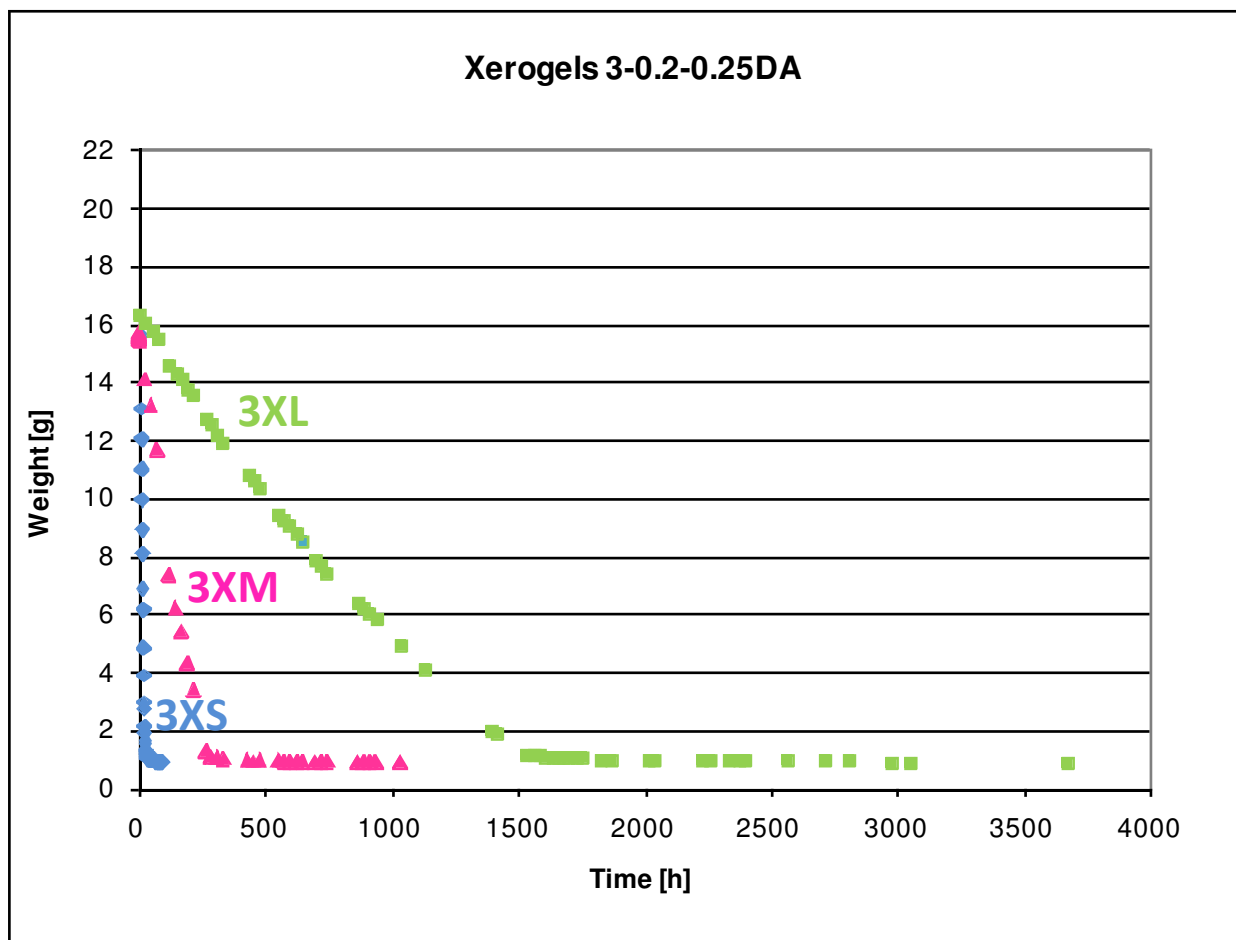


Figure II-27: Weight loss due to solvent evaporation of samples 3-0.2-0.25DA in different evaporation conditions

Figure II-28 shows the influence of supercritical drying and of evaporative drying in different conditions (see above) for sample 3-0.2-0.25DA.

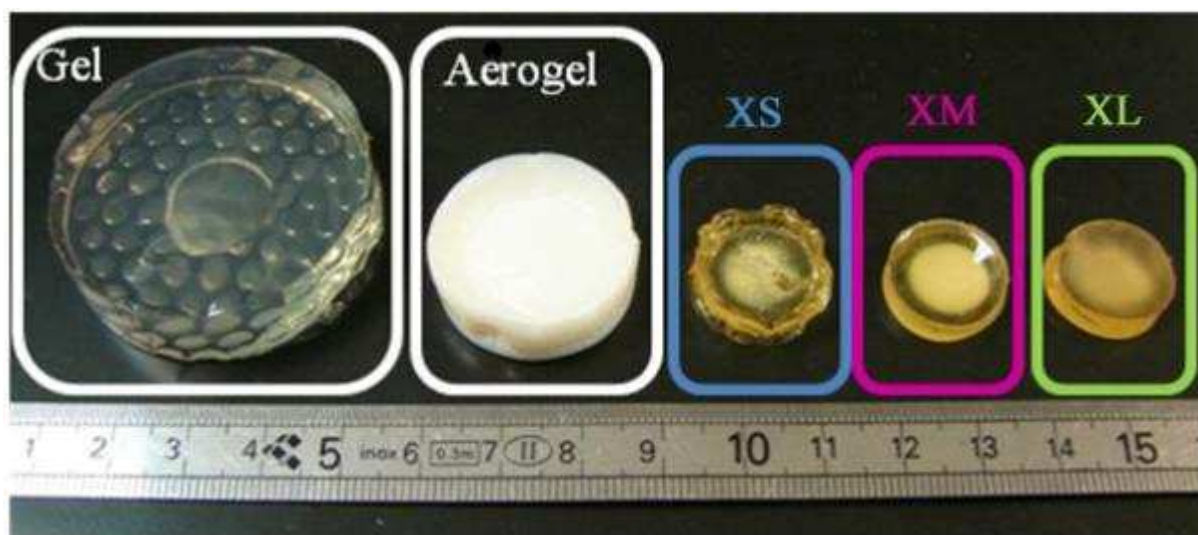


Figure II-28: Influence of drying process and evaporation kinetics on sample 3-0.2-0.25DA

Even though CAB gels shrink in the course of drying in supercritical CO₂, they shrink even more during evaporative drying. The xerogel dried at the rate, 3XS, has undergone the most pronounced shrinkage and deformation. Xerogels dried at lower drying rate, however, maintain their initial shape more or less but densify notably. In terms of deformation, even the gel dried supercritically deforms more, but obviously shrinks less than samples XM and XL. Mercury pycnometry and porosimetry confirm the impression of a pronounced densification for all xerogels (see table II-9).

Table II-9: Composition of organic aerogel catalyzed by different catalysts

		3-0.2-0.25DA	3XS	3XM	3XL	10-0.2-0.25DA	10XS	10XM	10XL	
ρ_b	[g/cm ³]	±0,02	0,49	1,27	1,29	1,27	0,80	1,31	1,26	1,28
ϵ		±0,05	0,62				0,37			
V_{SP}	[cm ³ /g]	±0,05	1,26				0,47			
V_{Hg}	[cm ³ /g]	±0,02	1,20	0,03	0,03	0,03	0,51	0,03	0,03	0,03
% V_{Hg}	[%]	±1	96%				109%			
V_{BJH}	[cm ³ /g]	±0,02	0,77				0,39			
% V_{BJH}	[%]	±1	61%				83%			
S_{BET}	[m ² /g]	±10	179				171			
L_{Hg}	[nm]	±1	12				13			
L_{BJH}	[nm]	±1	5				11			

On the basis of these results, supercritical drying seems to be the only drying method able to create porous CAB gel monoliths. The xerogels' bulk density is almost identical with the skeletal density determined for CAB aerogels of about 1.28 g/cm³, but the initial monolithic character of the gel is maintained.

3.2.3. Organic Aerogel Elemental Composition

Elemental analysis of the organic CAB aerogels has been carried out in order to know the elemental composition and to compare if different catalysts influence the composition, for example by being retained in the gel matrix. Results obtained on three representative CAB aerogel samples having been synthesized using the same %CA and I/CA, but different catalysts are presented in table II-10. Note that the catalyst quantity employed varies with catalyst type.

Table II-10: Composition of organic aerogel catalyzed by different catalysts

		<i>Theory: 3 %CA, I/CA=0.2, any catalyst</i>	<i>3-0.2-5DD</i>	<i>3-0.2-0.25DA</i>	<i>3-0.2-100P</i>
C	wt.-%	52.7	53.4	52.9	52.3
H	wt.-%	5.5	6.0	5.6	5.6
N	wt.-%	1.8	1.9	1.8	1.6
O	wt.-%	39.9	35.5	39.5	39.4
Sn	wt.-%	-	1.2	-	-
Total	wt.-%	100	98.0	99.8	98.9

The elemental composition is similar for aerogels catalyzed by different agents and close to the theoretical aerogel composition (calculated according to the sol-gel composition for a gel also containing 3 %CA with an I/CA of 0.2) in all cases. For nearly stoichiometrically cross-linked gels (I/CA of 0.2) the weight percentage of carbon lies thus around 53%, the hydrogen content around 6%, and the oxygen content just below 2%. In terms of oxygen content a small difference for aerogels catalyzed by DD and those catalyzed by DA and P may be observed. Aerogels catalyzed by DD contain less oxygen, about 35%, in comparison to DA- and P-catalyzed aerogels containing more than 39% oxygen. In addition, aerogels catalyzed using DD feature a small content of tin of about 1%.

The content of tin for DD-catalyzed aerogels implies retention of the catalyst in the polymer network even after washing and drying of the gels. As discussed before, DD is a quite cumbersome molecule (see figure II-4) and the possibility of catalyst retention in the gel matrix or in the gel's porosity because of the catalyst molecules dimension, as proposed by Fischer [Fis 2006], seems coherent. Another possibility is the formation of isocyanate/tin alkoxide complexes without a subsequent alcoholysis, which normally causes the release of the tin alkoxide (see figure II-6). This might be the case especially for a hyperstoichiometric concentration of isocyanate, *e.g.* at an I/CA of 1.

Although DA and P catalysts contain nitrogen atoms, aerogels catalyzed with DA and with P feature a nitrogen content a bit lower than that of DD-catalyzed aerogels and even lower than the theoretical values. Therefore, this slight difference in nitrogen content between aerogels catalyzed by DD and those catalyzed by DA and P, indicates clearly that neither DA nor P molecules are retained within the aerogels (even more so for P of which relatively high quantities are used compared to catalysis through DA). Evidently, DA- as well as P-molecules are smaller than DD-molecules (figure II-4) and therefore less likely to be trapped within the porous network of the gel. Additionally, neither of them seems to form a complex with one of the starting compounds (see section 2.4 on catalyst mechanisms).

4. Conclusion

On the basis of literature research, we have focused on studying carbon aerogels synthesized by pyrolyzing cellulose-acetate-based aerogels. CAB aerogels are prepared by supercritically drying gels synthesized *via* sol-gel method.

The influence of different sol-gel parameters, namely precursor and catalyst concentration and type, on the the gelation process have been examined. The gelation process has been studied in terms of

gelation time and volumetric shrinkage due to syneresis. The macroscopic effects of drying (*e.g.* deformation) in supercritical CO₂, subcritical drying in air, and lyophilisation on the cellulosic gels have been studied. Supercritical drying in CO₂ has been identified to be the only method resulting in mesoporous CAB OA. The structure of the organic aerogels has been analyzed by SEM microscopy, helium pycnometry, mercury porosimetry and pycnometry, and nitrogen sorption. The elemental composition of CAB OA has been determined by elemental analysis. The influence of the different sol-gel parameters on sol evolution and aerogel structure is very complex, but through variations of the different sol-gel parameters and different drying processes a structurally different CAB OA may be synthesized. Bulk densities as low as 0.16 g/cm³ and as high as values approaching the skeletal density have been found. Porous volumes determined by Hg porosimetry range between 0.03 and about 5.3 cm³/g and s_{BET} between around 40 and 350 m²/g.

In conclusion, a broad range of CAB aerogels have been generated by varying the sol-gel synthesis parameters. The porous structure of CAB aerogels depends particularly on the concentration and ratio of the two precursors (cellulose acetate and MDI). The catalyst nature and type, nonetheless, has also been found to play a role in determining the organic aerogels structure. In addition, the type of catalyst used may also have a slight influence on the aerogel's elemental composition, if catalyst molecules are trapped inside the aerogel (as is for example the case of DD-catalyzed aerogels).

After having synthesized organic CAB aerogels of different structures, the influence of the organic aerogel structure on the structure of the carbon aerogel are examined in chapter III.

Chapter III: Cellulose-acetate-based Carbon Aerogels

Cellulose acetate-based Carbon Aerogels

1. Introduction

As seen in chapter I.3.3, the characteristics of a carbon material (carbon structure, surface chemistry, etc.) depend importantly on the organic precursor and on the pyrolysis parameters.

Material-related influence: According to numerous publications, the precursor material used for pyrolysis does have an important influence on the resulting carbon material. The nature of the organic precursor (*e.g.* composition and structure) has been evidenced to play a role concerning the pyrolytic behavior and the quantity and composition of volatile matters emitted and liquid and solid fractions created during the pyrolysis process [Cou 2007] and the structure of the resulting carbon material [Ish 2004, Las 1999]. The porous structure of carbon aerogels (CA) has repeatedly been identified to be determined by the organic aerogel (OA) framework structure for several types of carbon aerogels (*e.g.* RF-based, cellulose-based, or polyvinyl chloride-based [Gui 2008, Ish 2004, Yam 2003]). Therefore, I have decided to study the influence of the cellulose-acetate-based organic aerogels (CAB OA) on (i) the structure and (ii) the composition of their carbon counterparts.

Pyrolysis-related influence: The influence of the inert pyrolysis atmosphere (N_2 and Ar) on the carbon structure and composition has been examined in this work. Different inert gases possess different thermal conductivities and have been found to have an influence on the resulting carbon material before [SuL 2007]. A slow heating rate has uniformly been used, aiming at a high solid yield [Mer 2006]. Additionally, the influence of the maximum pyrolysis temperature on the CA structure and composition has been studied for temperatures between 900 and 1100 °C. Pyrolysis maximum temperatures have been this high in order to prepare carbon compounds with a relatively high carbon content [Fis 2006].

On the whole, chapter III focuses on creating a broad range of structurally different carbon aerogels and on investigating and discussing the influence of different pyrolysis parameters on the resulting CA. To this end, I have examined (i) the evolution of CAB aerogels during pyrolysis in general (section 3.1), (ii) the influence of the OA on structure and composition of the resulting CA (section 3.2), and (iii) the influence of pyrolysis parameters (section 3.3) on structure and composition of the resulting CA. Structural changes occurring during pyrolysis and effects on mass loss, on the resulting carbon aerogels' structure, and on the composition have been studied.

2. Experimental

Cellulose-acetate-based organic gels have been synthesized by sol-gel method, based on the protocol described in chapter II. Cellulose acetate concentrations %CA of 3, 5, 10, or 15 and cross-linking ratios I/CA of 0.1, 0.2, or 1 have been examined. Organic gels have been catalyzed either by DD, DA, or P. Organic gels have been dried by indirect supercritical drying in CO_2 (if not stated otherwise) or by evaporative drying, as described in chapter II.

Pyrolysis has taken place under a continuous flow of 3 l/min of either N₂ or Ar. Samples have been heated linearly at a heating rate of 4 °C/min up to T_{max}. The maximum temperature T_{max} has been set to 900 °C, 1000 °C, or 1100 °C and has been maintained for 1 h (see figure III-1 for an example of a typical pyrolysis profile). Cooling has been left to thermal inertia.

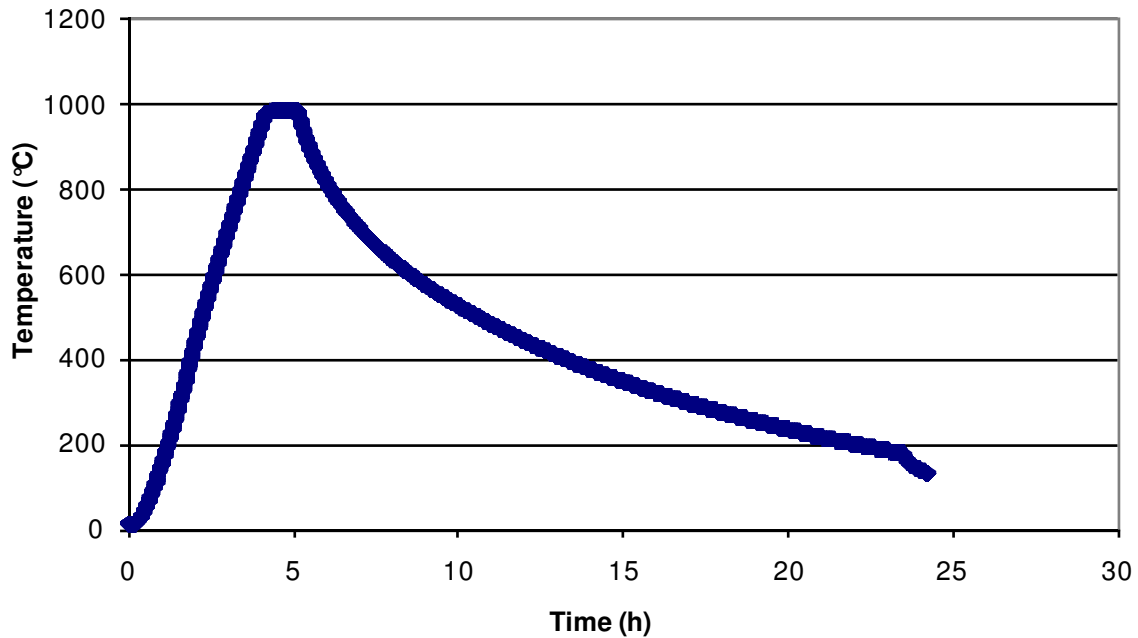


Figure III-1: Example of a pyrolysis profile of cellulose-acetate-based aerogels

Global mass loss due to pyrolysis Δm_{pyr} has been determined according to Equation III-1:

$$\Delta m_{pyr} = 100 \times \frac{(m_0 - m_f)}{m_0} \quad \text{Equation III-1}$$

with m_0 and m_f are the sample mass before and after pyrolysis respectively. CAB OA have been dried for 24h at 100 °C prior to pyrolysis. Mass loss due to pyrolysis Δm_{pyr} does therefore not include mass loss due to the evaporation of water or other COV potentially adsorbed. Real mass loss during pyrolysis Δm_{pyr} has been compared to the theoretical mass loss Δm_{th} assuming that all carbon atoms contained in the organic aerogel (carbon quantity theoretically introduced into the sol by the precursors) remains in the carbonaceous matrix after heat-treatment.

In order to study the evolution of CAB aerogels during pyrolysis, thermogravimetric analysis (TGA) coupled with Fourier Transformed Infrared (FTIR) Spectroscopy of the gas emitted during TGA and FTIR spectroscopy on the aerogel samples have been carried out. TGA (and simultaneous FTIR spectroscopy of the gas emitted) has been performed using a Setsys^{evolution} TG-DTA at a heating rate of 10 °C/min up to 1200 °C in a 30 ml/min N₂ flow. FTIR spectroscopy of the aerogel samples have been carried out using a Bruker Tensor 27 spectrometer. Samples have been analyzed in attenuated

total reflectance mode (ATR) using a Pike MIRacle accessory equipped with a Ge crystal (Pike Technology). The spectrum has been collected 256 times and corrected for the background noise. The multi-point baseline correction has been realized for each spectrum.

Structure and elemental composition of the carbonized CAB aerogel have been determined and observed as for organic CAB aerogels (see chapter II.2). Microporous volumes have been determined from N_2 adsorption using the t-plot method. Pore size distributions derived from Hg porosimetry have been established using the buckling theory for organic aerogels and using the Washburn equation for carbon aerogels, as CAB CA do not undergo compression during mercury porosimetry.

3. Results and Discussion

3.1. Evolution of Cellulose-acetate-based Aerogels during Pyrolysis

First macroscopic and microscopic perceivable characteristics are discussed, before the evolution of the aerogel during pyrolysis and the skeletal densities of the resulting carbon aerogel are analyzed.

3.1.1. Macroscopic Observation

CAB OA tend to lose their initial shape during pyrolysis. They seem to simultaneously shrink and foam (Figure III-2). Even surfaces cover the CAB CA bulk at least partly.



Figure III-2: Aerogel 15-0.2-100P before and after pyrolysis at 1000°C in N_2

This kind of phenomenon has already been observed previously for CAB aerogels [FiR 2007] and for other aerogels cross-linked by urethane bonds [Bie 1998, Koc 2005]. These aerogels have been seen to undergo a profound modification of the framework structure due to a partial fusion of the solid network during carbonization.

3.1.2. Micrographic Observation

Although the “blowing” effect caused by pyrolysis of CAB aerogels can be seen by the mere eye, the carbon aerogels’ surfaces seem to be at least partly even on SEM micrographs as can be seen the lower part of Figure III-3. Also visible on Figure III-3, is the difference between the even seeming surface (visible in the lower part of figure III-3) and the porous bulk of the carbon aerogel (visible in the upper part of figure III-3).

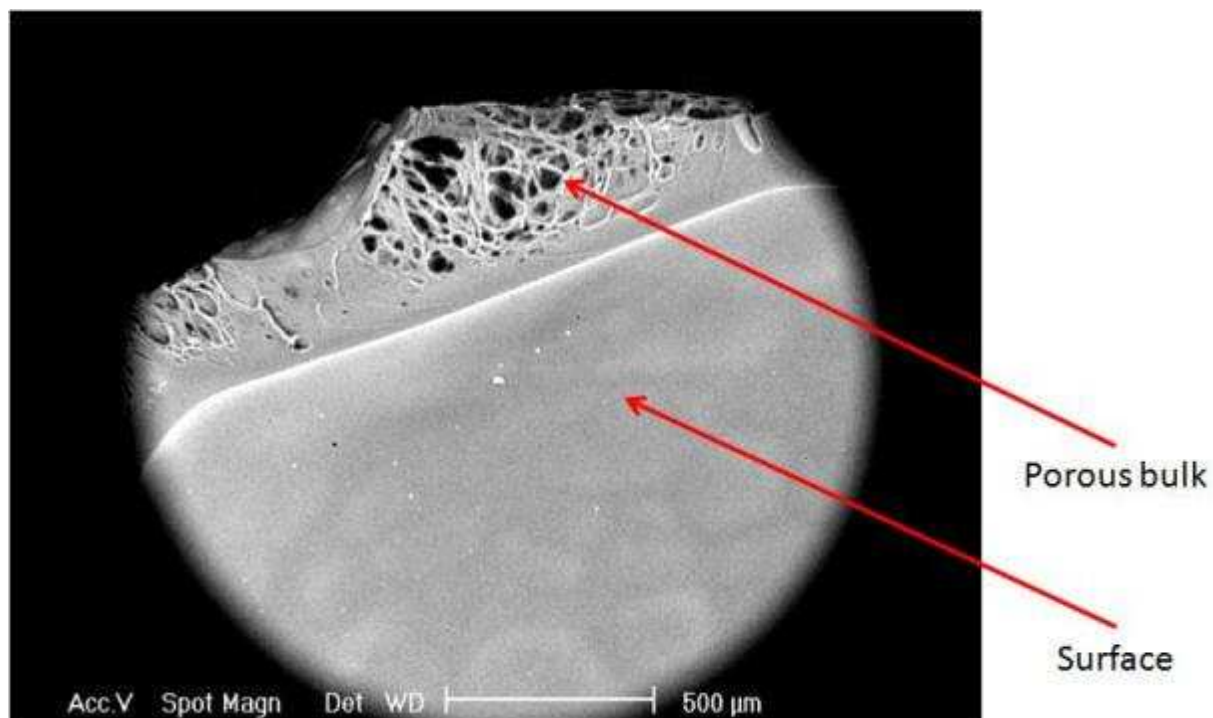


Figure III-3: SEM of carbon aerogel sample 15-0.2-1DA pyrolyzed at 900° N₂

Even though the surface of the CAB CA seems even and little porous, a close-up (figure III-4) reveals macropores ranging from several hundred nanometers to some micrometers.

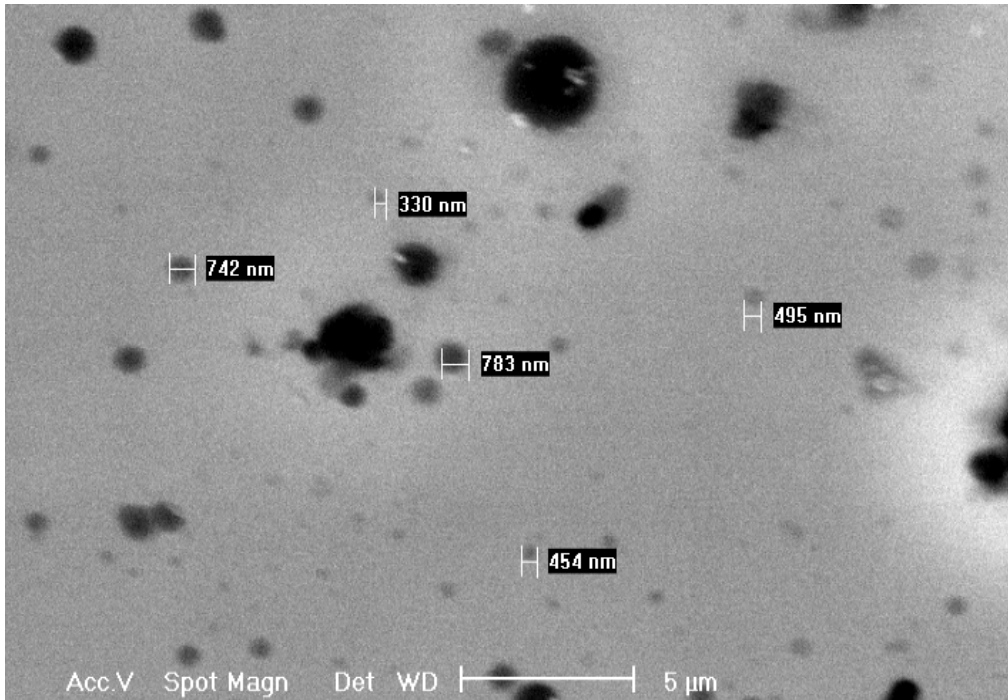


Figure III-4: SEM of the surface of carbon aerogel sample 15-0.2-1DA pyrolyzed at 900°C in N₂

The carbon aerogels' bulk, example to be seen in figure III-5, consists of thin walls also containing micrometer-sized pores.

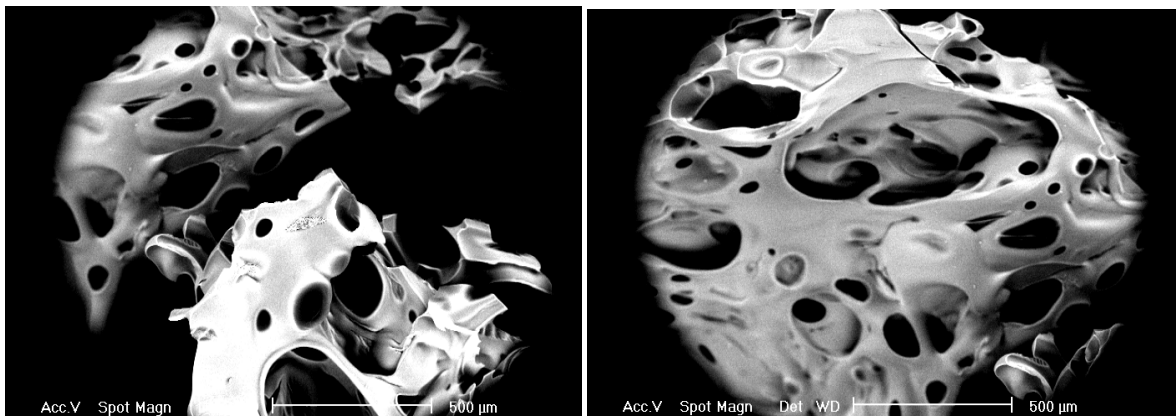


Figure III-5: SEM of the bulk of carbon aerogel sample 15-0.2-5DD pyrolyzed at 900°C in N₂

Typically, a high concentration of macropores can be found within the bulk of all CAB CA. Macropore walls, however, seem to be finely structured according to SEM and TEM observations of ground carbon aerogels (figures III-6 and III-7 respectively).

The carbon aerogel's solid skeleton seems to be composed of small pseudo-spherical aggregates having characteristic dimensions of approximately some tens of nanometers (see figures III-6 and III-7).

The magnification of a carbon grain, confirms the CAB CAs' quasi-amorphous character. No large graphitized areas can be distinguished (see figure III-8).

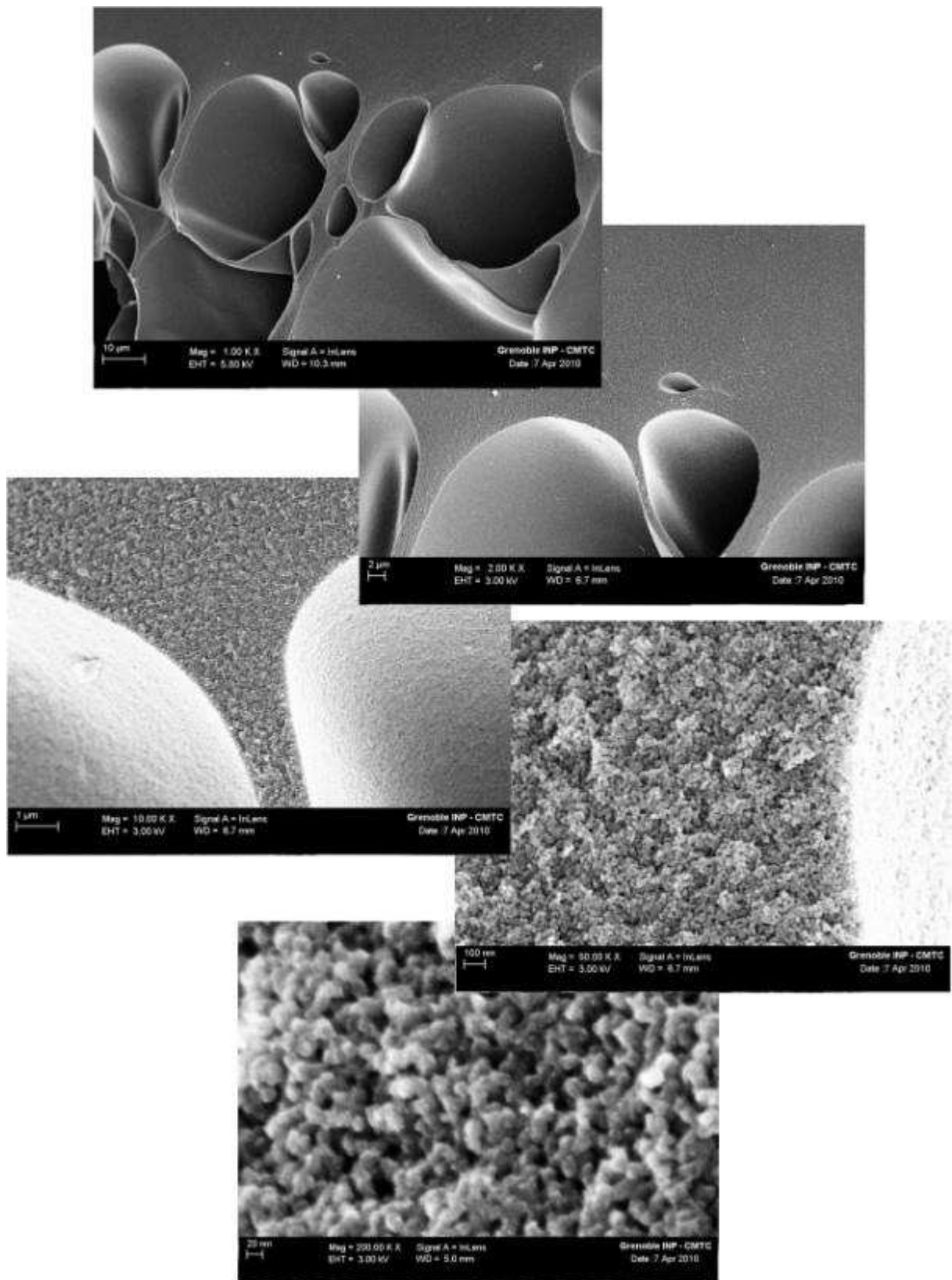


Figure III-6: SEM of the bulk of CAB CA sample 10-0.2-0.25DA pyrolyzed at 1000°C in N₂

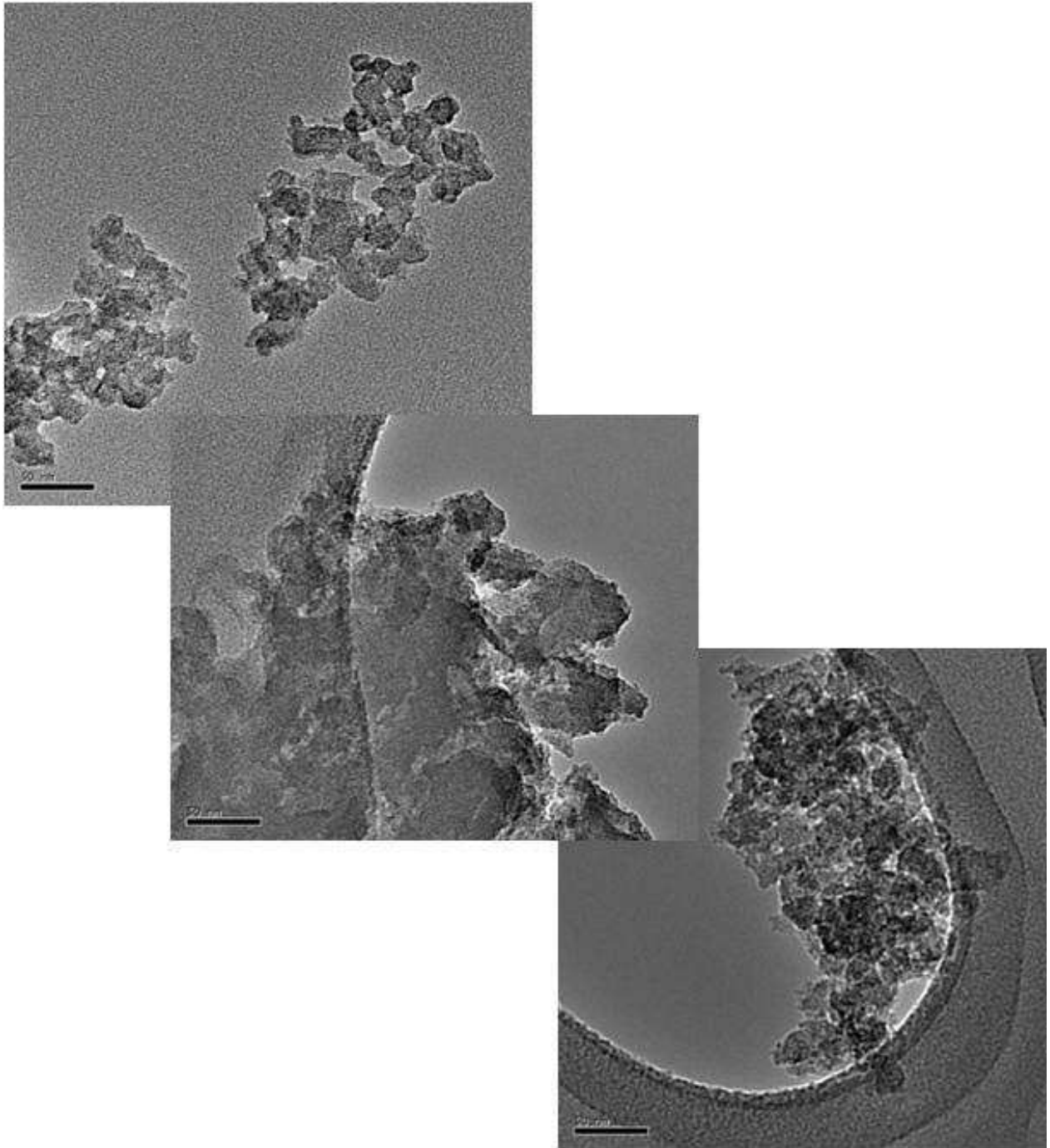


Figure III-7: TEM of carbon aerogel sample 15-0.2-1DA pyrolyzed at 1000°C in N₂ (courtesy of Dr. J. Rooke)

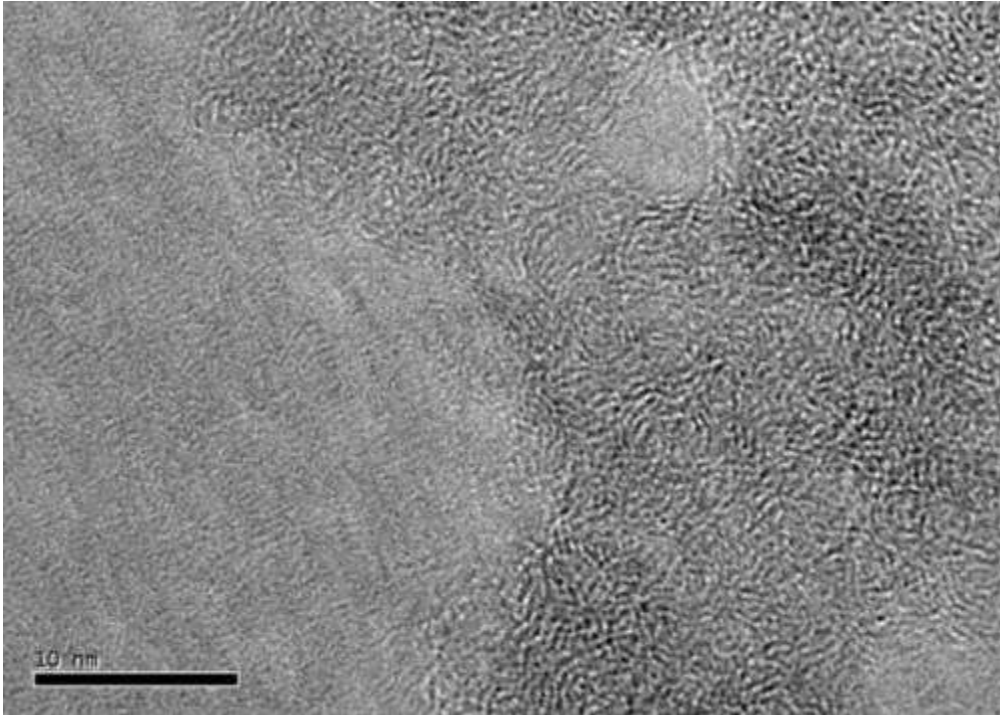


Figure III-8: TEM close-up of carbon aerogel sample 15-5-1DA pyrolyzed at 1000°C in N₂ (courtesy of Dr. J. Rooke)

3.1.3. Evolution of cellulose-acetate-based aerogels during pyrolysis

Thermal degradation behaviour of CAB aerogels differs completely from the behaviour observed for many other organic aerogels, often keeping their initial shape but shrink and therewith densify (*e.g.* in the case of RF-based, cellulose-based, and polyvinyl chloride-based aerogels [Gui 2008, Ish 2004, Yam 2003]). Cellulose diacetate is a thermoplastic polymer and melts before degradation. It possesses a melting temperature at around 235 °C, only some degrees below its' degradation temperature [Zug 2004]. Using DTA, figure III-9, Fischer found that the endothermic peak corresponding to the melting temperature of cellulose acetate at around 235 °C has also been visible for CAB aerogels [Fis 2006], but not so for pure cellulose. This observation already indicates that CAB materials also experiment melting during pyrolysis.

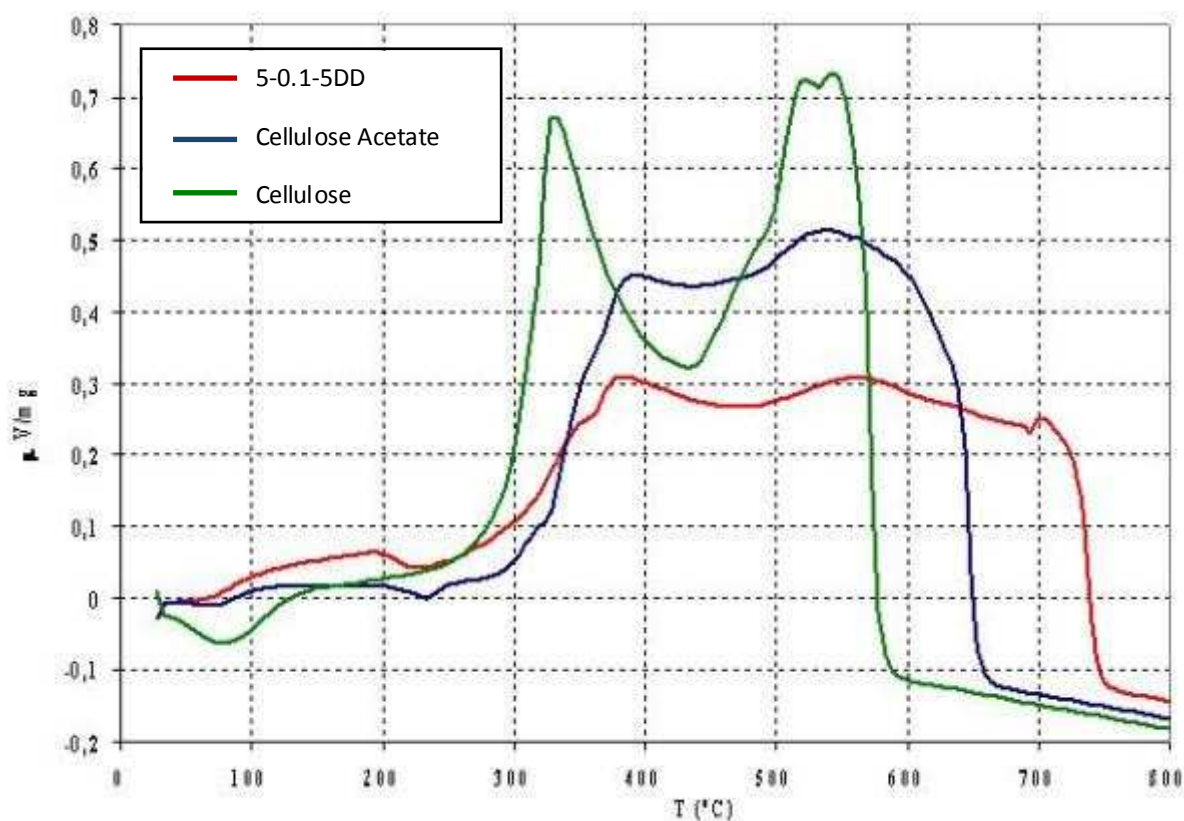


Figure III-9: DTA curves of cellulose, cellulose acetate, and cellulose-acetate-based aerogel 5-0.1-5DD [Fis 2006]

Thermogravimetric analysis in N_2 (figures III-10 and III-11 for a DD- and a DA-catalyzed aerogel, respectively) has borne out this assumption. The existence of reactions occurring at about 235 °C in the pyrolysis of CAB aerogels, corresponding approximately to the melting temperature of cellulose acetate, are confirmed by an endothermic peak. The abrupt rise of the curve beginning at about 270 °C and resulting in an exothermic peak, paralleling abrupt mass loss, corresponds to thermal degradation. Further, the heat flow stays positive but rather regular, pointing at an overall exothermic process, although pyrolysis of CAB aerogels begins as endothermic process (see figures III-10 and III-11). The formation of char has been found to be an exothermic process, whereas the formation of volatile compounds is endothermic (for the pyrolysis of cellulose) [Mil 1996]. During the pyrolysis of CAB aerogels, a gaseous fraction is formed in parallel to the solid carbonaceous fraction – endothermic and exothermic processes also seem to overlap. From the TGA results, hinting at an overall exothermic process, it can be assumed that the formation of volatile compounds is limited and char formation does outweigh the energetic balance over almost the entire period of pyrolysis.

Results from TGA for the DD-catalyzed sample, figure III-10, and the DA-catalyzed sample, figure III-11, are similar. The aerogels' behaviour during pyrolysis, like the mass loss, does not seem to be influenced by the catalyst type used in the sol-gel process. Neither TGA curve shows peaks due to a catalytic agent having been detained in the gel matrix.

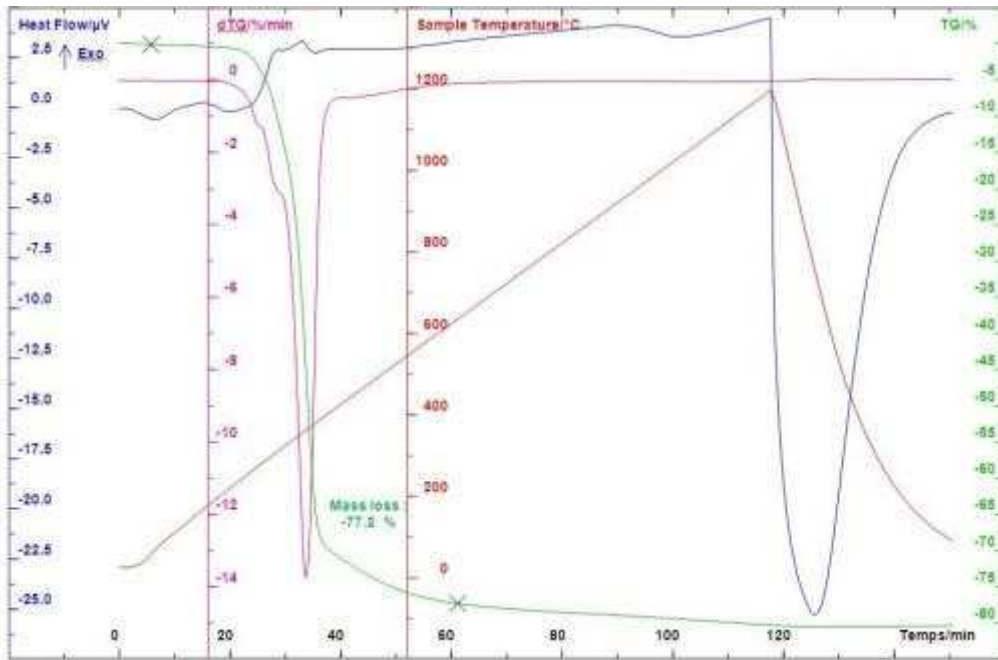


Figure III-10: TGA of aerogel sample 5-0.1-5DD

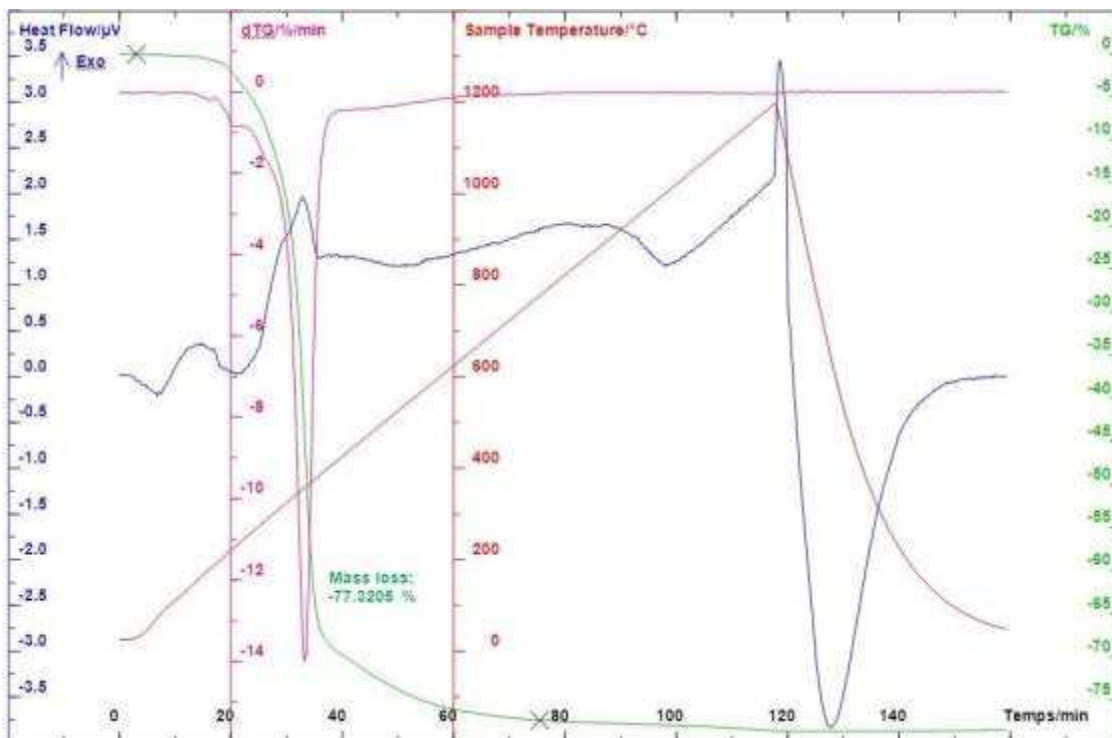


Figure III-11: TGA of aerogel sample 5-0.1-1DA

Another endothermic peak can be witnessed at some degrees below 100 °C, probably corresponding to the evaporation of water having been absorbed by the aerogel [Zug 2004]. CAB OA, as well as CAB CA, adsorb water during storage in ambient conditions which may be desorbed by heating the aerogel to moderate temperatures (*e.g.* 100 °C), as can be seen in table III-1. The mass loss of different OA (with a near-stoichiometric ratio of precursors) due to the elimination of water contained in the organic matrices is at 3%, whereas it amounts to 9% for their carbon counterpart.

CAB CA is able to take up more H₂O from air humidity than CAB OA and can thus be considered to be more hydrophilic.

Table III-1: CAB aerogel mass dependency on H₂O adsorption; Δm have been determined by comparison with the initial sample weight (stored in ambient conditions for 14 days)

	Δm_1	Δm_2	Δm_3
After:	+2 days	+7 days	+2 days
Conditions:	100 °C	25°C, 50% RH	100 °C
3-0.2-0.25DA	-3 wt. -%	3 wt. -%	-3 wt. -%
10-0.2-0.25DA	-3 wt. -%	3 wt. -%	-3 wt. -%
15-0.2-0.25DA	-3 wt. -%	3 wt. -%	-3 wt. -%
3-0.2-100P	-3 wt. -%	3 wt. -%	-3 wt. -%
10-0.2-100P	-3 wt. -%	3 wt. -%	-3 wt. -%
10-0.2-100P/1000 °C/N₂	-9 wt. -%	9 wt. -%	-9 wt. -%

Results from FTIR-IR gas spectroscopy analysis of the gases being emitted during TGA have confirmed results obtained by Fischer (see Table III-2). The endothermic peak at around 100 °C can effectively be attributed to the desorption of H₂O, while thermal degradation begins with the generation of CO₂ around 250 °C (see also figures III-10 and III-11), followed mainly by the evolution of other small carbon-containing molecules.

Table III-2: FTIR-IR analysis of TGA gases of cellulose-acetate-based aerogels (up to 1000 °C) [Fis 2006]

Gas species	Temperature range (± 5 °C)
Water - H₂O	Ambient temperature to 150 °C
Carbon dioxide - CO₂	255 to 1000 °C
Acetic acid - C₂H₄O₂	300 to 500 °C
N,N-dimethyl-1,4-phenylenediamine - C₈H₁₂N₂	310 to 330 °C
Carbon monoxide - CO	360 to 1000 °C
Methane - CH₄	410 to 755 °C
2,4-Dimethylaniline - C₈H₁₁N	470 to 590 °C
Ammonia - NH₃	480 to 840 °C

Thermal degradation of CAB aerogels leads to a partial gasification of the OA during heat treatment, releasing oxygen, nitrogen, hydrogen and carbon-based products. The generation of the gaseous carbon-containing compounds results in a partial loss of carbon due to the breaking of thermally instable chemical bonds. Therefore, the partial gasification of the CAB aerogel results in elevated mass losses, for example to a mass loss of around 77% between roughly 100 °C and 675 °C for aerogels 5-0.1-5DD and 5-0.1-1DA (see figures III-10 and III-11). The highest mass loss can be observed between 200 and 400 °C. This temperature range differs slightly from the temperature range observed by Biesmans et al. between 400 °C and 600 °C for aerogels cross-linked by urethane bonds [Bie 1998]. Evidently, the thermal degradation temperature depends on the aerogel precursor rather than on the type of cross-links.

The global mass loss Δm_{pyr} of CAB aerogels due to pyrolysis lies between the mass losses of the precursors cellulose acetate and MDI (see Table III-3). Experimental Δm_{pyr} for CAB aerogels is generally situated between 70% and 80% for temperatures around 1000 °C (see section 3.2 and 3.3 for more information), *i.e.* significantly higher than Δm_{th} , both for precursors and aerogels.

Table III-3: Real and theoretical mass loss of cellulose acetate, MDI, and CAB aerogel sample 10-0.2-0.25DA during pyrolysis (pyrolysis at 1000 °C in N₂, heating rate of 4°C/min)

	Δm_{pyr}	Δm_{th}
Cellulose acetate	92 wt.-%	51 wt.-%
PMDI	66 wt.-%	27 wt.-%
10-0.2-0.25DA	75 wt.-%	53 wt.-%

In conclusion, in the course of pyrolysis, CAB aerogels first undergo melting and subsequently thermal degradation (in the form of breaking thermally instable bonds leading to partial gasification of the aerogel). Gaseous degradation products seem to leak out from the melted CAB aerogel network in the form of bubbles, apparently inducing the formation of visible large macropores (see figures III-3 and III-5).

3.1.4. Evolution of the Surface Chemistry during Pyrolysis

CAB OA and CA sample 10-0.2-0.25DA have been examined by FTIR in order to understand the evolution of the chemical groups during carbonisation. The spectral features of the CAB OA include both the cellulose acetate and MDI bands (figure III-12). The bands at 1045, 1160 and 1230 cm⁻¹ correspond to C-O glucose links, involving C-O-C stretching in the pyranose rings. The presence of C=O acetate groups is reflected by the presence of the peaks at 1740 and 1640 cm⁻¹, corresponding to the symmetric and asymmetric modes of C=O stretching, respectively. CH bonds give rise to the peaks at 2927, 2855 (C-H aliphatic stretch) and 1375 cm⁻¹ (deformation mode of CH bond). Aromatic cycles of PMDI account for the peaks present at 880, and 3030 cm⁻¹, corresponding to the CH out-of-plane deformations in aromatic rings and =C-H stretching modes, respectively. The presence of distinct peaks at 1512 and 1530 cm⁻¹ corresponds to urethane bonds, confirming that a reaction has taken place between cellulose acetate and PMDI. Peaks at 3490 and 3368 cm⁻¹ are associated with the free and chemically bonded NH group, respectively. The lack of a peak at 2265 cm⁻¹ in the spectrum of the organic aerogel indicates that all isocyanate N=C=O groups of the PMDI have reacted with oxygen groups of cellulose.

The FTIR spectrum of a CAB CA pyrolyzed at 600 °C and at 1000 °C in N₂ is also shown in figure III-12. At 600 °C, peaks at 1740, 1230 and 1046 cm⁻¹ corresponding to the C=O, C-O-C and C-O structures, disappear. This indicates that the most prominent process accompanying the carbonisation of the cellulosic aerogel is the degradation of the oxygen functionalities. Simultaneously, a decrease in the intensity of the aliphatic 2860-2960 cm⁻¹ band and the emergence of an aromatic peak at 3050 cm⁻¹ indicate the dehydrogenation and aromatisation of the structure. The appearance of very intense peaks at 1600 and 1440 cm⁻¹, corresponding to the C=C and C=N containing rings, also confirms that aromatisation is taking place. The peaks at 760, 805 and 875 cm⁻¹ are attributed to hydrogen atoms in the aromatic rings of different degree of substitution (four neighbouring H, two and one free atom of hydrogen in aromatic ring, respectively). Since the intensity of the peaks increases in the order 875

< 805 < 760, it may be concluded that for CAB CA pyrolyzed at 600 °C a major part of the carbon aerogel's structure is involved in less condensed heteroaromatic rings.

Thermal treatment of the CAB aerogel at a temperature of 1000°C leads to a further degradation of oxygen functionalities, confirmed by the disappearance of the peak at 1045 cm⁻¹. Moreover, hydrogen from the aromatic rings is released according to the disappearance of the peaks at 760 and 805 cm⁻¹.

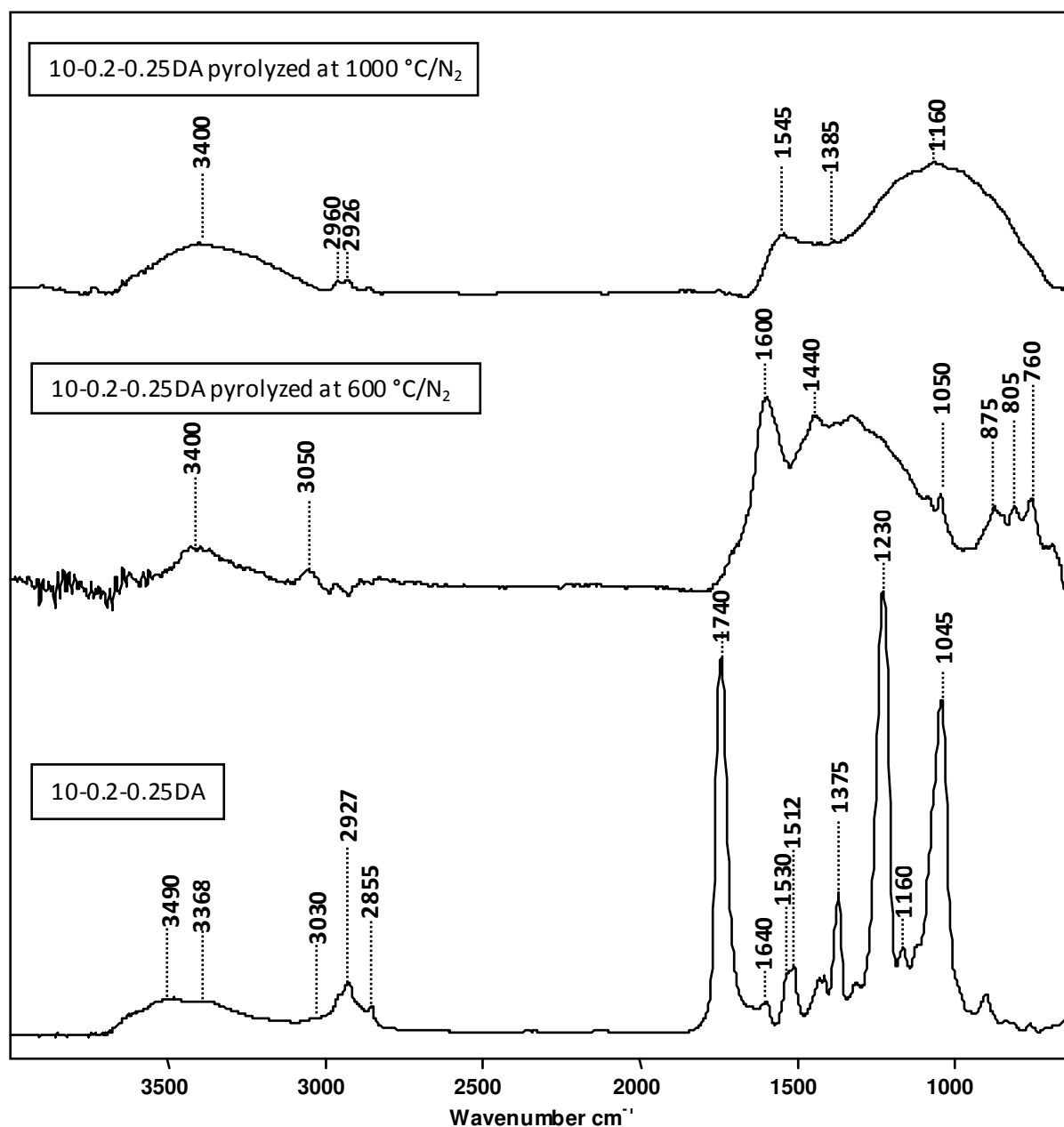


Figure III-12: Evolution of chemical functionalities on thermal treatment of the organic aerogel analyzed by FTIR

3.1.5. Skeletal Density

Skeletal densities of DA- and P-catalyzed carbon aerogels have been determined by He pycnometry (see Table III-4). Skeletal density is about 2.1 g/cm³ for both carbon aerogels analyzed. A dependence on the catalyst cannot be observed.

Table III-4: Skeletal density of organic and cellulose aerogels (pyrolyzed at 1000 °C in N₂) as determined by He pycnometry

Skeletal density (g/cm ³)	10-0.2-0.25DA	10-0.2-100P
Organic Aerogel	1.30	1.26
Carbon Aerogel (1000 °C/N₂)	2.14	2.11

3.1.6. Reproducibility of the Carbon Aerogel Preparation

As the solid network of the CAB OA melts during pyrolysis and “bubbling” takes place, the reproducibility of CAB CA structures is questionable. Therefore, I have carried out a study on the reproducibility of a representative CAB aerogel sample 10-0.2-0.25DA. Three organic samples of this formulation have been synthesized, dried in supercritical CO₂, and subsequently pyrolyzed at 1000 °C in N₂. Results of structural analysis for these six samples may be seen in table III-5.

Table III-5: Study of reproducibility for CAB OA and CA on the example of samples 10-0.2-0.25DA

DA-catalyzed aerogels			OA 10-0.2-0.25DA			CA 10-0.2-0.25DA (1000 °C/N ₂)		
			OA 1	OA 2	OA 3	CA 1	CA 2	CA 3
ρ_b	[g/cm ³]	± 0,02	0,90	0,76	0,81	0,13	0,18	0,18
ε		± 0,05	0,29	0,41	0,37	0,94	0,91	0,91
V_{SP}	[cm ³ /g]	± 0,05	0,33	0,54	0,46	7,10	5,05	4,99
V_{Hg}	[cm ³ /g]	± 0,02	0,38	0,56	0,52	5,67	4,84	4,60
% V_{Hg}	[%]	± 1	117%	104%	112%	80%	96%	92%
V_{BJH}	[cm ³ /g]	± 0,02	0,36	0,24	0,35	0,39	0,33	0,32
% V_{BJH}	[%]	± 1	111%	44%	77%	5%	7%	6%
S_{BET}	[m ² /g]	± 10	141	97	122	252	240	250
V_μ	[cm ³ /g]	± 0,01	0	0	0	0,05	0,05	0,06
L_{Hg}	[nm]	± 1	13	11	14	15	14	15
L_{BJH}	[nm]	± 1	11	9	12	12 & 22	12 & 14	12 & 18

The reproducibility study for CAB OA and CA on the example of sample 10-0.2-0.25DA shows clearly that sol-gel synthesis of CAB aerogels is very sensitive. The three different OA samples of the same formulation display densities, porous volumes, specific surface areas, and mean pore sizes approximately in the same range, but are nevertheless subject to variation. CA counterparts, however, present similar structural features.

3.2. Influence of the pristine Organic Aerogel

The influence of different CAB OA on the CAB CA resulting from pyrolysis in terms of structure and composition is analyzed and discussed.

Aerogels of 3, 10, and 15 %CA and a ratio I/CA of 1, 0.1, and 0.2 have been synthesized using different catalysts (DD, DA, or P). All CAB OA have been pyrolyzed at 900 °C in N₂. Additionally, CAB xerogels (see chapter II.3.2.2) have been pyrolyzed at 1000 °C and compared to their CA homologue.

3.2.1. Influence of Organic Aerogel Structure on the Carbon Aerogel Structure

The results of structural analysis for aerogels catalyzed by DD, DA, and P can be seen in tables III-6, III-7, and III-8, respectively. Carbon xerogel structural characteristics before and after pyrolysis at 1000 °C in N₂ can be seen in table III-9.

Mass losses increase with decreasing I/CA (see tables III-6, III-7, and III-8). This tendency is in accordance with theoretically expected mass losses and at the same time bears out a conclusion of F. Fischer [Fis 2006] on an existing influence of sol composition onto Δm_{pyr} during pyrolysis.

The aerogel structure changes during pyrolysis due to the combined effect of melting and thermal degradation, *i.e.* bubbling. However, carbonization of CAB OA results in the creation of porous and nanostructured carbon material, even for CAB organic xerogels being very dense and nearly not porous.

No direct, clear dependency of the CAB CA structure on its precursor OA stand, but some general tendencies seem to exist and are summarized below.

CA are frequently less dense than their organic counterparts (note that exceptions occur notably at 3 %CA). Bulk densities ρ_b for CAB CA range from 0.09 g/cm³ to 1.26 g/cm³. Porosities lie between 0.40 and 0.96, with lowest ϵ generally found for an I/CA of 1.

Specific porous volumes determined by Hg porosimetry V_{Hg} tend to increase during pyrolysis (with exceptions mostly found at 3 %CA) and are between 0.17 and 10.9 cm³/g, representing usually at least 80 % of the total specific porous volume ($\%V_{\text{Hg}} \in [53\% ; 99\%]$). This behaviour is mainly due to the “bubbling” phenomenon, occurring during pyrolysis. V_{BJH} decrease mostly during pyrolysis, reaching values as low as 0.02 for aerogels of an I/CA of 1. On the other hand, some microporosity is usually generated in the course of pyrolysis ($V_{\text{t-plot}}$ of up to 0.08 cm³/g for CAB CA as compared to 0 cm³/g for all CAB OA). Meso- and micropore volumes make up a non-negligible but small part (often roughly around 0.35 to 0.40 cm³/g and significantly less than 0.1, respectively) of the overall specific pore volume V_{sp} (as high as 11.2 cm³/g). N₂ adsorption describes only a very small percentage of the porosity ($\%V_{\text{BJH}} \in [1\% ; 13\%]$ and $V_{\text{t-plot}}$ almost negligible). Clearly, in most cases, Hg porosimetry describes almost the entire porosity whereas N₂ adsorption only covers a minor part of the porosity (see figures III-13 and III-14 for an example of results from Hg porosimetry and N₂ adsorption on CAB CA, respectively). Accordingly, the highest fraction of the specific pore volume is made up of macropores being generated during pyrolysis. This is particularly obvious for carbon xerogels having been nearly non-porous before pyrolysis but featuring higher V_{Hg} than their aerogel homologues after pyrolysis. However, the carbon xerogels' V_{BJH} and $V_{\text{t-plot}}$ are lower than that of their aerogel homologues.

Specific surface areas s_{BET} increase in most cases during pyrolysis and range from approximately 215 to 430 m²/g for aerogels. Carbon xerogel s_{BET} are lower than that of their aerogel homologues, *i.e.*

between 100 and 150 m²/g which is approximately half of the aerogels' s_{BET} . The increase of s_{BET} during pyrolysis might partly be explained by an increase in microporosity.

Table III-6: Structure of organic aerogels and their carbon counterparts depending on %CA and I/CA for DD-catalyzed gels pyrolyzed at 900 °C in N₂

DD-catalyzed aerogels			3-1-5DD	3-0.2-5DD	3-0.1-5DD	10-1-5DD	10-0.2-5DD	10-0.1-5DD	15-1-5DD	15-0.2-5DD	15-0.1-5DD
Organic aerogels											
ρ_b	[g/cm ³]	±0,02	0,28	0,18	0,27	1,13	0,38	0,20	0,88	0,56	0,37
V_{Hg}	[cm ³ /g]	±0,02	0,94	4,04	2,96	0,14	1,92	4,15	0,36	1,00	1,94
V_{BJH}	[cm ³ /g]	±0,02	0,85	1,65	0,35	0,07	1,85	0,81	0,33	0,87	1,37
S_{BET}	[m ² /g]	±10	220	242	140	43	353	250	182	249	215
L_{Hg}	[nm]	±1	13	34	19	9	23	30	11	13	22
L_{BJH}	[nm]	±1	5	4	4	5	28	5	7	18	52
Carbon aerogels											
Δm	[%]	±0,5	71	78	85	71	76	81	72	76	81
ρ_b	[g/cm ³]	±0,02	- ^{b)}	0,26	0,31	0,83	0,20	0,09	1,26	0,38	0,10
ϵ		±0,05	- ^{b)}	0,88	0,85	0,61	0,91	0,96	0,40	0,82	0,95
V_{SP}	[cm ³ /g]	±0,05	- ^{b)}	3,40	2,77	0,73	4,63	11,22	0,32	2,18	9,23
V_{Hg}	[cm ³ /g]	±0,02	- ^{b)}	2,99	2,22	0,59	4,42	10,90	0,17	1,84	8,73
% V_{Hg}	[%]	±1	- ^{b)}	88%	80%	80%	96%	97%	53%	85%	95%
V_{BJH}	[cm ³ /g]	±0,02	0,04	0,29	0,24	0,02	0,50	0,58	0,03	0,29	0,38
% V_{BJH}	[%]	±1	- ^{b)}	9%	9%	3%	11%	5%	9%	13%	4%
V_{t-plot}	[cm ³ /g]	±0,01	0,00	0,02	0,03	0,00	0,08	0,04	0,00	0,05	0,03
S_{BET}	[m ² /g]	±10	- ^{a)}	238	236	- ^{a)}	398	427	- ^{a)}	265	277
L_{Hg}	[nm]	±1	5	34	6	50	14	10	140	11	9
L_{BJH}	[nm]	±1	5	5	5	4	4	5	3	4	4

^{a)} Active surface values below detection limits

^{b)} Analysis has not been carried out due to lack of sufficient material

Table III-7: Structure of organic aerogels and their carbon counterparts depending on %CA and I/CA for DA-catalyzed gels pyrolyzed at 900 °C in N₂

DA-catalyzed aerogels			3-1-1DA	3-0.2-1DA	3-0.1-1DA	10-1-1DA	10-0.2-1DA	10-0.1-1DA	15-1-1DA	15-0.2-1DA	15-0.1-1DA
Organic aerogels											
ρ_b	[g/cm ³]	±0,02	0,50	0,39	0,38	1,04	0,73	0,47	1,14	0,82	0,68
V_{Hg}	[cm ³ /g]	±0,02	1,24	1,92	1,89	0,19	0,61	1,35	0,12	0,44	0,75
V_{BJH}	[cm ³ /g]	±0,02	1,13	1,66	0,69	0,16	0,62	0,87	0,03	0,33	0,50
S_{BET}	[m ² /g]	±10	290	257	113	137	217	225	- ^{a)}	146	173
L_{Hg}	[nm]	±1	16	15	13	9	13	19	9	13	16
L_{BJH}	[nm]	±1	4	-	50	5	11	16	38	7	12
Carbon aerogels											
Δm	[%]	±0,5	70	78	80	69	76	79	68	77	78
ρ_b	[g/cm ³]	±0,02	0,19	0,18	0,24	0,44	0,25	0,27	0,26	0,18	0,23
ϵ		±0,05	0,91	0,92	0,89	0,79	0,88	0,87	0,88	0,91	0,89
V_{SP}	[cm ³ /g]	±0,05	4,87	5,17	3,67	1,81	3,52	3,21	3,38	5,11	3,82
V_{Hg}	[cm ³ /g]	±0,02	4,37	4,73	3,22	1,67	3,25	2,95	3,03	4,93	3,49
% V_{Hg}	[%]	±1	90%	91%	88%	92%	92%	92%	90%	96%	91%
V_{BJH}	[cm ³ /g]	±0,02	0,03	0,39	0,31	0,03	0,33	0,39	0,39	0,42	0,36
% V_{BJH}	[%]	±1	1%	8%	8%	1%	9%	12%	11%	8%	9%
V_{t-plot}	[cm ³ /g]	±0,01	0,00	0,08	0,01	0,00	0,05	0,01	0,03	0,07	0,03
S_{BET}	[m ² /g]	±10	- ^{a)}	423	220	- ^{a)}	278	300	299	356	310
L_{Hg}	[nm]	±1	-	34	7	-	8	9	-	14	10
L_{BJH}	[nm]	±1	4	5	5	4	4	5	5	4	5

^{a)} Active surface values below detection limits

Table III-8: Structure of organic aerogels and their carbon counterparts depending on %CA and I/CA for P-catalyzed gels pyrolyzed at 900 °C in N₂

P-catalyzed aerogels			3-1-25P	3-0.2-25P	3-0.1-25P	10-1-25P	10-0.2-25P	10-0.1-25P	15-1-25P	15-0.2-25P	15-0.1-25P
Organic aerogels											
ρ_b	[g/cm ³]	±0,02	0,45	0,16	0,14	1,17	0,62	0,35	1,21	0,87	0,56
V _{Hg}	[cm ³ /g]	±0,02	1,42	5,20	6,04	0,11	0,85	2,03	0,08	0,39	1,06
V _{BJH}	[cm ³ /g]	±0,02	1,31	0,99	1,36	0,03	1,04	1,36	0,04	0,34	0,81
S _{BET}	[m ² /g]	±10	264	204	200	- ^{a)}	346	272	- ^{a)}	162	260
L _{Hg}	[nm]	±1	17	34	37	9	17	22	7.5	12	18
L _{BJH}	[nm]	±1	28	3	28	4	12	32	4	7	14
Carbon aerogels											
Δm	[%]	±0,5	68	83	80	70	80	80	67	76	78
ρ_b	[g/cm ³]	±0,02	0,60	0,18	0,23	1,06	0,12	0,13	0,71	0,18	0,20
ϵ		±0,05	0,72	0,92	0,89	0,50	0,94	0,94	0,66	0,91	0,91
V _{SP}	[cm ³ /g]	±0,05	1,20	5,14	3,80	0,47	7,59	6,99	0,93	5,05	4,55
V _{Hg}	[cm ³ /g]	±0,02	1,03	4,70	3,37	0,34	7,54	6,67	0,81	4,81	4,14
% V _{Hg}	[%]	±1	86%	91%	89%	71%	99%	95%	87%	95%	91%
V _{BJH}	[cm ³ /g]	±0,02	0,04	0,39	0,39	0,03	0,39	0,36	0,07	0,35	0,46
% V _{BJH}	[%]	±1	3%	8%	10%	6%	5%	5%	8%	7%	10%
V _{t-plot}	[cm ³ /g]	±0,01	0,00	0,07	0,01	0,00	0,04	0,01	0,00	0,03	0,02
S _{BET}	[m ² /g]	±10	- ^{a)}	398	261	- ^{a)}	307	268	- ^{a)}	215	319
L _{Hg}	[nm]	±1	-	10	10	-	11	8	-	12	9
L _{BJH}	[nm]	±1	4	4	4	4	4	4	3	14	4

^{a)} Active surface values below detection limits

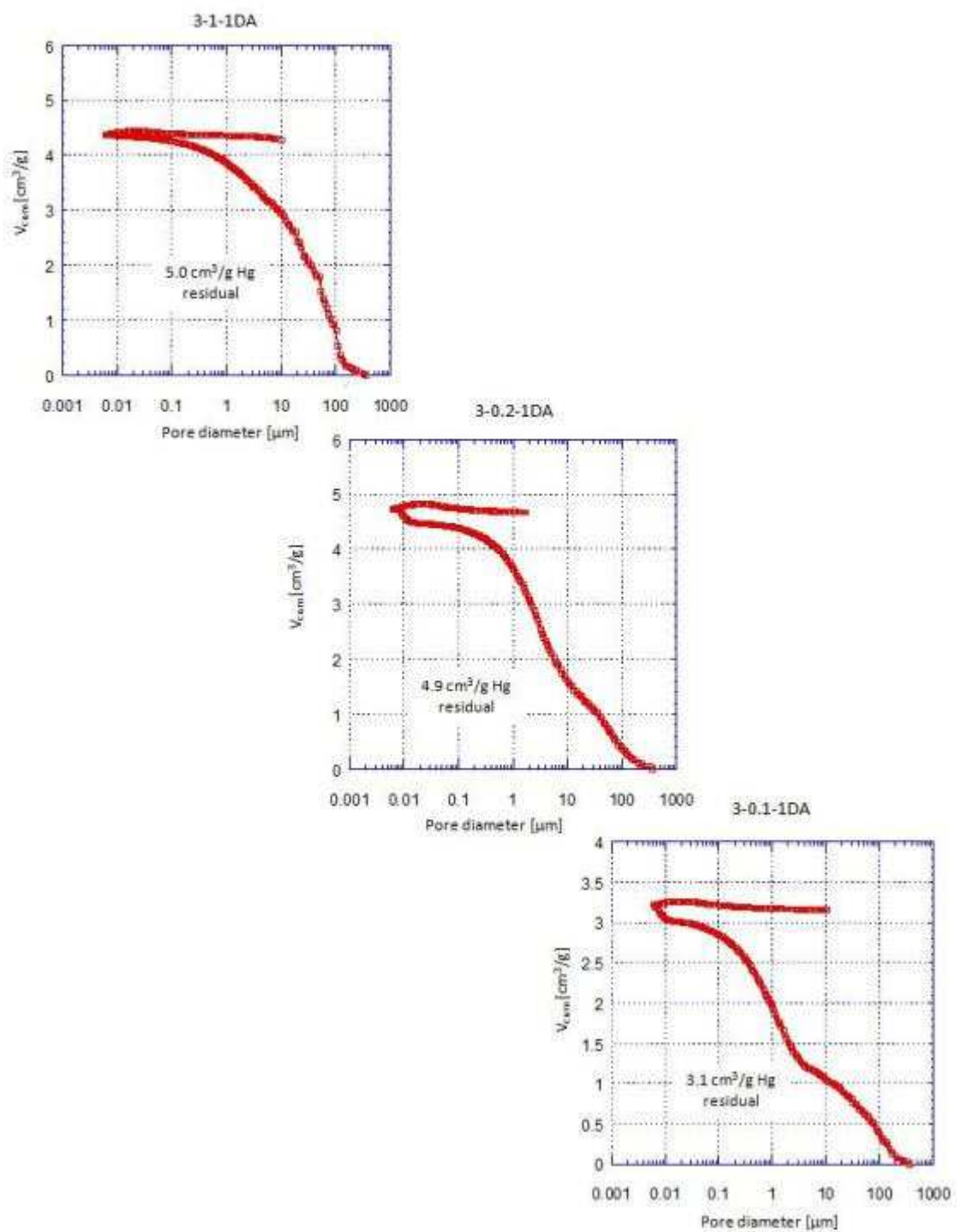


Figure III-13: Cumulative intruded pore volume as a function of pore size obtained by Hg porosimetry for carbon samples 3-1-1DA, 3-0.2-1DA, and 3-0.1-1DA pyrolyzed at 900 °C in N_2

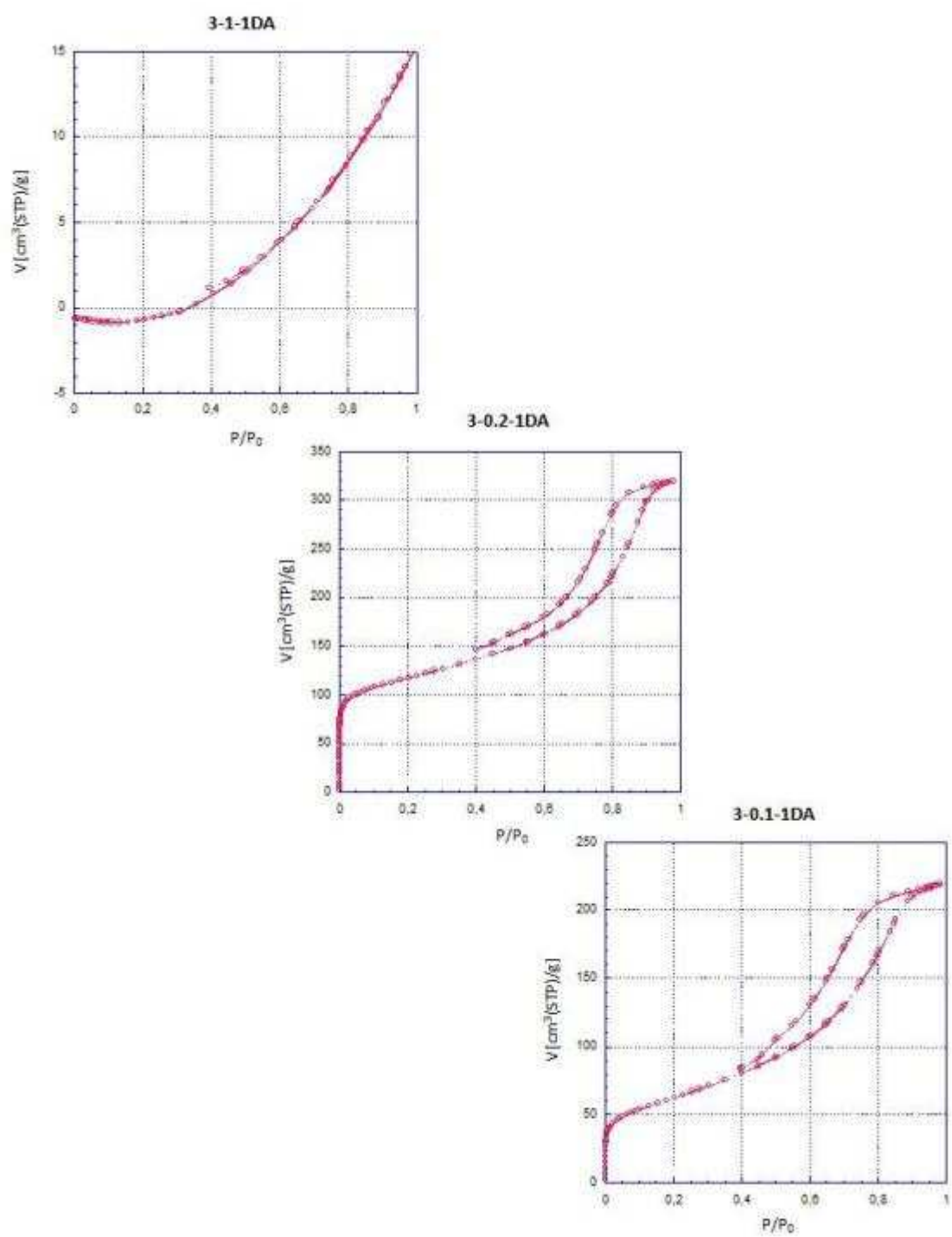


Figure III-14: N_2 adsorption isotherms for carbon samples 3-1-1DA, 3-0.2-1DA, and 3-0.1-1DA pyrolyzed at 900 °C in N_2

Table III-9: Structure of organic aerogels and xerogels and their carbon counterparts depending pyrolyzed at 1000 °C in N₂

			3-5-0.25DA	3XS	3XM	3XL	10-5-0.25DA	10XS	10XM	10XL
Organic samples										
ρ_b	[g/cm ³]	±0,02	0,49	1,27	1,29	1,27	0,80	1,31	1,26	1,28
V_{Hg}	[cm ³ /g]	±0,02	1,20	0,03	0,03	0,03	0,51	0,03	0,03	0,03
V_{BJH}	[cm ³ /g]	±0,02	0,77				0,39			
S_{BET}	[m ² /g]	±10	179				171			
L_{Hg}	[nm]	±1	12				13			
L_{BJH}	[nm]	±1	5				11			
Carbon samples										
ρ_b	[g/cm ³]	±0,02	0,19	0,13	0,21	0,15	0,29	0,18	0,10	0,12
ϵ		±0,05	0,91	0,94	0,90	0,93	0,86	0,92	0,95	0,94
V_{SP}	[cm ³ /g]	±0,05	4,90	7,22	4,31	6,37	2,98	5,14	9,14	7,93
V_{Hg}	[cm ³ /g]	±0,02	4,49	7,15	4,04	5,88	2,73	5,07	8,86	7,56
% V_{Hg}	[%]	±1	92%	99%	94%	92%	91%	99%	97%	95%
V_{BJH}	[cm ³ /g]	±0,02	0,35	0,30	0,27	0,29	0,35	0,31	0,30	0,29
% V_{BJH}	[%]	±1	7%	4%	6%	5%	12%	6%	3%	4%
V_{t-plot}	[cm ³ /g]	±0,01	0,05	0,00	0,00	0,00	0,03	0,00	0,00	0,01
S_{BET}	[m ² /g]	±10	275	123	103	120	237	134	138	142
L_{Hg}	[nm]	±1	12	13	13	11	11	12	10	10
L_{BJH}	[nm]	±1	11	9	9	9	4	9	8	8

During pyrolysis, CAB aerogels display a behavior similar to other aerogels samples cross-linked by urethane bonds. Although CAB aerogels tend to become lighter in the process of pyrolysis, studies on other organic aerogels found that mass loss is inclined to bring about a densification of the aerogel [Koc 2005]. Polyurethane aerogels by Biesmans et al. [Bie 1998], for example, tripled their density during pyrolysis at 600 °C. Due to densification macroporous volumes are often prone to decrease, as are pore sizes in general [Tam 1998, Boc 1998]. This comparison shows that the use of a macromolecular polyester like cellulose acetate (instead of monomeric polyols) has a certain influence on the resulting CA's structure.

At the same time microporosity is known to emerge [Boc 1998, Ish 2004] at increasing temperatures up to a temperature above which open porosity closes [Rei 1998]. An increasing amount of micropores would increase specific surface areas, as is the case for CAB CA. Nonetheless, for polyurethane aerogels, Biesmans et al. [Bie 1998] found microporosity to increase at temperatures above 400 °C, but at the same time s_{BET} to decrease by more than two-thirds for a pyrolysis temperature of 800 °C. Therefore, it is quite possible, that CAB aerogels pyrolyzed at temperatures below 900 °C might feature specific surface areas even higher than those to be found tables III-6 to III-8. The influence of the pyrolysis temperature on the aerogels' structure is further explored and discussed in section 3.3.

3.2.2. Influence of Organic Aerogel Composition on Carbon Aerogel Composition

The elemental composition of organic and carbon aerogels pyrolyzed at 900 °C in N₂ has been determined (see Table III-10).

Table III-10: Composition of DA- and P-catalyzed organic and carbon aerogels (pyrolyzed at 900 °C in N₂)

	3-0.2-0.25DA	3-0.2-0.25DA 900 °C/N₂	3-0.2-100P	3-0.2-100P 900 °C/N₂
C [wt.-%]	52.9	88.3	52.3	87.2
H [wt.-%]	5.6	0.4	5.6	0.9
O [wt.-%]	39.5	2.9	39.4	6.1
N [wt.-%]	1.8	3.5	1.6	3.6
Total [wt.-%]	99.8	95.1	98.9	97.8

The carbon content of CAB aerogels pyrolyzed at 900 °C in N₂ is about 90 wt.-% for all samples. A fair concentration of heteroatoms (oxygen and nitrogen) persists in the carbonaceous matrix after pyrolysis, as a comparison between aerogels before and after pyrolysis shows. The (high) content in heteroatoms is a particularity of carbons obtained from the pyrolysis of an organic material. The oxygen content in the CA is about 5 wt.-%, *i.e.* reduced by about 80 % as compared to the OA. Similarly, the majority of hydrogen is released during carbonization. This observation also suggests that two main degradation reactions, accompanying the rupture of the cellulosic units, occur: the decomposition of oxygen groups and dehydrogenation/aromatization of the structure. In contrast, the nitrogen content is higher for CA than for OA samples, which indicates that nitrogen atoms introduced with the MDI molecules are partly retained in the structure of the final pyrolyzed carbon material.

The total of the elements C, H, O, and N contained in CAB aerogels before and after pyrolysis differs, *i.e.* decreases. For one part this difference may be caused by the error of the analysis device (see chapter II.2) and the fact that C, H, and N quantities on the one hand and O quantities, on the other hand, are measured in two different experiments. However, the total of these four elements being lower for CA than for OA might hint at an uptake of impurities during the pyrolysis process.

Tin traces have been detected in DD-catalyzed organic aerogels (see chapter II.3). According to F. Fischer, these tin trace persist in corresponding carbon aerogels and make up as much as 3 % of the carbons [Fis 2006]. As tin content may be detrimental to numerous applications in electrochemical energy storage and conversion and due to the fact that DD is a toxic agent, DD-containing gels have not been examined more closely in the following part of this work.

3.3. Influence of Pyrolysis Parameters

DA- and P-catalyzed CAB aerogels have been pyrolyzed at different temperatures in different inert atmospheres to investigate the influence of (i) the pyrolysis temperature T_{\max} and (ii) the pyrolysis atmosphere on the aerogel structure and composition.

3.3.1. Influence on Carbon Aerogel Structure

DA- and P-catalyzed CAB aerogels of near-stoichiometric precursor concentration have been pyrolyzed at 900 °C, 1000 °C, and 1100 °C in N₂. Additionally, DA-catalyzed CAB aerogels have been pyrolyzed in Ar. The nanostructures of the resulting CA have been compared to the OA precursor.

Mass loss appears to increase slightly with pyrolysis temperature (see Tables III-11, III-12, and III-13 for a comparison of DA- and P-catalyzed aerogels pyrolyzed in N₂ at 3 %CA, 10 %CA, and 15 %CA, respectively, and tables III-14, III-15, and III-16 for DA-catalyzed aerogels pyrolyzed in N₂ and Ar at 3 %CA, 10 %CA, and 15 %CA, respectively).

Bulk density ρ_b does not appear to depend on maximum pyrolysis temperature nor on pyrolysis atmosphere. Generally, P-catalyzed CA feature lower ρ_b than DA-catalyzed CA (between 0.11 and 0.21 g/cm³ and 0.19 and 0.37 g/cm³, respectively). Accordingly, ϵ and V_{Hg} are somewhat higher for P-catalyzed CA (between 0.9 and 0.95 and 4.3 to 8.5 cm³/g for ϵ and V_{Hg} , respectively) than for DA-catalyzed CA (between 0.8 and 0.9 and 1.8 to 4.5 cm³/g for ϵ and V_{Hg} , respectively). % V_{Hg} are relatively close to 100%, particularly for P-catalyzed CA. However, neither of these parameters seems to depend on T_{max} nor on the type of inert pyrolysis atmosphere. Mesoporous volumes V_{BJH} are basically very similar for all samples, varying only between 0.25 and 0.45 cm³/g. % V_{BJH} are all below 16%, indicating that the specific pore volume in all CAB CA is mainly controlled by the macropores volume.

Microporosity is created during pyrolysis, but V_{t-plot} stay relatively low for most samples (*i.e.* mostly significantly lower than 0.2 cm³/g). Unlike macro- and mesoporous volumes, however, the microporous volume shows a tendency to decrease with increasing T_{max} (see for example figure III-15).

CAB CA feature a large range of specific surface areas between around 160 and 500 m²/g. L_{BJH} lie almost uniformly in the small mesopore range around 5 nm, with some exceptions around 10 nm.

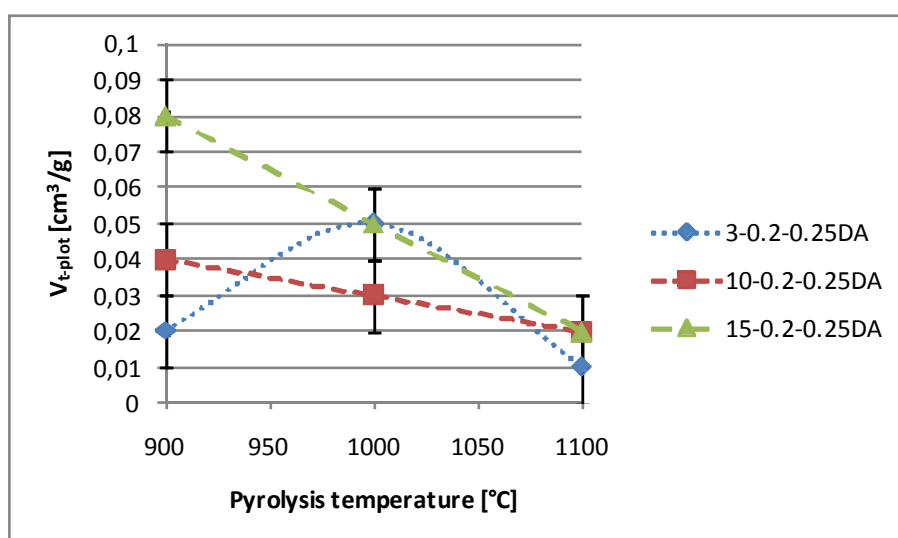


Figure III-15: Evolution of V_{t-plot} with T_{max} for DA-catalyzed aerogels pyrolyzed in N₂

Table III-11: Structural characteristics of CAB aerogels 3-0.2-0.25DA and 3-0.2-100P if pyrolyzed at different temperatures in N₂

	3-0.2-0.25DA			3-0.2-100P					
	OA	CA - pyrolysis in N ₂			OA	CA - pyrolysis in N ₂			
		900 °C	1000 °C	1100 °C		900 °C	1000 °C	1100 °C	
Δm [%]	$\pm 0,5$	74,5	76	77		74	74,5	79	
ρ_b [g/cm ³]	$\pm 0,02$	0,49	0,21	0,19	0,33	0,16	0,12	0,14	0,12
ϵ	$\pm 0,05$	0,62	0,90	0,91	0,84	0,88	0,94	0,94	0,94
V_{SP} [cm ³ /g]	$\pm 0,05$	1,26	4,24	4,90	2,52	5,63	7,79	6,88	7,93
V_{Hg} [cm ³ /g]	$\pm 0,02$	1,20	4,09	4,49	3,80	5,27	7,46	6,59	7,74
% V_{Hg} [%]	± 1	96%	96%	92%	151%	94%	96%	96%	98%
V_{BJH} [cm ³ /g]	$\pm 0,02$	0,77	0,42	0,35	0,39	0,99	0,41	0,37	0,38
% V_{BJH} [%]	± 1	61%	10%	7%	15%	18%	5%	5%	5%
$V_{t\text{-plot}}$ [cm ³ /g]	$\pm 0,01$	0,00	0,02	0,05	0,01	0,00	0,14	0,01	0,03
S_{BET} [m ² /g]	± 10	179	264	275	192	224	513	188	248
L_{Hg} [nm]	± 1	12	13	12	13	33	14	14	14
L_{BJH} [nm]	± 1	5	5	11	6	4	5	5	4

Table III-12: Structural characteristics of CAB aerogels 10-0.2-0.25DA and 10-0.2-100P if pyrolyzed at different temperatures in N₂

	10-0.2-0.25DA			10-0.2-100P					
	OA	CA - pyrolysis in N ₂			OA	CA - pyrolysis in N ₂			
		900 °C	1000 °C	1100 °C		900 °C	1000 °C	1100 °C	
Δm [%]	$\pm 0,5$	74,5	75	75,5		72	72,3	77,5	
ρ_b [g/cm ³]	$\pm 0,02$	0,80	0,26	0,29	0,28	0,54	0,14	0,11	0,12
ϵ	$\pm 0,05$	0,37	0,88	0,86	0,87	0,58	0,94	0,95	0,94
V_{SP} [cm ³ /g]	$\pm 0,05$	0,47	3,41	2,98	3,16	1,07	6,88	8,53	8,07
V_{Hg} [cm ³ /g]	$\pm 0,02$	0,51	2,73	2,73	2,83	1,03	6,67	8,06	7,44
% V_{Hg} [%]	± 1	109%	80%	91%	90%	96%	97%	94%	92%
V_{BJH} [cm ³ /g]	$\pm 0,02$	0,39	0,35	0,35	0,32	0,76	0,34	0,31	0,37
% V_{BJH} [%]	± 1	83%	10%	12%	10%	71%	5%	4%	5%
$V_{t\text{-plot}}$ [cm ³ /g]	$\pm 0,01$	0	0,04	0,03	0,02	0,00	0,09	0,02	0,08
S_{BET} [m ² /g]	± 10	171	261	237	196	235	366	186	373
L_{Hg} [nm]	± 1	13	11	11	11	16	13	13	13
L_{BJH} [nm]	± 1	11	5	4	11	16	4	4	3

Table III-13: Structural characteristics of CAB aerogels 15-0.2-0.25DA and 15-0.2-100P if pyrolyzed at different temperatures in N₂

	15-0.2-0.25DA			15-0.2-100P					
	OA	CA - pyrolysis in N ₂			OA	CA - pyrolysis in N ₂			
		900 °C	1000 °C	1100 °C		900 °C	1000 °C	1100 °C	
Δm [%]	$\pm 0,5$	75	75,5	75,5		73	72,5	76,5	
ρ_b [g/cm ³]	$\pm 0,02$	0,84	0,30	0,37	0,31	0,85	0,13	0,16	0,17
ϵ	$\pm 0,05$	0,34	0,86	0,82	0,85	0,34	0,94	0,92	0,92
V_{SP} [cm ³ /g]	$\pm 0,05$	0,41	2,88	2,20	2,71	0,40	7,16	5,68	5,41
V_{Hg} [cm ³ /g]	$\pm 0,02$	0,41	2,52	1,83	2,29	0,41	6,67	5,26	5,18
% V_{Hg} [%]	± 1	100%	88%	83%	85%	104%	93%	93%	96%
V_{BJH} [cm ³ /g]	$\pm 0,02$	0,35	0,36	0,35	0,32	0,34	0,36	0,37	0,39
% V_{BJH} [%]	± 1	85%	13%	16%	12%	85%	5%	6%	7%
$V_{t\text{-plot}}$ [cm ³ /g]	$\pm 0,01$	0,00	0,08	0,05	0,02	0,00	0,07	0,03	0,03
S_{BET} [m ² /g]	± 10	171	365	271	195	148	337	219	243
L_{Hg} [nm]	± 1	13	10	10	11	13	13	13	13
L_{BJH} [nm]	± 1	9	5	5	11	11	4	4	3

Table III-14: Structural characteristics of CAB aerogel 3-0.2-0.25DA if pyrolyzed at different temperatures in different atmospheres

3-0.2-0.25DA			OA	CA - pyrolysis in N ₂			CA - pyrolysis in Ar		
				900 °C	1000 °C	1100 °C	900 °C	1000 °C	1100 °C
Δm	[%]	$\pm 0,5$		74,5	76	77	75,5	76,5	76
ρ_b	[g/cm ³]	$\pm 0,02$	0,49	0,21	0,19	0,33	0,21	0,19	0,27
ϵ		$\pm 0,05$	0,62	0,90	0,91	0,84	0,90	0,91	0,87
V _{SP}	[cm ³ /g]	$\pm 0,05$	1,26	4,24	4,90	2,52	4,35	4,93	3,30
V _{Hg}	[cm ³ /g]	$\pm 0,02$	1,20	4,09	4,49	3,80	3,88	4,53	3,04
% V _{Hg}	[%]	± 1	96%	96%	92%	151%	89%	92%	92%
V _{BJH}	[cm ³ /g]	$\pm 0,02$	0,77	0,42	0,35	0,39	0,39	0,38	0,35
% V _{BJH}	[%]	± 1	61%	10%	7%	15%	9%	8%	11%
V _{t-pilot}	[cm ³ /g]	$\pm 0,01$	0,00	0,02	0,05	0,01	0,03	0,02	0,00
S _{BET}	[m ² /g]	± 10	179	264	275	192	259	231	163
L _{Hg}	[nm]	± 1	12	13	12	13	12	13	12
L _{BJH}	[nm]	± 1	5	5	11	6	4	4	5

Table III-15: Structural characteristics of CAB aerogel 10-0.2-0.25DA if pyrolyzed at different temperatures in different atmospheres

10-0.2-0.25DA			OA	CA - pyrolysis in N ₂			CA - pyrolysis in Ar		
				900 °C	1000 °C	1100 °C	900 °C	1000 °C	1100 °C
Δm	[%]	$\pm 0,5$		74,5	75	75,5	75,5	76	75,5
ρ_b	[g/cm ³]	$\pm 0,02$	0,80	0,26	0,29	0,28	0,21	0,31	0,21
ϵ		$\pm 0,05$	0,37	0,88	0,86	0,87	0,90	0,85	0,90
V _{SP}	[cm ³ /g]	$\pm 0,05$	0,47	3,41	2,98	3,16	4,24	2,77	4,40
V _{Hg}	[cm ³ /g]	$\pm 0,02$	0,51	2,73	2,73	2,83	4,00	2,51	3,96
% V _{Hg}	[%]	± 1	109%	80%	91%	90%	94%	91%	90%
V _{BJH}	[cm ³ /g]	$\pm 0,02$	0,39	0,35	0,35	0,32	0,33	0,36	0,37
% V _{BJH}	[%]	± 1	83%	10%	12%	10%	8%	13%	8%
V _{t-pilot}	[cm ³ /g]	$\pm 0,01$	0	0,04	0,03	0,02	0,05	0,05	0,01
S _{BET}	[m ² /g]	± 10	171	261	237	196	303	273	181
L _{Hg}	[nm]	± 1	13	11	11	11	12	11	12
L _{BJH}	[nm]	± 1	11	5	4	11	4	6	4

Table III-16: Structural characteristics of CAB aerogel 15-0.2-0.25DA if pyrolyzed at different temperatures in different atmospheres

15-0.2-0.25DA			OA	CA - pyrolysis in N ₂			CA - pyrolysis in Ar		
				900 °C	1000 °C	1100 °C	900 °C	1000 °C	1100 °C
Δm	[%]	$\pm 0,5$		75	75,5	75,5	75,5	76	75,5
ρ_b	[g/cm ³]	$\pm 0,02$	0,84	0,30	0,37	0,31	0,22	0,26	0,28
ϵ		$\pm 0,05$	0,34	0,86	0,82	0,85	0,89	0,88	0,86
V _{SP}	[cm ³ /g]	$\pm 0,05$	0,41	2,88	2,20	2,71	4,03	3,37	3,04
V _{Hg}	[cm ³ /g]	$\pm 0,02$	0,41	2,52	1,83	2,29	3,66	2,97	2,77
% V _{Hg}	[%]	± 1	100%	88%	83%	85%	91%	88%	91%
V _{BJH}	[cm ³ /g]	$\pm 0,02$	0,35	0,36	0,35	0,32	0,35	0,32	0,38
% V _{BJH}	[%]	± 1	85%	13%	16%	12%	9%	10%	12%
V _{t-pilot}	[cm ³ /g]	$\pm 0,01$	0,00	0,08	0,05	0,02	0,05	0,03	0,13
S _{BET}	[m ² /g]	± 10	171	365	271	195	293	228	500
L _{Hg}	[nm]	± 1	13	10	10	11	12	11	11
L _{BJH}	[nm]	± 1	9	5	5	11	5	11	4

The specific surface area s_{BET} of CAB aerogels generally augments during pyrolysis (see also section 3.2), but decreases with higher T_{max} as can be seen for example in figure III-16. In their studies on polyurethane-based aerogels, Biesmann et al. [Bie 1998] found s_{BET} to decrease with increasing T_{max} due to a densification of the aerogel during pyrolysis. CAB aerogels of stoichiometric precursor ratio (*i.e.* I/CA = 0.2), however, do not densify during pyrolysis or with increasing T_{max} pyrolysis. Other studies found BET surface area to increase with higher T_{max} due to the creation of microporosity [Fey

2002, Ari 2007]. For CAB CA, the decrease in s_{BET} seems to be directly correlated to the tendency of $V_{\text{t-plot}}$ to decrease for increasing T_{max} .

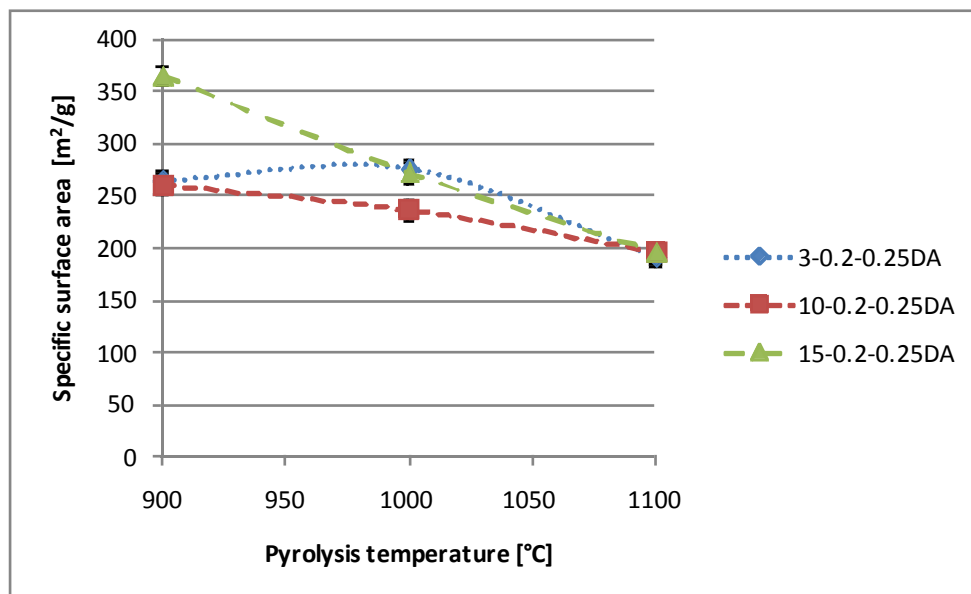


Figure III-16: Evolution of s_{BET} with T_{max} for DA-catalyzed aerogels pyrolyzed in N_2

In conclusion, maximum pyrolysis temperature T_{max} seems to have an influence on the specific surface area and the microporous volume of CAB CA. With increasing T_{max} , s_{BET} and $V_{\text{t-plot}}$ decrease. The type of inert pyrolysis atmosphere, on the other hand, does not seem to have a pronounced or clear effect on the structural characteristics of the CAB CA.

3.3.2. Influence on Carbon Aerogel Composition

The elemental composition of organic and carbon aerogels has been determined for DA-catalyzed and P-catalyzed aerogels of different precursor concentrations %CA, pyrolyzed at 900 °C, 1000 °C, and 1100 °C in N_2 and for DA-catalyzed aerogels additionally in Ar. Table III-17 shows the results of elemental analysis for DA- and P-catalyzed aerogels pyrolyzed in N_2 , table III-18 the difference of DA-catalyzed aerogels pyrolyzed in N_2 and in Ar.

Values from elemental analysis have proven to be oftentimes not very close to 100%, mainly indicating the presence of impurities. Therefore, for simplifying the interpretation of results from elemental analysis, I have normalized the mass of the elements C, H, O, and N by dividing them by the total mass of C, H, O, and N (see tables III-19 and III-20). Also some total values have been found to be above 100%, possibly partly due to the error of the analysis device (*i.e.* ± 0.3 wt.-%), but still more probably due to an inhomogeneity of the sample in question evidenced by the quantification of C, H, and N and the quantification of O being carried out in two different experiments (see chapter II.2.3.3).

Table III-17: Elemental compositions of DA- and P-catalyzed CAB CA of different %CA as a function of T_{max} (pyrolysis in N_2)

		DA-catalyzed, N_2 atmosphere			P-catalyzed, N_2 atmosphere		
		900 °C	1000 °C	1100 °C	900 °C	1000 °C	1100 °C
3-0.2-100P	C [Wt.-%]	88,3	88,7	90,0	87,2	88,5	89,5
	H [Wt.-%]	0,4	0,3	0,3	0,9	1,0	0,7
	O [Wt.-%]	2,9	2,6	3,2	6,1	5,8	5,2
	N [Wt.-%]	3,5	2,8	1,7	3,6	3,0	1,7
	Total	95,1	94,4	95,2	97,8	98,3	97,1
10-0.2-100P	C [Wt.-%]	86,7	87,7	91,6	87,1	87,0	90,6
	H [Wt.-%]	1,0	0,9	0,6	1,0	0,9	0,8
	O [Wt.-%]	5,0	5,0	4,2	5,6	5,4	3,9
	N [Wt.-%]	3,5	3,2	2,1	4,0	3,4	2,0
	Total	96,3	96,9	98,5	97,7	96,7	97,3
15-0.2-100P	C [Wt.-%]	89,5	90,5	89,7	87,7	89,1	91,3
	H [Wt.-%]	0,4	0,3	0,5	1,0	0,9	1,0
	O [Wt.-%]	6,9	2,4	3,1	5,2	4,7	4,0
	N [Wt.-%]	3,6	2,9	1,9	3,9	3,3	2,1
	Total	100,4	96,0	95,3	97,7	98,0	98,4

Table III-18: Elemental compositions of DA-catalyzed CAB CA of different %CA as a function of T_{max} and pyrolysis atmosphere

DA-catalyzed		N_2			Ar		
		900 °C	1000 °C	1100 °C	900 °C	1000 °C	1100 °C
3-0.2-0.25DA	C [Wt.-%]	88,3	88,7	90,0	88,5	90,3	91,1
	H [Wt.-%]	0,4	0,3	0,3	0,9	0,9	0,7
	O [Wt.-%]	2,9	2,6	3,2	5,7	5,4	4,3
	N [Wt.-%]	3,5	2,8	1,7	3,6	1,6	2,0
	Total	95,1	94,4	95,2	98,7	98,2	98,1
10-0.2-0.25DA	C [Wt.-%]	86,7	87,7	91,6	88,8	89,9	90,0
	H [Wt.-%]	1,0	0,9	0,6	1,0	0,8	0,8
	O [Wt.-%]	5,0	5,0	4,2	5,4	5,0	4,0
	N [Wt.-%]	3,5	3,2	2,1	4,0	3,1	2,2
	Total	96,3	96,9	98,5	99,3	98,8	97,0
15-0.2-0.25DA	C [Wt.-%]	89,5	90,5	89,7	87,1	88,5	90,8
	H [Wt.-%]	0,4	0,3	0,5	1,0	0,9	1,0
	O [Wt.-%]	6,9	2,4	3,1	5,0	4,5	5,0
	N [Wt.-%]	3,6	2,9	1,9	3,9	2,2	3,5
	Total	100,4	96,0	95,3	97,1	96,0	100,3

Table III-19: Normalized elemental compositions of DA- and P-catalyzed CAB CA of different %CA as a function of T_{max} (pyrolysis in N_2)

		DA-catalyzed, N_2 atmosphere - normalized			P-catalyzed, N_2 atmosphere- normalized		
		900 °C	1000 °C	1100 °C	900 °C	1000 °C	1100 °C
3-0.2-100P	C [Wt.-%]	92,8	93,9	94,6	89,2	90,1	92,1
	H [Wt.-%]	0,5	0,3	0,3	1,0	1,0	0,8
	O [Wt.-%]	3,1	2,8	3,3	6,2	5,9	5,4
	N [Wt.-%]	3,6	3,0	1,8	3,6	3,1	1,7
	Total	100,0	100,0	100,0	100,0	100,0	100,0
10-0.2-100P	C [Wt.-%]	90,1	90,6	93,0	89,2	90,0	93,1
	H [Wt.-%]	1,1	1,0	0,6	1,0	0,9	0,8
	O [Wt.-%]	5,2	5,2	4,2	5,8	5,6	4,0
	N [Wt.-%]	3,7	3,3	2,1	4,1	3,5	2,1
	Total	100,0	100,0	100,0	100,0	100,0	100,0
15-0.2-100P	C [Wt.-%]	89,2	94,3	94,1	89,7	90,9	92,7
	H [Wt.-%]	0,4	0,3	0,6	1,0	0,9	1,0
	O [Wt.-%]	6,9	2,5	3,3	5,3	4,8	4,1
	N [Wt.-%]	3,5	3,0	2,0	4,0	3,4	2,2
	Total	100,0	100,0	100,0	100,0	100,0	100,0

Table III-20: Normalized elemental compositions of DA-catalyzed CAB CA of different %CA as a function of T_{max} and pyrolysis atmosphere

DA-catalyzed		N_2 - normalized			Ar - normalized		
		900 °C	1000 °C	1100 °C	900 °C	1000 °C	1100 °C
3-0.2-0.25DA	C [Wt.-%]	92,8	93,9	94,6	89,7	92,0	92,9
	H [Wt.-%]	0,5	0,3	0,3	0,9	0,9	0,7
	O [Wt.-%]	3,1	2,8	3,3	5,8	5,5	4,3
	N [Wt.-%]	3,6	3,0	1,8	3,7	1,7	2,1
	Total	100,0	100,0	100,0	100,0	100,0	100,0
10-0.2-0.25DA	C [Wt.-%]	90,1	90,6	93,0	89,5	91,0	92,8
	H [Wt.-%]	1,1	1,0	0,6	1,0	0,8	0,8
	O [Wt.-%]	5,2	5,2	4,2	5,4	5,1	4,2
	N [Wt.-%]	3,7	3,3	2,1	4,1	3,2	2,2
	Total	100,0	100,0	100,0	100,0	100,0	100,0
15-0.2-0.25DA	C [Wt.-%]	89,2	94,3	94,1	89,7	92,2	90,5
	H [Wt.-%]	0,4	0,3	0,6	1,1	0,9	1,0
	O [Wt.-%]	6,9	2,5	3,3	5,2	4,7	5,0
	N [Wt.-%]	3,5	3,0	2,0	4,1	2,3	3,5
	Total	100,0	100,0	100,0	100,0	100,0	100,0

The weight-% of carbon increases with maximum pyrolysis temperature, but remains at about 91,7% \pm 3% for the pyrolysis temperature range between 900 °C and 1100 °C (for normalized values). The concentration of the heteratoms oxygen and nitrogen, as well as of hydrogen decreases in the meantime, as was to be expected [Fey 2002].

After pyrolysis, a large concentration of heteratoms remains in the carbonaceous matrix for all T_{max} . The quantity of carbon could maybe be increased, and that of remaining heteratoms decreased, if pyrolysis has been carried out in even higher T_{max} . Oxygen seems to be the heteratom of which the highest quantity persists during pyrolysis.

The quantity of remaining heteratoms does not seem to depend on the type of inert atmosphere.

4. Conclusion

Chapter III examines and discusses (i) the evolution of CAB aerogels during pyrolysis, (ii) the influence of the OA used as precursors on the resulting CA, and (iii) the influence of pyrolysis parameters on the resulting CAB CA. The influence of the organic precursor, T_{max} and pyrolysis atmosphere on carbon aerogel structure and composition has been analyzed.

Hyper(macro)porous but nanostructured carbonaceous materials are prepared by pyrolyzing CAB aero- and xerogels. A bubbling phenomenon, related to heating the aerogel above the cellulose acetate's melting temperature and subsequent partial gasification of the organic matrix during thermal degradation, takes place. Gaseous degradation products of CAB OA in the form of bubbles apparently induce the formation of visible large pores, by leaking out of the melted aerogel network. Two different levels of porosity are thus generated: micro- and mesoporosity together with micro- to millimetre-sized macroporosity.

Pyrolysis of the CAB OA results basically in the degradation of the oxygen and nitrogen functionalities and dehydrogenation and aromatisation of the structure.

Although pyrolysis brings about modifications between the structure of the OA and the CA, the structure of the OA, and therefore sol-gel synthesis and drying parameters, does not seem to have a significant influence on the carbon structure. Bulk densities tend to decrease and porosities to increase with pyrolysis. Hg porosimetry has been able to characterize most of the porous volume contained in the CAB CA generally increasing with pyrolysis (although exceptions to this behaviour are to be found for 3 %CA). A minor amount of microporosity is created during pyrolysis and accordingly specific surface areas have increased. Organic xerogels, having been nearly not porous before pyrolysis, develop an even higher quantity of macroporous volume than aerogels, but less micro- and mesopores.

A particularity of carbons obtained from the pyrolysis of CAB aerogels, is their high content in heteroatoms (*i.e.* nitrogen and oxygen from the precursor). CAB CA contain around 90% carbon and 10% of heteroatoms mainly in the form of oxygen and nitrogen plus some hydrogen, for CAB CA pyrolyzed at 900 °C in N₂.

Maximum pyrolysis temperature has been found to have an influence on structure and on composition of resulting CAB CA, whereas pyrolysis atmosphere could not be evidenced to have an effect on the resulting carbon material. Specific surface area and microporosity increase during pyrolysis from CAB OA to CAB CA. However, with increasing maximum pyrolysis temperature, specific surface area and microporosity decrease. The carbon content of CAB CA has been found to increase with maximum pyrolysis temperature, but remains at about 92% for samples pyrolyzed between 900 °C and 1100 °C. The concentration of the heteratoms decreases with increasing maximum pyrolysis temperature.

In conclusion, even though precursor structure, pyrolysis temperature and atmosphere have varied, CAB CA prepared in this study featured very similar structures and compositions.

Chapter IV: Modification of the Cellulose-acetate based Carbon Aerogels - Structure and Surface Chemistry

Modification of the Cellulose-acetate-based Carbon Aerogels: Structure and Surface Chemistry

1. Introduction

In order to synthesize cellulose-based carbon material, I have synthesized organic aerogels based on cellulose acetate (chapter II) and pyrolyzed them to obtain carbon aerogels (chapter III). In order to obtain a broad range of structurally different CAB CA we have studied the influence of synthesis and pyrolysis parameters. However, CAB CA structure and elemental composition have been found to depend only marginally on the CAB organic aerogel used as precursor and on pyrolysis parameters. Therefore, I have explored different possibilities of modifying the CAB aerogel structure (chapter IV.2) and surface chemistry (chapter IV.3).

2. Modification of the Carbon Aerogel Structure

To modify the CAB CA structure, I have investigated (i) physical activation to augment the degree of porosity and specific surface area (chapter IV.2.1.) and (ii) the synthesis of CAB aerogels/cellulose powder composites to create monolithic CAB CA samples and to limit the “bubbling” phenomenon during pyrolysis (chapter IV.2.2.).

2.1. Physical Activation

So as to modify preferably structure, I have decided to examine physical/thermal activation of CAB CA. Agents for physical activation are oxygen-containing gases, such as air, steam, carbon dioxide (CO₂), or mixtures of oxygen-containing gases or oxygen and inert gases. Each activation agent has a different influence. Steam and CO₂ are the physical activating agents most widely used, due to their availability and competitive cost. Activation in steam widens existing pores. Even though some microporosity can be generated in the process of activation in steam, depending on the activation parameters, micropores are not necessarily created [Rod 1995]. CO₂, on the other hand, produces narrow microporosity at burn-offs⁴ of less than 20%, followed mainly by the widening of this microporosity up to about 40 to 50% burn-off [Rod 1995]. As high microporosity results in high specific surface areas, I have decided to examine physical activation in CO₂.

The evolution of the structure (*i.e.* of the porous network) depends obviously significantly on the degree of burn-off. The burn-off is strongly influenced by activation temperature, gas flow, and activation duration. The burn-off increases with the activation temperature and the activation duration [Rod 1995, Pas 2002]. In this work, I have chosen to activate CAB CA at different temperatures between 850 °C and 1050 °C.

⁴ The burn-off designates the mass loss during activation due to the partial oxidation and therefore gasification of the carbon material.

2.1.1. Experimental

2.1.1.1. Carbon aerogel synthesis

The study on the influence of activation has been carried out using CAB CA 10-0.2-0.25DA as representative material. CAB gels have been synthesized following the protocol given in chapter II. Gels have been dried in supercritical CO₂ chosen as default drying process in this work (see also chapter II). CAB CA have been prepared by pyrolyzing the precursor OA at 1000 °C in N₂, according to the pyrolysis protocol established in chapter III.

2.1.1.2. Activation

Carbon aerogels have been ground to obtain carbon powder. Carbon powder has been dried at 110 °C for about 12 h before activation to eliminate H₂O traces. For physical activation the carbon powder has been heated up to the activation temperature at 4 °C/min in N₂. Upon reaching the activation temperature, the atmosphere has been switched to the activation atmosphere, *i.e.* CO₂. Duration at activation temperature in activation atmosphere has been 2 h for all experiments. Activation has been carried out at 850 °C, 950 °C, and 1050 °C have been chosen. After activation, the carbon material has been cooled down in N₂ through thermal inertia. An example of the activation's temperature profile can be seen in figure IV-1. The gas flow has been held constant at 1 l_{CO₂}/min for the inert atmosphere N₂ and the activation agent CO₂.

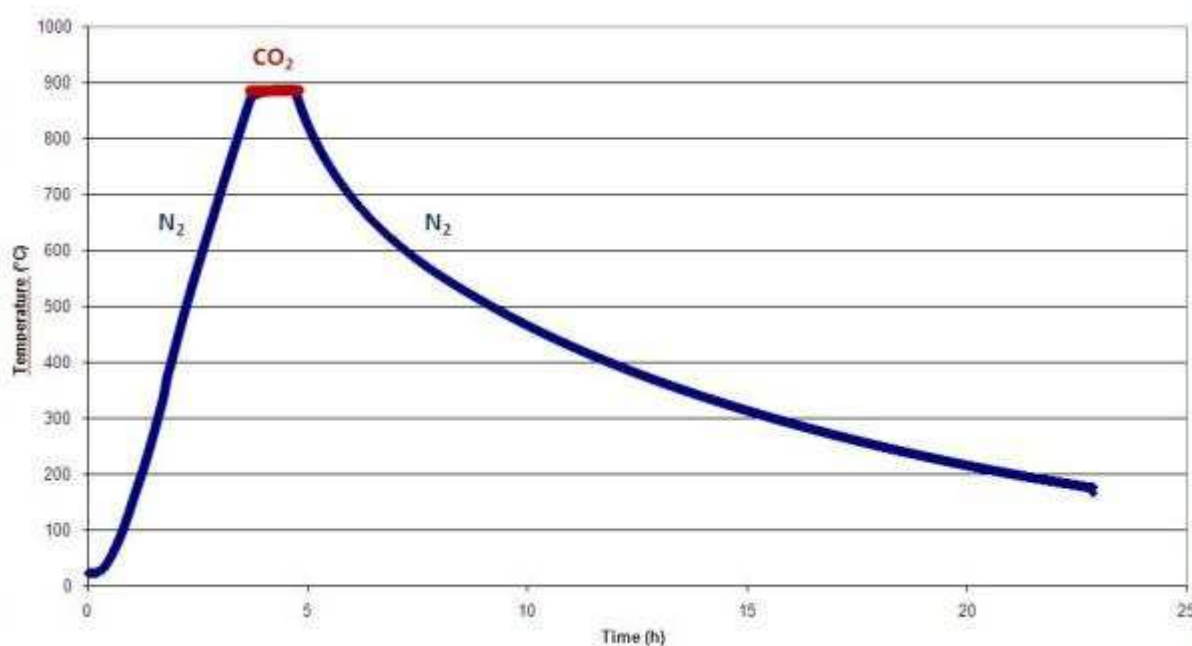


Figure IV-1: Example of an activation profile of CAB CA

2.1.1.3. Structural and Chemical Analysis

Porous properties, structure and elemental composition have been analyzed by nitrogen adsorption and elemental analysis, respectively, as described in chapter II. The mean size of pores contributing to the microporous volume calculated according to the t-plot method is referred to as L_{2t}.

2.1.2. Results and Discussion

2.1.2.1. Structure

For activation, CAB CA has been ground. CAB CA powder (see figure IV-2) does not reveal any macroporosity within the carbon material.

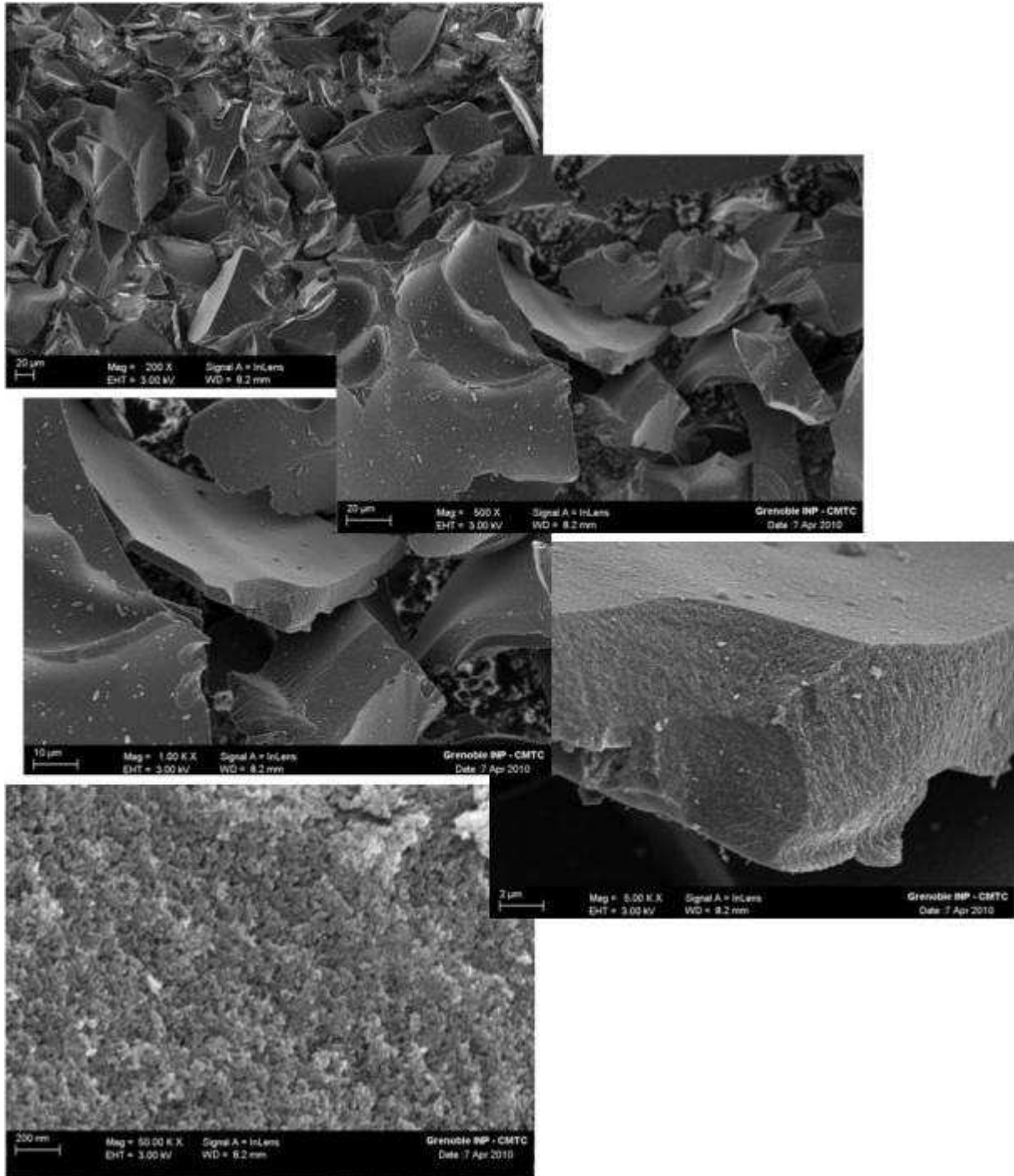


Figure IV-2: SEM of CAB CA powder 10-0.2-0.25DA activated at 950 °C for 2 h

The structure of the CA powder before and after activation has been analyzed by N₂ adsorption. Hg porosimetry has not been carried out, as CAB CA powder does not feature big macropores anymore. Results of the structural analysis can be seen in table IV-1.

Table IV-1: Structure of CAB CA 10-0.2-0.25DA before and after activation at different temperatures

10-0.2-0.25DA			Pristine	CO ₂ activated		
				850 °C	950 °C	1050 °C
Burn-off	[%]	±1		6.5 %	52 %	75%
V_{BJH}	[cm ³ /g]	±0.02	0.35	0.29	0.63	0.94
V_{t-plot}	[cm ³ /g]	±0.01	0.03	0.19	0.70	0.75
S_{BET}	[m ² /g]	±10	237	620	2106	2147
L_{BJH}	[nm]	±1	4	10	8	4
L_{2t}	[nm]	±0.05	0.65	0.58	0.72	0.89

The activation treatment brings about radical structural modifications, as expected increasing surface area and porous volumes.

As seen in table IV-1, burn-off also increases with activation temperature. In a first experiment burn-off for CAB CA 10-0.2-0.25DA after activation at 950°C for 2 h has been observed to be about 50% (sample whose results from structural analysis can be seen in table IV-1 and from elemental analysis in table IV-2). In ulterior experiments, however, we have found burn-offs of about 35% for above-mentioned activation parameters (samples have not undergone structural analysis). This lower burn-off value seems more logic when looking at figure IV-3, as burn-offs have been found to increase linearly with activation temperature before [Rod 1995]. The burn-off of over 50% having been observed at first is probably due to a deviation of the scheduled activation conditions. However, structural characterization and elemental analysis for CAB CA 10-0.2-0.25DA having been activated at 950 °C have been carried out on the sample featuring a burn-off of about 50%.

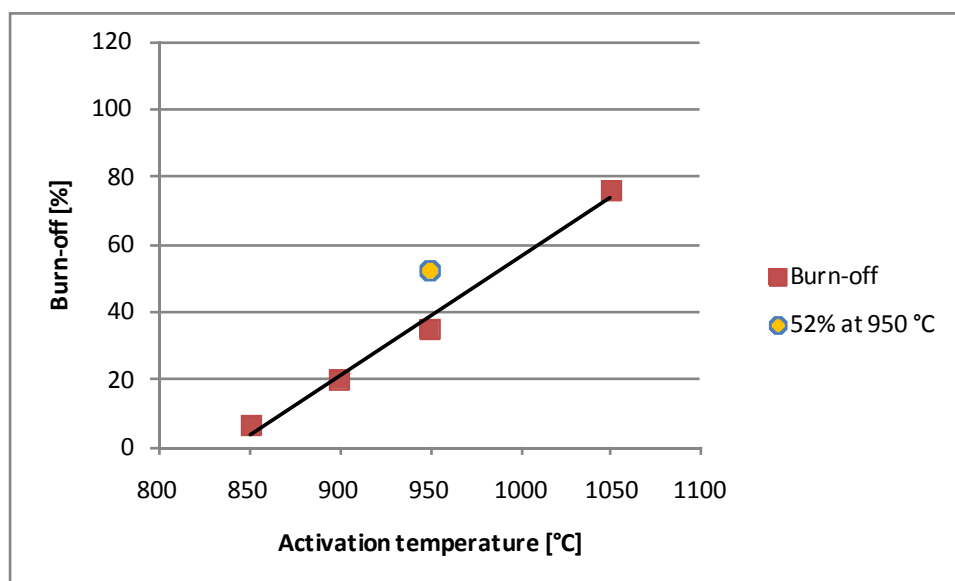


Figure IV-3: Evolution of the burn-off for CAB CA activated in CO₂ for 2 h and linear trend line

As expected, s_{BET} increases with activation temperature and therefore with burn-off (see table IV-1 and figure IV-4).

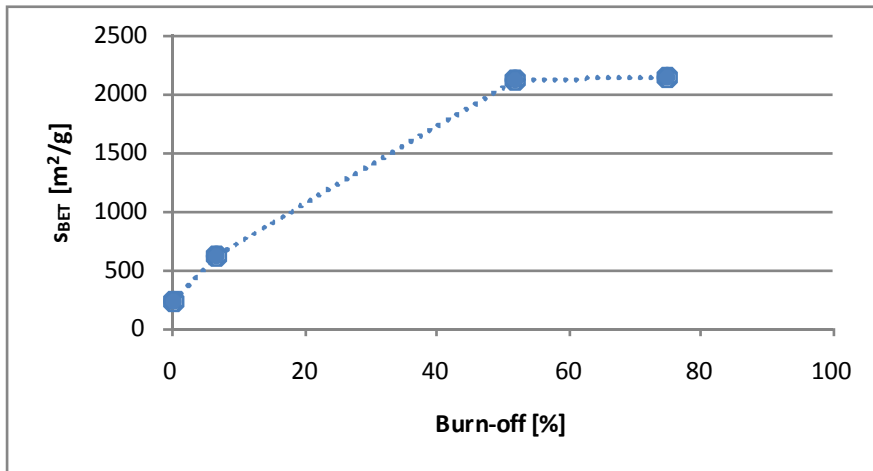


Figure IV-4: Evolution of s_{BET} with burn-off during activation in CO_2

The specific surface area increases steeply at least up to the about 50% burn-off for the points measured in this work. Beyond this burn-off, specific surface area still increases but much less drastically. This behavior may be explained by the evolution of the micro- and mesoporous volumes with the burn-off. Both micro- and mesoporous volumes increase. Mesoporous volume rather linearly with activation temperature and burn-off (see figure IV-5), microporous volume increases notably at least up to the burn-off reached at 950 °C but only very slightly above. These findings bear out those of Rodríguez-Reinoso, Molina-Sabio, and González [Rod 1995], having found that microporosity is generated but also widened during activation. According to their findings, microporosity is certainly created up to about 20% burn-off, but widening is by far the determining mechanism above 30-40% burn-off. Similar results have been found for RF CA (*i.e.* creation of microporosity and widening of micropores at higher burn-offs like 50% [Han 1996]). For CAB CA, the increase of microporous volume slows down remarkably for higher burn-offs indicating that less micropores are created and existing microporosity rather widens at higher burn-offs (see figure IV-5).

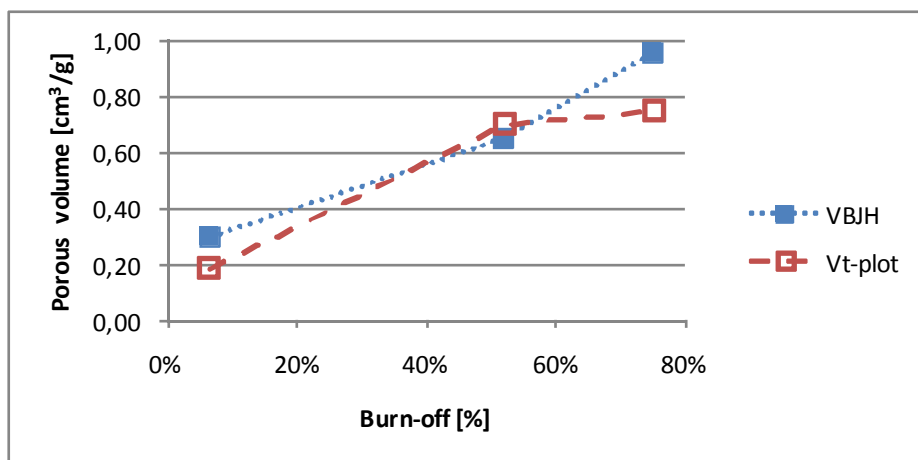


Figure IV-5: Evolution of porous volumes during activation in CO_2

Although L_{2t} augments with activation temperature, *i.e.* with burn-off, it is lower for activation at 850 °C than for the CAB CA before activation. This phenomenon confirms that narrow micropores are created at lower burn-off and widen subsequently [Rod 1995].

2.1.2.2. Elemental Composition

The elemental composition of CAB CA samples activated at 850 °C, 950 °C, and 1050 °C has been analyzed by elemental analysis (see table IV-2).

Table IV-2: Composition of CAB CA 10-0.2-0.25DA pyrolyzed at 1000 °C in N_2 before and after activation in CO_2 for 2 h

10-0.2-0.25DA	Pristine Sample	CO_2 activated		
		850 °C	950 °C	1050 °C
%C [wt.-%]	87.7	87.1	91.6	91.0
%H [wt.-%]	0.9	0.9	0.6	0.4
%O [wt.-%]	5.4	6.1	3.1	2.4
%N [wt.-%]	3.4	2.7	2.9	2.6
Total [wt.-%]	96.7	96.8	98.2	96.4

Obviously, carbon still makes up the highest fraction of the activated aerogel. The quantity of heteroatoms (notably oxygen) and hydrogen decreases with higher activation temperatures. However, oxygen content is higher for carbon material activated at 850 °C than for CAB CA not having been activated. This difference in oxygen content might be explained by an interaction of CO_2 with the carbon surface during activation, followed by a decrease in oxygen content with increasing activation temperature due to the breaking of thermally unstable C-O bonds. Oxygen-containing surface groups are known to decompose at different temperatures, originating CO and CO_2 . These tendencies are maintained if the masses of C, H, O, and N are normalized by the total mass.

2.1.3. Conclusion on Activation

CAB CA have been activated in CO_2 for 2h at temperatures between 850 and 1050 °C. The burn-off increases almost linearly with activation temperature. Porous volumes and s_{BET} increase with the burn-off due to the creation of microporosity and the widening of existing pores. Thus, CAB CA with specific surface areas of up to around 2150 m^2/g have been generated.

2.2. Cellulose-acetate-based Aerogel/Cellulose Powder Composites

CAB gels undergo pronounced shrinkage during drying and CAB aerogels shrink and their structure is somewhat modified during pyrolysis (see chapter III). In order to limit shrinkage and to better control the CAB CA structure, I have examined the possibility of generating CAB aerogel composites. An advantage of the sol-gel method is the possibility of introducing compounds into the sol and thus creating aerogel composites. Compounds introduced into the sol may be of different nature, such as ceramic or carbon particles or inorganic and organic polymers [Pet 2001]. The creation of RF CA composites by introducing other compounds into the sol during the sol-gel synthesis has been investigated previously to increase the CA's mechanical strength [Pet 2001, Sch 2001].

To investigate the possibility of creating CAB gels relatively resistant to shrinkage during drying, aerogel monoliths resisting “bubbling” during pyrolysis, and to reinforce the CAB aerogel I have chosen to study the effects of introducing cellulose powder (CP) into the sol. An advantage of using cellulose is the fact that its chemical affinity with CO₂ is better than that of cellulose acetate and that it does not melt before thermal degradation. In addition, cellulose fibre containing organic materials have been shown to possess an increased mechanical strength [Oua 2009]. Cellulose may therefore help to control the CAB aerogels’ structure during drying in supercritical CO₂ and to limit the deformation of the OA during pyrolysis.

2.2.1. Experimental

The sol for CAB CA containing cellulose has been prepared according to the protocol described in chapter II, for OA 10-0.2-100P. Once the sol has been prepared, microcrystalline cellulose powder (Cellulose powder DS-0, Fluka, CAS 9004-34-6, particle size of around 20 μm) has been added. In order to allow for a good dispersion of CP in the sol, pyridine has been used as catalyst based on the relatively long gelation times for P-catalyzed samples. Three samples of the formulation 10-0.2-100P containing different amounts of microcrystalline cellulose, referred to as PA, PB, and PC, have been synthesized (see table IV-3). The quantity of cellulose powder introduced into the sol, referred to as **%Cellulose**, is given in mass percentage versus solvent.

Cellulose-containing CAB OAs have been supercritically dried (see chapter II.2 for details) and subsequently pyrolyzed at 1000 °C in N₂ (refer to chapter III). Carbonaceous CAB aerogel/CP composites are referred to as samples PAC, PBC, and PCC.

Table IV-3: Composition of cellulose powder containing CAB aerogel samples based on CAB aerogel formulation 10-0.2-100P

<i>OAs</i>	<i>Sol</i>	<i>%Cellulose</i>
10-0.2-100P	10-0.2-100P	0
PA	10-0.2-100P	5
PB	10-0.2-100P	10
PC	10-0.2-100P	15

The structure has been analyzed by N₂ adsorption and Hg pycnometry and porosimetry as described in chapter II.

2.2.2. Results and Discussion

2.2.2.1. Macro- and Microscopic Observation

Shrinking due to drying in supercritical CO₂ for cellulose-containing CAB aerogels is obviously much lower than the 75-85% normally underwent by CAB aerogels (see chapter II), as visible from figure IV-6.



Figure IV-6: Cellulose-containing gel 10-0.2-100PC (left) and corresponding aerogel (right)

The degree of shrinking and the ability to conserve the original form depend on the quantity of cellulose added to the sol (see figure IV-7). Sample PA containing the lowest quantity of cellulose powder shrinks and deforms most of all CAB aerogel/CP composites; sample PC containing the highest quantity of microcrystalline cellulose shrinks and deforms the least. The increased resistance to shrinkage during supercritical drying may be a result of an enhanced mechanical strength, but may also principally be due to a better chemical affinity of the compound material (*i.e.* of cellulose) with CO₂ used in the drying process [Gav 2007] (see chapter II.3.2.1.1).



Figure IV-7: Cellulose-containing aerogels PA containing 5 %Cellulose (left), PB containing 10 %Cellulose (middle), and PC containing 15 %Cellulose (right)

Figure IV-8 shows the cellulose-containing CAB OA and CA of sample PC. Carbons, as well as organics, maintain their original form much better if cellulose powder is introduced into the sol, as has been intended by synthesizing CAB aerogel/CP compounds. Nonetheless, the aerogel shrinks notably during pyrolysis. Shrinking takes place, as cellulose is known to shrink during heat treatment [Pet 2001]. Although not deformed by “bubbling”, carbon aerogels burst open. These openings are probably created by gaseous compounds resulting from partial gasification of the CAB aerogel and the cellulose during thermal degradation.



Figure IV-8: Cellulose-containing OA PC (left) and its carbonaceous counterpart CA PCC (right)

SEM micrographs of the organic CAB aerogel/CP compound and the carbonaceous counterpart can be seen in figures IV-9 and IV-10, respectively. The CP particles of about 20 μm are densely enveloped and seemingly held together by the CAB OA.

Upon pyrolysis, the CAB aerogel melts and macropores are formed. However, the cellulose powder incorporated in the CAB OA seems to provide a solid framework to which the CAB CA adheres. The organic aerogel does not only seem to envelop the CP (figure IV-9), but also to hold the different CP particles together even after pyrolysis (figure IV-10). The CAB aerogel enveloping the CP consists of sphere-like particles typical for an aerogel. The cellulose framework of the CAB aerogel/CP composites seems to inhibit the deformation by “bubbling”, as cellulose does not melt before thermal degradation.

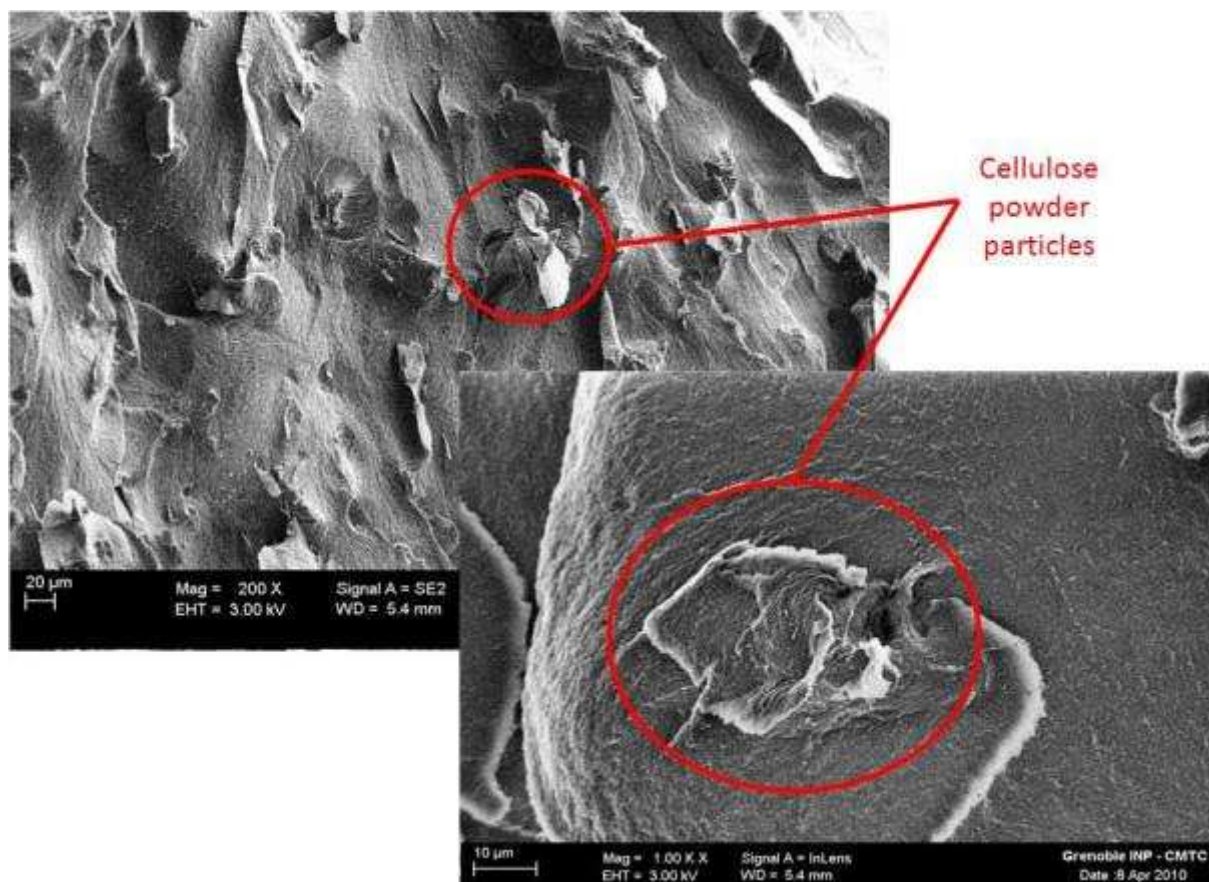


Figure IV-9: SEM of CAB aerogel/CP composite organic sample PB containing 10 %Cellulose

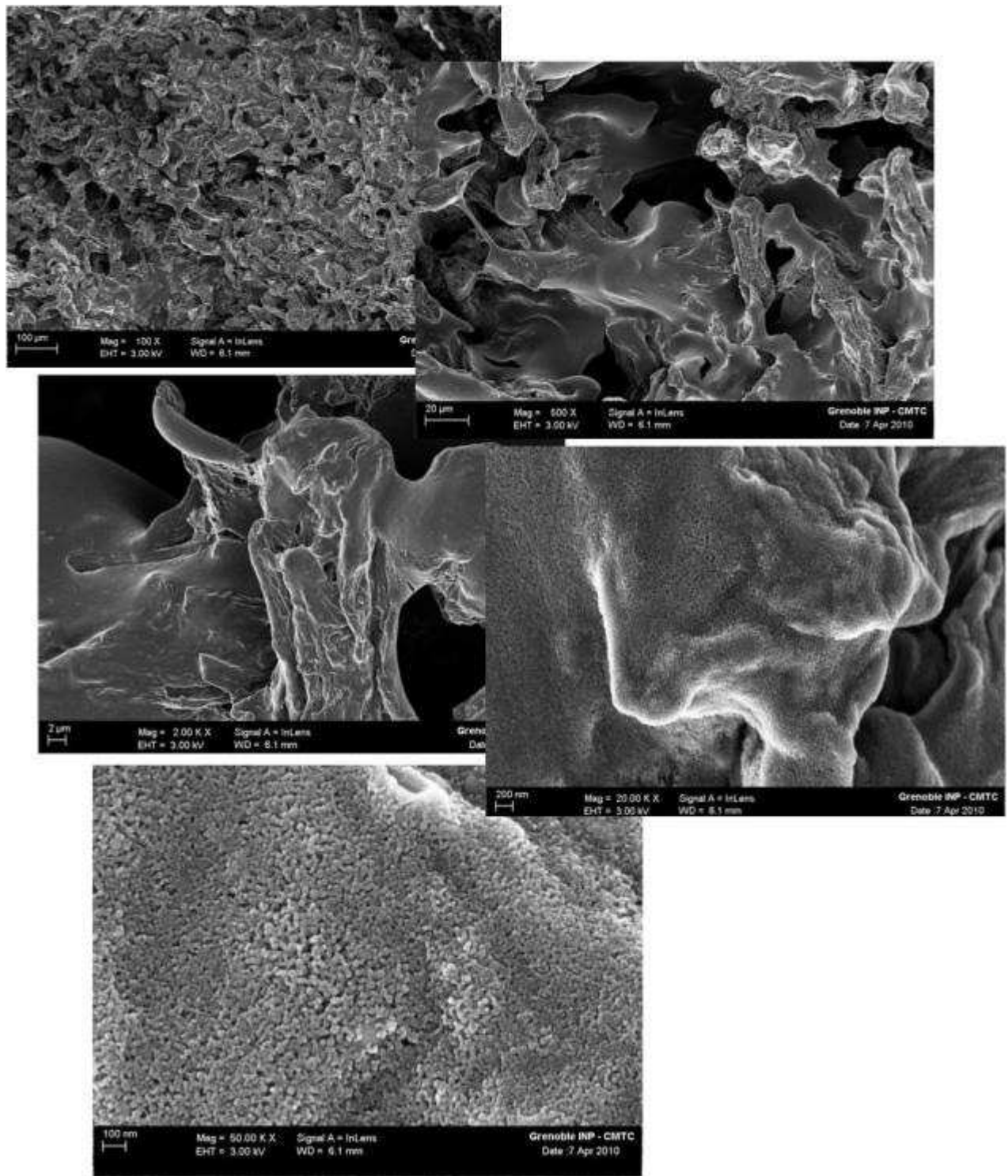


Figure IV-10: SEM of CAB aerogel/CP composite carbon sample PBC containing 10 %Cellulose

2.2.2.2. Structural Analysis of Organic Composites

The results of the structural analysis of cellulose-containing CAB OAs can be found in table IV-4.

Table IV-4: Structure of organic CAB aerogel/CP composites

			10-0.2-100P	PA	PB	PC
ρ_b	[g/cm ³]	±0.02	0.54	0.43	0.69	0.48
V_{Hg}	[cm ³ /g]	±0.02	1.05	1.64	1.50	1.43
V_{BJH}	[cm ³ /g]	±0.02	0.76	0.50	0.19	1.14
V_{μ}	[cm ³ /g]	±0.01	0	0	0	0
S_{BET}	[m ² /g]	±10	235	97	76	267
L_{BJH}	[nm]	±1	16	44	18	32

The bulk density of the CAB aerogel/CP compounds does not seem to be systematically higher than that of CAB OA not containing cellulose, probably due to a reduced shrinking rate during supercritical drying. Even though the total volume V_{Hg} for all samples containing cellulose is higher than that of CAB OA 10-0.2-100P, it decreases slightly with the %Cellulose (see figure IV-11) and is thus lowest for sample PC. Specific surface areas are much lower for samples PA and PB as compared to the CAB OA 10-0.2-100P not containing any cellulose powder. Sample PC, however, features a specific surface even superior to that of CAB OA 10-0.2-100P, probably due to a mesoporous volume V_{BJH} largely exceeding that of the other aerogels. This tendency may be explained by the introduction of a relatively high amount of cellulose. Although cellulose is a nearly non-porous material with small surface areas it accounts for a significantly enhanced chemical affinity with CO₂ (and therefore only very limited shrinking during supercritical drying in CO₂) with an increasing amount of cellulose content. Accordingly, the organic sample PC maintains a high quantity of mesopores due to the high degree of preservation of its shape during supercritical drying, but exhibits a lower total porous volume than samples PA and PB due a higher content of cellulose powder within the aerogel.

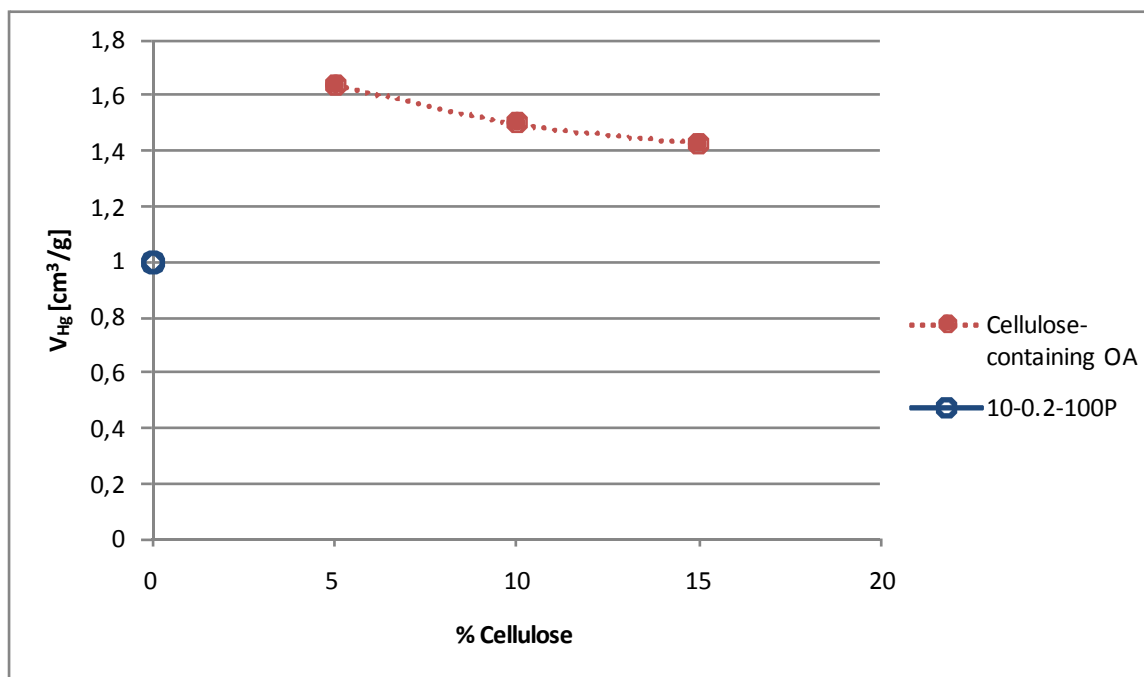


Figure IV-11: V_{Hg} versus cellulose content in CAB OA 10-0.2-100P

2.2.2.3. Structural Analysis of Carbonized Composites

The results of the structural analysis of carbonized CAB aerogel/CP composite monoliths can be seen in table IV-5.

Table IV-5: Structure of cellulose-containing carbon aerogels

			10-0.2-100PC	PAC	PBC	PCC
Δm	[%]	± 0.5	72.5	78	79.5	80
ρ_b	[g/cm ³]	± 0.02	0.11	0.25	0.32	0.36
V_{Hg}	[cm ³ /g]	± 0.02	8.06	3.15	2.34	2.24
V_{BJH}	[cm ³ /g]	± 0.02	0.31	0.27	0.31	0.22
V_{μ}	[cm ³ /g]	± 0.01	0,02	0,01	0,01	0,00
S_{BET}	[m ² /g]	± 10	186	115	127	75
L_{Hg}	[nm]	± 1	13	15	14	15
L_{BJH}	[nm]	± 1	4	12	10	14

Densities, as expected, are higher for cellulose-containing carbon samples in general, increasing with cellulose content (see figure IV-12). Specific surface areas for cellulose-containing samples after pyrolysis are lower than CAB CA 10-0.2-100P not containing any cellulose powder.

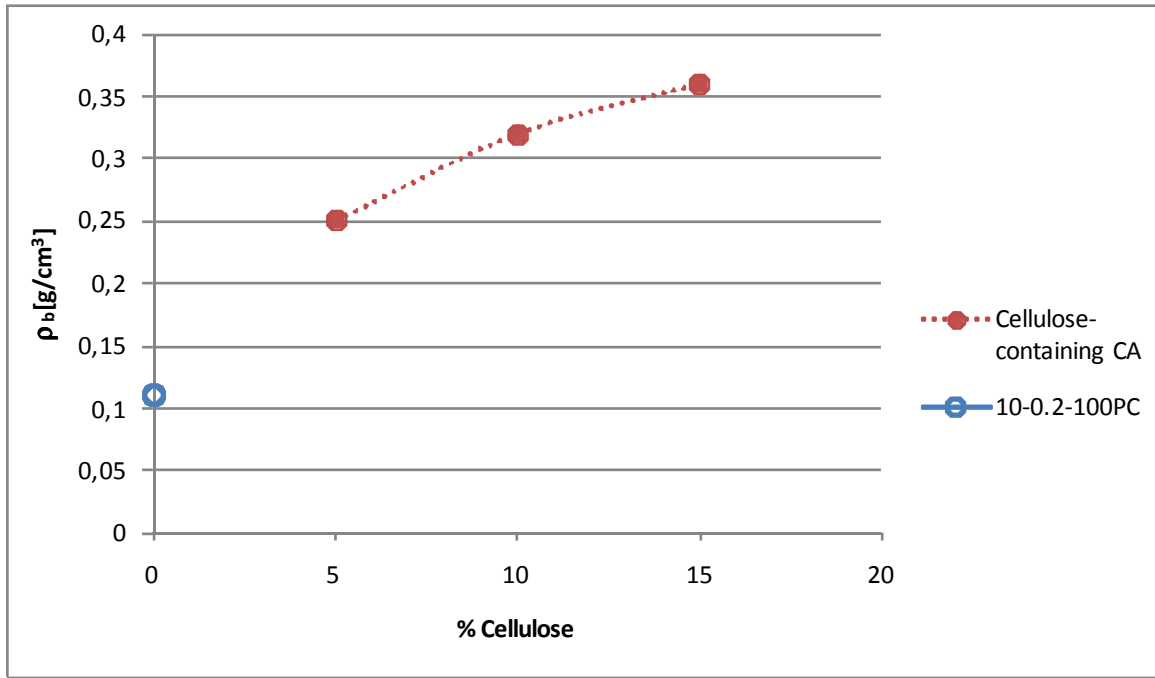


Figure IV-12: ρ_b versus cellulose content in CAB CA 10-0.2-100P

Total porous volume V_{Hg} also decreases with %Cellulose, but values remain above those of the corresponding organic samples (see figure IV-13), probably because less macropores are formed as the cellulose framework restrains the formation of bubble-shaped cavities. Mesoporous volumes, as well as microporous volumes, of carbonized CAB aerogel/CP composites seem to be lower for cellulose-containing CAs.

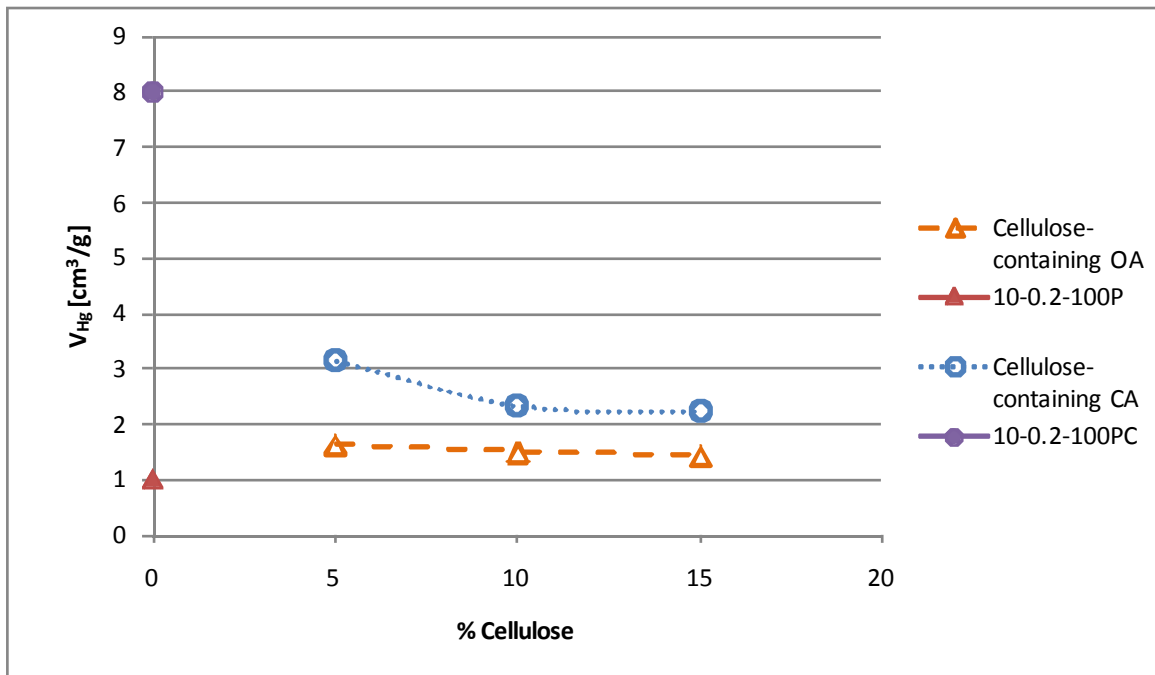


Figure IV-13: V_{Hg} versus cellulose content in CAB CA 10-0.2-100P

CA 10-0.2-100PC exhibits a very high total porous volume V_{Hg} , but only a very small amount of this porosity can be attributed to mesopores, according to the % V_{BJH} . The greatest part of the porosity

must thus consist of macropores, probably a result of the combination of melting and partial gasification during thermal degradation. Cellulose-containing aerogels, however, feature smaller macropore volumes, hinting at a lesser formation of macropores during pyrolysis. The fact that less macropores are created during the pyrolysis of CAB aerogels containing cellulose may be attributed to the high degree of shape preservation of these samples during pyrolysis. The cellulose seems to provide a framework resisting to “bubbling”, although the quantity of gaseous degradation products is even superior to that of conventional CAB aerogels (see Δm in table IV-5). The higher mass loss of CAB aerogel/CP composites as compared to CAB aerogels not containing any cellulose can easily be explained by the mass loss of CP. Although, the theoretical mass loss of cellulose would be of 55.5% [Don 1998], cellulose has reportedly been found to feature mass losses of up to over 90% [Pet 2001]. The cellulose powder used in this study loses around 81.5% of its mass upon pyrolysis at 1000 °C during 1 h, which is superior to the mass loss of the CAB aerogel. Accordingly, the mass loss for CAB aerogel/CP composites increases with an increasing content of CP.

2.2.3. Conclusion on Cellulose-acetate-based Aerogel/Cellulose Powder Composites

CAB aerogel/CP composites have been prepared to study the possibility of limiting the shrinkage of the CAB aerogel during drying and pyrolysis and to minimize “bubbling”.

Organic and carbonaceous CAB aerogel/CP composites maintain their original form better upon the introduction of CP into the sol. Shrinkage due to drying in supercritical CO₂ has much been reduced, probably due to a better chemical affinity of cellulose with CO₂. During pyrolysis, the composite aerogels do not “bubble”. Nonetheless the composite samples burst open to create an opening for evacuating the gaseous compounds resulting from partial gasification during thermal degradation.

Carbonaceous CAB aerogel/CP composites are of higher density and have lower macroporous volumes and specific surface areas than CAB CA not containing cellulose. The structure of the organic aerogel composites seems to be maintained better throughout pyrolysis than the structure of pure CAB aerogels, most likely as a result of the cellulose contained in the composites as cellulose does neither melt nor deform during pyrolysis.

3. Modification of the Carbon Aerogel Surface Chemistry

The structure of the carbon materials is crucial, but is not the exclusive factor determining the performance of the different carbons in different applications. The carbon surface chemistry also plays an important role in all applications in which the carbon comes into contact with a fluid, due to inevitable interactions of the fluid with the carbon surface. Surface functional groups (*e.g.* O- and N-containing groups) influence the carbon behaviour for example in terms of charge transfer, blocking of reactive sites, possible redox reactions, wettability, etc. [Swi 2004, Ser 2008]. Functionalised carbons can be prepared directly from heteroatom-containing precursors [Gui 2007, Mac 2005, Lah 1999, Bra 1993], or heteroatoms can be added by various different post-treatments [Lot 2007, Jur 2003, Jan 1994, Muñ 1998].

To obtain CA with different surface chemistry, I have examined different methods of introducing oxygen and/or nitrogen-containing functional groups. The chemical methods having been applied allow producing a wide range of functionalized carbon aerogels differing in terms of oxygen and nitrogen groups, their distribution and basicity. The aim of this study has been to observe the impact of the chemical surface groups only. Therefore, relatively “soft” treatments have been employed to modify the surface chemistry so as to limit the modification of the carbon structure.

Oxidation, is aimed at introducing O-containing functional groups on the carbon surface, rather than modifying the structure (as is the case with conventional chemical activation). CAB CA samples have been oxidized by H_2O_2 and HNO_3 in this study. In order to introduce N-containing functional groups on the carbon surface ammonisation (*i.e.* reaction with gaseous ammonia), a rather well-known and much exploited method [Jan 1994] has been examined. So as to investigate another different method of introducing nitrogen, I have chosen to examine the effects of co-heating of the CA and melamine. This method is based on works of Gorgulho et al. [Gor 2009] and Pérez-Cadenas et al. [Pér 2008], dealing with the synthesis of nitrogen-containing resorcinol-formaldehyde carbon xerogels prepared by introducing nitrogen-containing polymer precursors (*i.e.* melamine, pyridine, or urea-containing units).

The aim of this study has been to create CAB CAs with different surface chemistries, but also to understand the complex chemistry of functionalized CAB CAs resulting from different synthesis pathways.

This study has been carried out in collaboration with Bartosz Grzyb during his post-doctorate at the CEP/Mines ParisTech. Results of this study have been published in Carbon [Grz 2010].

3.1. Experimental

3.1.1. Carbon Aerogel Synthesis

For the study on the influence of modifying the CAB CA surface chemistry, sample CA 10-0.2-0.25DA has been used as precursor for all surface treatments.

CAB OA 10-0.2-0.25DA has been synthesized by sol-gel method, according to the protocol presented in chapter II, subsequently dried supercritically (see also chapter II) and finally pyrolyzed at either 1000 °C (referred to as CA1) or 1050 °C (by J.-F. Maréché, LCSM, UHP2, Nancy; referred to as CA2) in N_2 (see chapter III).

3.1.2. Chemical Modification of the Carbon Aerogel

The surface chemistry of the CAB CA1 has been modified by oxidation and/or introduction of nitrogen.

CA1 powder (particles between 5 and 40 μm) has been oxidised in a solution of H_2O_2 (5 N) or HNO_3 (4 N) for 48 h at ambient temperature under continuous stirring. Samples have been rinsed with distilled water until the pH stabilized. Subsequently, resultant carbons have been dried at 120 °C for

12 h. Oxidized carbons are referred to as CA1H and CA1N for samples treated with H₂O₂ and HNO₃, respectively (see table IV-6).

In order to introduce N-containing functional groups, CAB CA has either been co-heat-treated with melamine or ammonized. For the co-heat-treatment of carbon with melamine, the CA1 sample has been impregnated with melamine, before the impregnated sample has undergone heat-treatment. CA1 powder (9 g) has been dispersed in a melamine suspension (6 g of melamine in 50 mL of ethanol) and stirred at room temperature for 5 h. After filtering, the CA1/melamine mixture has been heat-treated at 750 °C in nitrogen flow during 1 h, resulting in the carbon CA1M (see table IV-6). The procedure has principally been carried out described in the work of Seredych et al. [Ser 2008].

For ammonisation CAB CA sample CA2 has been used. Powders of CA2 and CA2N (CA2 oxidised by stirring in 4 N HNO₃ for 48 h) have been treated with gaseous ammonia, resulting in samples CA2AM and CA2NAM respectively. For the ammonisation step, 3 g of carbon powder have been placed in a Pyrex tube. The carbon powder has been heated up to 400 °C in air. At 400 °C carbon powder has been fluidized by an ammonia flow with a flow rate of 50 mL/min for 3 h. After treatment, the reactor has been cooled down to ambient temperature in air. As ammonisation has been carried out at relatively low temperature, sample CA2 has been chosen as precursor for ammonization treatment. Upon ammonization at only 400 °C, a part of the oxygen functionalities may not react. CA2 should contain less heteroatoms than CA1, due to pyrolysis at a higher temperature leading to the breaking of thermally instable chemical bonds at higher temperatures (see chapter III), and should therefore contain a limited number of un-reacted oxygen groups after ammonization treatment.

Table IV-6: Chemically modified carbon aerogels

	<i>Precursor</i>	<i>Treatment</i>
CA1	OA 10-0.2-0.25DA	Pyrolysis at 1000 °C/N ₂ , 1 h
CA2	OA 10-0.2-0.25DA	Pyrolysis at 1050 °C/N ₂ , 1 h
CA1H	CA1	H ₂ O ₂ (5 N), T _{amb} , 48 h
CA1N	CA1	HNO ₃ (4 N), T _{amb} , 48 h
CA1M	CA1	Co-heat-treatment with melamine at 750 °C/N ₂ , 1 h
CA2N	CA2	HNO ₃ (4 N), T _{amb} , for 48 h
CA2AM	CA2	Ammonisation, 400 °C/NH ₃ , 3 h
CA2NAM	CA2N	Ammonisation, 400 °C/NH ₃ , 3 h

3.1.3. Structural Analysis

Structural properties of all the samples have been obtained by N₂ adsorption–desorption and helium pycnometry. Hg porosimetry has additionally been carried out for a choice of samples, namely carbon powder CA1 and its derivatives after chemical modification.

N₂ adsorption and desorption isotherms have been measured at -196 °C with a Fisons Sorptomatic 1990 after outgassing at 10⁻³Pa for 24h at ambient temperature. Analyses have been carried out by N. Job (Laboratoire de Génie Chimique, Université de Liège, Liège, Belgium). He and Hg pycnometry have been carried out according to specifications in chapter II.

The mesopore volume, V_{meso} , has been determined by the Broekhoff-de Boer method and the micropore volume, V_{DUB} , by the Dubinin–Radushkevich equation. The minimum and maximum mesopore diameter, $d_{p,\text{min}}$ and $d_{p,\text{max}}$, *i.e.* the pore diameter limit under which smaller mesopores represent 5% and 95% of the total mesopore volume, respectively, have been deduced from pore size distribution provided by the Broekhoff–de Boer method applied to the adsorption branch of the isotherm and assuming an open cylinder geometry.

3.1.4. Analysis of Chemical Properties

Elemental composition has been determined as described in chapter II.

The surface chemistry of the carbon aerogels has been characterized by Fourier transform infrared spectroscopy (FTIR), X-ray photoelectron spectroscopy (XPS), Boehm method and pH of the point zero charge measurement (pH_{pzc}).

FTIR spectroscopy on the aerogel samples has been carried out according to specifications given in chapter III.

The XPS analyses have been carried out using a VG Scientific Multilab apparatus using $K\alpha$ radiation (1486.6 eV). The sample charging has been corrected using the OPs peak ($E_{\text{b(OPs)}} = 284.6$ eV) as an internal standard. A non-linear, Shirley-type baseline and an iterative least-squares fitting algorithm have been used to decompose the peaks, the curves being taken as 70 % Gaussian and 30 % Lorentzian. XPS analyses have been carried out by D. Bégin (LMSPC, ECPM, Strasbourg, France) and deconvolutions by B. Grzyb (CEP, Mines ParisTech, Sophia Antipolis, France).

Acidic and basic surface groups have determined according to the method of Boehm and co-workers [Kap 1999]. The carbon aerogel powder (0.5 g) has been dispersed in 0.05 N sodium hydroxide (25 mL) and in 0.05 N hydrochloric acid (25 mL). The vials have been sealed and shaken for 24 h, and then 8 mL of each filtrate has been pipetted and the excess of base or acid has been titrated with HCl or NaOH. The numbers of all acidic sites (of various types) have been calculated under the assumption that NaOH neutralises carboxyl, phenolic and lactonic groups. The number of surface basic sites has been calculated from the amount of hydrochloric acid that reacted with the carbon.

To measure the pH_{pzc} , 0.5 g of carbon powder has been added to 10 mL of CO_2 -free distilled water and the suspension has been shaken for 24 h to reach equilibrium. The final pH of the suspension has been taken as the pH_{pzc} of the carbon material [Mac 2005, Lás 2001].

3.2. Results and Discussion

3.2.1. Structure

Results of mercury porosimetry for samples based on CA1 (see table IV-7) indicate that all samples seem to be nearly exclusively microporous and mesoporous, with only a very small quantity of macropores, if present at all. In addition, mercury porosimetry measurements have been less precise than values from nitrogen adsorption in this case, as measurements have been carried out on carbon powders and the volume variation observed at low pressure corresponds rather to intrusion between

the carbon powder grains than to porosity. Therefore, nitrogen adsorption has been deemed to be sufficient to obtain the whole pore size distribution and pore volume.

Table IV-7: Porous volumes of non-modified and modified CA1 from nitrogen absorption and mercury porosimetry

			CA1	CA1H	CA1N	CA1M
V_{meso}	[cm ³ /g]	±0.02	0.28	0.24	0.23	0.23
V_{Hg}	[cm ³ /g]	±0.02	0.28	0.27	0.23	0.25

Structural characteristics of CA1 and CA2 before and after chemical modification can be found in table IV-8. All samples, with the exception of the ammonised samples, display low porosity: total pore volumes between 0.23 and 0.30 cm³/g and specific surface areas range between 117-165 m²/g. Carbon aerogels obtained from CA1 are mainly mesoporous, with mesopores constituting about 80 % of the pore volume.

Table IV-8: Structure of carbon aerogels before and after chemical treatment

			CA1	CA1H	CA1N	CA1M	CA2	CA2AM	CA2NAM
ρ_s	[g/cm ³]	±0.02	1.92	2.07	2.00	2.00	2.05	2.02	2.03
V_{DUB}	[cm ³ /g]	±0.01	0.07	0.06	0.05	0.06	0.05	0.12	0.12
V_{meso}	[cm ³ /g]	±0.02	0.23	0.24	0.23	0.23	0.18	0.23	0.22
s_{BET}	[m ² /g]	±10	165	152	121	130	117	280	277
$d_{p,min}$	[nm]	±1	9	8	9	9	8	9	8
$d_{p,max}$	[nm]	±1	14	14	15	15	15	14	14

Oxidation (with H₂O₂ or HNO₃) and treatment with melamine tend to slightly decrease in the s_{BET} value, apparently due the formation of the functional groups blocking the access to the pores (table IV-8). This phenomenon is mainly observed in the case of the oxidized material CA1N prepared by treatment of the CA1 in nitric acid (121 m²/g vs. 165 m²/g, respectively). The loss of the porosity is more pronounced (27 % of BET value) than for other samples. For CA1H obtained by the reaction of CA1 with H₂O₂, the decrease of the BET value is not significant. In the case of CA2, the treatment at higher temperature, 1050 °C vs. 1000 °C, results in a smaller s_{BET} than for CA1 (117 m²/g vs. 165 m²/g, respectively).

Treatment with ammonia gives more porous carbons: samples CA2AM and CA2NAM display similar specific surface areas (280 and 277 m²/g, respectively). Ammonia acts like an activating agent, promoting porosity development. The general trend consists in the creation of micro- and mesoporosity as well as in the widening of existing pores due to the ammonia treatment [Man 2001, Bim 1998]. Ammonisation mainly promotes a development of the microporosity and, to a lower extent, of the mesopores.

3.2.2. Elemental Composition

The elemental composition of all carbon aerogel samples is presented in table IV-9. CA1 and CA2 display a very different composition with regard to its organic precursor OA 10-0.2-0.25DA, maintaining about 20 % of the initial oxygen atoms in the bulk.

The oxidation of the carbon aerogel with nitric acid and hydrogen peroxide induces the incorporation of an additional 5 wt.-% of oxygen compared to CA1. The oxygen content is slightly higher for the CA1N than for CA1H sample (10.3 instead of 9.6 wt.-%). This result is in good agreement with previously reported data indicating a higher reactivity of the nitric acid [Kin 1988]. The high oxygen content of sample CA1N corresponds also to a higher loss of the porosity (27 % of BET value) than for other samples (see table IV-8) and a higher acid/base modification of the CA1N's surface (see table IV-10).

Co-heat treatment of the carbon aerogel with melamine gives a nitrogen-rich carbon: CA1M displays a nitrogen content of 6.7 wt.-%, *i.e.* twice as high as its precursor CA1 (3.0 wt.-%).

CA2 contains a lower amount of oxygen as compared to CA1, which can be explained by the higher pyrolysis temperature (see chapter III on the influence of pyrolysis temperature). Ammonisation of CA2 leads to the incorporation of an additional 1.5 wt.-% of nitrogen: the nitrogen content of sample CA2 amounts to 2.9 wt.-% and to 4.5 wt.-% in the case of CA2AM. The percentage of nitrogen in CA2AM and CA2HAM samples is very similar (4.5 and 4.6 wt. %, respectively), demonstrating that the oxidation of CA2 prior to the ammonia treatment did not result in any beneficial effect in terms of nitrogen incorporation. Probably, the temperature of the ammonisation used in this study has not been high enough to promote the reaction of ammonia with the previously introduced oxygen groups [Zaw 2003]. Nonetheless, the data presented in table IV-9 show that CA2N loses 50 % of oxygen during its ammonisation (from 6.7 wt.-% for CA2N to 3.2 wt.-% for CA2NAM), most likely due to the thermal decomposition of oxygen groups and/or their reaction with ammonia.

Table IV-9: Elemental composition of the CAB OA and derived CA [wt.-%]

Sample	%C	%H	%N	%O	N/C_{at}	O/C_{at}	N/O_{at}
OA 10-0.2-0.25DA	52.9	5.6	1.8	39.5	0.03	0.57	0.02
CA1	91.1	0.9	3.0	5.1	0.03	0.04	0.03
CA1H	86.3	0.9	3.1	9.6	0.03	0.08	0.03
CA1N	85.4	0.9	3.4	10.3	0.03	0.09	0.03
CA1M	87.1	1.1	6.7	5.1	0.07	0.04	0.06
CA2	92.6	0.8	2.9	2.8	0.03	0.02	0.03
CA2N	87.1	1.2	3.2	6.7	0.03	0.06	0.03
CA2AM	90.5	0.8	4.5	2.8	0.04	0.02	0.04
CA2NAM	89.1	0.9	4.6	3.2	0.04	0.03	0.04

3.2.3. Evolution of the Surface Chemistry on the Chemical Treatment of the Carbon Aerogels

Porous carbons possessing a surface featuring a majority of acidic functional groups can be distinguished from carbons featuring a majority of basic functional groups on their surface. Hence, methods like pH_{pzc} measurement and mass titration are very useful to characterize the surface chemistry. Results from acid/base titration presented in table IV-10 indicate that CA1 displays a basic character, with a concentration of basic groups of 0.50 mmol/g, largely exceeding the amount of acidic groups (0.14 mmol/g). The higher pyrolysis temperature for sample CA2 does not result in the reduction of functional surface groups, but in a modification of the surface groups' character. On CA2 more acidic groups can be found, while the number of basic functional groups has decreased. The changes in the surface groups' character is mirrored in the evolution of the pH_{pzc} value, which changes from rather basic to acid (7.1 for CA1 pyrolyzed at 1000 °C, to 4.6 for sample CA2 pyrolyzed at 1050 °C).

Treatment with melamine and ammonia has been intended to enhance the basicity of the carbon aerogels, while oxidation treatments with either H_2O_2 or HNO_3 have been performed in order to introduce acidic groups on carbons. Acid/base titration shows that all tested functionalisation methods employed within the scope of this work lead to an increase in the density of the surface groups. As expected, both oxidation treatments (with H_2O_2 or HNO_3) enhance the number of acidic surface groups from 0.14 mmol/g to 0.57 mmol/g for CA1H and to 0.67 mmol/g for CA1N, while the density of the basic groups decreases considerably. These modifications are reflected in the slight decrease of the pH_{pzc} value: from 7.1 (CA1) to 6.4 (CA1H) and 6.3 (CA1N).

Table IV-10: Acid-base properties of the functionalised carbon aerogels

Sample	Acidic groups [mmol/g]	Basic groups [mmol/g]	Acidic and basic groups [mmol/g]	pH_{pzc}
CA1	0.14	0.50	0.63	7.1
CA2	0.28	0.33	0.62	4.6
CA1H	0.57	0.33	0.90	6.4
CA1N	0.67	0.27	0.94	6.3
CA1M	0.23	0.41	0.64	7.1
CA2AM	0.05	0.61	0.66	9.5
CA2NAM	0.09	0.61	0.70	9.0

Quite unexpectedly, the co-heat treatment of CA1 with melamine does not enhance its basicity. Contrary to effects described by Seredych et al. [Ser 2008], the basicity of CA1M is slightly lower than that of its precursor CA1, while the N/C ratio is twice as high as in case of the parent carbon. Since the concentration of the acidic groups in the treated sample is higher than in the case of CA1, this

behaviour could be explained by an increased oxidation of the surface during the storage of the carbon due to the fixation of oxygen on nascent carbon atoms left on the CA surface after the treatment.

The treatment with ammonia gives the most basic materials, considering the concentrations of basic groups close to 0.60 mmol/g for both CA2AM and CA2NAM samples. The data presented in table IV-10 show that ammonisation does not consist solely in the introduction of basic nitrogen groups, but also in the reduction of the acidic oxygen groups. The concentration of acidic O-containing groups is effectively lowest in CA2AM and CA2NAM (0.05 and 0.09 mmol/g respectively). A higher concentration of acidic groups measured for CA2NAM indicates that a part of the oxygen groups introduced by the previous oxidation treatment with nitric acid has not been reduced by ammonia. Earlier studies have shown that the effect of ammonisation depends on the temperature of the process; some acidic functionalities may not react at a lower temperature [Jan 1994].

The surface chemistry of the carbon aerogels CA1 and CA2 acting as precursors for the different surface modification treatments and of the functionalised carbon aerogels has also been studied using FTIR and XPS spectroscopy. Figure IV-14 presents the FTIR spectra of sample CA1 and its derivatives prepared by the oxidations and treatment with melamine. The main process accompanying the oxidations with HNO_3 and H_2O_2 materials is the formation of carboxylic groups, manifested in a moderate increase of the bands at 1720 and 1170 cm^{-1} (C=O and C-O stretching in carboxylic groups [Zaw 1989]). The peak at 1720 cm^{-1} is more intense in the case of the HNO_3 -treated carbon aerogel. This observation bears out previously published results indicating that oxygen groups resulting from oxidation in HNO_3 have a more acidic character [Kin 1988] as compared to oxygen groups resulting from oxidation in H_2O_2 . In parallel, the band at 1040-1060 cm^{-1} , associated with the C-O stretching in alcohols, decreases. This behaviour suggests that C-OH groups are oxidized to carboxylic functionalities. Also, the oxidation treatment is accompanied by an increase in the peak at 1530-1570 cm^{-1} , indicating the formation of quinone groups.

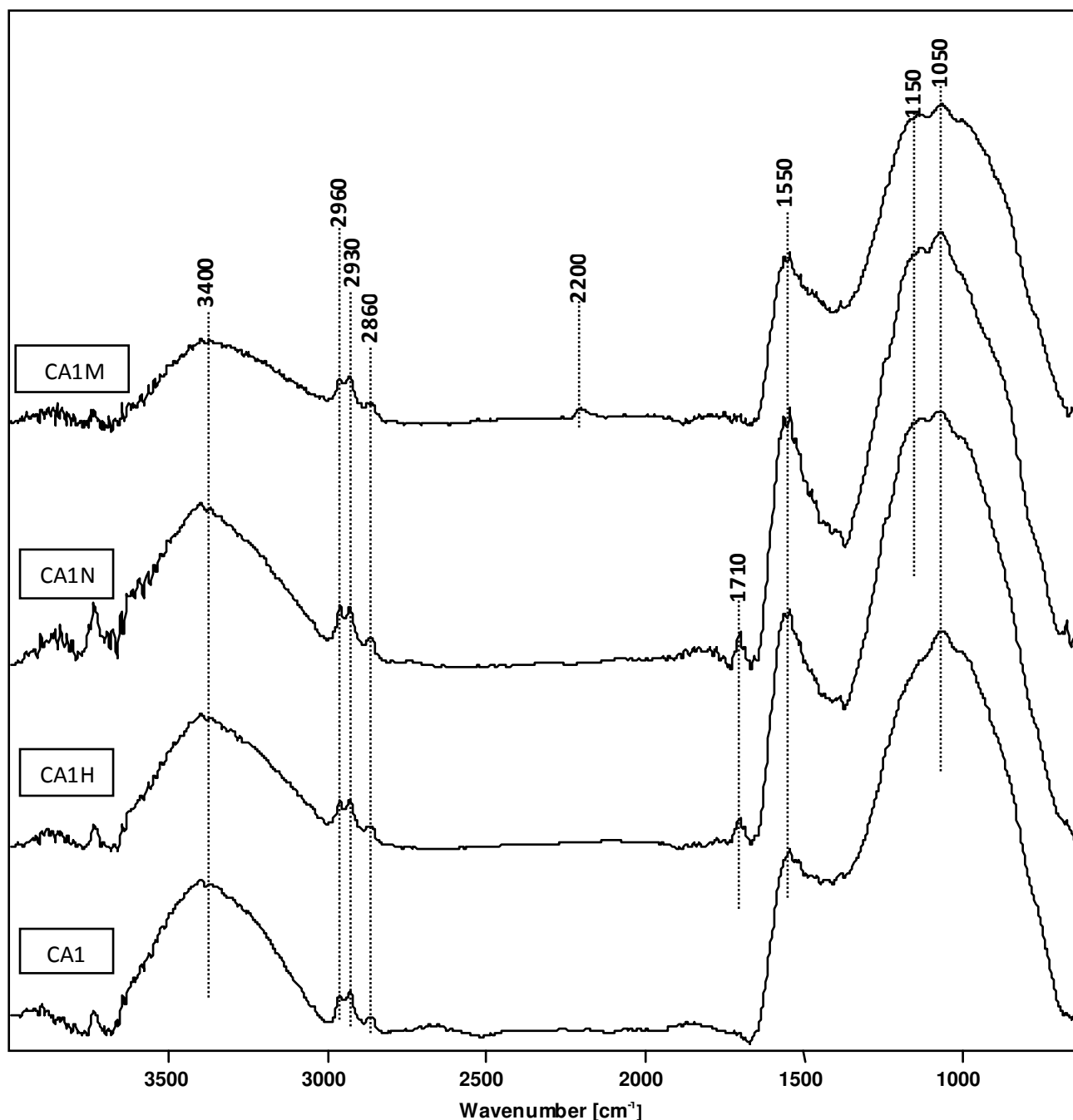


Figure IV-14: FTIR spectra of chemically treated carbon aerogels.

The spectrum of CA1M fairly resembles that of its precursor CA1. Slightly more intense absorbance in the 1150 cm^{-1} region suggests that some esters/lactone compounds are formed, probably due to oxidation of nascent carbon atoms left on the CA surface after the treatment (during storage of the material). In addition, a small but sharp peak at 2200 cm^{-1} is observed, indicating that some oxidised forms of nitrogen functionalities have been formed.

The chemical transformations occurring during ammonia treatment of the carbon aerogel have been examined based on the subtraction results of the respective FTIR spectra (see figure IV-15).

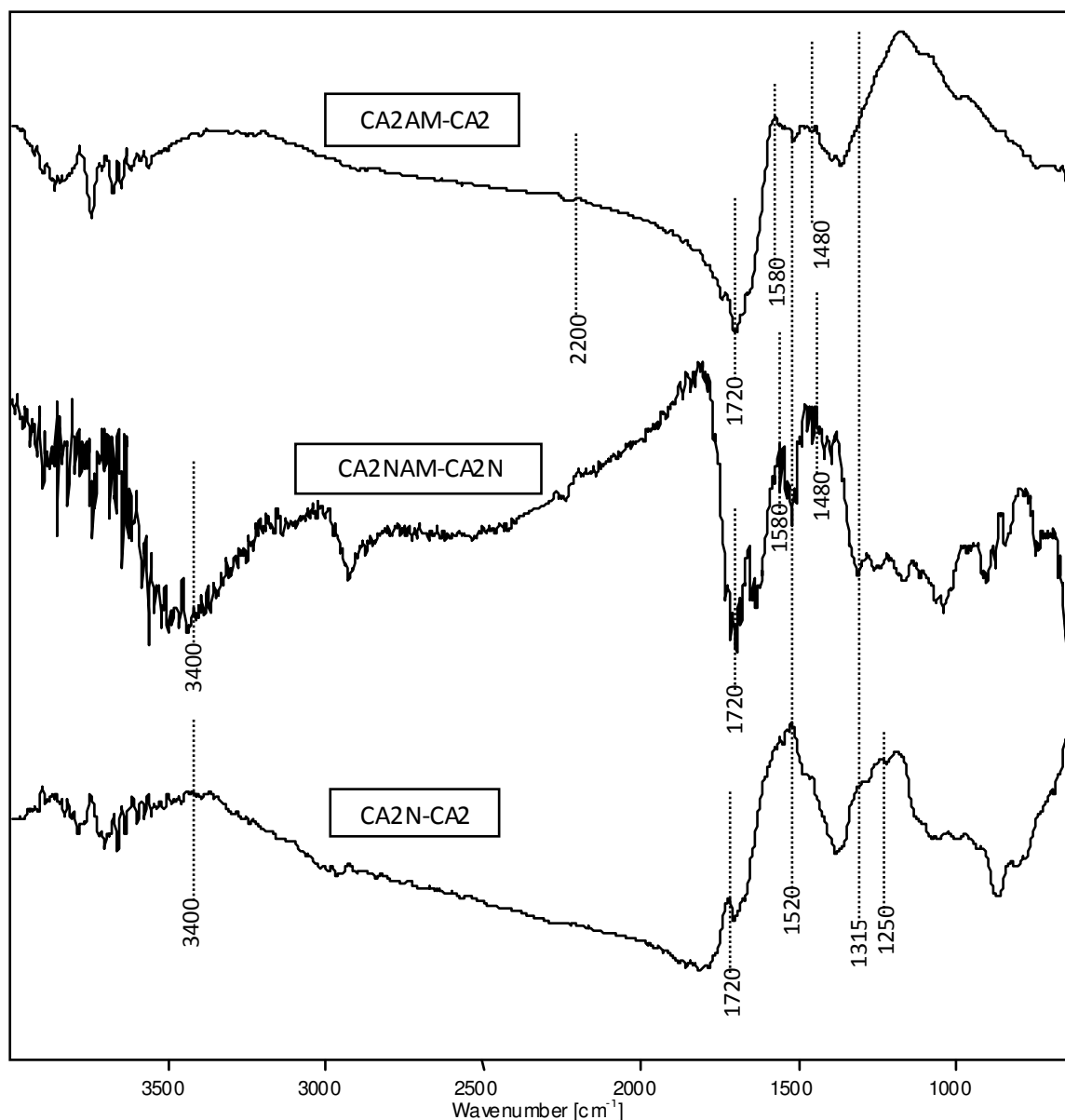


Figure IV-15: FTIR difference spectra of ammonised carbon aerogels.

Positive peaks appearing in the 1720, 1250, 1560 and 3400 cm^{-1} zone of the difference spectra of CA2N vs. CA2 (figure IV-15) confirm an introduction of carboxylic and quinone groups during oxidation with nitric acid. Moreover, bands at 1520 and 1315 cm^{-1} correspond to the asymmetric and symmetric stretching of the NO_2 groups [Zaw 1989], indicating that nitrite groups are also introduced by the nitric acid treatment. The nitrite functionalities are subsequently removed by the ammonia treatment, which can be deduced from the presence of negative peaks at 1520 and 1315 cm^{-1} in the difference spectra of CA2NAM vs. CA2N. The reductive role of ammonia can also be observed in the removal of the carboxyl groups, visible as negative peaks at 1720 cm^{-1} in the respective difference spectra (CA2NAM vs. CA2N and CA2N vs. CA2). These observations bear out the results of the elemental analysis (table IV-9), since the oxygen content measured in the ammonised samples is distinctly lower than in their respective precursors CA2 and CA2N. Apparently, oxygen groups are partly removed during ammonisation. The presence of a small positive peak at 2200 cm^{-1} in the

difference spectrum of the CA2AM vs. CA2 and CA2NAM vs. CA2N indicates that isocyanate species containing the N=C=O functional groups are formed on the reaction of CA2 and CA2N with ammonia.

XPS data provide more precise insight into the evolution of the surface groups during thermal treatment of the carbon aerogel. The C1s spectra of CA1 and the functionalised aerogels on the basis of CA1 (*i.e.* CA1H, CA1N, and CA1M) are presented in figure IV-16. As can be concluded from the deconvolutions of the C1s envelope (table IV-11), the major part of the carbon atoms contributes to the non-functionalised skeleton (ranging from 69.8 to 55.1 % of the total surface carbons in case of the CA1 and CA1H carbon, respectively). The relative percentage of non-functionalised carbon in CA1H, CA1N and CA1M is considerably lower than in case of CA1. This finding is in agreement with the higher degree of the functionalisation of these products (see table IV-10). The remaining part of carbon atoms is mainly involved in ethers and alcohols and C-N linkages (binding energy 286.1 eV). Considering the effect of oxidation, C1s spectrum of CA1H reveals an increase in the intensity of the peaks at 286.1, 287.8, and 289.2 eV demonstrating that the oxidation treatment in H₂O₂ is accompanied by the formation of a variety of groups containing C-O and C=O. The peak at 286.1 eV is most intense for CA1H, implying that mainly alcohols and ethers are formed by oxidation in H₂O₂. In contrast, the oxidation with nitric acid is primarily accompanied by the incorporation of esters, lactones and carboxylic groups, as can be deduced from the increase in intensity of the peak centred at 289.2 eV.

Table IV-11: XPS data (envelope C1s)

b.e. [eV]	Assignment	CA1	CA1H	CA1N	CA1M	CA2	CA2N	CA2AM	CA2NAM
284.6 (± 0.1 eV)	non functionalised carbon	69.8	55.1	66.4	57.9	57.1	50.2	70.3	65.7
286.1 (± 0.1 eV)	carbon linked to oxygen or nitrogen by a simple bond	20.1	27.8	18.5	25.9	18.1	22.0	16.3	14.0
287.8 (± 0.1 eV)	carbon linked to oxygen by a double bond (ketones, quinones, or amides)	5.7	9.5	7.0	5.9	13.8	15.9	5.1	10.4
289.2 (± 0.1 eV)	C=O in esters, lactones, anhydrides, acids	3.5	5.3	7.4	8.7	7.0	7.6	4.6	5.5
290.8 (± 0.1 eV)	plasmon / π-π* transitions	0.9	2.2	0.7	1.7	4.0	4.3	3.6	4.4

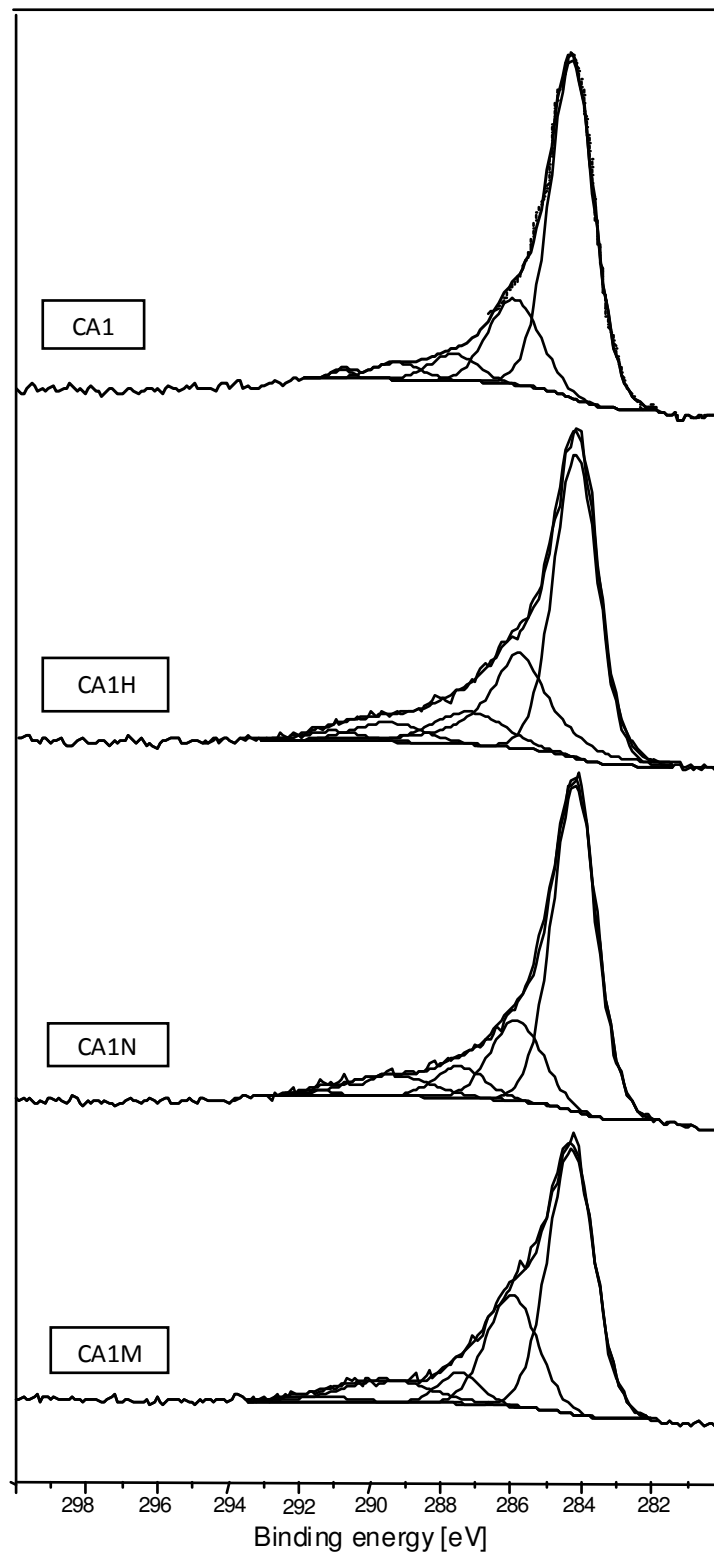


Figure IV-16: C1s XPS spectra of carbon aerogels

These observations are further supported by the deconvolution of the O1s envelopes (table IV-12 and figure IV-17). The peak at 533.5 eV corresponding to C-O-C increases in the case of CA1H, and decreases for CA1N. Similarly, the peak at 530.6 eV, related to C=O carboxyl moieties, is more intense in the CA1N acid-treated sample. The most relevant effect of the co-heat-treatment with melamine is

the incorporation of nitrogen functionalities as observed in the rise of the peak at 286.1 eV. Quite unexpectedly, a substantial quantity of the C=O groups (corresponding to the peak at 289.2 eV) is present in this sample. Probably these functionalities are formed after carbonisation, during the storage of the sample [Kin 1988].

Table IV-12: XPS data (envelope O1s)

b.e. [eV]	Assignment	CA1	CA1H	CA1N	CA1M	CA2	CA2N	CA2AM	CA2NAM
530.6 (±0.2 eV)	C=O in carboxyl	19.0	18.1	24.2	9.4	10.0	12.0	10.9	17.0
532.3 (±0.3 eV)	C=O in ester, amides	39.3	30.2	39.0	28.3	17.5	19.5	18.2	24.2
533.5 (±0.2 eV)	C-O-C (ethers)	24.7	30.8	23.5	28.4	29.7	26.2	27.7	25.7
534.3 (±0.2 eV)	C-OH, N-O-C	12.1	11.9	7.8	30.1	27.5	26.3	32.2	25.7
536.3 (±0.4 eV)	H ₂ O, O ₂ ads.	4.9	8.0	5.5	3.8	15.3	16.0	11.0	7.4

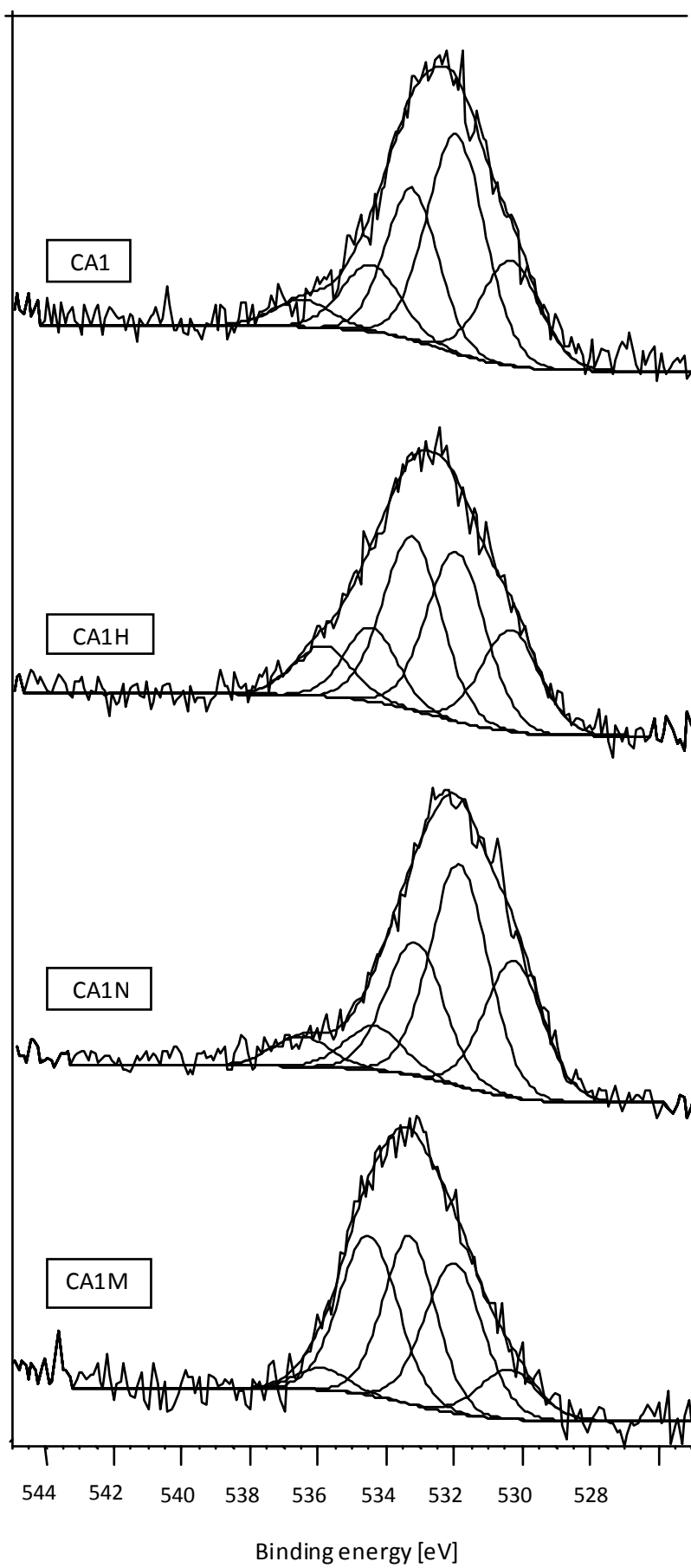


Figure IV-17: O1s XPS spectra of carbon aerogels

XPS N1s spectra of carbon aerogels (figure IV-18) have been fitted by four components of binding energies of about 398.7, 400.3, 401.4 and 404.3 eV. The peaks are assigned to different forms of nitrogen atoms substituted for carbon in the graphene layer: N-6, N-5, N-Q and N-X respectively [Pel 1995]. In CA1, nitrogen is mainly found in the form of N-5 (46.3 % of nitrogen atoms), corresponding to pyrrolic/pyridonic functionalities (Table IV-13). Both oxidation processes affect the nitrogen groups similarly. A decrease in the intensity of the N-6 peak is accompanied by a simultaneous increase of the N-5 peak. This phenomenon can be explained by the introduction of oxygen groups into pyridinic rings, resulting in the formation of pyridonic functionalities. Nitrogen groups in oxidised carbons are thus mainly present in N-6/N-5 non-condensed forms, involving approximately 90 % of surface atoms. The main effect of the treatment with melamine consists in a very strong increase in pyridinic nitrogen (of about 20 % as compared to CA1), while N-Q forms become much less abundant. This behaviour may be due to the rather moderate temperature of the heat treatment (750 °C), possibly not being high enough to promote the condensation of N-6 rings. Further, the peak at 402 eV (N-X) is stronger in CA1M than in the other samples. This energy has frequently been reported to represent different forms of oxidised nitrogen atoms, which points, in concordance with the FTIR spectrum, at a presence of $-N=C=O$ bonds.

Table IV-13: XPS data (envelope N1s)

<i>b.e. [eV]</i>	<i>Assignment</i>	<i>CA1</i>	<i>CA1H</i>	<i>CA1N</i>	<i>CA1M</i>	<i>CA2</i>	<i>CA2N</i>	<i>CA2AM</i>	<i>CA2NAM</i>
398.7 <i>(±0.3 eV)</i>	N6	37.6	33.6	32.7	53.5	28.3	21.6	35.7	28.9
400.3 <i>(±0.3 eV)</i>	N5	46.3	52.1	51.4	29.4	19.3	25.8	17.2	34.7
401.4 <i>(±0.5 eV)</i>	NQ	12.5	10.1	9.3	8.3	40.9	23.1	40.4	28.7
402-405	NX	3.6	4.2	6.6	8.8	11.5	8.8	6.7	7.7
406.2 <i>(±0.3 eV)</i>	NO ₂	0.0	0.0	0.0	0.0	0.0	20.7	0.0	0.0

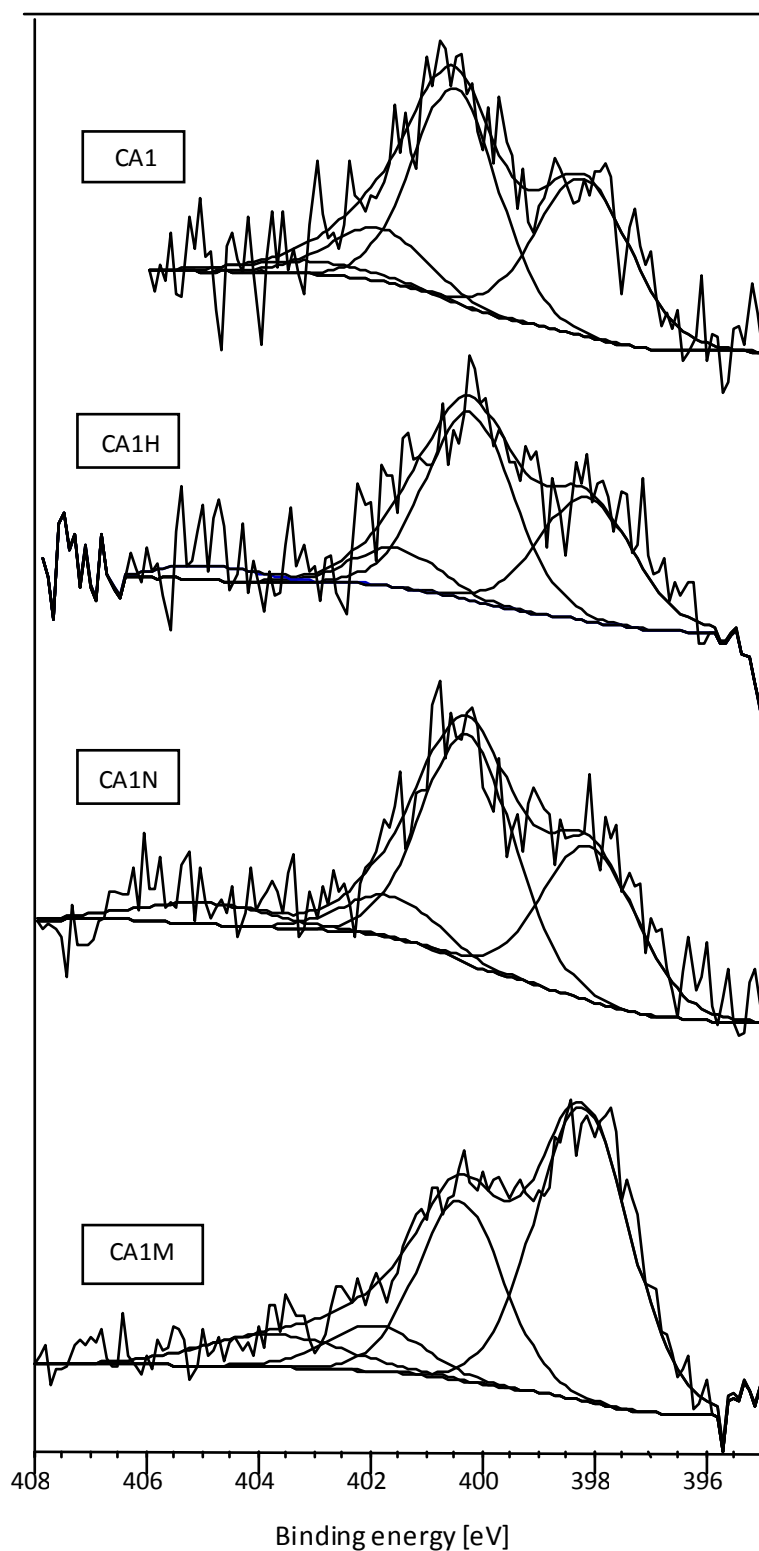


Figure IV-18: N1s XPS spectra of carbon aerogels.

Similarly, XPS has also been used to examine the transformations of the oxygen and nitrogen groups during ammonisation.

Deconvolution of the XPS C1s envelope (figure IV-19 and table IV-11) indicates that the percentage of non-functionalized carbon atoms in CA2 drops to approximately 50 % after oxidation with a nitric

acid (in the case of sample CA2N). Contrarily, the ratio of non-functionalized carbon atoms increases to approximately 70 % after treatment with ammonia. This behaviour can be linked to the removal of a part of the oxygen- and nitrogen-containing groups due to the reductive action of ammonia. Apparently, peaks at 286.1, 287.8 and 289.2 eV, corresponding respectively to the C-O/C-N, C=O and COOH functionalities become less intense in the CA2AM and CA2NAM samples.

Deconvolutions of XPS N1s envelopes for ammonised samples are presented in figure IV-20 and table IV-13. Activation leads to the condensation of pyridinic rings, as 40 % of the nitrogen atoms present in CA2 are found in the “quaternary” form. The oxidation with nitric acid is accompanied by a decrease of the amount of the N-6 form in favour of N-5 functionalities due to the oxidation of a part of the pyridinic groups to the pyridonic form. However, the most striking effect of the oxidation treatment with nitric acid is the formation of nitrite groups involving about 20 % of the nitrogen atoms in CA2N.

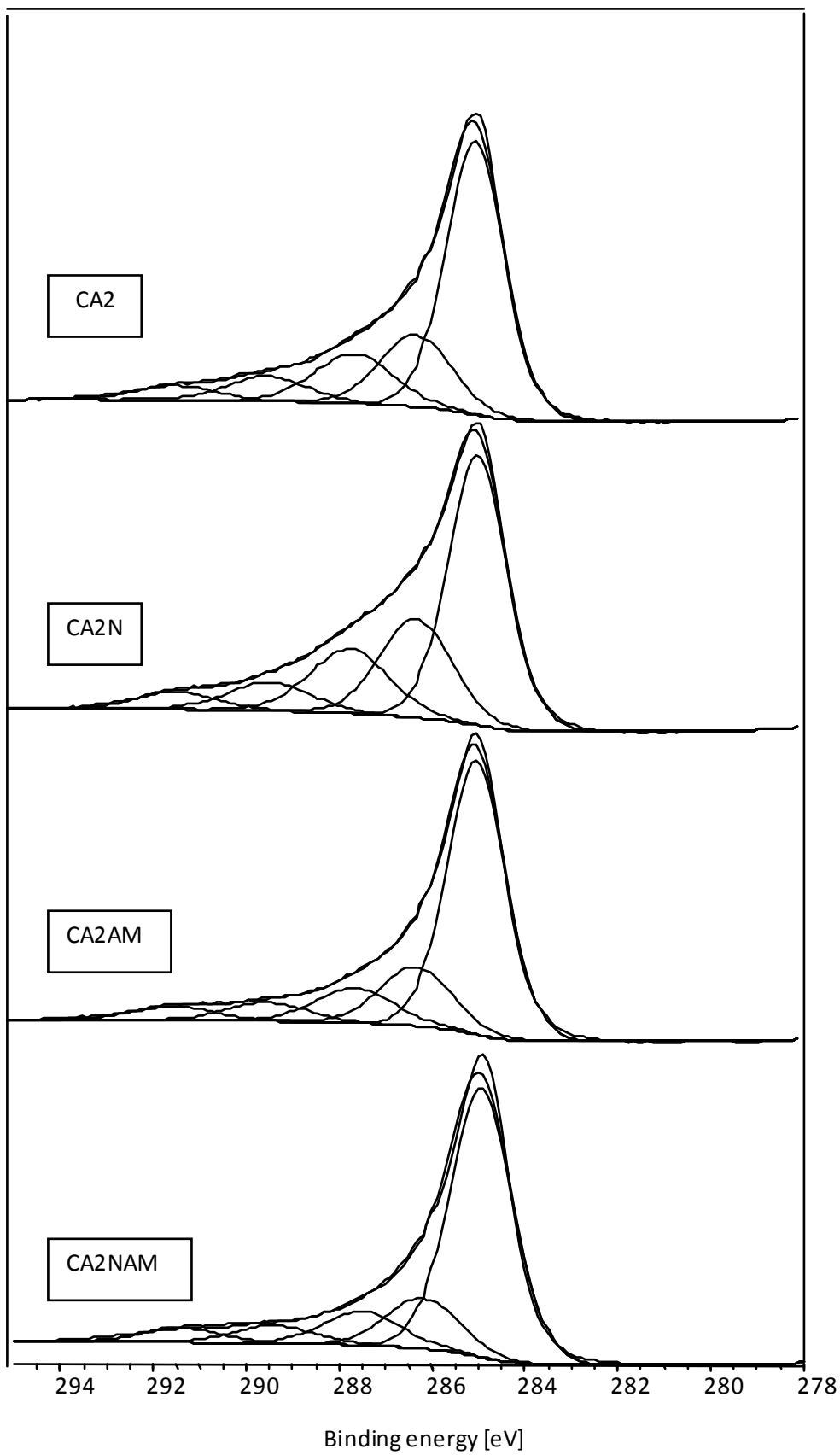


Figure IV-19: C1s XPS spectra of ammonised carbon aerogels

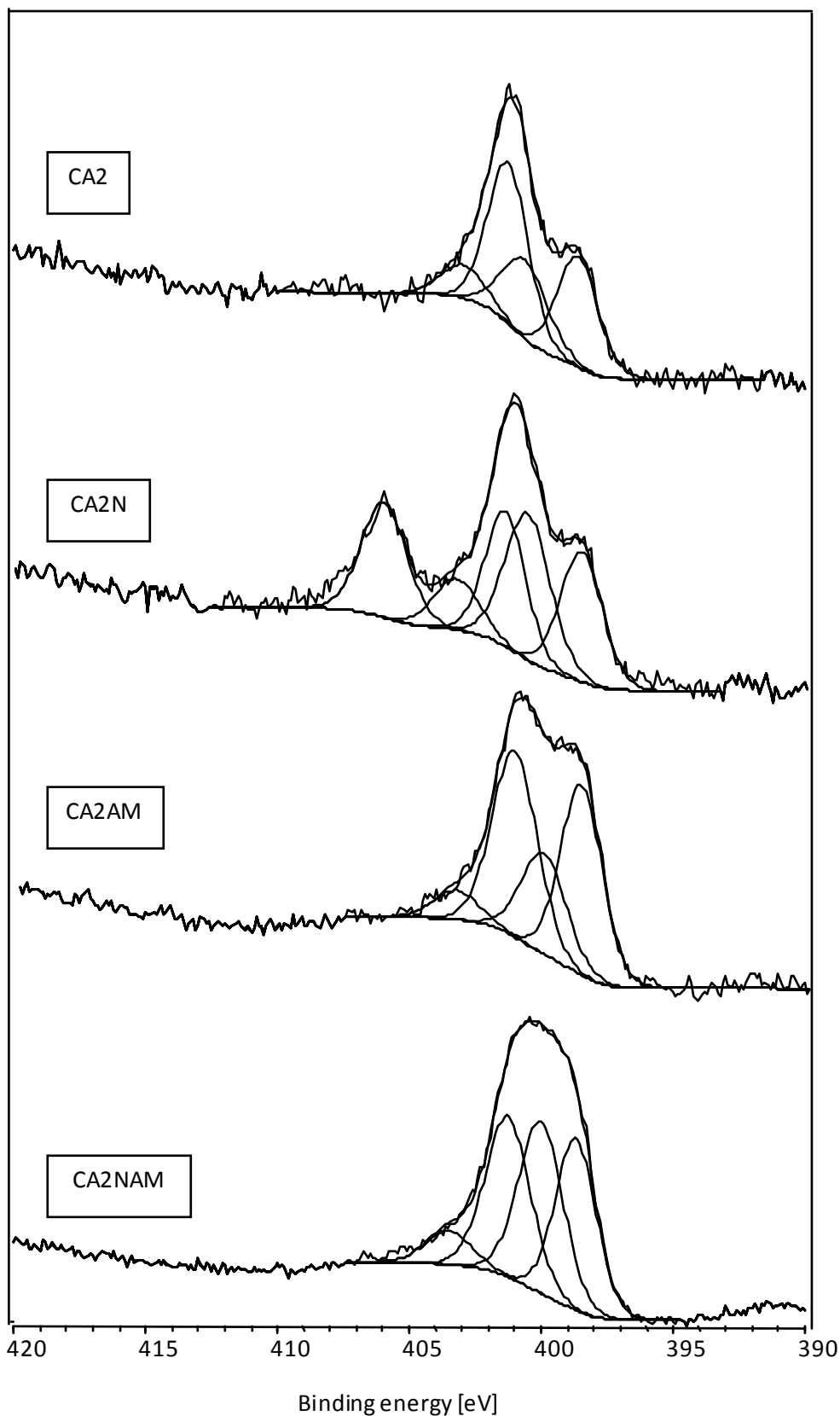


Figure IV-20: N1s XPS spectra of ammonised carbon aerogels

The XPS data confirm the reductive role of ammonia on the oxygen-containing functionalities. After ammonisation of the CA2N sample, NO₂ groups are completely transformed into other nitrogen

functionalities, bearing out the FTIR results. Moreover, the intensity of the peak at 402 eV decreases due to the ammonisation while the N-6 peak at 398.7 eV increases. This phenomenon might be attributed to the transformation of the oxidized N-X functionalities to pyridinic oxygen-free groups. Oxidized N-species, corresponding to the N-X form of nitrogen, are slightly more abundant for CA2NAM. The transformation of the carboxylic groups by oxidation with nitric acid and reaction with ammonia can also be traced as the percentage of the 530.6 eV peak in the O1s spectrum (figure IV-21). Obviously, this peak becomes more intense after oxidation with nitric acid. However, in the case of the CA2NAM sample, this peak is surprisingly intense.

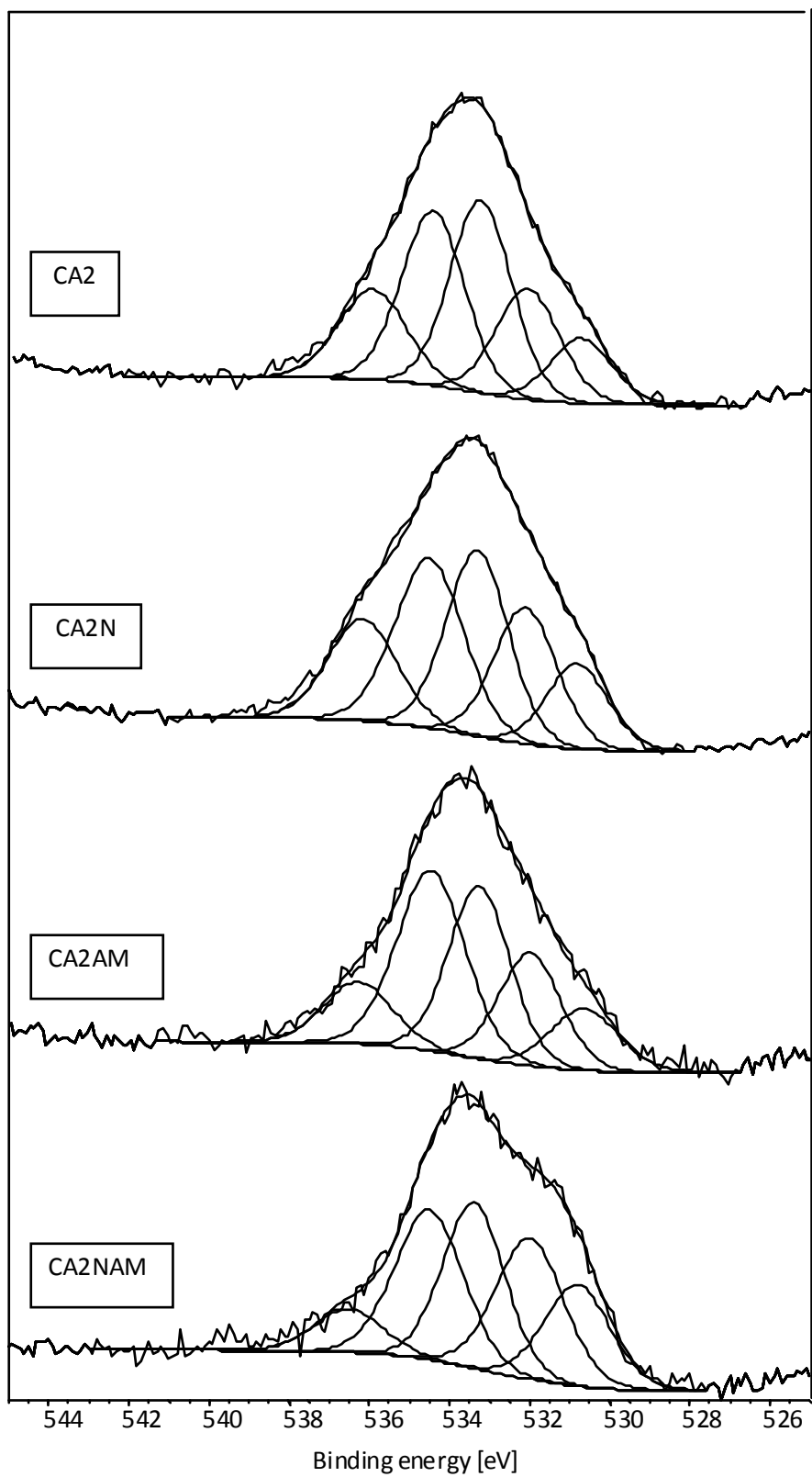


Figure IV-21: O1s XPS spectra of ammonised carbon aerogels.

3.2.4. Heterogeneity of Carbon Aerogels

XPS provides information concerning superficial atomic layers. Depending on the analysis conditions, the spectral information can be extracted from 1 to 10 nm depth [Rat 1997]. Comparing the values of the oxygen and nitrogen atomic concentration derived from XPS and conventional elemental analysis, the difference between surface composition and bulk composition can be estimated. Figure IV-22 relates the N/C atomic ratio obtained from the two methods. Evidently, nitrogen is homogeneously distributed in all the samples derived from CA1. Particularly, in the case of the most nitrogen-enriched sample (CA1M), both values are very similar (0.082 and 0.084 measured by conventional elemental analysis and XPS, respectively), demonstrating that co-heating of the carbon aerogel with the melamine leads to a homogeneous product. On the contrary, in the carbon aerogels prepared by ammonisation, nitrogen groups are formed mainly on the surface. Likewise, figure IV-23 presents the comparison for the O/C atomic ratio. Clearly, nitric acid penetrates deeper into the carbon than H_2O_2 thus giving a more homogeneous distribution of oxygen functionalities for CA1N than for CA1H. Interestingly, in the ammonised samples, the oxygen content is very similar in the bulk and on the surface (about 0.023 and 0.027 for CA2AM and CA2NAM, respectively). This confirms the previously described role of ammonia to remove superficial oxygen functionalities. The differences between O-content in the bulk and on the surface for carbons CA1, CA1M, and also for CA2, meanwhile, point at an oxidation of the CAs if in contact with air.

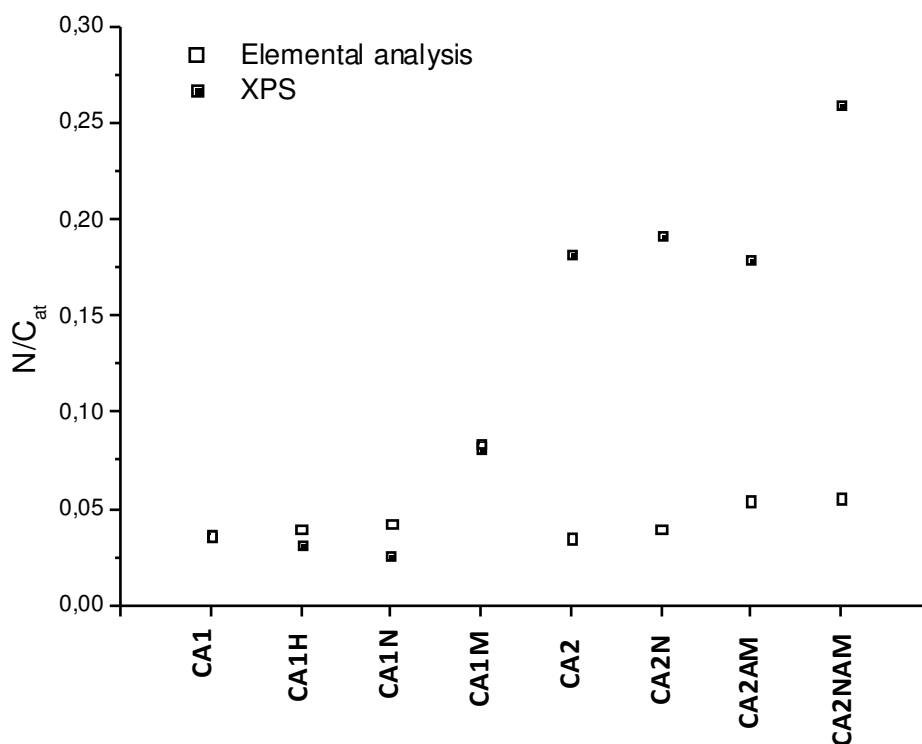


Figure IV-22: N/C atomic ratio based on the XPS and elemental analysis

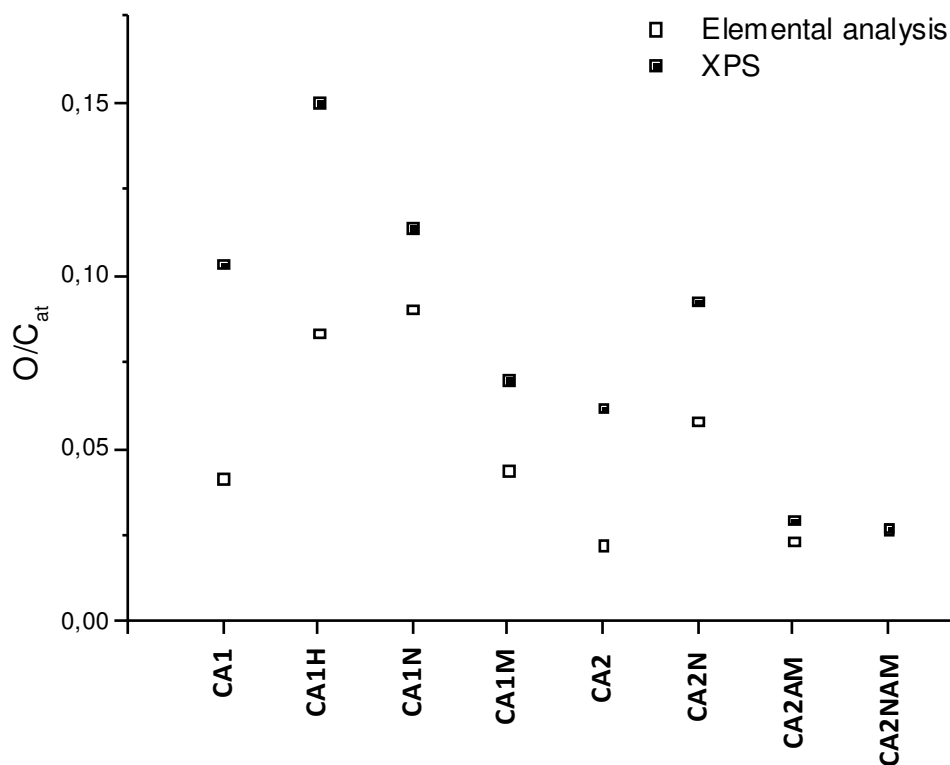


Figure IV-23: O/C atomic ratio based on the XPS and elemental analysis

3.3. Conclusion on the Modification of the Carbon Aerogel Surface Chemistry

The surface chemistry of CAB CA has been functionalized using different treatments. Samples have been oxidized by H_2O_2 and HNO_3 and/or enriched in nitrogen by reaction with ammonia in gaseous phase or by co-heating with melamine. Chemical treatment modifies the porosity of the CAB CA at least slightly. Resultant samples are mainly mesoporous, with a low porosity development (s_{BET} between 121 and 280 m^2/g). CA samples treated in ammonia undergo the most pronounced structural changes, due to major modifications in the micropore scale. Additionally, treatment in ammonia produces the most basic materials, mostly due to the removal of acidic oxygen groups and the transformation/introduction of nitrogen groups occurring in the outer atomic layers. The methods used for modifying the CA surface chemistry in this study allow adjusting the chemical composition, elemental composition, and acid/base properties of the CAB CA. The possibility of preparing a large panel of nanostructured carbon materials with different types and quantities of oxygen- or nitrogen-containing surface groups has been demonstrated.

4. Conclusion

In order to modify the CAB CA characteristics, I have examined the influence of several treatments aiming at changing the carbon's structure or its elemental composition and surface chemistry. In this work, I have investigated the influence of physical activation on the CAB CA, the introduction of cellulose powder into the CAB sol, and chemical treatment of the CAB CA.

To create CAB CA with higher porosity and specific surface areas, I have modified the CAB CA cellulose-acetate-based carbon aerogel structure by physical activation in CO₂ at temperatures between 850 and 1050 °C. The activation treatment brings about radical structural modifications, increasing surface area and porosity. Nanostructured carbons with specific surface areas of over 2000 m²/g and micro- and mesoporous volumes of 0.75 and 0.95 cm³/g, respectively, have been created. In addition to modifying the carbon structure, activation also modifies the CA surface chemistry. Oxygen-containing functionalities seem to be created during activation in CO₂ at a temperature of 850 °C, but to be decomposed alongside initially present O-containing functional groups at 950 °C or 1050 °C.

To be able to control the shrinkage of the aerogel, I have investigated the influence of introducing microcrystalline cellulose powder into the cellulose-acetate sol. CAB OA and CA containing cellulose powder have been synthesized. Cellulose-containing CAB OA and CA maintain their original shape during drying and pyrolysis the better the more cellulose powder is introduced into the sol. During pyrolysis, CAs do not “bubble”, but still burst open to create an opening for evacuating the gaseous compounds resulting from partial gasification during thermal degradation. Cellulose-containing CAB CA have lower specific surface areas and lower macroporous volumes, but higher densities than CAB CA not containing cellulose. The original OA structure seems to be maintained much better throughout pyrolysis if cellulose powder is contained. The introduction of cellulose seems to be one of the most important measures in order to modify and control the CAB CA structure.

To obtain CA with different surface chemistries and to understand the development of the complex chemistry of CAB CA during different functionalizing treatments, I have examined different methods of introducing oxygen and/or nitrogen-containing functional groups. CAB CA samples have been oxidized by H₂O₂ and HNO₃ and/or enriched in nitrogen by reaction with ammonia in gaseous phase or by co-heating with melamine. The chemical methods having been applied allow producing a wide range of functionalized carbon aerogels differing in terms of oxygen and nitrogen groups, their distribution and basicity. In addition, all treatments have modified the carbon's porosity and specific surface area at least slightly.

**Chapter V: Electrochemical Analysis of
Cellulose-acetate-based Carbon
Aerogels on the example of an EDLC**

Electrochemical analysis of cellulose-acetate based carbon aerogels as Electrochemical Double Layer Capacitor electrode material

1. Introduction

Nanostructured carbon material is required for a multitude of applications (see chapter I), including electrochemical energy storage in electrochemical double layer capacitors (EDLCs) and batteries.

Electrochemical energy storage methods are usually very efficient at storing electrical energy, because no conversion of electrical energy into another type of energy (*e.g.* potential or kinetic mechanical energy, thermal energy, etc.) before storage is required.

Electrochemical energy storage devices can store electrical charges (i) indirectly or (ii) directly:

- (i) indirect storage of electrical energy involves oxidation and reduction reactions
- (ii) direct storage of electrical energy resorts to electrostatic interactions.

Capacitors and batteries both store electrical energy through electrochemical processes, albeit using different mechanisms. Batteries resort to indirect storage of electrical energy, while conventional capacitors and EDLC store electrical energy directly.

Considering the energy storage mechanisms' differences, it is obvious that electrical energy is converted to chemical energy in the course of indirect storage processes and that only direct storage of electrical energy does not involve any kind of energy conversion step and associated losses at all. Therefore, capacitors and EDLC feature advantageous fast time constants for charge and discharge, a high efficiency, almost unlimited cycle life, and long-term stability [Win 2004].

Further, batteries and capacitors differ also in terms of performance. Energy storage devices are generally distinguished in terms of two performance criteria: (i) power and (ii) energy. Schematically,

- (i) Energy is the capacity to do work. In electrical energy storage devices this is the amount of charges stored which can be released to effect work.
- (ii) Power is the speed at which energy is transferred, in this case the rate of charge and discharge.

These characteristics and how they compare in different devices is illustrated in the Ragone plot in figure I-1.

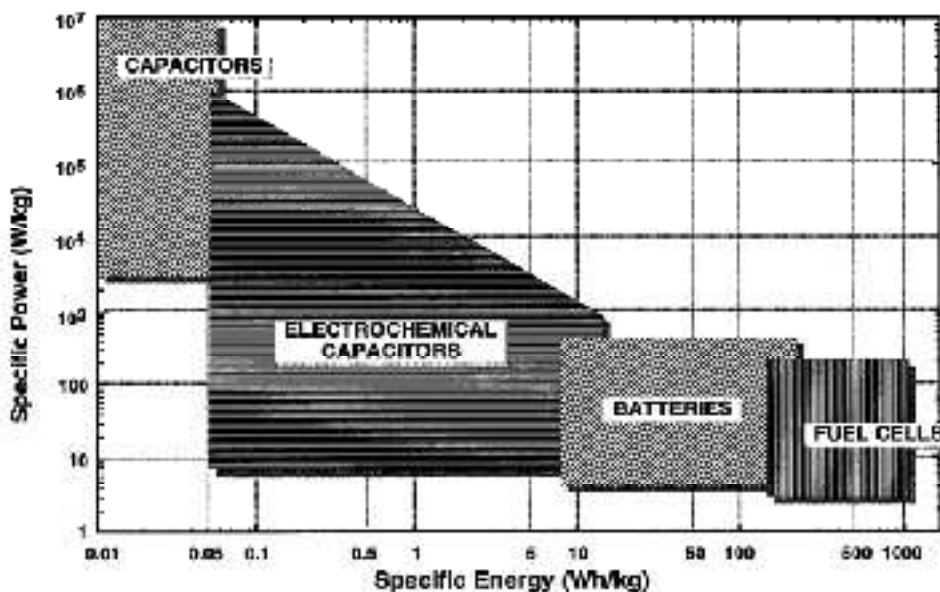


Figure V-1: Schematic Ragone plot for various energy storage and conversion devices [Köt 2000]

EDLCs are high-power systems, unlike batteries which are high-energy systems but are usually unable to respond to high power demands. In comparison to batteries, EDLCs are capable of efficiently and quickly discharging the stored energy. Energy and power capabilities for batteries and capacitors depend on their energy storage mechanisms. While capacitors assemble charges electrostatically at the electrode's surface, batteries store the charges through redox reactions between electrolyte and the electrode material. These mechanisms determine the quantity of electrons which can be stored on the electrode (and therefore energy density) as well as discharge rates (and therefore power capabilities). The impact of the energy storage mechanism on energy and power capabilities for batteries and EDLCs are discussed below.

Energy: According to an exemplary calculation by B.E. Conway [Con 1999], the average EDLC can store about 0.2 electrons per atom of carbon (as double-layer charge) at a voltage of 1 V. In comparison, redox reactions in batteries involve usually 1 or 2 electron charges per atom of carbon. Typically, EDLCs can hence store only 10 to 20% (at 1 V) of the energy batteries are able to store. However, various approaches to improve the energy density in EDLCs are being investigated (see section 2.3 on *Potential improvement of EDLC assembly*).

Power: The power capability depends on the time discharge reactions take. Electrostatic reactions are not subject to kinetic limitations, contrary to redox reactions. The charge release of EDLCs is therefore much faster than in batteries, resulting in relatively high power capability. However, the power density of EDLCs is finally limited, not by reaction kinetics but by the electrolyte's ion diffusion and migration capacities [Con 1999].

Due to these considerations it is quite obvious that batteries cannot be substituted through EDLCs, but rather used as complementary devices. Nonetheless, augmenting energy but also power

capabilities (while limiting leakage current, *i.e.* self discharge) remains of foremost importance in EDLC development.

The performance of CAB CA in electrochemical energy storage and conversion devices has been studied in the course of the ANR project Carbocell. CAB CA have been evaluated in the form of electrode material for PEMFC (LEPMI/INPG) [Roo 2009] and Li/SOCl₂ batteries (SAFT R&D). During my thesis, I have additionally evaluated the electrochemical performance of a broad variety of CAB CA samples if used as EDLC electrode material.

2. State of the Art: EDLC

2.1. EDLC Design

2.1.1. Conventional Capacitor

A capacitor stores electrical charges, and thereby electrical energy, by physically separating charges of opposite polarity but equal magnitude. Through this charge separation an electrical field, and thus a voltage, develops between the two conductors on which the opposite charges accumulate.

The simplest capacitor assembly is a parallel plate capacitor. It is composed of two conductive electrodes (the plates) separated by a dielectric (an insulating substance), as can be seen in figure V-2.

The energy capability of electrochemical energy storage devices depends significantly on the capacitance. The capacitance, C [F], that is the amount of charge stored on each plate for a given potential difference or voltage, of such a device is governed by the following equation:

$$C = (\epsilon_r \epsilon_0 A) / d \quad \text{Equation V-1}$$

The capacitance is linearly proportional to the surface area A [m²] of the plate. It is also proportional to the relative permittivity of the dielectric between the two plates, ϵ_r , but inversely proportional to the distance, d [m] between the plates. The permittivity of free space $\epsilon_0 = 8,854 * 10^{-12}$ Fm⁻¹ is constant [Köt 2000].

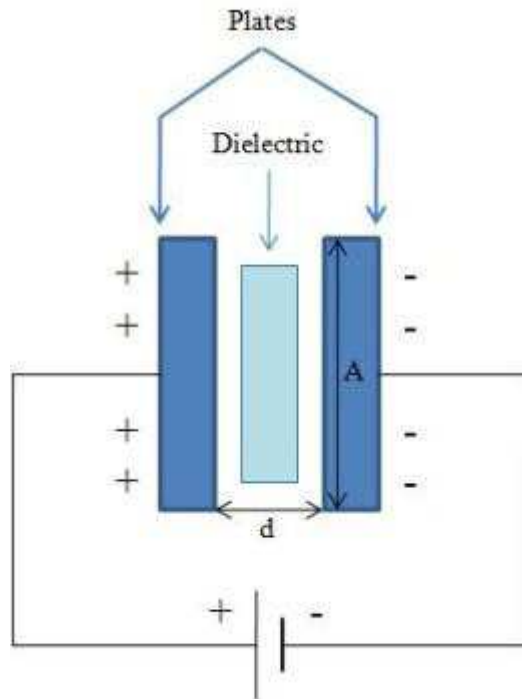


Figure V-2: Schematic representation of a conventional capacitor assembly

2.1.2. EDLC Assembly

In an EDLC several developments have been put into practice to enhance the capacitance.

As opposed to a conventional parallel plate capacitor, consisting of two parallel conductive plates being separated by a dielectric (classically air), a symmetric carbon-based EDLC assembly (figure V-3) is composed of:

- two current collectors,
- two carbon electrodes featuring a high surface area,
- an ion-conducting separator which is used as dielectric,
- an electrolyte.

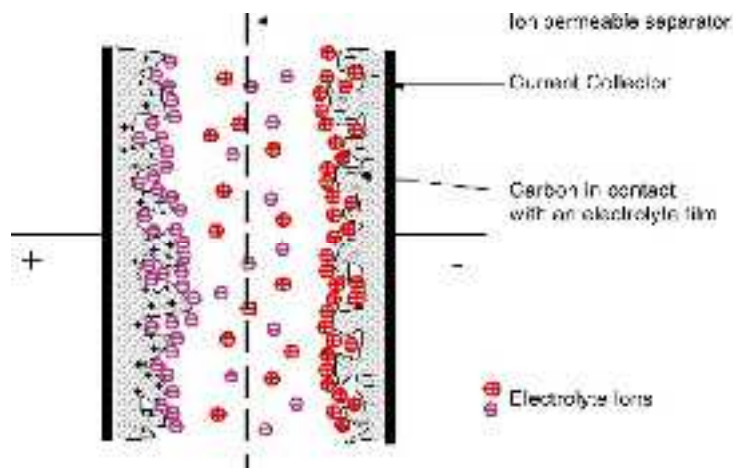


Figure V-3: Schematic representation of a carbon-based electrochemical double layer capacitor (in its charged state) [Pan 2006]

Upon charging an EDLC, opposite charges accumulate (i) in the bulk of the two parallel electrodes and (ii) at the electrode/electrolyte interface. Accordingly, at each of the two electrodes a layer of opposite polarities is generated. The opposite charges at each electrode are thus only separated by the phase boundary between electrode and electrolyte. For electrolytic solutions, a diffuse layer joins this compact layer at the electrode surface (except in the case of micropores) as can schematically be seen in figure V-4. Compact and diffuse layer together give the name to the electrical double layer [Bar 2001]. A thin dielectric, the separator, separates the two parallel electrodes so as to avoid a short circuit. Although the separator needs to be electronically insulating, it must be ionically conductive to let the electrolyte's ions roam freely.

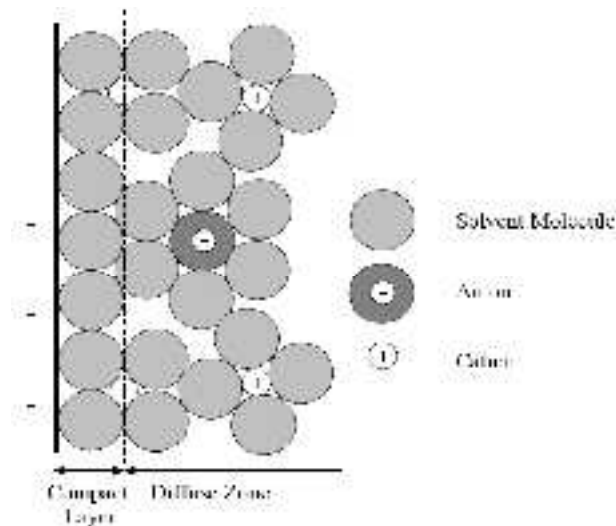


Figure V-4: Schematic representation of the electrical double layer [Dru 2001]

In summary, EDLCs can store considerably more energy than conventional capacitors, as a result of (i) the very small distance d (see equation V-1) between the charges of opposite polarity constituted only by the phase boundary between electrode and adjacent electrolyte (amounting only to about molecular diameter) and (ii) the utilization of electrode material with high accessible surface areas [Con 1999, Pan 2006].

2.2.Importance of the EDLC Electrode

One of the most crucial components in all EDLCs is the electrode. The electrode is in contact with all components of the EDLC and interacts closely with collector and electrolyte. Power and energy storage capabilities of EDLCs are closely linked to the physical and chemical characteristics of the electrodes through resistivity and capacitance. Requirements on structure, composition, and surface chemistry of the EDLC electrode material are therefore quite stringent. In addition to power and energy, the EDLC electrode material has also a significant influence on leakage current and self-discharge. The leakage current is considered to be the current necessary to maintain a capacitor in the charged state. The self-discharge corresponds to the voltage loss with time after full charging of a capacitor.

Carbon is commonly used as electrode material in commercially available EDLCs [Pan 2006]. The advantage of carbon is its availability, versatility, and the multitude of possible combinations of chemical and physical properties, such as:

- ⇒ high conductivity
- ⇒ high surface-area range
- ⇒ controlled pore structure
- ⇒ good corrosion resistance in acidic as well as in basic solutions
- ⇒ high temperature stability
- ⇒ processability and compatibility in composite materials
- ⇒ relatively low cost

2.3.Potential Improvement of EDLC Assembly

2.3.1. Improvement of Energy and Power Capabilities

In order to improve energy and power capabilities, it is important to know that these parameters depend on the EDLCs' capacitance, resistance and voltage.

For EDLCs the energy E [Wh] is defined as:

$$E = \frac{1}{2} CV^2 \quad \text{Equation V-2}$$

and the power P [W] is given by:

$$P = V^2/4R \quad \text{Equation V-3}$$

where C [F] stands for capacitance, V [V] for voltage, and R [Ω] for the device resistance.

According to equations V-1 to V-3, the energy of an EDLC can be increased by:

- (i) increasing the capacitance C
 - ⇒ increasing the area A
 - ⇒ decreasing the distance d between the charges of opposite polarities
 - ⇒ increasing the relative permittivity of the dielectric ϵ_r
- (ii) increasing the voltage V

Power can be increased by:

- (i) increasing the voltage V
- (ii) decreasing the resistance R

Numerous interdependences and commercial constraints (*e.g.* concerning size of the device or voltage) complicate the optimization of an EDLC and different types of EDLC may be needed for different applications [Wad 2006].

An augmentation of energy or power has, according to equations V-1 to V-3, to be based upon an optimization of capacitance, voltage, or device resistance. Any of these optimizations can only be effected by the adaptation of collector, electrode structure and composition, separator material, and the chemical composition of the electrolyte, or a combination of several of these elements. A major approach to increase the EDLCs performance is the optimization of the electrode. Still other approaches in order to increase the EDLCs energy density include:

- ⇒ the utilization of an organic electrolyte instead of an aqueous electrolyte to increase the possible operating voltage range
- ⇒ the introduction of pseudocapacitive effects to increase the capacitance
- ⇒ the assembly of asymmetric hybrid capacitors to increase the capacitance and the possible operating voltage.

All of these approaches aiming at increasing an EDLCs power and energy density are described more thoroughly below.

2.3.2. Electrode structure

In order to limit the internal resistance, the resistivity of the electrode material (depending on the material's electrical conductivity and structure) needs to be low. Other sources contributing to the internal resistance of the EDLC further include i) the interfacial resistance between the electrode and the current collector and ii) the ionic (diffusion) resistance of ions moving in small pores [Pan 2006]. Resistance induced by these sources therefore also depends indirectly or partly on the electrode material used in the electrode, as does capacitance. In order to enhance the electrodes capacitance, the pore structure and volumes needs to be optimized.

Capacitance depends on the electrode surface accessible to the electrolyte's ions. In theory, the highest capacitances may be reached using a material with a high microporous volume due to narrow micropores as these seem to be responsible for charges accumulation. A universal ideal structure for electrode material in terms of pore size distribution does not exist, but an ideal relation of pore size to ion size might exist [Ani 2006]. The ideal pore size depends on the electrolyte and thus on the ion size. Chmiola et al. [CYG 2006] propose this might be the desolvated ion size for applications which require longer discharge times. Recent studies show that 0.7 nm and 0.8 nm are adequate pore sizes for aqueous and organic electrolytes respectively [Vix 2005, RaK 2006]. Also, adequate pore sizes for positive and negative electrodes corresponding to the electrolyte's anion and cation sizes, respectively, have been found to differ [Seg 2010]. However, narrow micropores may restrict or retard the electrolyte diffusion and thereby contribute to high time constants. The time constant τ [s], determined according to equation V-4, indicates how fast the electrode can be charged/discharged [Fra 2001].

$$\tau = R \cdot C$$

Equation V-4

A high time constant implies a poor frequency response and hence a low rate capability. In addition to pore size, pore shape and tortuosity also seem to have an influence on the capacitance and in particular on the frequency response behavior of the material [Pan 2006, CYD 2006].

In conclusion, the resistance of the electrode material decreases for material with a lower porosity, but capacitance increases (at least for low charge and discharge rates) if the electrode material features a high microporous volume. Therefore, an optimization of the electrode material's pore size distribution taking into account the operating frequency may be necessary.

2.3.3. Organic Electrolytes

The operating voltage V of EDLCs is generally determined by the stability range of the electrolyte. Aqueous electrolytes decompose at $\sim 1,23$ V. Non-aqueous electrolytes have been developed, which allow operation at voltages of up to 3,5 V.

Non-aqueous organic electrolytes (*e.g.* tetraethylammonium tetrafluoroborate in acetonitrile) have, on the other hand, a lower ionic conductivity and therefore a higher electric resistivity. This leads to higher internal resistances R . The relative permittivity ϵ_r of aqueous electrolytes is higher than for organic electrolytes (*e.g.* about 37 for acetonitrile as opposed to 82 for 1M H_2SO_4 solution at a temperature around 20 °C) [Cli 2005]. Therefore, EDLCs operating with aqueous electrolytes would feature higher capacitances according to equation V-1, if not for the higher possible operating voltage for organic electrolytes. Power and energy densities are consequently higher for organic electrolytes (compare equations V-2 and V-3). In contrast, organic electrolytes often decompose with time. The decomposition products risk blocking a part of the carbon's porosity thereby decreasing the accessible pore surface. Accordingly, the capacitance decreases and the resistance increases. Also, organic electrolytes may be toxic and dangerous for the environment, contrary to most aqueous electrolytes [Con 1999, Aza 2007, Kho 2008].

2.3.4. Pseudocapacitance

The energy storage mechanism of carbon-based symmetrical electrochemical capacitors depends generally on electrostatic interactions between the carbon surface and the ions. Nonetheless collateral phenomena can arise. Very important and often arising phenomena are for example redox reactions between the active material's surface functionalities and the electrolyte. The effects of this compartment are directly measurable as capacitance, even if the charges are not only stored electrostatically as is the case in capacitors, but to a great extent also through an electron transfer across the double layer. Therefore this type of electrochemical capacitor is often called a "pseudocapacitor". A charge and mass transfer between the electrode and the electrolyte takes place and the composition of the electrode and the transferred charges changes proportionally with the applied voltage. Total capacitance in this case is thus the total energy stored electrostatically on the electrode surface and energy stored through faradaic reactions with functional groups on the electrode surface [Con 1999, Mor 2000, Fra 2001].

In addition to undergoing pseudocapacitive reactions, functional groups present on the carbon surface may induce a surface polarity improving the wettability of the carbon in aqueous solutions. Also, certain surface functionalities may provide more available sites for the adsorption of ions due to an enhanced dipole affinity. Thus the electronic charge density may undergo local changes, in contrast to the "conventional" double layer where the number of ions involved matches the charge density developed on the electrode. Thus, an excess specific double layer capacitance may be induced locally [Hsi 2002]. Although both of these mechanisms may not be called pseudocapacitive

and cannot be determined as such, they may change the capacitance capability of the electrode as a result of a variety of functional groups.

Electrode material used in pseudocapacitors may consist of carbon containing a high number of heteroatoms or carbon being doped with (or completely consisting of) metal oxides (*e.g.* ruthenium oxide). Furthermore, pseudocapacitor electrodes may consist of conducting polymers instead of carbon (*e.g.* polyaniline), or of carbon/polymer composites [Zhe 1995, Fra 2001, Sug 2005, RaL 2006].

2.3.5. Hybrid Capacitor

A hybrid capacitor is an asymmetric capacitor containing different types of positive and negative electrodes in terms of electrode material. In general, the cathode consists of a metal oxide (*e.g.* MnO_2) or a conducting polymer, while the anode uses to be a nanostructured carbon compound.

The charge storage mechanism of the cathode is clearly of pseudocapacitive type (oxidation of the cathode material upon positive polarization). At the anode, energy is stored electrostatically as electrical double layer until reaching the value at which the electrolyte decomposes (in aqueous electrolytes hydrogen is generated at 0 V for very low pH, *i.e.* of almost 0). At still lower values of negative polarization, the electrolyte decomposes at the anode. In the case of aqueous electrolytes it has been found, that in the beginning, the hydrogen produced in this step is instantly adsorbed in the carbon electrode's nanometer-sized pores. This pseudocapacitive behavior allows negative polarization to values even a bit lower than theoretical decomposition voltage.

The major advantage of such a hybrid system is thus the utilization of pseudocapacitance in combination with extended operating voltages [Kho 2006].

Additionally, the capacitance of an EDLC corresponds to a series connection of two capacitors, each one corresponding to one of the two EDLC electrode/electrolyte interfaces (see figure V-5).



Figure V-5: EDLC capacitance represented as connection in series of electrode capacitances

Therefore, the capacitance of the EDLC can be calculated on the basis of the capacitance of each of the two electrodes:

$$\frac{1}{C_{EDLC}} = \frac{1}{C_{ElectrodeA}} + \frac{1}{C_{ElectrodeB}} \quad \text{Equation V-5}$$

The capacitance of the EDLC is thus dominated by the electrode featuring the lowest performance. If the positive and the negative EDLC electrode consist of the same material, a capacity improvement of either electrode by modifying the chemistry of the material tends to result in the deterioration of the opposite electrode's performance and accordingly, of the whole capacitor [Jur 2003].

Consequently, the interest of asymmetric EDLC assemblies in order to adjust each electrode to its operating conditions (*e.g.* adjustment of the porosity of positive and negative electrode to the electrolyte's anion and cation size, respectively) is considerable.

2.4. Targeted Performance

Commercially available EDLC cell assemblies may feature very different performance characteristics (such as capacitance, maximum energy and power, and weight of the device), depending on operation criteria (including operating voltage, peak and continuous current), adapted to the requirements of the application. Therefore, it is difficult to determine common commercial performance characteristics to which results obtained in this work may be compared.

Furthermore, the performance of an EDLC depends significantly on the EDLC assembly. Important parameters include the connection resistance, current collector material, contact between current collector and electrode, electrode composition and geometry, separator type and thickness, electrolyte type and concentration, and applied operating voltage. Additionally, characteristic values can be determined using different analysis methods. However, these values depend also on the analysis method and analysis parameters employed. In this work, I have compared different CAB CA samples and other carbons if used as electrode material in the same type of home-made test cell assembly. However, results obtained in this work can hardly be compared to characteristic values having been obtained using a different test cell or different analysis methods and/or analysis parameters.

Even if comparing is difficult, as explicated above, interesting raw values published for carbon aerogels are given below. CA investigated have mostly been on the basis of resorcinol-formaldehyde aerogels, but also on the basis of cresol-formaldehyde aerogels [Zhu 2006]. Carbon xerogels [Hwa 2004, Lee 2010], regular CA and activated CA [LiW 2006, Sch 2001, Prö 2002], or still CA having undergone surface treatment (*e.g.* use of surfactants) [Fan 2006, Fan 2007, Hal 2010] have been examined. Capacitances as high as 80 F/g (1M H₂SO₄) for carbon xerogels [Lee 2010], 110 F/g (6M KOH) for regular [LiW 2006] and 220 F/g (6M H₂SO₄) for activated [Hwa 2004] carbon aerogels have been obtained (depending on CA structure, test cell assembly, and analysis methods).

3. Experimental Section

3.1. EDLC Test Bench Assembly

Monolithic carbon material has been grinded in an agate mortar to obtain a carbon powder. Carbon powder has been mixed with PTFE (Polytetrafluoroethylene 60 wt.-%, Sigma Aldrich) in a mass ratio of 9:1. For better homogenization, the carbon/PTFE-mixture has been fluidized by ethanol (purity of at least 99.8 %, Sigma-Aldrich). The carbon/PTFE mixture has been spread out heeding a thickness of 300 µm. After the ethanol had vaporized in ambient conditions, two circular electrodes of a diameter of 16 mm have been cut. Subsequently, the electrodes have been dried at 120°C for 2 h.

The two carbon electrodes have been placed on gold current collectors (diameter of 16 mm) of the home-made test cell. A quartz microfibers filter (Fisher Bioblock, 0293A00001) has been used as

separator. The electrolyte used has been a 1M aqueous solution of sulfuric acid H_2SO_4 (Sigma Aldrich).

The electrochemical performance of the different electrode pairs has been examined on an EDLC test bench consisting of:

- ⇒ A home-made two-electrode test cell with gold current collectors,
- ⇒ a potentiostat with associated software to display the recorded signals (BioLogic HCP-803 potentiostat/galvanostat with EC-Lab[®] software V9.45).

The EDLC test cell assembly can be seen in figure V-6, the test bench in figure V-7.

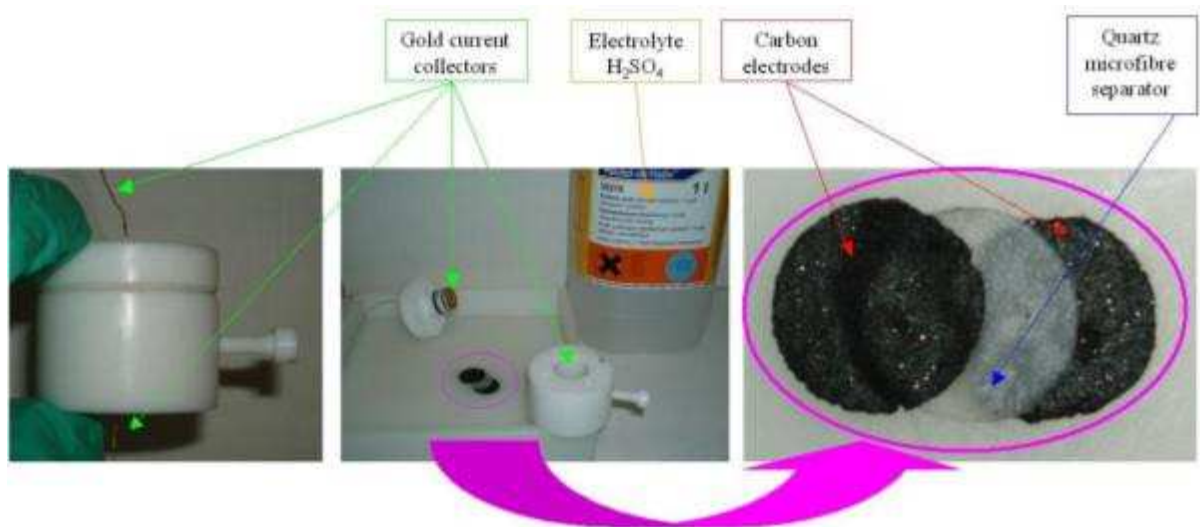


Figure V-6: EDLC test cell assembly

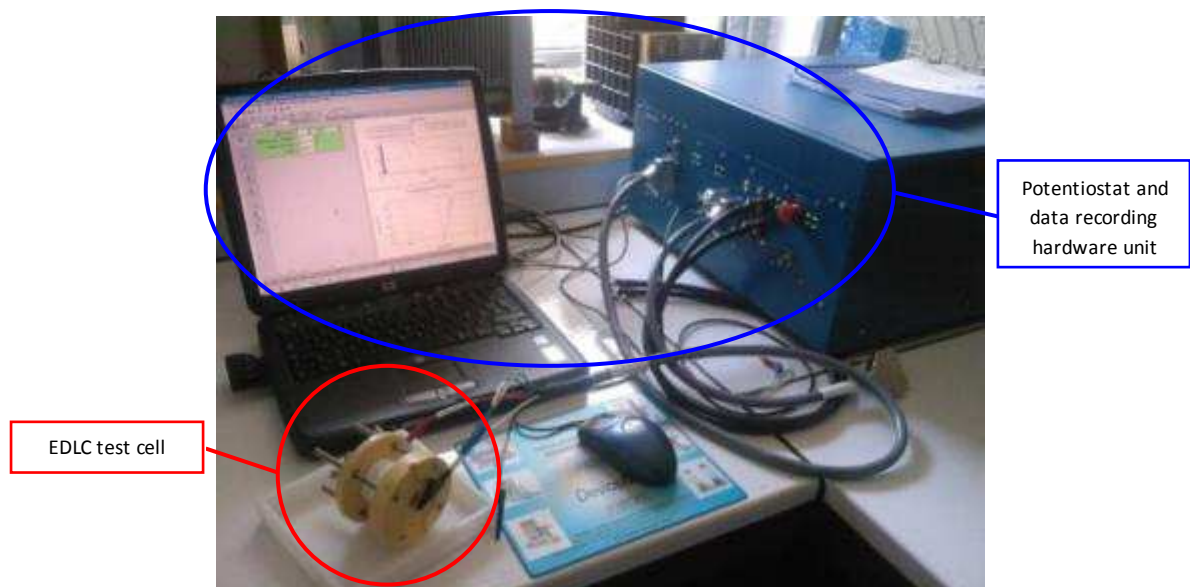


Figure V-7: EDLC test bench

3.2. Analysis Methods

3.2.1. Analysis of EDLC Performance

To investigate the CAB CAs' electrochemical performance and the influence of their different characteristics on their energy storage performance, they have been tested in the form of electrodes in an EDLC test bench. Common techniques for evaluating the capacitance include cyclic voltammetry, galvanostatic charge and discharge, and impedance spectroscopy [Fra 2001].

Capacitance and ESR may be determined using different analysis methods (*e.g.* capacitance may be determined using cyclic voltammetry, but also EIS or galvanostatic cycling). Values obtained depend not only on the analysis method, but also significantly on the analysis parameters employed. Throughout this work characteristic values have been determined according to the analysis methods and parameters described below.

In this work cyclic voltammetry, electrochemical impedance spectroscopy (EIS), leakage current measurement, and self discharge measurements have been used in order to evaluate the carbon material. On the basis of results from these analysis methods volumetric and specific (*i.e.* gravimetric) capacitances $C_{\text{volumetric}}$ and C_{specific} , equivalent series resistance **ESR** and surface resistance $\text{ESR}_{\text{surface}}$, specific energy E_{specific} , specific power P_{specific} , time constant τ , leakage current, and self-discharge have been estimated.

Capacitance values have been determined from cyclic voltammetry according to equation V-8 (in section 3.2.2 on cyclic voltammetry). The scan rate for cyclic voltammetry experiments has been fixed at 20 mV/s and the operating voltage range to 0 to 1 V. Specific (gravimetric) and volumetric capacitances have been determined by relating the capacitance to carbon mass contained in the electrode and volume of the electrode respectively: capacitance values are expressed per single electrode. Additionally, cyclic voltammetry has allowed checking for pseudocapacitive contribution. Resistance and capacitance have been determined as a function of frequency by impedance spectroscopy measurements (see section 3.2.3 on electrochemical impedance spectroscopy for details on how resistance and capacitance have been determined). Impedance measurements have been conducted at a constant voltage mode of 0.5 V. Impedance spectroscopy spectra have been recorded in the frequency range from 1 mHz to 100 kHz (the frequency of imposed signal has been scanned logarithmically at 6 points for each decade from the high frequency region) at an amplitude of 20 mV. The resistance has been determined for three points: at 9524 Hz, at 58 Hz, and at 0.11 Hz. The ESR has been determined by impedance spectroscopy at a frequency of 0.11 Hz. In order to plot the capacitance as a function of frequency, the capacitance from electrochemical impedance spectroscopy has been determined according to equation V-14 (section 3.2.3). The leakage current has been measured for a cell charged at 1 V for 2 h. Self discharge has been observed directly after leakage current experiments (charging the test cell to 1 V for 2 h) for 24 h. Energy, power, and time constant have been calculated using capacitance values estimated from cyclic voltammetry at 20 mV/s and the ESR taken at 0.11 Hz from electrochemical impedance spectroscopy, according to equations I-2, I-3, and I-4, respectively.

The analysis methods used to determine the EDLCs characteristics values in this work, *i.e.* cyclic voltammetry and electrochemical impedance spectroscopy, are discussed below.

3.2.2. Cyclic Voltammetry

In voltammetry experiments, a potential varying linearly in time is applied to the EDLC. The time and the potential-dependant current response are recorded. This method is called a linear voltage sweep or, if applied in repetitive mode, cyclic voltammetry. The direction of current in cyclic voltammetry is periodically reversed at reaching the maximum and minimum potential amplitude (see figure V-8).

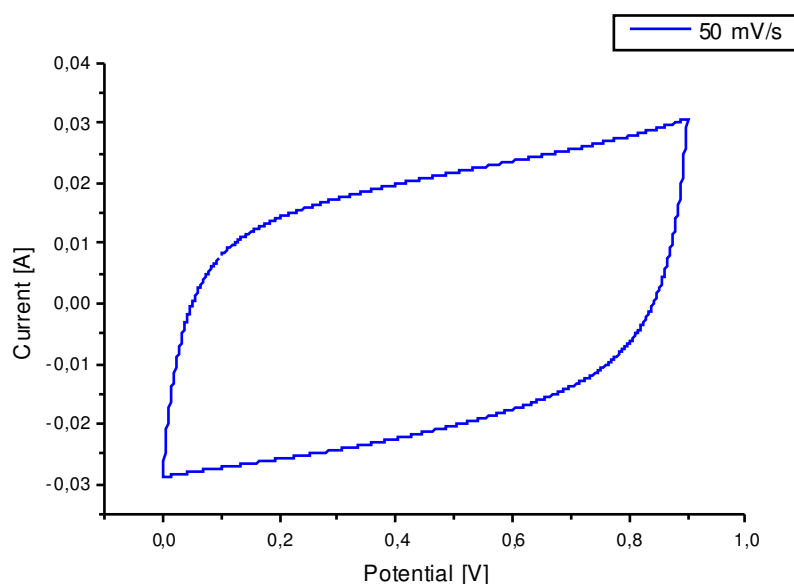


Figure V-8: Cyclic voltammetry current response (at sweep rate 50 mV/s) of sample CAB CA 15-0.2-0.25 DA pyrolyzed at 1000 °C in N_2

In an ideal capacitor (with no resistance), the capacitance does not depend on the potential. In this case cyclic voltammetry records a rectangular current response, symmetrical around the zero-current line. In real capacitors, however, resistances like diffusion limitations arise and result in a capacitance which is not constant but varies with the applied potential or with the sweep rate (*i.e.* the rate of variation of the potential). An EDLC can therefore be represented schematically by an equivalent electrical circuit model of capacitances and resistors connected in series and in parallel. Figure V-9 shows schematically the charge/discharge voltammetry characteristics of (a) an ideal capacitor, (b) an ideal capacitor connected in series with an ideal resistor, and (c) an ideal capacitor connected in parallel with an ideal resistor.

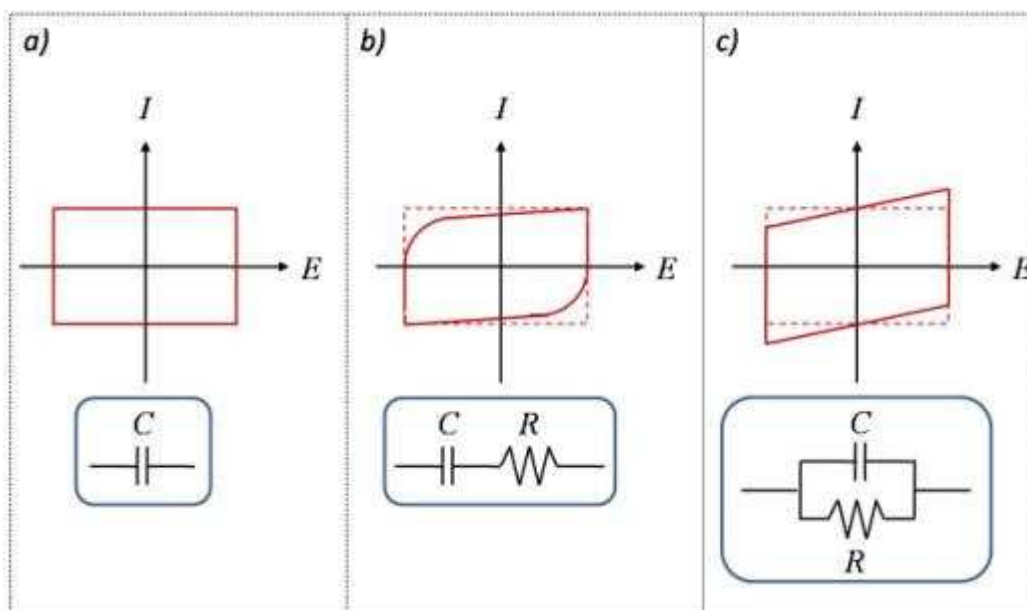


Figure V-9: Voltammogram of a) an ideal capacitor, b) an ideal capacitor connected in series with an ideal resistor, and c) an ideal capacitor connected in parallel with an ideal resistor

Real capacitors often display voltammograms similar to a combination of curves b) and c) of figure V-9 and rely to some degree on pseudocapacitance. Pronounced pseudocapacitive behaviour is revealed by cyclic voltammetry in the form of peaks similar (although often much less pronounced) to the peaks in voltammogram in figure V-10.

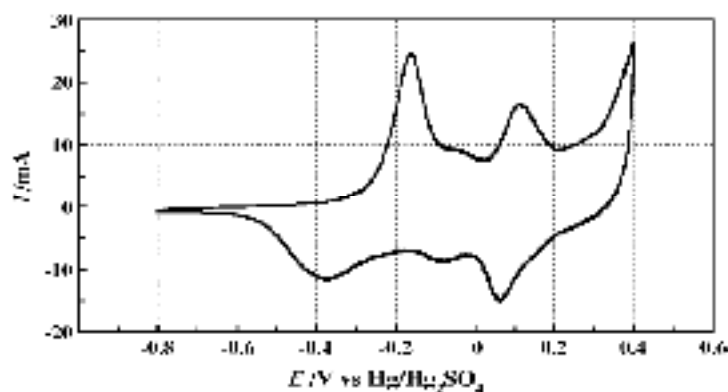


Figure V-10: Cyclic voltammogram of a polyaniline/multiwalled carbon nanotube pellet electrode in $1\text{M H}_2\text{SO}_4$ [Kho 2005]

In accordance with theory, the value of the current response in cyclic voltammetry augments gradually with increasing potential sweep range (figure V-11). Nonetheless, the specific capacitance decreases with increasing potential sweep range. According to [Kim 2005] this phenomenon may be due to ions larger than the electrode's pore size blocking the entrances of the small nanometer-sized pores and thus reducing specific capacitance. At lower sweep ranges, however, such ions have sufficient time to enter tortuous pore networks and even small pores by desolvating [CYG 2006].

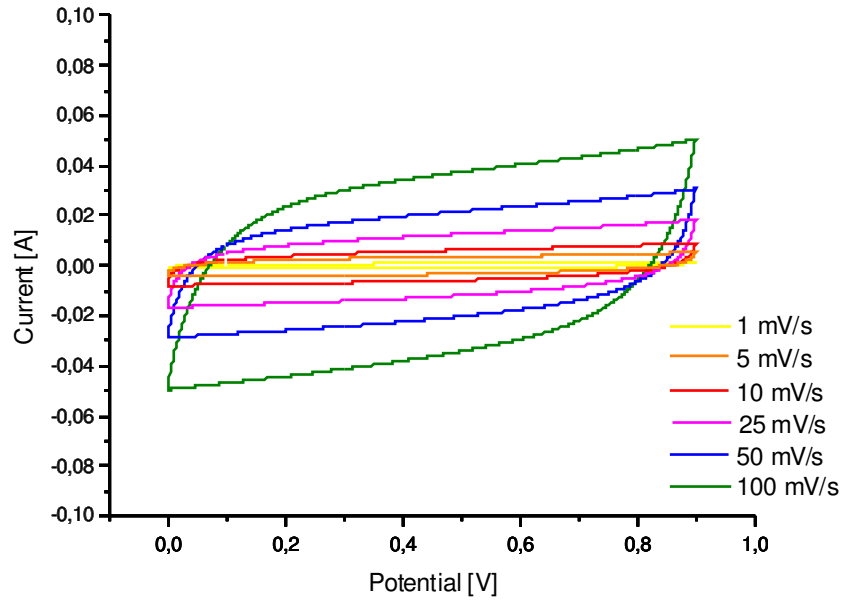


Figure V-11: Cyclic voltammogram of CAB CA 15-0.2-0.25 DA pyrolyzed at 1000 °C in N₂ at different sweep rates

For an EDLC the response current to a linear voltage sweep is:

$$I(t) = C (dV(t)/dt) \quad \text{Equation V-6}$$

where $I(t)$ [A] is the response current, C [F] the EDLC capacitance, $V(t)$ [V] the operating voltage, t [s] the time, and $v = \pm dV/dt$ [V/s] the voltage sweep or scan rate.

The capacitance can thus be determined according to

$$C = I(t)/v \quad \text{Equation V-7}$$

Simplified, equation I-7 becomes

$$C = (S/\Delta V) (1/v) \quad \text{Equation V-8}$$

where S [VA] the surface of the curve $I(t) = f(V(t))$, and ΔV [V] the absolute value voltage range examined [Con 1999, Mor 2000].

3.2.3. Electrochemical Impedance Spectroscopy

EDLC are real capacitors, therefore, they do not exhibit the pure capacitive behaviour of an ideal capacitor without any kind of resistivity. They also feature resistive behaviour due to the existence of different electronic resistances (bulk resistivity of the electrode material, *i.e.* particle-particle contacts, particle-current-collector contacts, the bulk current-collector and external wires, etc.) and

ionic resistances (*e.g.* separator resistance, resistance due to ion conduction in electrolyte in the electrode pores, etc.) within the cell [Kim 2004, Con 1999].

Electrical resistance, *i.e.* the ability of an element to resist the flow of electrical current, can be defined by Ohm's law

$$R = \frac{V}{I} \quad \text{Equation V-9}$$

Ohm's law, however, defines the relationship between resistance, potential and current for ideal resistors only. Ideal resistors obey Ohm's law at all current and voltage levels and frequencies. Furthermore, upon application of an alternating current (AC) the response signal of the voltage is in phase with the current. Real resistors, however, may not always follow Ohm's law but be frequency-dependent and current and voltage may be dephased if the cell is driven with AC (see figure V-12) [Gam 2007].

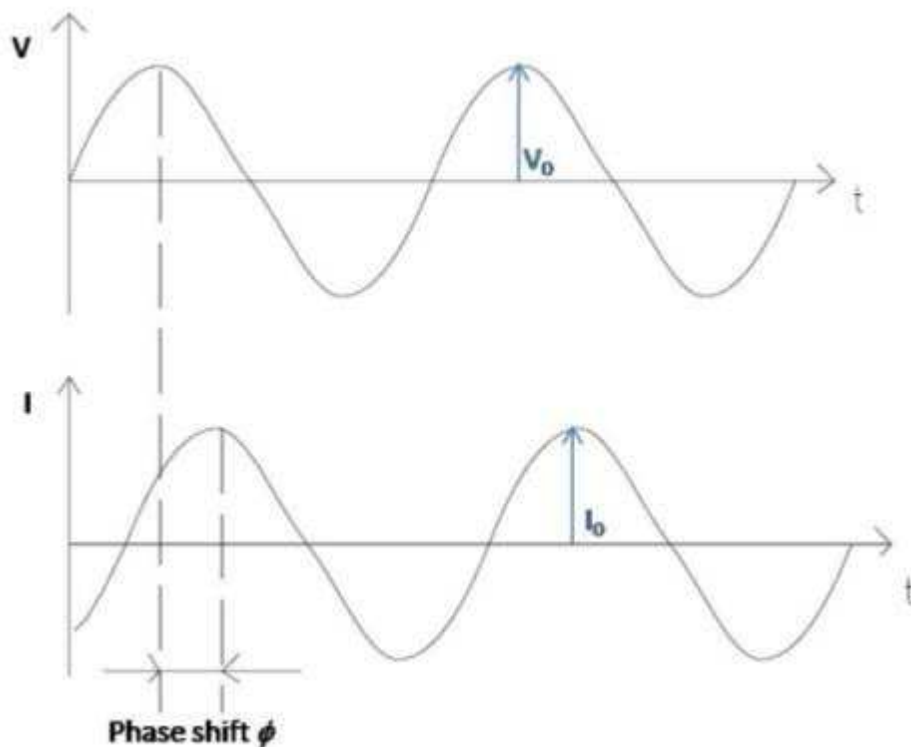


Figure V-12: Sinusoidal voltage excitation and exemplary current response of a real resistor

The resistance of real resistors to AC is referred to as impedance. Impedance can, therefore, also be defined as the ability of an element to resist the flow of electrical alternating current, only that impedance is not limited by the simplifications which apply to an ideal resistor.

EIS measurements are usually carried out at a stationary potential. A sinusoidal AC potential

$$V(t) = V_0 \cos(\omega t) \quad \text{Equation V-10}$$

of small amplitude V_0 and radial frequency ω [s^{-1}] is applied to the electrochemical cell. The response current to this excitation is measured. The response to a sinusoidal potential (for a small excitation signal) is a sinusoidal AC current signal of amplitude I_0 at the same frequency as the potential signal, but shifted in phase ϕ (see figure V-12)

$$I(t) = I_0 \cos(\omega t - \phi). \quad \text{Equation V-11}$$

Although the current response would not be dephased for an ideal resistor, it is shifted in phase for any device featuring a reactive impedance (*i.e.* capacitors or inductors) as compared to a mere resistive impedance [Las 2001, Aza 2003, Köt 2006, Gam 2007].

The impedance may be determined by an equation equivalent to Ohm's Law taking into account the phase shift:

$$Z = \frac{V(t)}{I(t)} = \frac{V_0 \cos(\omega t)}{I_0 \cos(\omega t - \phi)} = Z_0 \frac{\cos(\omega t)}{\cos(\omega t - \phi)} \quad \text{Equation V-12}$$

For reasons of convenience (simpler calculations), the impedance may be expressed as a complex number in terms of a magnitude Z_0 and phase shift ϕ :

$$Z = Z_0(\cos\phi + j\sin\phi). \quad \text{Equation V-13}$$

A resistor's impedance only has a real component $Z = \text{Re}Z = R$ (no reactive or imaginary impedance) and is generally independent of frequency. A capacitance's impedance has only an imaginary impedance component. The potential signal is phase shifted -90° with respect to the current signal: $Z = \text{Im}Z = \frac{1}{j\omega C}$. The impedance of a capacitor is frequency-dependent: it

decreases with increasing frequency. As an EDLC can be represented by an equivalent electrical circuit model of capacitances and resistors connected in series and in parallel, its current response to a voltage excitation contains a real part (representing the EDLC's resistance) and an imaginary part (from which the capacitance can be deduced) depending on frequency.

The impedance, in terms of real and imaginary parts, is often represented in a Nyquist plot. The Nyquist plot shows the imaginary part $-\text{Im}Z(\omega)$ of the impedance in function of the real part $\text{Re}Z(\omega)$. Each point in the plot shows the impedance at one frequency.

- An ideal resistor, because not frequency-dependent, would consist of only one point on the real axis $\text{Re}Z(\omega)$.
- An ideal capacitor would consist of a vertical line at $\text{Re}Z(\omega) = 0$ only.

- For a connection in series of an ideal capacitor and an ideal resistor of a resistance R , the vertical line would be shifted on the real axis by the amount of R (see figure V-13).

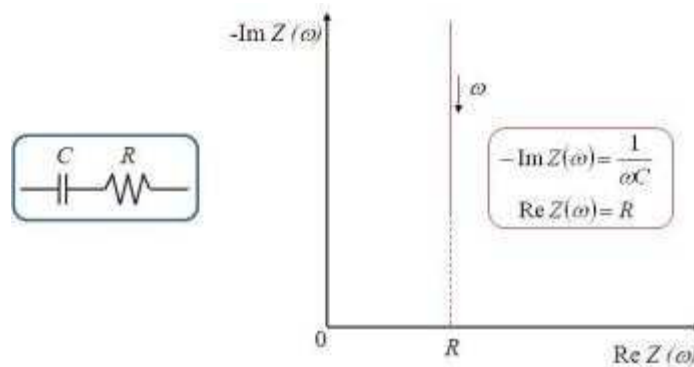


Figure V-13: Equivalent circuit and Nyquist plot of a capacitance C and a resistance R connected in series

- An ideal capacitor connected in parallel to an ideal resistance, however, would result in a semi-circle between $\text{Re } Z(\omega) = 0$ and $\text{Re } Z(\omega) = R$ (see figure V-14).

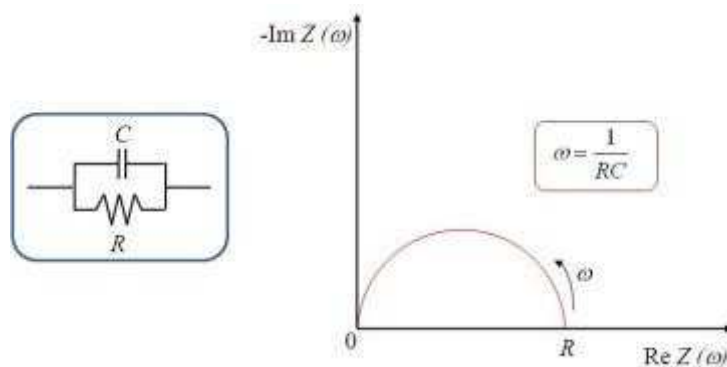


Figure V-14: Equivalent circuit and Nyquist plot of a capacitance C and a resistance R connected in parallel

- For equivalent circuits of capacitances and resistances connected in series and in parallel, thought to represent real capacitors, three different zones may be distinguished in the Nyquist diagram. As can be seen for the example of the equivalent circuit shown in figure V-15, the Nyquist plot of an EDLC begins oftentimes at a point $\text{Re } Z(\omega) \neq 0$ of the real axis. First, the plot may feature a loop at high frequencies. Second, the value for $-\text{Im } Z(\omega)$ increases continually. At intermediate frequencies the plot reaches an angle of about 45° . Third, at low frequencies the plot approaches a quasi-vertical.

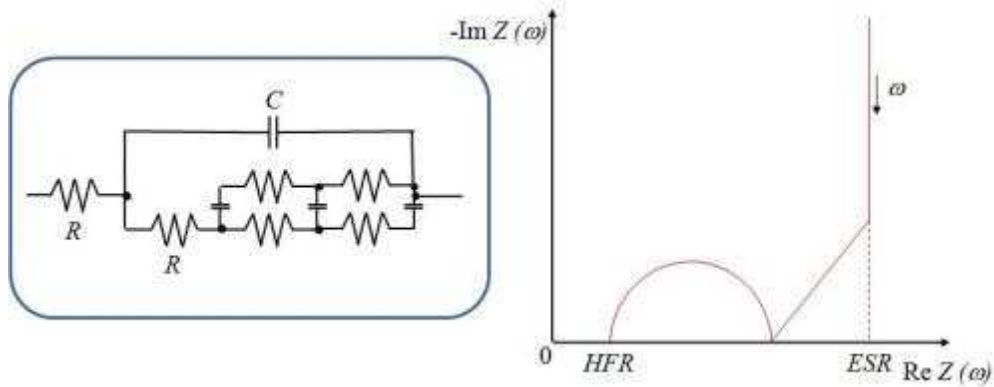


Figure V-15: Equivalent circuit and Nyquist plot of several capacitances and resistances connected in series and in parallel (based on [Las 2001])

For EDLC, however, often either no loop or only the beginning of the loop can be observed merging directly with the angle of 45° without showing a significant decline of the imaginary value between the two zones (see for example figure V-16).

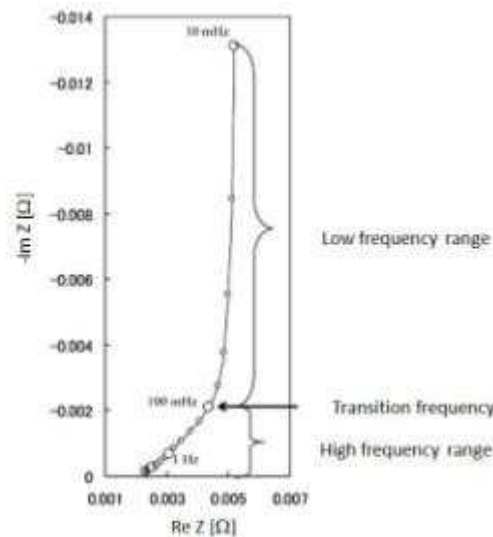


Figure V-16: Experimentally determined Nyquist plot of an EDLC by HONDA R&D Ultra capacitor (frequency range 1 kHz-10 mHz, charging voltage 2V, measurement temperature 278 K) (based on [Ita 2007])

EDLC have been described by Taberna, Simon, and Fauvarque as devices oscillating between two states: resistance at high frequencies and capacitance at low frequencies. Between these two states it behaves like a resistance-capacitance transmission line circuit [Tab 2003]. The impedance behaviour of an EDLC is described more thoroughly below.

- at very high frequencies (close to 60 kHz):
At very high frequencies, the imaginary part $-\text{Im} Z(\omega)$ tends to zero, *i.e.* behaves almost like a resistor. This resistance, called high frequency resistance HFR, is mostly due to frequency independent factors. The main components of the HFR consist of the ionic resistance of the electrolyte and the intrinsic electrical resistance of the electrodes (including intra- and inter-particle resistances), and contact quality between electrode and current collector (responsible for the formation of high frequency loops). Nonetheless, the HFR also

includes the resistance of current collector and connectivity [Gam 2001, Prö 2002, Aza 2003, Tab 2006, Yoo 2010].

- at intermediate frequencies (around 1-100 Hz):

The 45° slope in the Nyquist plot at intermediate frequencies is usually called the distributed resistance. The distributed (electrolyte) resistance is generally assigned to the electrode's porous structure extending into the depth of the pore. The distributed resistance is coupled with distributed interfacial capacitance elements, resulting in a non-uniform distribution of effective resistance and capacitance but a distribution depending on the rate of charge and discharge. Both resistances and capacitances are created by the diffusion of electrolyte ions within the pores of the EDLC electrode material. Mesopores in carbon electrodes, for example, are more easily accessible for the electrolyte than micropores. The real part of the impedance $\text{Re} Z(\omega)$ of mesoporous electrodes is therefore less frequency-dependent and the capacitive behaviour begins to show at lower resistance. In general, however, charging and discharging at low rates allow the electrolyte to penetrate into narrow or deep pores increasing the resistance but also the capacitance by accessing additional surface area. The distributed resistance obviously depends on the porous characteristics of the electrode (in combination with the electrolyte used), but also on the electrode's thickness [Gam 2001, Las 2001, Aza 2003, Tab 2003, Köt 2006, Pan 2006].

- At low frequencies (less than 1 Hz):

At decreasing frequencies, the current is increasingly propagating into inner pore sites of the electrode leading the imaginary part of the impedance to increase suddenly. The Nyquist plot tends to a vertical line characteristic of capacitive behaviour. The real value $\text{Re} Z(\omega)$ of the quasi-vertical part of the Nyquist plot corresponds to the equivalent series resistance ESR for low frequencies. Theoretically, the plot should become a vertical line. However, pores not easily accessible to the electrolyte's ions may result in long electrolyte pathways. This characteristic, slightly dependent on frequency, results in a resistance causing a deviation of the real plot from the ideal plot towards increasing values of $\text{Re} Z$. Accordingly, lower ESR values are associated with a better accessible carbon surface [Gam 2001, Prö 2002, Tab 2003, Köt 2006].

Resistance as well as capacitance may be plotted as a function of frequency. Capacitance can be derived from the imaginary part of the impedance by

$$C = \frac{1}{\omega \text{Im} Z} = \frac{1}{2\pi f \text{Im} Z} \quad \text{Equation V-14}$$

where $\omega = 2\pi f$.

Figure V-17 shows the resistance in function of frequency of a typical commercially available EDLC in comparison to that of an ideal capacitor. The resistance of a real capacitor decreases with increasing frequency. Figure V-18 shows the capacitance behavior for the same commercially available EDLC, as compared to that of an ideal capacitor, as a function of frequency. In reality, the capacitance is

highest at low frequencies, due to increasing participation of inner pore sites in the charge storage. The sudden deterioration of capacitance indicates the frequency (cut-off frequency) until which the energy of the capacitor can be withdrawn [Prö 2002, Kie 2004, Köt 2006]. For frequencies above the cut-off frequency, the surface area ceases to be utilized adequately [Zho 2008].

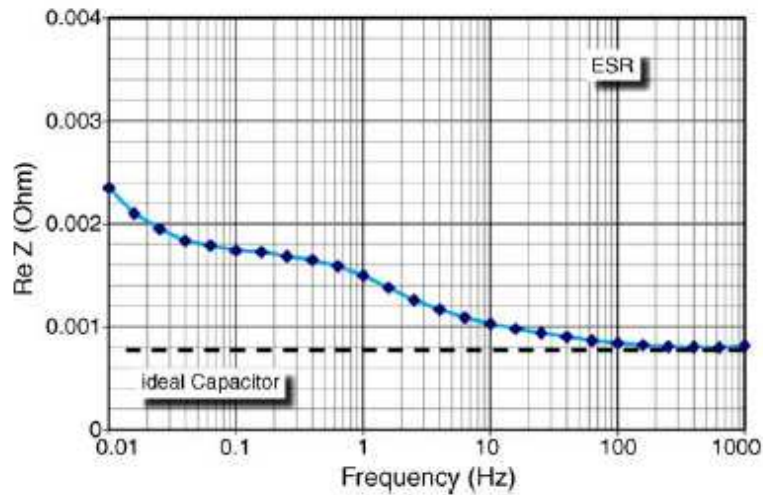


Figure V-17: Resistance of a typical EDLC (blue line) and an ideal capacitor (dashed line) as function of frequency [Köt 2006]

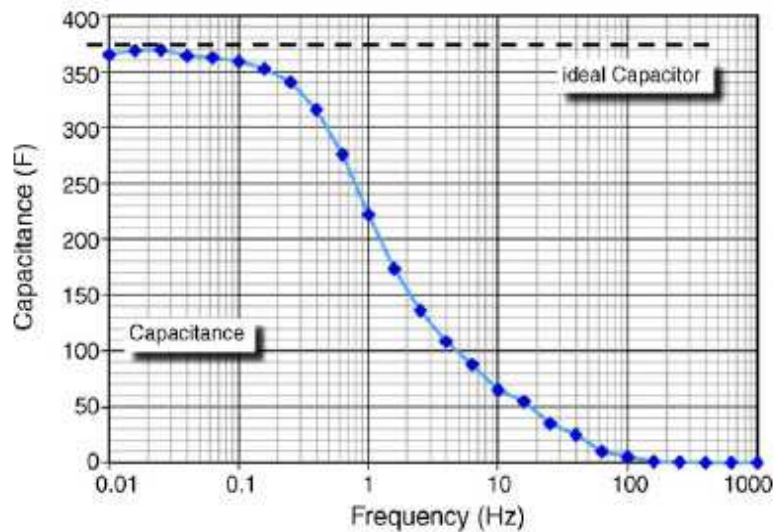


Figure V-18: Capacitance of a typical EDLC (blue line) and an ideal capacitor (dashed line) as function of frequency [Köt 2006]

3.3. Carbon Samples

Although it is known that highest capacitances may be reached using microporous carbon for EDLC electrode material (see section 1.3 on the potential improvement of EDLC assembly), the performance of different CAB aerogels if used as EDLC electrode material has been examined. This study aimed at investigating the influence of different structures or surface chemistries of CAB aerogels and at revealing the complexity of superposed phenomena for this new type of material.

Several CAB carbon aerogels and xerogels, synthesized during my thesis, have been evaluated (see table I-1). Sample CAB CA 10-0.2-0.25DA has been used as reference CAB CA material. In order to investigate effects due to different structures, CAB xerogels (see chapter III), activated CAB CA (see chapter IV), and a CAB aerogel/CP compound have been examined. Effects due to the surface chemistry have been studied using CAB CA having been oxidized or into which nitrogen has been introduced (see chapter IV).

Table V-1: CAB CA and related material for analysis as EDLC electrode material

Sample	S_{BET} m²/g	V_{mesopores} cm³/g	V_{μpores} cm³/g	d_p nm	Preparation
CA1 ^{b)}	165	0,23	0,07	12	10-0.2-0.25DA, 1000 °C/N ₂ , referred to as CA1 in chapter IV
CA2 ^{b)}	117	0,18	0,05	13	10-0.2-0.25DA, 1100 °C/N ₂ , referred to as CA2 in chapter IV
1XL ^{a,c)}	142	0,29	0,01	8	10-0.2-0.25DA, Xerogel (slow controlled evaporation), 1000 °C/N ₂ (chapter II)
A850 ^{e)}	620	0,29	0,2	10	10-0.2-0.25DA, 1000 °C/N ₂ , activated at 850 °C/CO ₂ /2h (chapter IV)
A950 ^{e)}	2106	0,63	0,7	8	10-0.2-0.25DA, 1000 °C/N ₂ , activated at 950 °C/CO ₂ /2h (chapter IV)
A1050 ^{c)}	2147	0,94	0,75	4	10-0.2-0.25DA, 1000 °C/N ₂ , activated at 1050 °C/CO ₂ /2h (chapter IV)
PCC ^{a,c)}	75	0,22	0	114	CAB 10-0.2-0.25P CA/cellulose compound, 1000 °C/N ₂ (chapter IV)
CA1H ^{b)}	152	0,24	0,06	11	CA1, 5N H ₂ O ₂ /48h/T _{amb} (chapter IV)
CA1N ^{b)}	121	0,23	0,05	12	CA1, 4N HNO ₃ /48h/T _{amb} (chapter IV)
CA1M ^{b)}	130	0,23	0,06	12	CA1, co-heat-treatment with melamine at 750 °C/N ₂ (chapter IV)
CA2AM ^{b)}	280	0,23	0,12	12	CA2, ammonisation 400 °C/3h (chapter IV)
CA2NAM ^{b)}	277	0,22	0,12	11	CA2, 4N HNO ₃ /48h/T _{amb} , ammonisation 400 °C/3h (chapter IV)

^{a)} structural analysis on carbon aerogel monolith

^{b)} Mesoporous volume by Broekhoff de Boer, micropore volume and mean pore size by Dubinin-Radushkevich,

^{c)} Mesoporous volume by Barret-Joyner-Halenda, micropore volume and mean pore size determined by t-plot method

Sample type 10-0.2-0.25DA pyrolyzed at 1000 °C in N₂ has undergone structural analysis in monolithic form (results can be found in chapter III.3.2) as well as in powder form (chapter IV.3, where the sample is called CA1). Characteristics for sample 10-0.2-0.25DA presented in table V-1 correspond to the analysis results of the carbon powder featured in chapter IV.3. Additional information on sample 10XL is available in chapter II.3.2.2 and in chapter III.3.2.1 on xerogels. Samples A850, A950, and A1050 have been analyzed more closely in chapter IV.2.1 and sample PCC in chapter IV.2.2. More information on samples CA2, CA1H, CA1N, CA1M, CA2AM, and CA2NAM may be found in chapter IV.3.

Further, I have investigated the performance of different cellulose-based (cellulose powder and cellulose acetate powder, aerocellulose) and a commercially available carbon (Maxsorb) if used as EDLC electrode material (see table V-2). Organic aerocellulose gels have been synthesized by R. Sescousse (as a part of the project CARBOCELL) according to the protocol described in [Ses 2009]⁵ and subsequently washed first in water and then in acetone before having undergone supercritical drying in CO₂ (see chapter II for drying conditions) and pyrolysis (heating rate 2.2 °C/min, 800 °C final temperature for 200 minutes and 100 minutes for samples 1 and 2, respectively). Maxsorb has been provided by TIMCAL.

⁵ Aerocellulose 1 and 2 have been gelled at 50 °C (20 h and 55 h for samples 1 and 2, respectively) and regenerated in 10⁻³M acetic acid at 22 °C.

Table V-2: Cellulose-based and other carbon material for analysis as EDLC electrode material

Samples	S_{BET} m²/g	V_{mesopores} cm³/g	V_{μpores} cm³/g	d_p nm	Material
<i>CP</i>	-	-	-	-	Cellulose powder (CAS: 9004-34-6), 1000 °C/N ₂
<i>CAP</i>	-	-	-	-	Cellulose acetate powder (CAS: 9004-35-7), 1000 °C/N ₂
<i>Aerocellulose 1</i> ^{a,c)}	381	0,35	0,12	2	Cellulose-based carbon aerogel
<i>Aerocellulose 2</i> ^{a,c)}	407	0,23	0,10	4	Cellulose-based carbon aerogel
<i>Maxsorb</i>	2200 ^{d)}	-	-	-	formerly commercially available activated carbon

^{a)} structural analysis on carbon aerogel monolith

^{c)} Mesoporous volume by Barret-Joyner-Halenda, micropore volume and mean pore size determined by t-plot method

^{d)} according to TIMCAL (provider of Maxsorb for this work)

Characteristics of the electrodes made out of the carbon materials listed in tables V-1 and V-2 can be found in table V-3. The carbon mass for one electrode as seen in table V-3 is the mean value of the carbon mass contained in each of the two supposedly symmetric electrodes in order to calculate the specific capacitance per electrode. Of course this approach induces an error, as the electrodes can never be exactly equal. However, 3-electrode cell tests would have been required in order to study the real capacitance performance of positive and negative electrode separately.

Table V-3: Electrode characteristics for one electrode

Samples	Surface cm²	Volume cm³	Mass_{Carbon} mg	PTFE/Carbon wt.-%
<i>CA1</i>	2,01	0,06	33,7	9,9
<i>CA2</i>	2,01	0,06	37,9	11,2
<i>CP</i>	2,01	0,06	42,2	10,5
<i>CAP</i>	2,01	0,06	40,0	13,0
<i>10XL</i>	2,01	0,06	41,5	10,9
<i>A850</i>	2,01	0,06	32,2	12,3
<i>A950</i>	2,01	0,06	29,1	13,7
<i>A1050</i>	2,01	0,06	20,2	13,2
<i>PCC</i>	2,01	0,06	40,4	10,0
<i>CA1H</i>	2,01	0,06	37,1	10,0
<i>CA1N</i>	2,01	0,06	34,2	9,7
<i>CA1M</i>	2,01	0,06	34,7	10,0
<i>CA2AM</i>	2,01	0,06	34,0	10,0
<i>CA2NAM</i>	2,01	0,06	37,2	9,6
<i>Aerocellulose 1</i>	2,01	0,06	18,6	11,1
<i>Aerocellulose 2</i>	2,01	0,06	12,9	9,9
<i>Maxsorb</i>	2,01	0,06	29,4	11,9

4. Results and Discussion

4.1. Influence of Test Cell

As mentioned before (paragraph V.1.2), an EDLCs' electrochemical performance depends significantly on the test cell assembly and operating conditions. To gain knowledge of the used test cell's influence, particularly on the resistance, I have analyzed the performance of the test cell not

containing any carbon electrode. Figure V-19 shows the performance of the test cell assembly without carbon electrodes and with electrodes out of CAB CA1. As all CAB CA synthesized in the scope of chapter III possessed very similar structures, CAB CA sample CA1 has been chosen to act as reference in the analysis of EDLC performance.

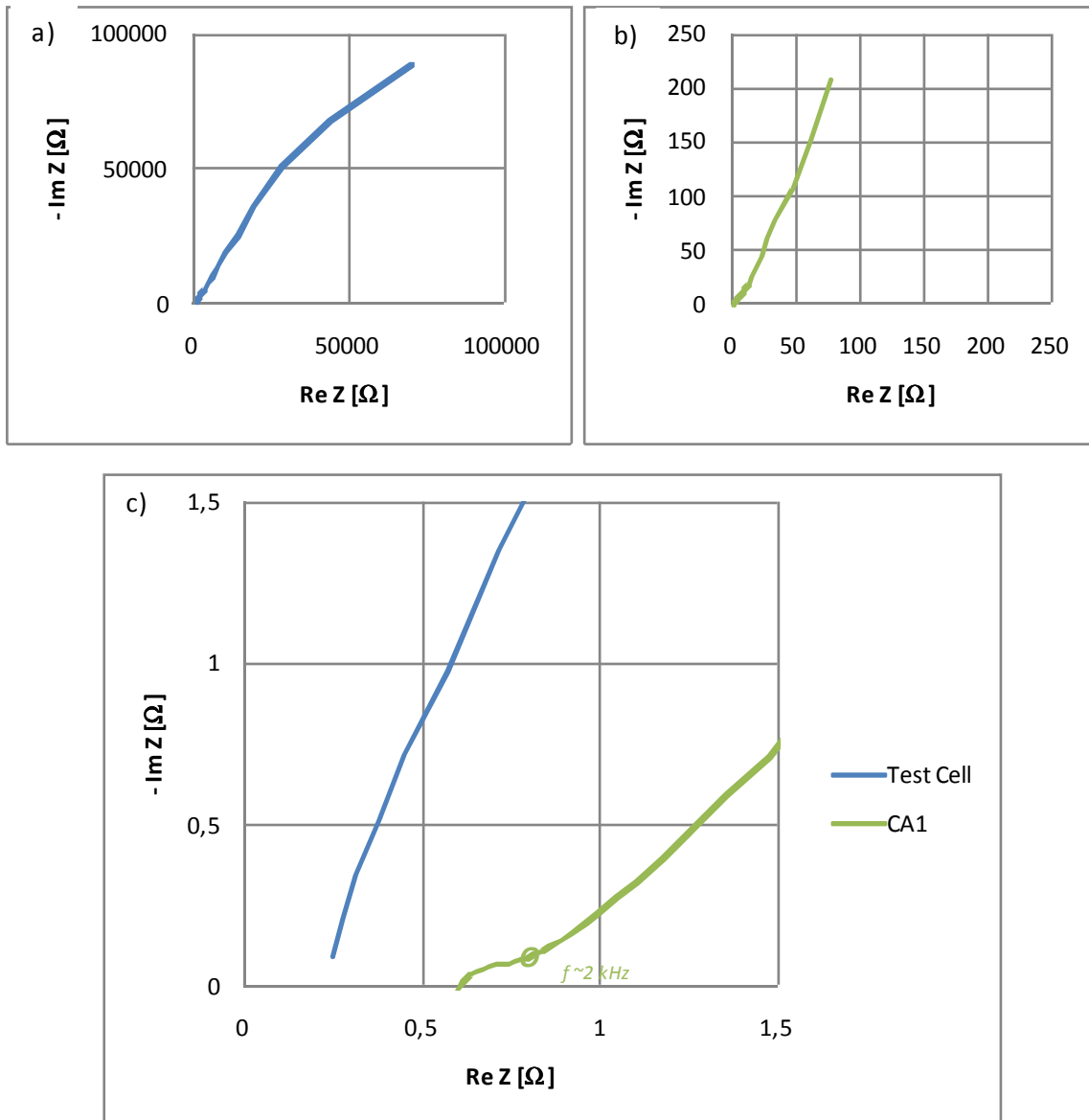


Figure V-19: Comparison of the Nyquist plot of a) the EDLC test bench assembly without electrodes (blue line) and b) CAB CA1 (green line) and c) close up of the high frequency region

Since the only difference in the test cell has been the absence (curve a) test cell) or presence (curve b) CA1) of CAB CA electrodes, the HFR value of the test cell can be attributed to the various resistances of the test cell assembly. The difference between the HFR of the test cell and those of CAB CA1 may thus be attributed to the carbon electrode. The frequency given for sample CA1 in curve c) indicates roughly the cut-off frequency.

The test cell's HFR is of around 0.25 Ω. Note that the HFR value of this assembly is much higher than that of commercial EDLC assemblies amounting generally to some mΩ only. The experimental assembly's HFR value thus makes up already about half of CA1's HFR value, for example.

4.2. Influence of Structure

4.2.1. Interest of Synthesizing Carbon Aerogels

In order to examine a possible interest of synthesizing CAB CA (even though melting and partial gasification modify the structure of the pristine CAB OA), cellulose powder (CP) and cellulose acetate powder (CAP) have been carbonized and their performance as EDLC electrode material has been compared to that of CAB CA1.

CAP features a remarkably low resistance at high frequencies (see figure V-20), may due to low inter-particle resistance, because of melting during pyrolysis. For this same reason, CA1 might also feature a lower HFR than the carbon issued from the cellulose-powder. Although CA1 possesses spherical particles, the contact between the particles seems to very good due to the partial melting CAB material undergoes during heat treatment processes (see chapter III.3.1.2 for SEM micrographs of CAB CA). Nonetheless, CA1 features a structure with high porosity, possibly deteriorating the conductivity as compared to CAP.

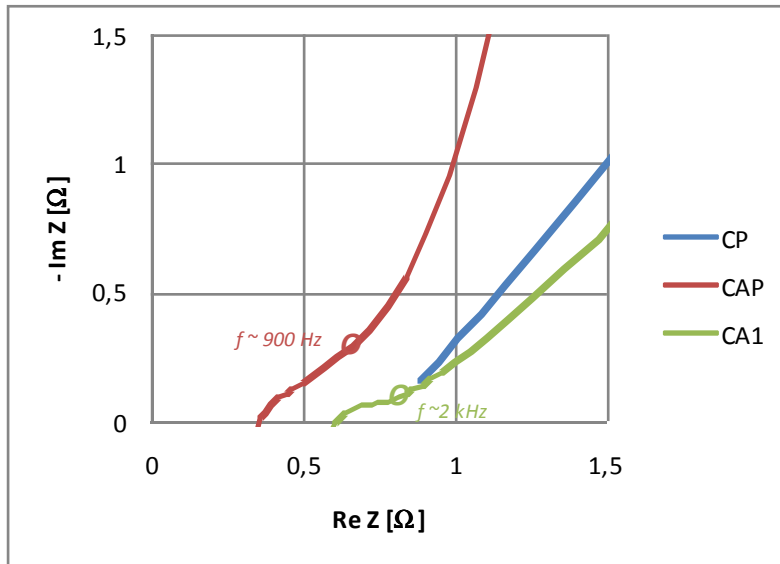


Figure V-20: High frequency region of Nyquist plot for CP, CAP, and CA1

At comparing the different carbons' resistance at different frequencies (table V-4 and figure V-21), however, it can be found that the resistance of CAP at low frequencies is much higher than that of CA1. The resistive part of the impedance increases even with decreasing frequencies down to 1 mHz, for all three samples.

Table V-4: Resistance in dependence of frequency for CA1, CP, and CAP

Frequency	9524 Hz		58 Hz		0,11 Hz	
	R Ω	R _{surface} Ω / cm^2	R Ω	R _{surface} Ω / cm^2	R Ω	R _{surface} Ω / cm^2
CA1	0,70	0,35	1,01	0,50	6,35	3,16
CP	1,40	0,69	15,60	7,76	239,70	119,22
CAP	0,44	0,22	1,17	0,58	105,87	52,66

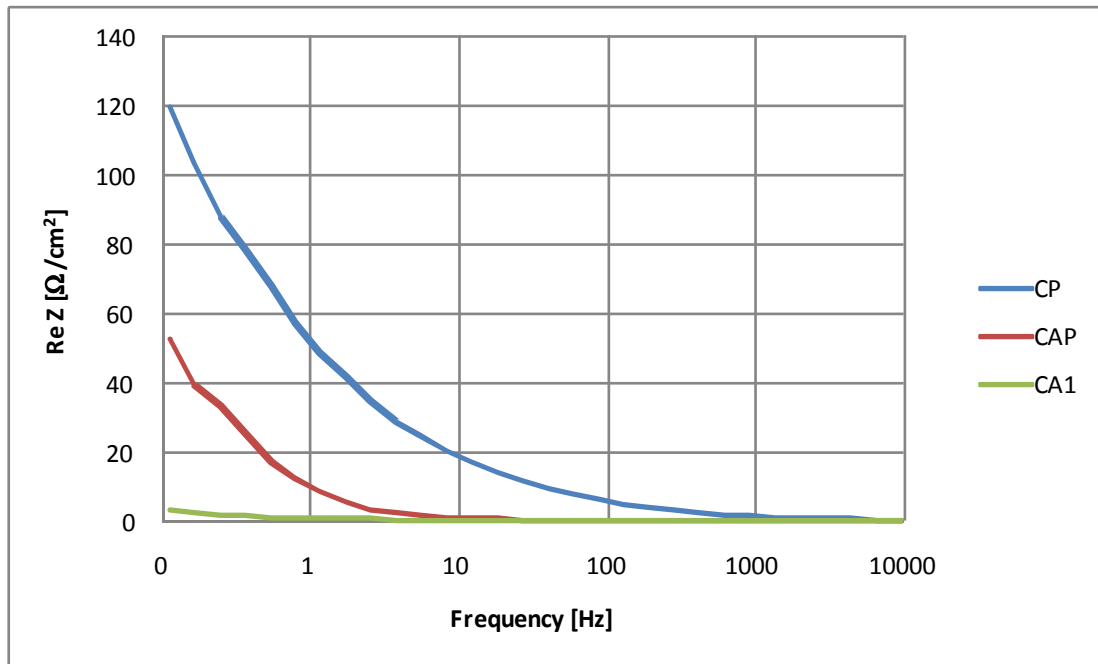


Figure V-21: Resistance as function of frequency for CP, CAP, and CA1

Figure V-22 shows the frequency-dependent evolution of capacity (normalized by the maximum value of capacity) for carbons CP, CAP, and CA.

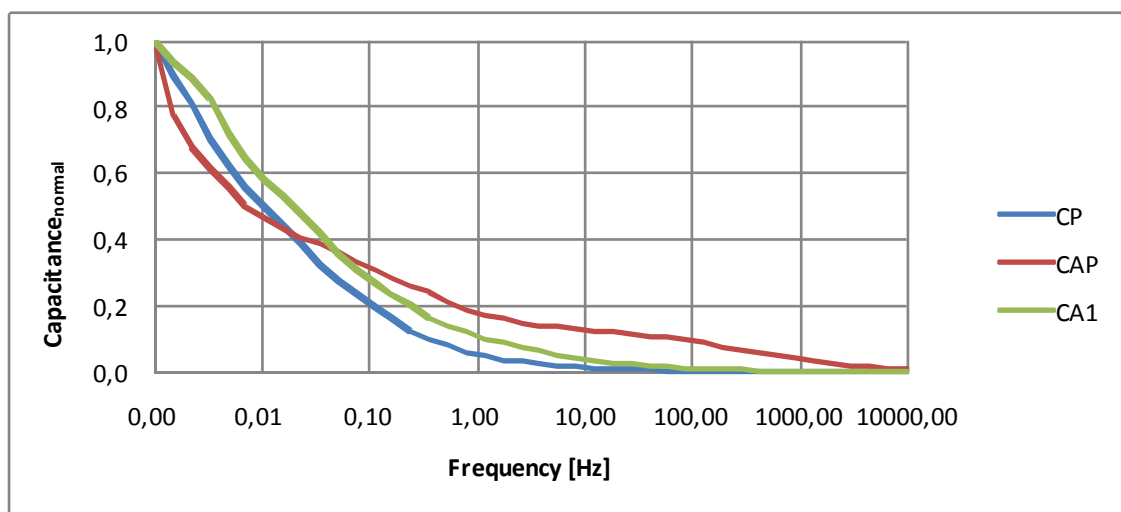


Figure V-22: Normalized capacitance as function of frequency for CP, CAP, and CA1

Capacitance, ESR (at 0.1 Hz), leakage current, energy and powder capabilities, and time constant τ of CP, CAP, and CA1 can be seen in table V-5. The capacitance capabilities of CP, CAP and CA1 are clearly different. CA1 possesses a much higher capacitance than the other two carbons, due to the nanostructure having been given to the aerogel by the sol-gel process. Although structural analysis of CP and CAP has not been carried out, carbon materials CP and CAP are obviously denser, *i.e.* less porous, than CAB CA1 (see values for carbon mass in electrode in table V-3). While the capacitance is highest for CA1, its ESR is lowest. Accordingly, energy and power capabilities are superior for carbon CA1.

Table V-5: Characteristic values of CA1, CP, and CAP

Samples	C_{volumetric} F/cm³	C_{specific} F/g_{carbon}	ESR Ω	ESR_{surface} Ω/cm²	I_{leakage} mA	E_{specific} Wh/kg_{carbon}	P_{specific} W/kg_{carbon}	τ s
CA1	8,64	15,48	6,35	3,16	0,24	0,54	585	3,3
CP	0,33	0,47	239,70	119,22	0,09	0,02	12	4,8
CAP	0,24	0,36	105,87	52,66	0,05	0,01	30	1,5

Even though CA1 has the highest leakage current (probably due to charge redistribution within the CA structure), its self-discharge (see figure V-23) is lowest. CAP discharges almost completely in only around 7 h, while CP also loses about 90 % of its initial voltage in 24 h. The discharge of CA1 is much less pronounced but makes up 50% of the initial voltage, nonetheless.

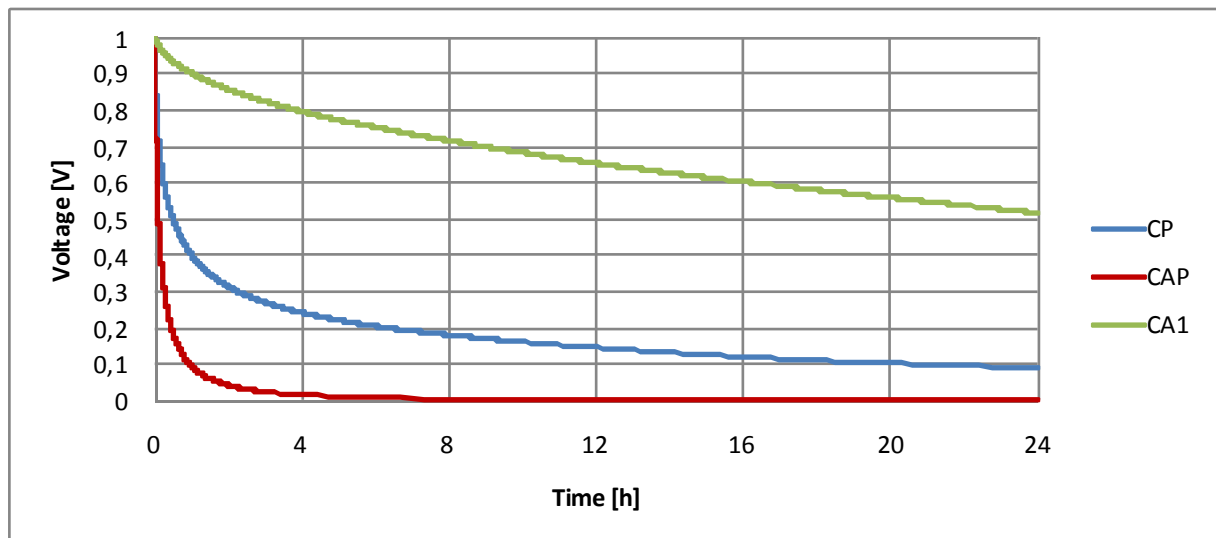


Figure V-23: Self discharge of carbons CP, CAP, and CA1

In conclusion, synthesizing CAB CA is advantageous for an application as EDLC electrode material, compared to simple cellulose powder or cellulose acetate powder carbonized in the same conditions. Although the initial structure of the CAB OA may not be maintained during pyrolysis (due to melting and partial gasification), CAB CA possess a non-negligible mesoporous volume together with a minor microporous volume. Capacitances are relatively low, corresponding to the not very elevated specific surface area and porous volume.

4.2.2. Xerogel Performance

The performance of a CAB carbon xerogel (sample 10XL, dried slowly in air as can be seen in chapter II.3.2.2) if used as EDLC electrode material has been analyzed and compared to that of a CAB CA of the same composition (CA1).

As seen in chapter II, very dense CAB organic xerogels are produced by evaporative drying. After carbonization, however, carbon xerogels are rather similar to their aerogel homologues (see chapter III.3.2.1). In comparison to sample CA1, they possess slightly less developed surface areas and microporous volumes (see table V-1).

The resistance of CAB CA1 and carbonized CAB 10XL is very similar (refer to figures V-24 and V-25 and table V-6), although mostly a bit lower for 10XL (especially in the low frequency region) probably due to its density (or at least its electrode density) being higher than that of CA1 (see table V-3).

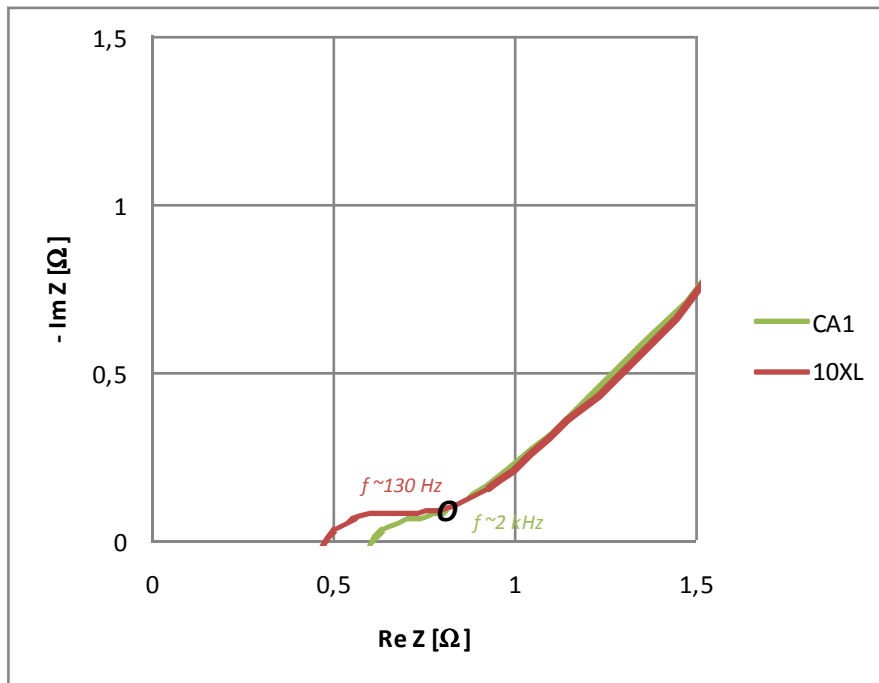


Figure V-24: High frequency region of Nyquist plot for CA1 and 10XL

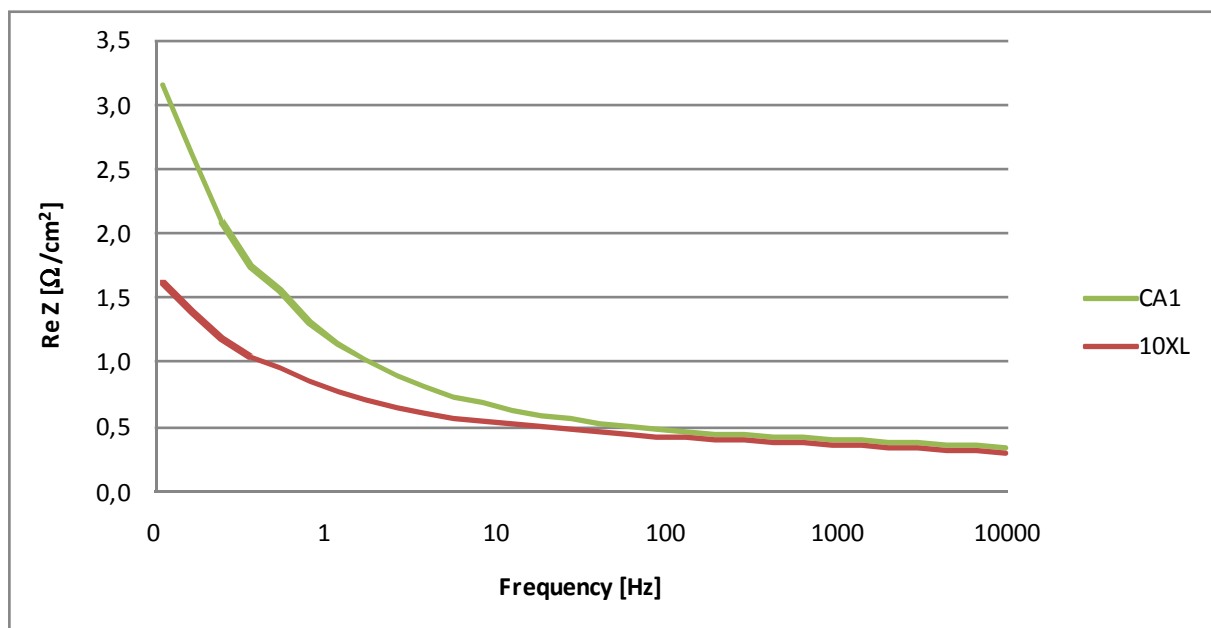


Figure V-25: Resistance as function of frequency for CA and 10XL

Table V-6: Resistance in dependence of frequency for CA1 and 10XL

Frequency	9524 Hz		58 Hz		0,11 Hz	
	R Ω	R _{surface} Ω /cm ²	R Ω	R _{surface} Ω /cm ²	R Ω	R _{surface} Ω /cm ²
CA1	0,70	0,35	1,01	0,50	6,35	3,16
10XL	0,60	0,30	0,89	0,44	3,24	1,61

In terms of capacitance, however, sample 10XL exhibits even higher values than CA1 (see table V-7). Nonetheless, the differences in capacitance are minor and the capacitance behavior of the differently dried gels remains very similar (see figure V-26). Although 10XL seems to be less microporous than CA1, it has a higher mesoporous volume and a smaller mean mesopore size, explaining the fact that the frequency at which the energy may be withdrawn effectively is slightly higher for 10XL.

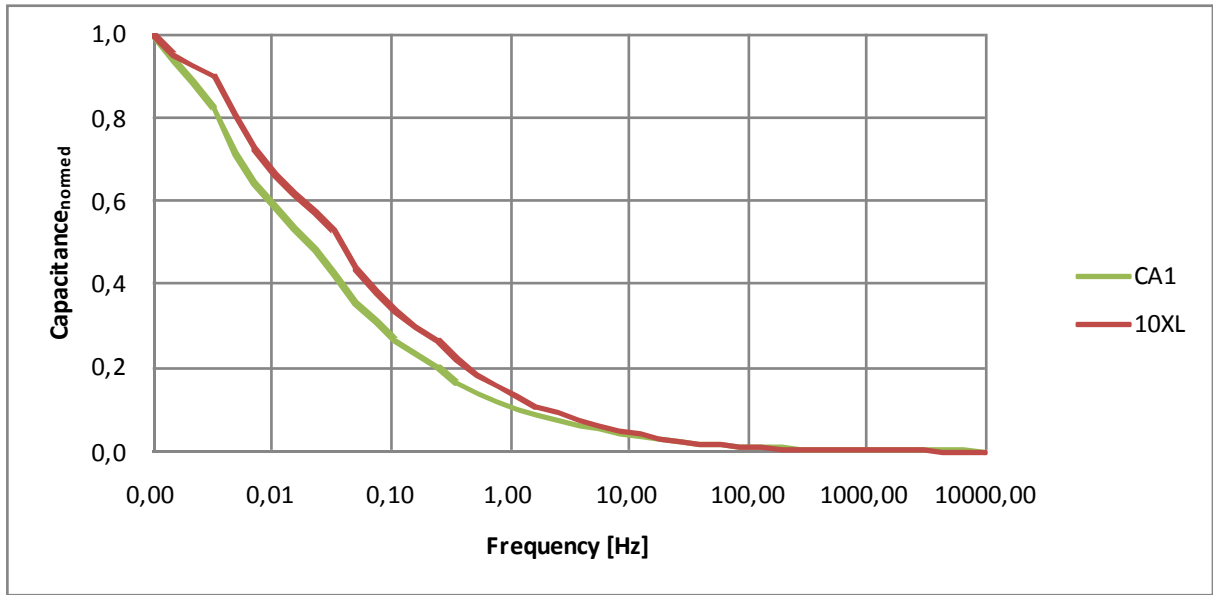


Figure V-26: Normalized capacitance as function of frequency for CA1 and 10XL

Table V-7: Characteristic values of CA1 and 10XL

Samples	$C_{\text{volumetric}}$ F/cm ³	C_{specific} F/g _{carbon}	ESR Ω	ESR _{surface} Ω / cm^2	I_{leakage} mA	E_{specific} Wh/kg _{carbon}	P_{specific} W/kg _{carbon}	τ s
CA1	8,64	15,48	6,35	3,16	0,24	0,54	585	3,3
10XL	16,21	23,54	3,24	1,61	0,32	0,82	929	3,2

Self discharge behavior (figure V-27) for aerogel CA1 and xerogel 10XL is rather similar, but shows a somewhat lesser discharge rate for the xerogel.

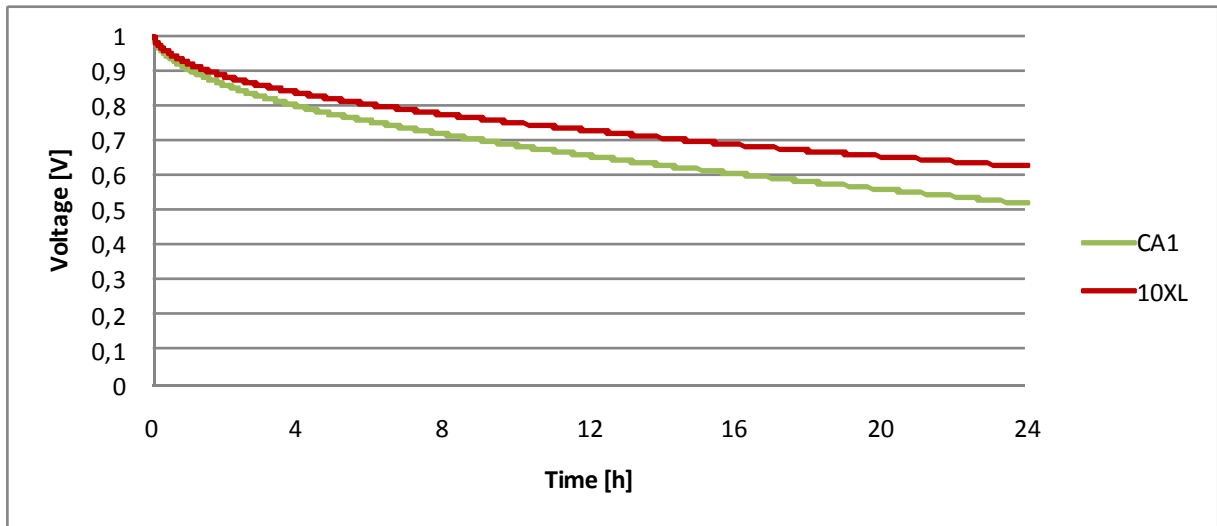


Figure V-27: Self discharge of carbons CA1 and 10XL

In conclusion, CAB 10XL shows performances comparable to those of a supercritically dried gel of the same formulation, *i.e.* CA1. Subcritical drying may thus be considered as an interesting alternative to energy- and cost-intensive supercritical drying.

4.2.3. Interest of Activation

The performance of CA1 (CAB CA of the formula 10-0.2-0.25DA) before and after activation at 850 °C, 950 °C, and 1050 °C (samples A850, A950, and A1050, respectively) has been analyzed in order to determine the interest of activation if CAB CAs is used as EDLC electrode material.

The HFR increases with increasing activation temperature (*i.e.* burn-off) for samples A850 and A950, but falls sharply for sample A1050 (see figure V-28 and table V-8). The increase of HFR for samples A850 and A950 may be due to an increase in porosity and therefore a decreased conductivity of the carbon. The low HFR for sample A1050 on the other hand might be explained by an improved electrical conductivity by exposing the sample to an activation temperature above the pyrolysis temperature and an accompanying increasingly ordered crystalline structure (*e.g.* bearing out results on increasing electrical conductivity for EDLC electrodes containing carbon treated at higher temperatures [Zho 2003, Hul 2006]).

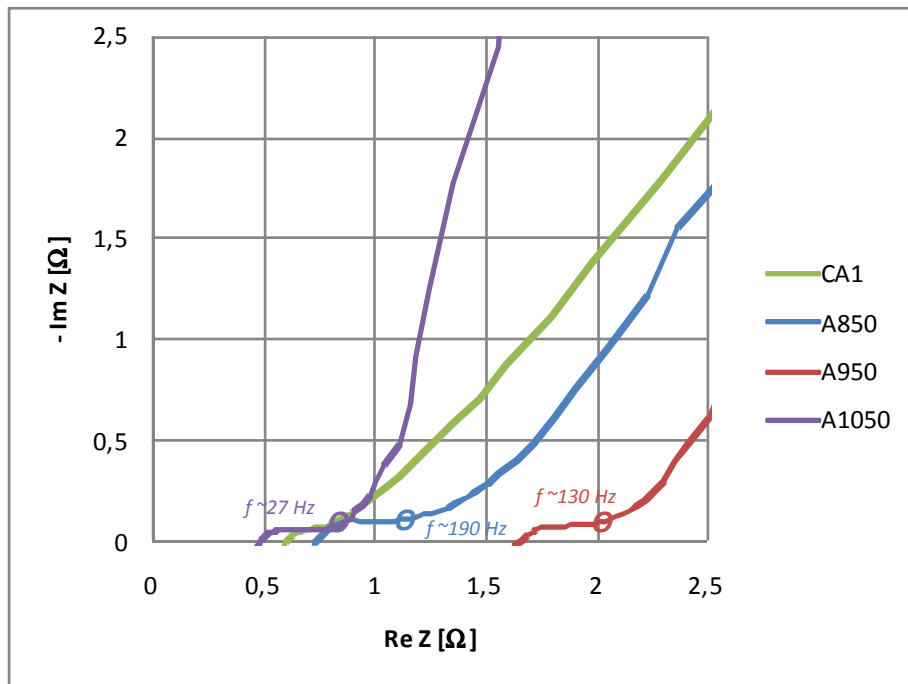


Figure V-28: High frequency region of Nyquist plot for CA1, A850, A950, and A1050

Table V-8: Resistance in dependence of frequency for CA1, A850, A950, A1050

Frequency	95 24 Hz		58 Hz		0, 11 Hz	
Samples	R Ω	R _{surface} Ω / cm ²	R Ω	R _{surface} Ω / cm ²	R Ω	R _{surface} Ω / cm ²
CA1	0,70	0,35	1,01	0,50	6,35	3,16
A850	0,93	0,46	1,29	0,64	3,54	1,76
A950	1,76	0,88	2,04	1,01	3,38	1,68
A1050	0,56	0,28	0,78	0,39	1,25	0,62

At low frequencies the resistance decreases with increasing activation temperature and therefore burn-off (see figure V-29). The Nyquist plot of sample A1050 is closest to a vertical line at low frequencies (see figure V-28), indicating a highly accessible surface. On the whole, increasing activation temperature increases the amount of surface area easily accessible for electrolyte ions (see figure V-30). The surface thus seems to become more easily accessible due to the widening of narrow micropores and the creation of a high mesoporous volume (refer to table V-1) resulting in the generation of wider pathways for the electrolyte ions. Also, oxygen-containing polar functional groups might be introduced on the carbon surface improving the wettability of the carbon surface for acidic aqueous electrolytes.

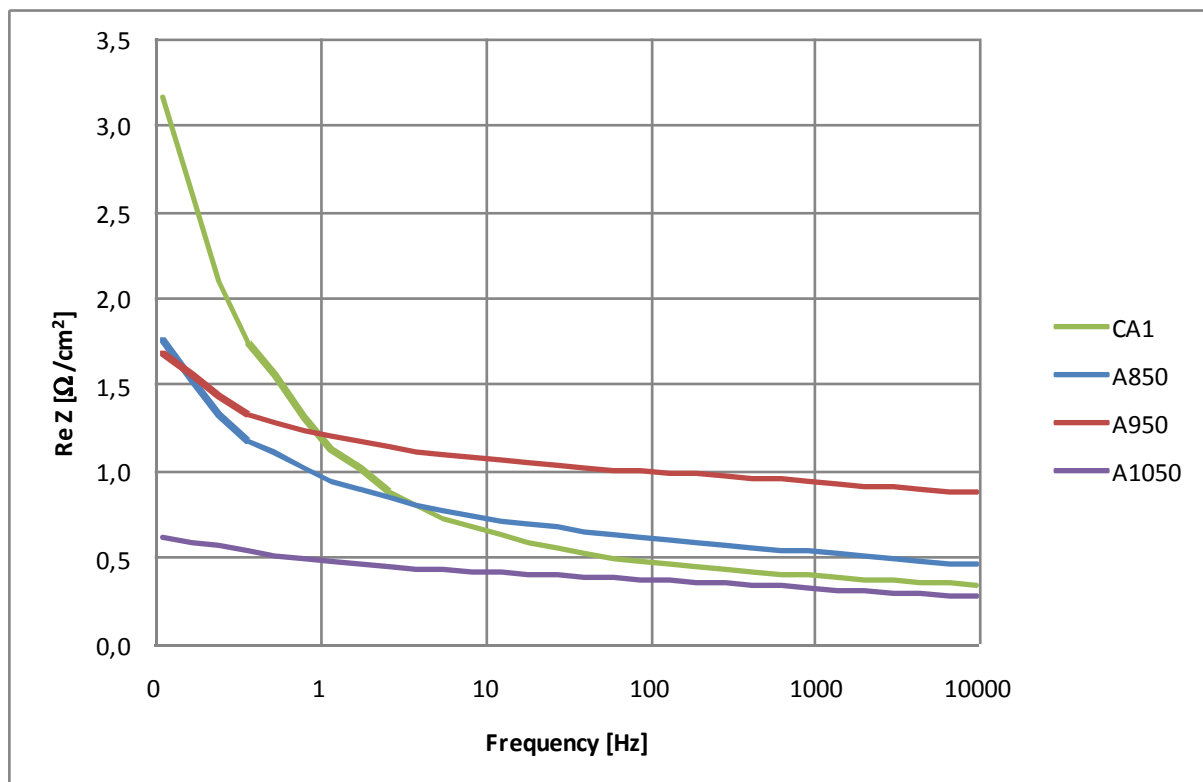


Figure V-29: Resistance as function of frequency for CA1, A850, A950, A1050

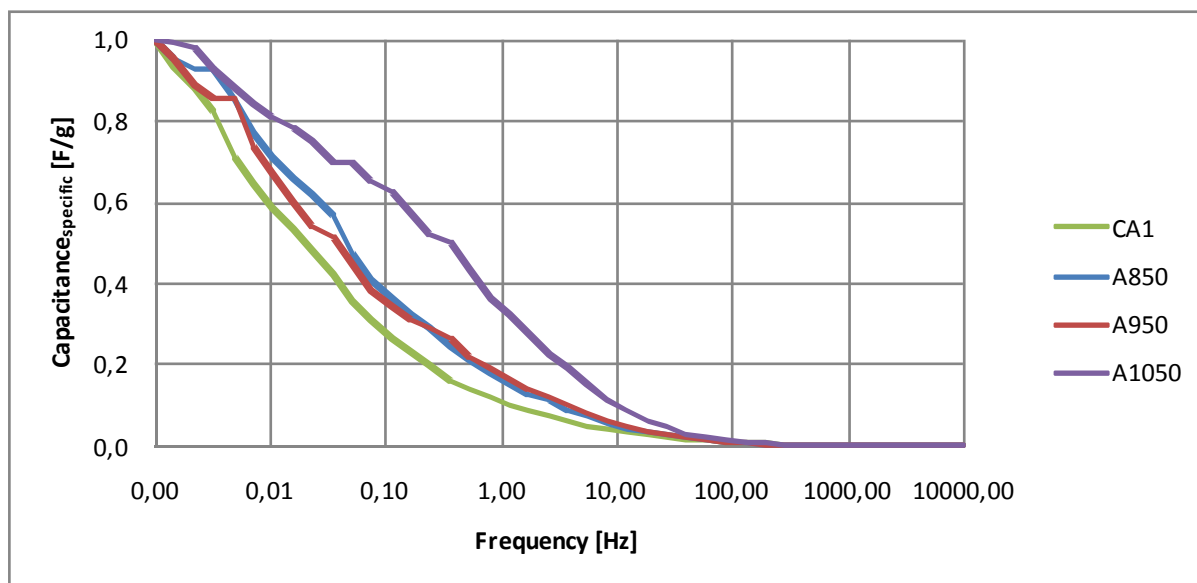


Figure V-30: Normalized capacitance as function of frequency for CA1, A850, A950, and A1050

Additionally, increasing activation temperatures increase the micropore volume in general (see table V-1) by creating microporosity, which certainly is the main reason for largely enhanced capacitances with increasing activation temperature (see figure V-31). In the literature, numerous authors have found that functional groups have been introduced on the carbon surface by activation in air or in CO₂. These surface functional groups may participate in improving the wettability of the carbon electrode, in the creation of local excess double layers, but also in pseudocapacitive reactions (e.g. quinone groups or pyrone-like structures) [Prö 2002, Hsi 2002, Hwa 2004, Hul 2006]. However, neither do results from elemental analysis for CAB CA activated in CO₂ (refer to table IV-2) indicate an introduction of O-containing surface groups (but rather a decrease of the oxygen content at activation temperatures above 850 °C), nor do cyclic voltammetry curves of the activated CAB CA do show any redox peaks. Nevertheless, to verify the absence of any redox humps (also of pseudocapacitive contributions due to the nature of the pristine CAB CA) cyclic voltammetry experiments at lower scan rates, in three-electrode cells, or for a different voltage range might be needed.

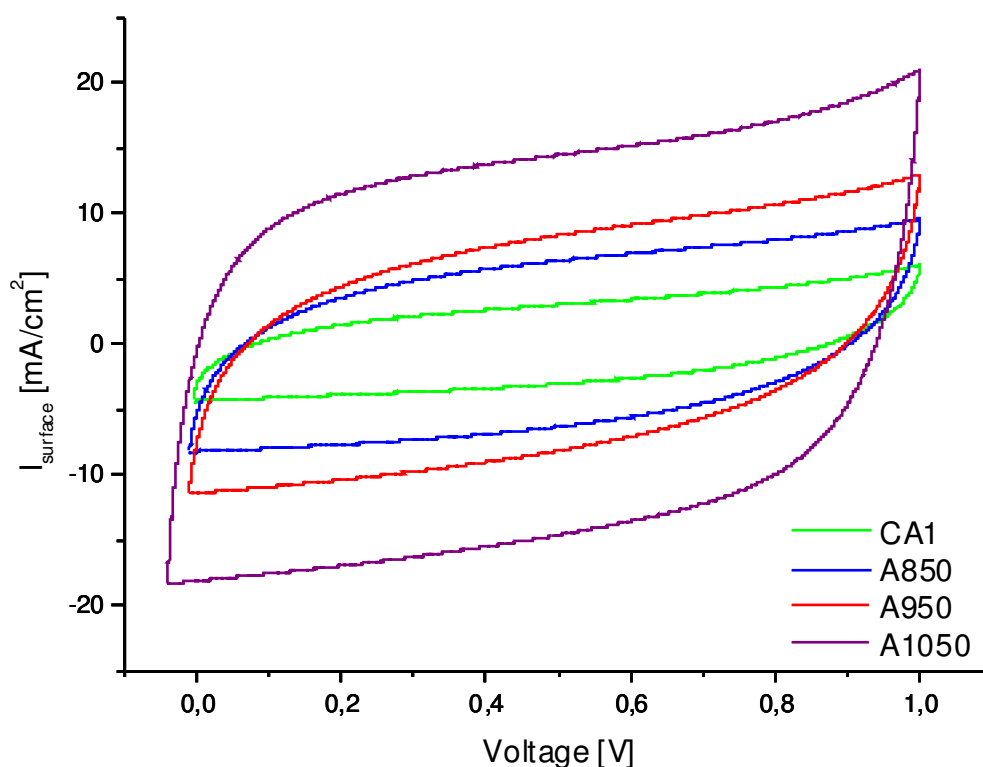


Figure V-31: Voltammogram for CA1, A850, A950, A1050

The characteristic values of non-activated and activated carbon samples are summarized in table V-9. While ESR decrease, capacitance and accordingly energy and power, increase significantly with activation temperature (*i.e.* burn-off).

Table V-9: Characteristic values of CA1, A850, A950, and A1050

Samples	C _{volumetric} F/cm ³	C _{specific} F/g _{carbon}	ESR Ω	ESR _{surface} Ω/cm ²	I _{leakage} mA	E _{specific} Wh/kg _{carbon}	P _{specific} W/kg _{carbon}	τ s
CA1	8,64	15,48	6,35	3,16	0,24	0,54	585	3,3
A850	17,79	33,32	3,54	1,76	0,27	1,16	1097	3,8
A950	23,27	48,23	3,38	1,68	0,40	1,67	1271	4,7
A1050	44,92	134,01	1,25	0,62	0,35	4,65	4946	3,4

Another benefit of activation in CO₂ seems to be a reduced self discharge of CAB CA in acidic aqueous electrolyte (see figure V-32). The leakage current of all activated CAB CA is above that of the non-treated sample CA1 (see table V-9). Frequently, the leakage current has been claimed to increase as a result of oxygen-containing surface groups [Hsi 2002, RaK 2006]. But although the leakage current is higher for all three activated samples than for the non-treated sample CA1, the self discharge is lower and visibly decreases with the activation temperature, as does the oxygen content of activated CAB CA samples. Higher leakage current might therefore rather be an effect of the modified structure, *i.e.* of a higher mesoporous volume and accompanying better circulation of electrolyte within the porosity. A lower self discharge for samples activated at higher temperatures is likely due to the samples' lower mean pore sizes resulting in a lower diffusion.

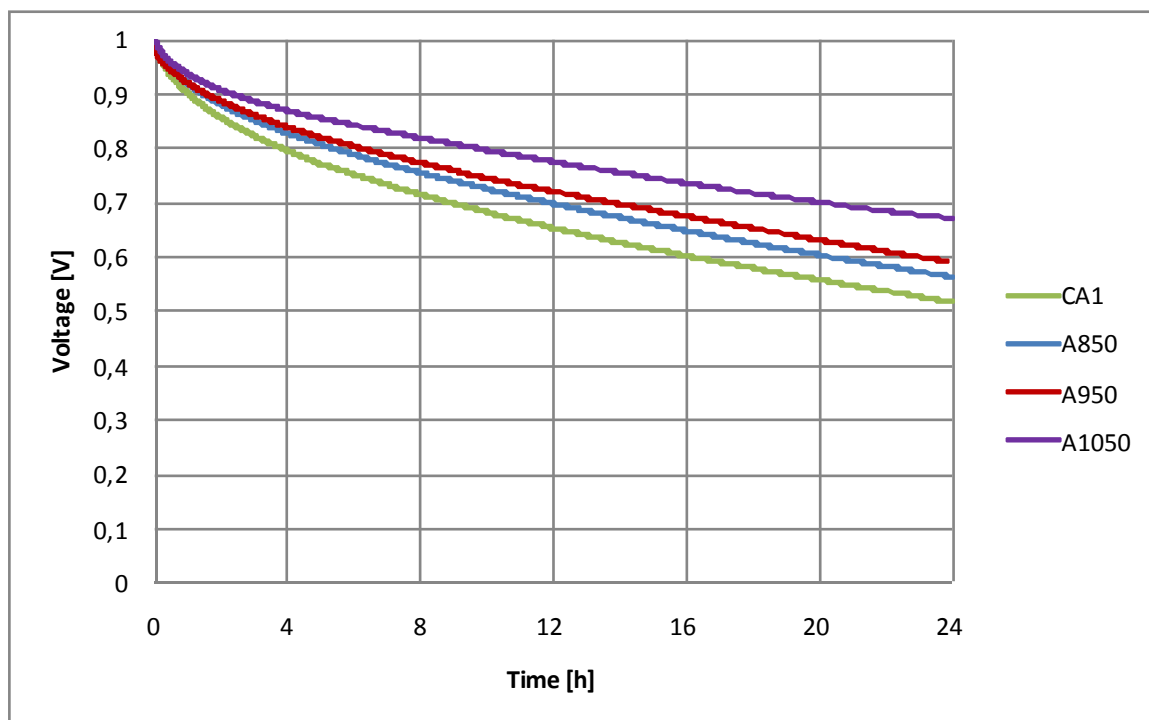


Figure V-32: Self discharge of carbons CA1, A850, A950, A1050

In conclusion, activation – by increasing microporous volume and specific surface area – increases the CAB CA’s capacitance and power and energy capability. In addition, activation in CO₂ seems to have a positive effect on the EDLCs self discharge. Therefore, activating CAB CA increases their performance for use as EDLC electrode material considerably.

4.2.4. Performance of Cellulose-acetate-based Aerogel/Cellulose Powder Composites

The performance of CAB aerogel/cellulose powder composite PCC (see chapter IV.2.2) as EDLC electrode material has been analyzed and compared to that of CAB CA1 not containing cellulose powder and to pyrolyzed cellulose powder (CP).

CAB aerogel/cellulose powder composite PCC has a lower resistance than CA1 (see table V-10 and figures V-33 and V-34).

Table V-10: Resistance in dependence of frequency for CA1, PCC, and CP

Frequency	9524 Hz		58 Hz		0,11 Hz	
	R Ω	R _{surface} Ω/cm ²	R Ω	R _{surface} Ω/cm ²	R Ω	R _{surface} Ω/cm ²
CA1	0,70	0,35	1,01	0,50	6,35	3,16
PCC	0,48	0,24	0,72	0,36	3,60	1,79
CP	1,40	0,69	15,60	7,76	239,70	119,22

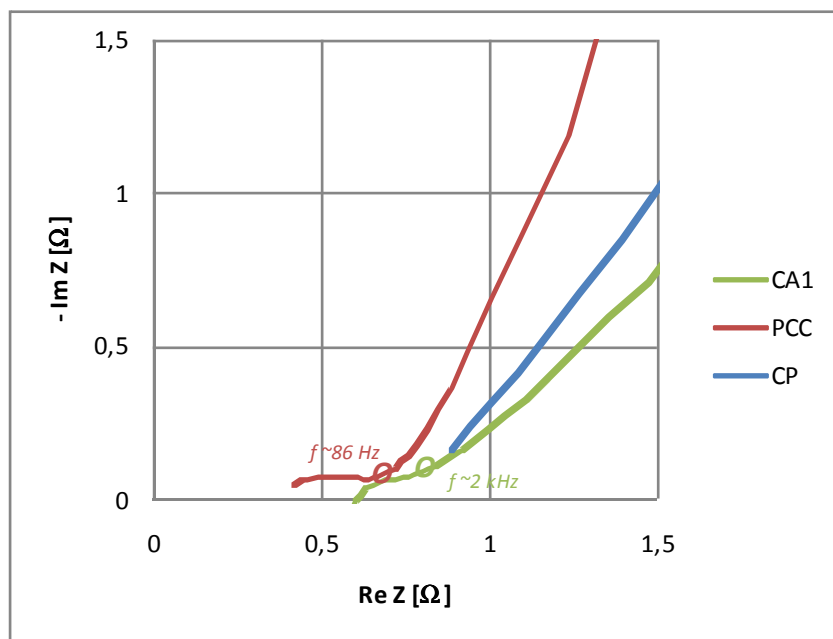


Figure V-33: High frequency region of Nyquist plot for CA1, PCC, and CP

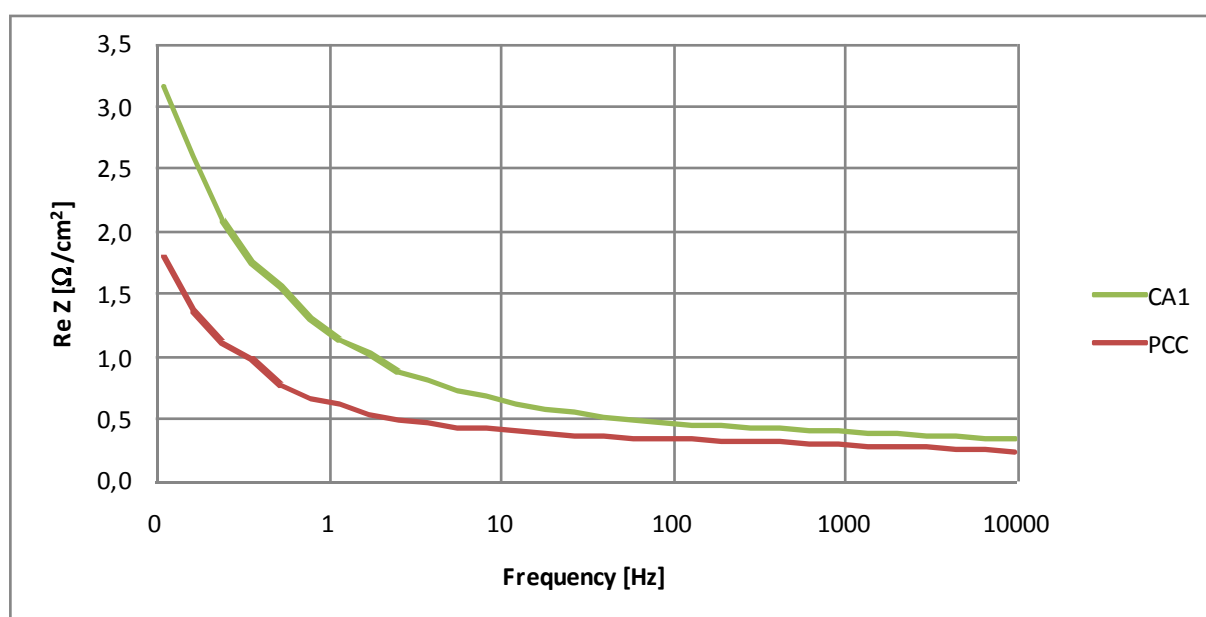


Figure V-34: Resistance as function of frequency for CA1 and PCC

The relatively low resistance values for PCC might be due to the carbon material's (or electrode's) higher density (refer to carbon mass contained in an electrode in table V-3) and accompanying lower porosity. Other reasons for PCC's relatively low ESR may be a higher average carbon powder particle size as a result of cellulose powder particles (and obviously fibres) being incorporated in the aerogel (and therefore less inter-particle boundaries) [Kie 2004] and low inter-particle resistance due to a good contact between the cellulose powder particles and the CAB CA having melted during pyrolysis (see figure V-35). The high frequency behavior of PCC as seen in its Nyquist plot in figure V-33 also hints at a poorer contact quality between PCC and the current collector (than for CA1 and the current collector), which could be a result of a larger carbon powder mean particle size.

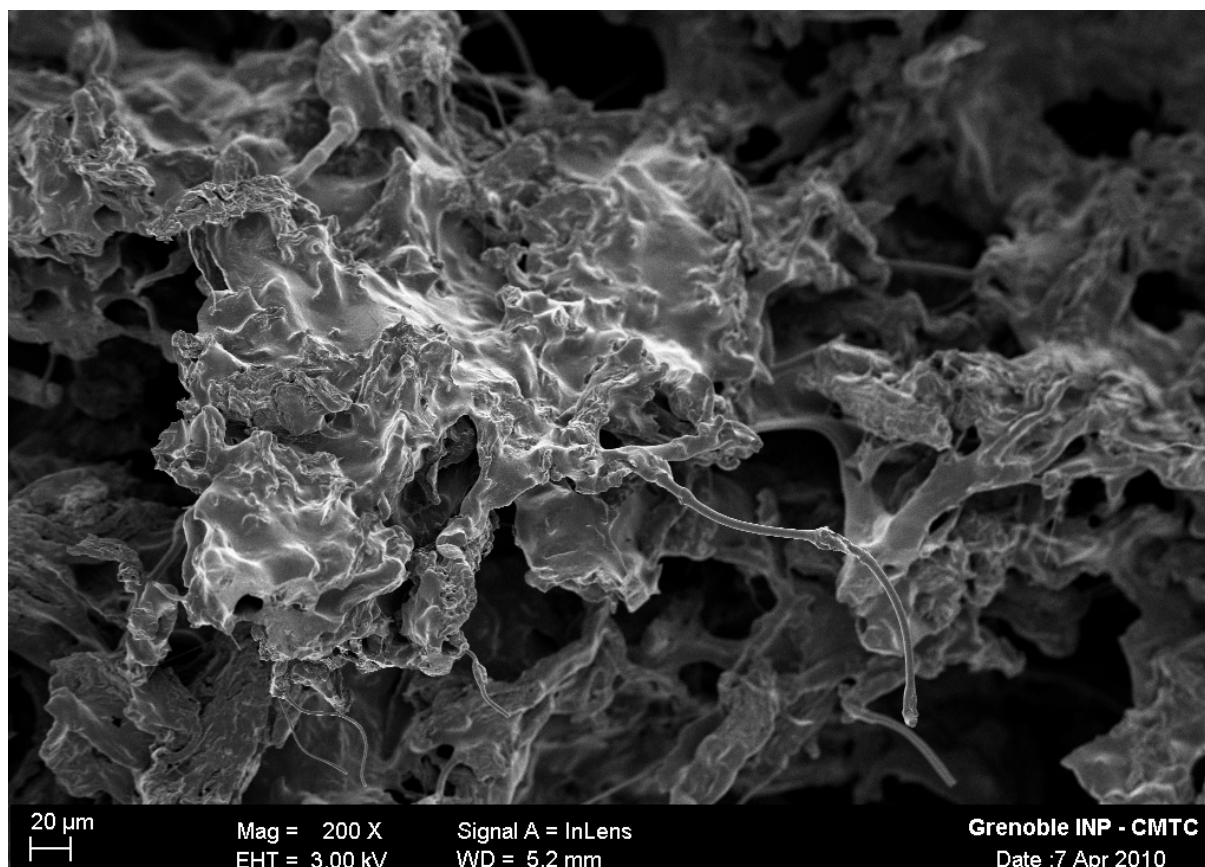


Figure V-35: SEM micrograph of carbonaceous CAB aerogel/CP composite and PCC

The high density of PCC (or at least of the PCC electrode) also results in a higher volumetric capacitance for PCC compared to CA1 (see table V-11). The specific capacitance for PCC, on the other hand, remains mostly inferior to that of CA1 (see figure V-36), which can be attributed to the less advantageous porous structure of PCC for application as EDLC electrode material (*i.e.* low specific surface area and a low micropore volume of only about $0.003 \text{ cm}^3/\text{g}$) as can be seen in table V-I.

Consequently, PCC's energy capabilities are lower than that of CA1, but its power capabilities and time constant are improved as a result of the low resistance of the CAB aerogel/cellulose composite. Not surprisingly, the carbon on the basis of cellulose powder embedded in the CAB aerogel yields much better results if applied as EDLC electrode material, than carbonized cellulose powder alone.

Table V-11: Characteristic values of CA1, PCC, and CP

Samples	C_{volumetric} F/cm³	C_{specific} F/g_{carbon}	ESR Ω	ESR_{surface} Ω/cm²	I_{leakage} mA	E_{specific} Wh/kg_{carbon}	P_{specific} W/kg_{carbon}	τ s
CA1	8,64	15,48	6,35	3,16	0,24	0,54	585	3,3
PCC	9,65	14,42	3,60	1,79	0,21	0,50	860	2,1
CP	0,33	0,47	239,70	119,22	0,09	0,02	12	4,8

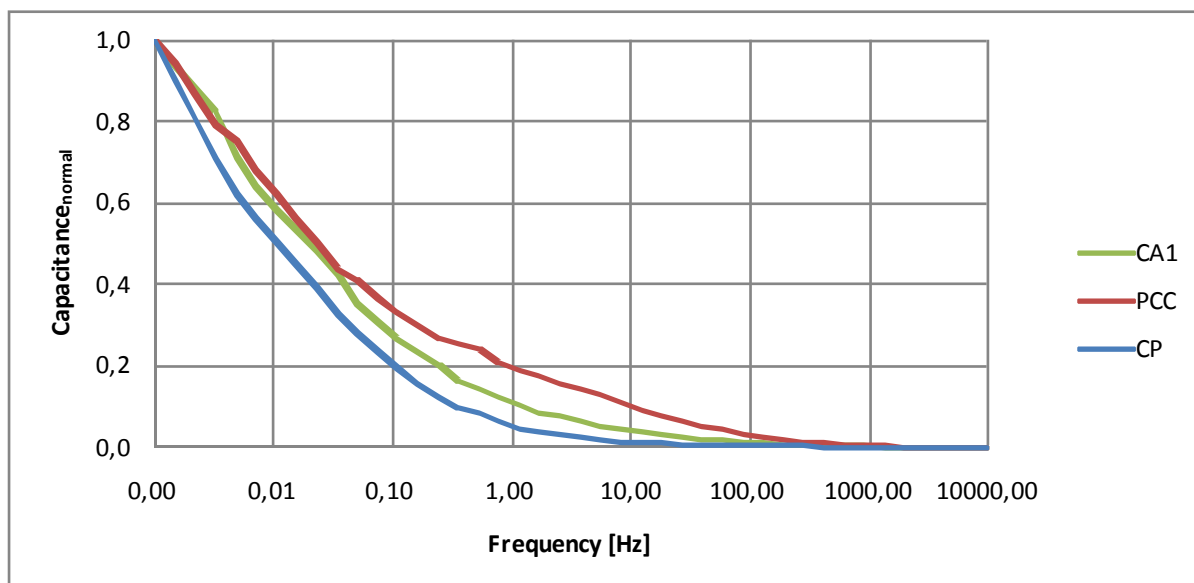


Figure V-36: Normalized capacitance as function of frequency for CA1, PCC, and CP

The self discharge of sample PCC is a little bit higher than for CAB CA1, but remains in a comparable value range (figure V-37).

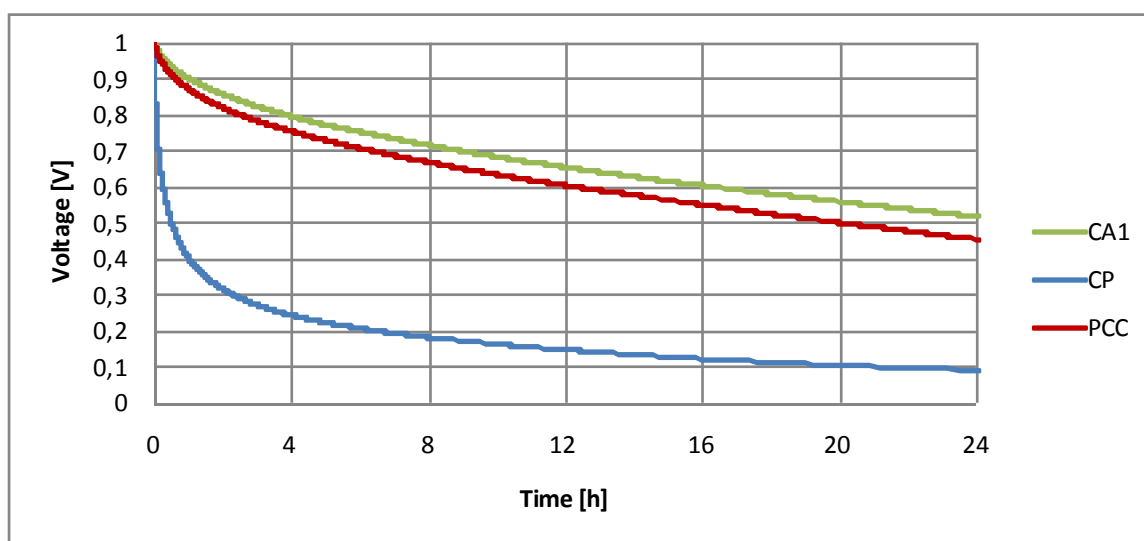


Figure V-37: Self discharge of carbons CA1, PCC, and CP

In conclusion, creating carbons on the basis of CAB aerogels containing cellulose powder seems to be interesting in view of decreasing the carbon's resistance. Lower resistance may be due only to lower porosity and higher density in comparison to CAB CA, but may also be due to the presence of carbonized cellulose particles (and fibres according to figure V-35) together with an enhanced contact between cellulose particles and CAB CA. In addition, a higher density through introduction of cellulose allow for a relatively high volumetric capacitance, even though micropore volume and specific surface area are inferior to those of CA1 not containing any cellulose powder.

4.3. Influence of Surface Chemistry

Electrochemical analysis of different CAB CA containing oxygen (CA1H, CA1N) and/or nitrogen surface functionalities (CA1M, CA2AM, CA2NAM) has been carried out, in order to discern influences of different surface chemistries.

4.3.1. Influence of oxidation

Oxidation of CAB CA1 drastically alters resistance and capacitance behavior. While oxidation in H_2O_2 decreases the carbon's resistance, oxidation in HNO_3 seems to increase the resistance at high frequencies (see table V-12 and figure V-38). This change resistive behavior at high frequencies may be induced by the presence of different functional groups on the carbon surface as a result of the two different oxidation treatments. Differences in surface chemistry may influence the wettability but also the contact quality between carbon electrode and current collector (visible in the high frequency region of the Nyquist plot in figure V-38). In addition, the distributed resistance seems to be most pronounced for CA1N, possibly due to the obstruction of a part of the porosity (especially microporosity, according to table V-1) by the introduction of O-containing functional groups during oxidation of CA1 with HNO_3 . In general, CA1 features a higher resistance than CA1H, but lower than CA1N (see figure V-39).

Table V-12: Resistance in dependence of frequency for CA1, CA1H, and CA1N

Frequency	9524 Hz		58 Hz		0,11 Hz	
Samples	R Ω	R_{surface} Ω / cm^2	R Ω	R_{surface} Ω / cm^2	R Ω	R_{surface} Ω / cm^2
CA1	0,70	0,35	1,01	0,50	6,35	3,16
CA1H	0,46	0,23	0,68	0,34	1,42	0,71
CA1N	1,82	0,91	2,32	1,15	5,93	2,95

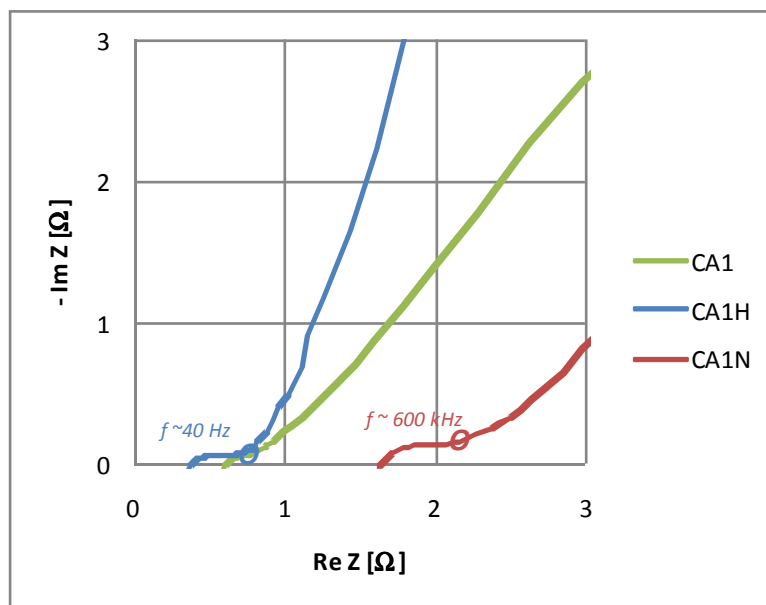


Figure V-38: High frequency region of Nyquist plot for CA1, CA1H, and CA1N

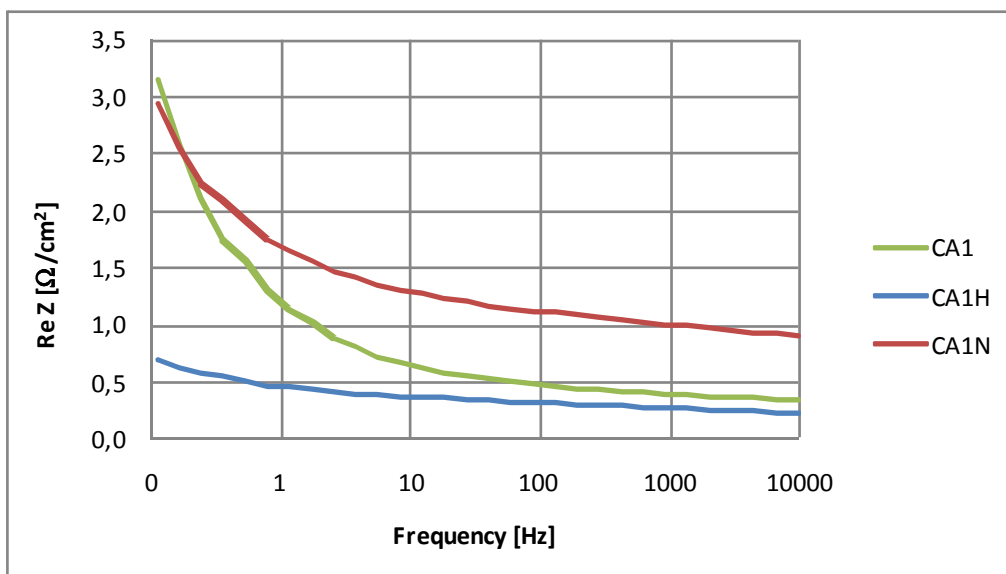


Figure V-39: Resistance as function of frequency for CA1, CA1H, and CA1N

Although oxidation in HNO_3 (sample CA1N) increases the electrode capacitance only very little, oxidation in H_2O_2 (sample CA1H) has a very pronounced influence on capacitance behavior and capability (see table V-13 and figures V-40 and V-41). The capacitance of CA1H is increased by a factor of four as compared to the capacitance of CA1. As the structure of both oxidized carbons, CA1H and even more so CA1N, seems to be less appropriate for an application as EDLC electrode material than that of CA1 (according to the results of N_2 sorption), improved EDLC performance may be attributed to the presence of oxygen-containing surface groups. As presented in the section on pseudocapacitance (section V.2.3), the presence of functional groups may change (i) the carbon's electron donor and acceptor characteristics and thereby the possibility of oxidation/reduction reactions to occur, (ii) surface polarity and thereby wettability, and (iii) the dipole affinity between carbon surface and electrolyte and thereby an excess double layer.

Table V-13: Characteristic values of CA1, CA1H, and CA1N

Samples	$C_{\text{volumetric}}$ F/cm^3	C_{specific} $\text{F}/\text{g}_{\text{carbon}}$	ESR Ω	$\text{ESR}_{\text{surface}}$ Ω/cm^2	I_{leakage} mA	E_{specific} $\text{Wh}/\text{kg}_{\text{carbon}}$	P_{specific} $\text{W}/\text{kg}_{\text{carbon}}$	τ s
CA1	8,64	15,48	6,35	3,16	0,24	0,54	585	3,3
CA1H	41,20	67,02	1,42	0,71	0,38	2,33	2374	3,5
CA1N	9,06	16,00	5,93	2,95	0,46	0,56	617	3,2

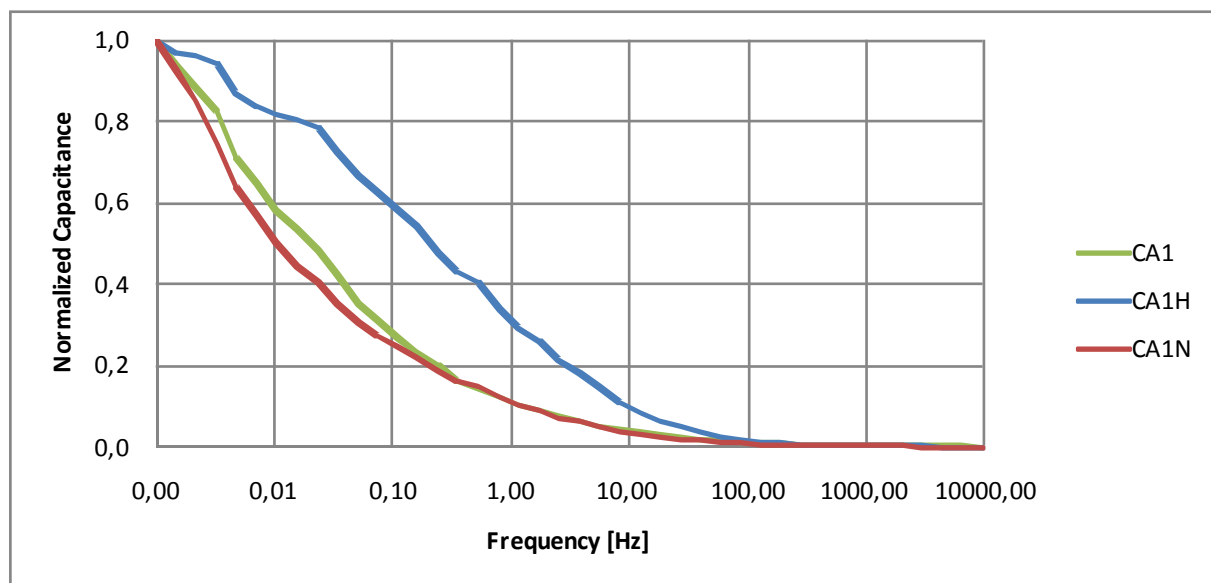


Figure V-40: Normalized capacitance as function of frequency for CA1, CA1H, CA1N

Although the behavior of carbons CA1H and CA1N (and maybe already of CA1) seem to be influenced by oxygen-containing surface functional groups, it is not clear which mechanisms are responsible for the altered behaviour. Sample CA1H, featuring the highest percentage of functional groups (45%), reaches the highest capacitances, while CA1, featuring the lowest percentage of functional groups (30%) has the lowest capacitances of samples CA1, CA1H, and CA1N (35% surface functionalities), according to the XPS data featured in table IV-11. The voltammograms of CA1, CA1H, and CA1N lack characteristic pseudocapacitive peaks. Nonetheless, all of the carbons tested contain surface functionalities which have been shown to undergo faradaic reactions with acidic aqueous electrolyte before, *e.g.* quinone groups for CA1H and CA1N (refer to chapter IV.3) [Hsi 2002, Ser 2009]. As O-containing functional groups (like quinone) and also N-containing functional groups due to the cellulosic nature of the aerogel (*e.g.* N-5) are present in all three samples, a pseudocapacitive contribution cannot be excluded, but have not been detected. However, CA1, CA1H, and CA1N have been tested exclusively in a 2-electrode cell. Also, redox humps might not be visible in the voltage range observed during cyclic voltammetry (*i.e.* 0-1 V). Reactions involving quinone/hydroquinone reactions or pyrone-like structures, for example, are most pronounced around 0.0 V and 0.1 V vs. Hg/Hg₂SO₄ (for cathodic and anodic current respectively) [RaL 2006]. An enhanced hydrophilic character, on the other hand, has been found for CA1H and CA1N according to the data from XPS analysis (table IV-12 in chapter IV).

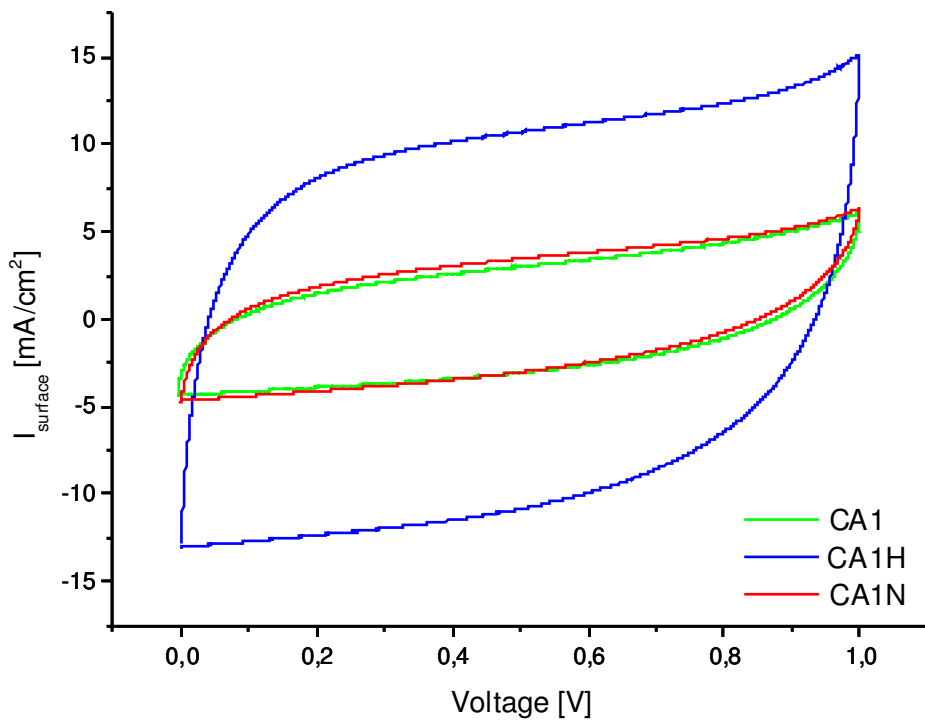


Figure V-41: Voltammogram for CA1, CA1H, and CA1N at 20 mV/s

In spite of an improved performance in terms of capacitance, energy and powder capabilities, the self discharge is clearly more pronounced for both oxygen-enriched CAB CA (see figure V-42). This behavior bears out the results of different authors reporting an increased leakage current for oxygen-containing carbon electrodes [Hsi 2002, RaK 2006]. Instead of a voltage loss of about 50% in 24 h (for sample CA1), both oxygen-containing carbons lose roughly 80% of the initial voltage.

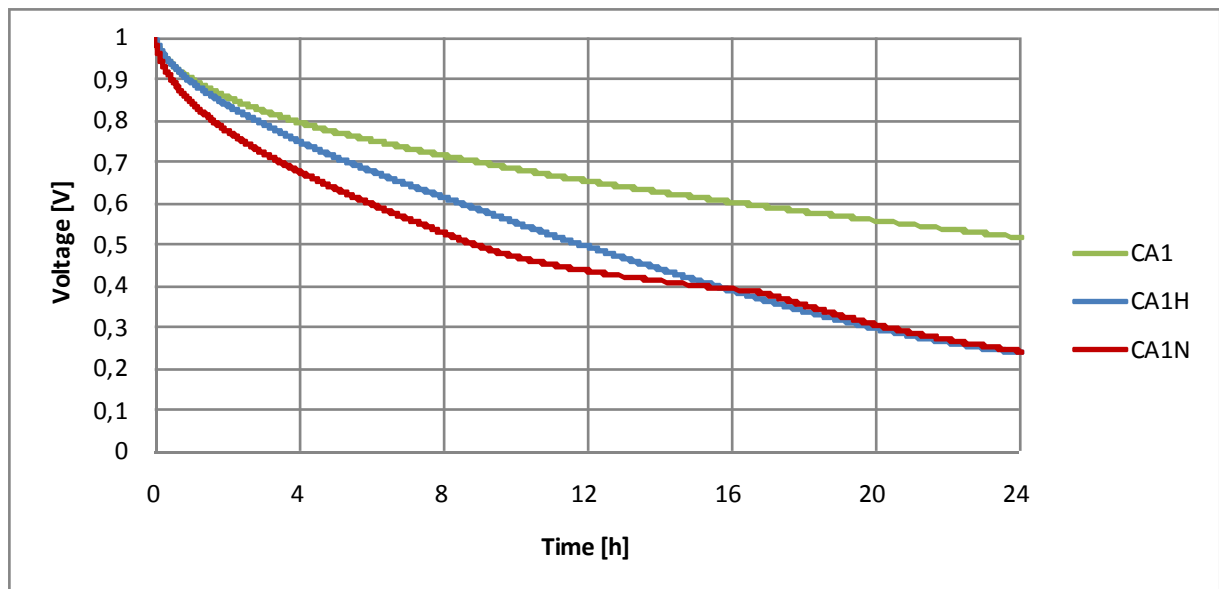


Figure V-42: Self discharge of carbons CA1, CA1H, CA1N

In conclusion, oxidation of carbon aerogels in HNO_3 and H_2O_2 and introducing oxygen surface functionalities helps improving the electrochemical performance of CAB CA in terms of energy and power capabilities, but leakage current and self-discharge rates are considerably increased at the same time.

4.3.2. Influence of Nitrogen Introduction

Introducing nitrogen functionalities seems to decrease the electrode resistance (see table V-14 and figures V-43 and V-44), probably due to an enhanced polarity and therefore wettability of the electrode material [Ser 2009]. CAB CA2 and carbon material derived from CA2 (*i.e.* CA2AM and CA2NAM) show clearly higher resistance values, seemingly due to the intrinsic electrical resistance of the electrode material, its intergranular contacts, and a poorer contact between electrode and current collector. Although the deterioration of specific surface area and porous volumes, as well as the decrease in oxygen content, between CA1 and CA2 corresponds to the difference in pyrolysis temperature (higher pyrolysis temperature for CA2), CA2 has been found to feature more surface functional groups than CA1 (40% for CA2 as compared to 30% for CA1). This difference in chemistry might be responsible for the higher HFR for CA2 and CA2-based samples.

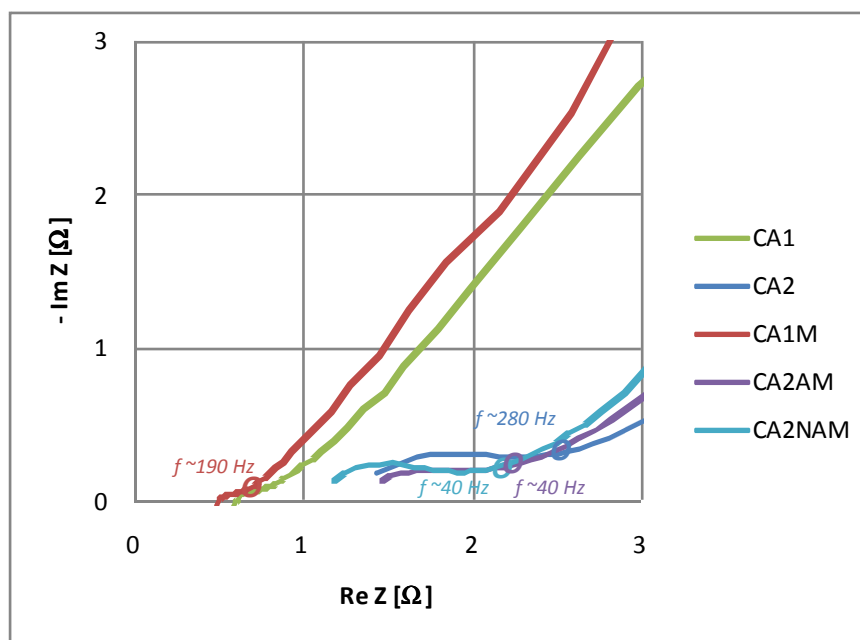


Figure V-43: High frequency region of Nyquist plot for CA1, CA2, CA1M, CA2AM, CA2NAM

Table V-14: Resistance in dependence of frequency for CA1, CA2, CA1M, CA2AM, and CA2NAM

Frequency	9524 Hz		58 Hz		0,11 Hz	
Samples	Resistance Ω	R_{surface} Ω / cm^2	R Ω	R_{surface} Ω / cm^2	R Ω	R_{surface} Ω / cm^2
CA1	0,70	0,35	1,01	0,50	6,35	3,16
CA2	1,84	0,91	2,80	1,39	8,71	4,33
CA1M	0,55	0,28	0,77	0,38	4,28	2,13
CA2AM	1,73	0,86	2,41	1,20	6,22	3,10
CA2NAM	1,52	0,76	2,18	1,08	4,74	2,36

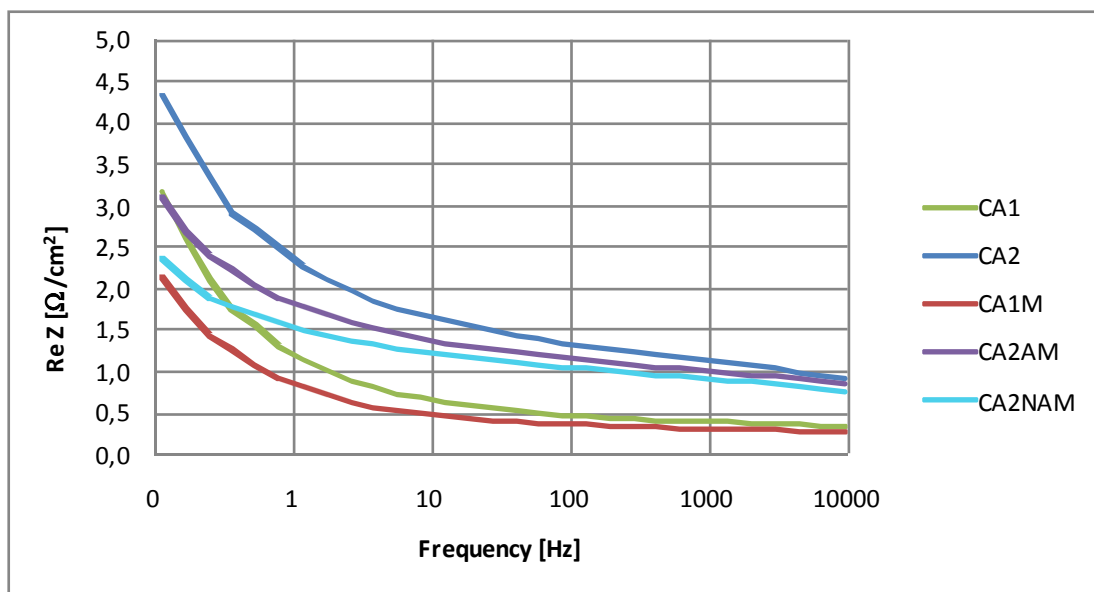


Figure V-44: Resistance as function of frequency for CA1, CA2, CA1M, CA2AM, and CA2NAM

Capacitance is increased for all nitrogen-enriched carbons, even if only slightly (see table V-15 and figure V-45). Even though the structure of sample CA1M is very similar to that of its carbonaceous precursor CA1, capacitances are increased and resistances are lower as compared to CA1. The increase in capacitance may be due to the influence of nitrogen-containing groups and/or of oxygen-containing groups having been created upon contact of carbon CA1M with the atmosphere leading to an adsorption of oxygen on its surface (see chapter IV). The decrease in resistance, however, may be due to a better wettability caused by the presence of hydrophilic functional groups on the carbon surface.

Capacitive behavior of CA2AM and CA2NAM is superior to that of their precursor carbon material CA2. Nonetheless, capacitances are far from what could have been expected in respect to their s_{BET} and microporous volume being above CA2. Carbon material CA2AM and CA2NAM feature surfaces of about twice the area of that of their precursor CA2, and also twice the micropore volume (see table V-1). The performance of the CA2AM and CA2NAM seems therefore to have deteriorated by increasing the amount of nitrogen-containing surface groups by ammonization. However, the difference in capacitance between CA2AM and CA2NAM (featuring comparable structural features) suggests that the difference in surface functionalities does play an important role (CA2NAM possesses more functional groups than CA2AM, *i.e.* 35% vs. 30% of carbon atoms functionalized). At the same time voltammogram shapes have deteriorated for samples CA2AM and CA2NAM. According to the XPS analysis carried out on samples CA2AM and CA2NAM, ammonization has rendered the samples more hydrophobic (table IV-12 in chapter IV).

Even though capacitance has repeatedly been reported to increase with N content of the carbon electrode (for acidic medium and basic nitrogen functionalities) [Hul 2005, Fra 2006, Ser 2009], the capacitance in dependence of surface area or pore volume has decreased with ammonization for samples CA2AM and CA2NAM. Both samples contain more nitrogen than their carbonaceous precursor and a high number of basic surface groups. An explanation to this behavior may be the use of a symmetric EDLC assembly, *i.e.* using the same material for both positive and negative plate. Although the capacity of one electrode may have been improved by introducing N-containing

functional groups, the parameters of the opposite electrode may have been deteriorated at the same time and the capacitance of the total EDLC assembly thus decreased. Jurewicz et al. have proposed to use electrodes of a balanced content of O- and N-containing functional groups so that the performance of both electrodes (of different polarities) may be improved at the same time [Jur 2003]. Not surprisingly, samples CA2AM and CA2NAM are the least balanced, *i.e.* feature the highest difference in quantity of acidic and basic surface groups, of all samples having been used in the study of modifying the CAB CA surface chemistry (CA1, CA1H, CA1N, CA1M, and CA2). In order to study these relations more closely, experiments in different electrolytes and at different current loads could be carried out in a 3-electrode cell.

Table V-15: Characteristic values of CA1, CA2, CA1M, CA2AM, and CA2NAM

Samples	$C_{\text{volumetric}}$ F/cm ³	C_{specific} F/g _{carbon}	ESR Ω	ESR_{surface} Ω/cm ²	I_{leakage} mA	E_{specific} Wh/kg _{carbon}	P_{specific} W/kg _{carbon}	τ s
CA1	8,64	15,48	6,35	3,16	0,24	0,54	585	3,3
CA2	8,99	14,33	8,71	4,33	0,23	0,50	557	3,2
CA1M	10,11	17,59	4,28	2,13	0,23	0,61	843	2,6
CA2AM	9,04	16,04	6,22	3,10	0,58	0,56	591	3,4
CA2NAM	12,89	20,90	4,74	2,36	0,34	0,73	1424	1,8

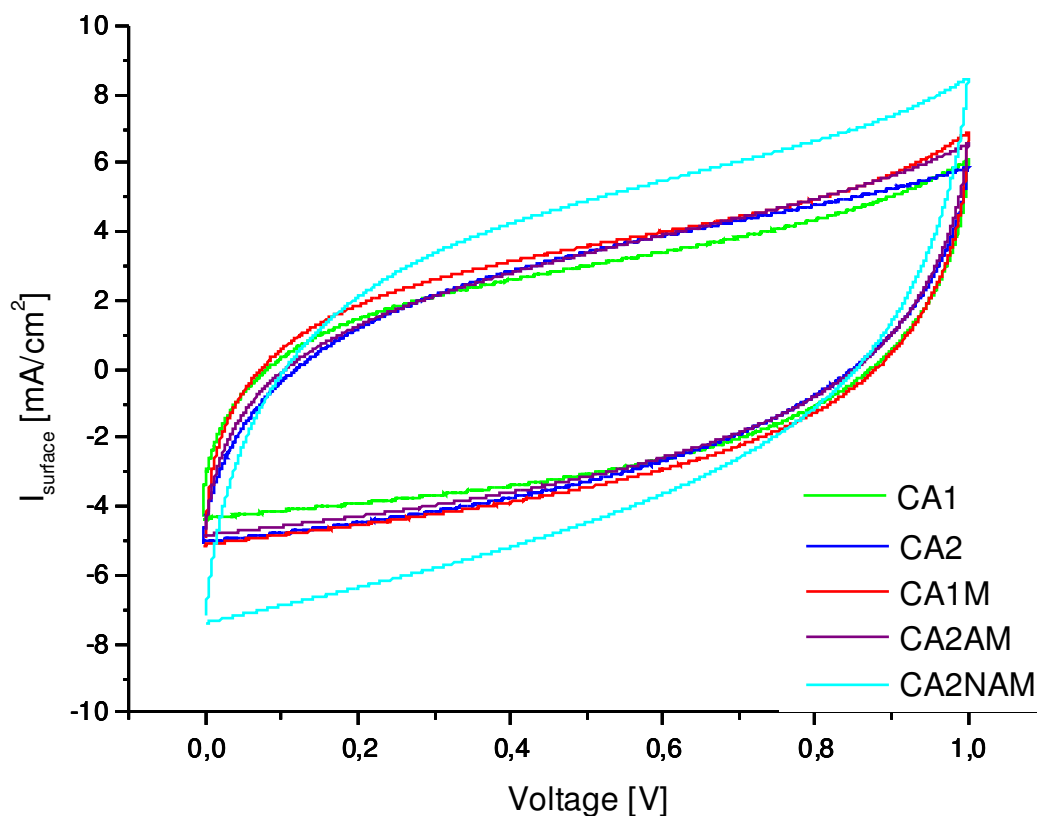


Figure V-45: Voltammogram for CA1, CA2, CA1M, CA2AM, and CA2NAM at 20 mV/s

Capacitive behavior in dependence of the frequency, however, does not differ noticeably (see figure V-46). Even though CA2AM and CA2NAM possess higher S_{BET} and $V_{\mu pores}$ the accessibility for ions to the carbon surface does not seem to have been altered at all.

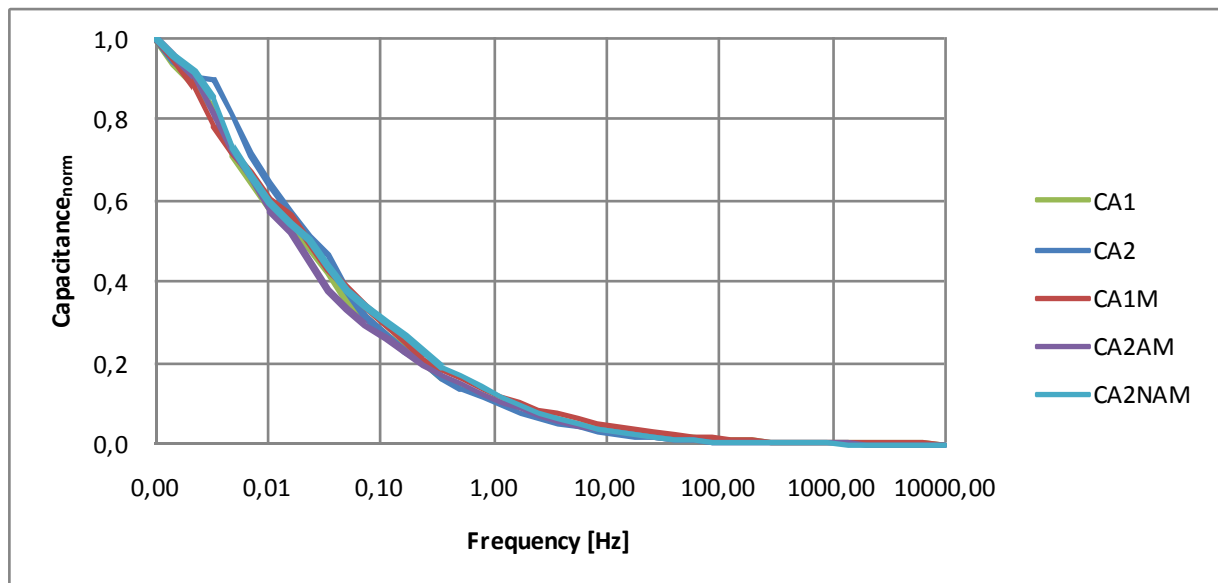


Figure V-46: Normalized capacitance as function of frequency for CA1, CA2, CA1M, CA2AM, CA2NAM

Figure V-47 shows the self discharge for the different carbons before and after introduction of nitrogen on the carbon surface. The introduction of N has been found to decrease leakage current and self-discharge [Jur 2006]. CAB CA1 features the lowest self discharge rate. CA1M features a lower leakage current but a higher discharge rate. CA2AM and CA2NAM, on the other hand, have a more pronounced leakage current than their carbonaceous precursor CA2, but their self discharge is lower than that of sample CA2.

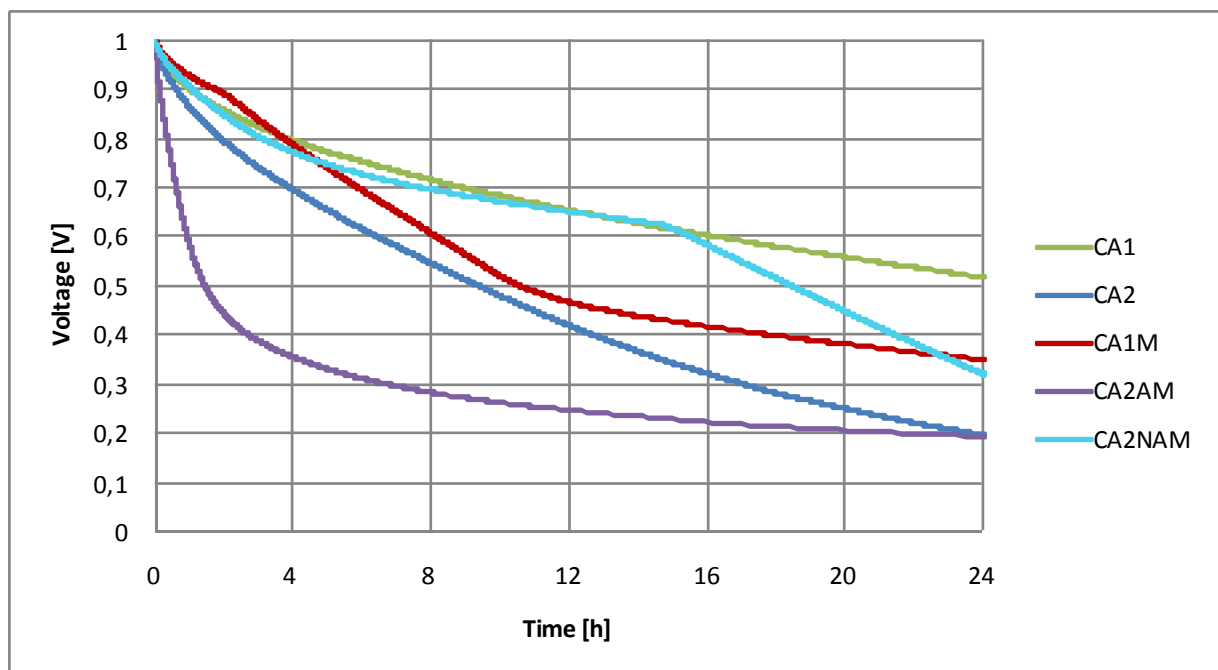


Figure V-47: Self discharge of carbons CA1, CA2, CA1M, CA2AM, and CA2NAM

In conclusion, modification of the surface chemistry by introducing N-containing surface groups changes the electrode performance. Although the performances could have been improved for sample CA1M, the changes in surface chemistry for both ammonized samples (CA2AM, CA2NAM) have not been found to be beneficial for the overall performance of the capacitor. Also, benefits of nitrogen introduction, in terms of pseudocapacitive contribution to capacitance, could not have been demonstrated.

4.4. Comparison with other Nanostructured Carbons

4.4.1. Comparison of different cellulose-based carbon aerogels

CAB CA have been compared with other carbonized cellulose-based aerogels, so-called aerocellulose (Aerocellulose 1, Aerocellulose 2). Aerocellulose samples are synthesized by the dissolution and subsequent regeneration of cellulose (see section 3.3).

Both aerocellulose samples exhibit very low resistance values (see table V-16 and figures V-48 and V-49). The HFR of Aerocellulose 1 and Aerocellulose 2 are similar. The ESR at low frequencies of Aerocellulose 2, on the contrary, amounts to only half of that of Aerocellulose 1 and only to a fourth of that of CA1. The low resistance values for aerocellulose are probably due to the nature of the cellulose-based carbon, significantly governed by the organic precursor (in this case cellulose). The favorable ESR of Aerocellulose 2 as compared to Aerocellulose 1 might be a result of a slightly higher oxygen content, known to be able to have a beneficial influence on the wettability of the carbon surface [Kin 1988, Con 1999].

Table V-16: Resistance in dependence of frequency for CA1, Aerocellulose 1, and Aerocellulose 2

Frequency	9524 Hz		58 Hz		0,11 Hz	
Samples	R	R_{surface}	R	R_{surface}	R	R_{surface}
	Ω	Ω/cm²	Ω	Ω/cm²	Ω	Ω/cm²
<i>CA1</i>	0,70	0,35	1,01	0,50	6,35	3,16
<i>Aerocellulose 1</i>	0,28	0,14	0,44	0,22	3,25	1,61
<i>Aerocellulose 2</i>	0,28	0,14	0,40	0,20	1,21	0,60

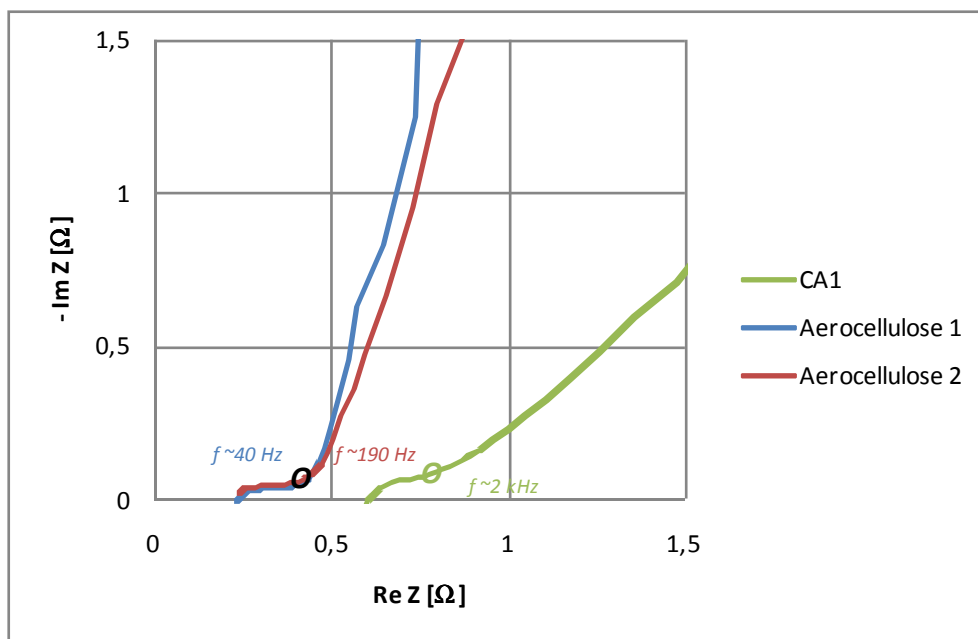


Figure V-48: High frequency region of Nyquist plot for CA1, Aerocellulose 1, and Aerocellulose 2

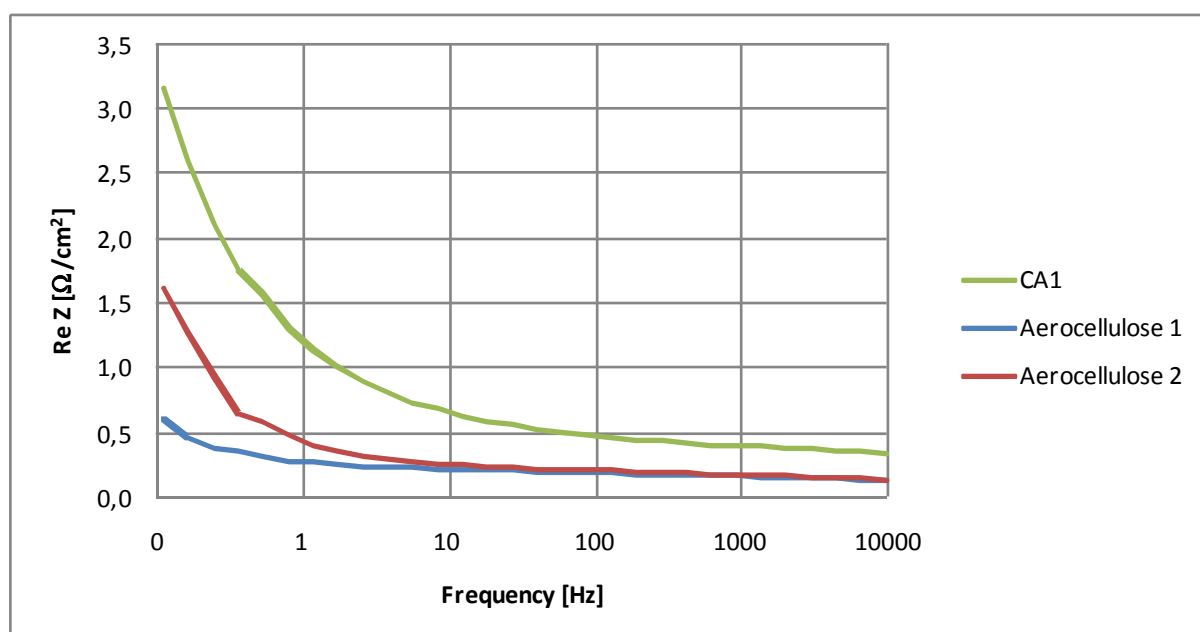


Figure V-49: Resistance as function of frequency for CA1, Aerocellulose1, and Aerocellulose 2

Aerocellulose samples 1 and 2 display a specific capacitance higher than that of CAB CA1, but not necessarily a higher volumetric capacitance (table V-17). Aerocellulose 1 features the highest capacitance. Although Aerocellulose 2 possesses a higher s_{BET} , its meso- and micropore volume as well as the mean pore size are lower than for Aerocellulose 1 (see table V-2). Additionally, the quantity of residual heteroatoms and impurities (e.g. O, H, and Na) is slightly higher in the Aerocellulose 2 sample (Aerocellulose 1: 87.9 wt.-%C, 0.7 wt.-%H, 5.5 wt.-%O, 0.15 wt.-%Na, 94.25 wt.-% total; Aerocellulose 2: 89.17 wt.-%C, 0.97 wt.-%H, 5.71 wt.-%O, 0.19 wt.-%Na, 96.05 wt.-% total). Although the differences between samples Aerocellulose 1 and 2 seem marginal, Aerocellulose 1 features capacitances almost twice as high as Aerocellulose 2.

Table V-17: Characteristic values of CA1, Aerocellulose 1, and Aerocellulose 2

Samples	$C_{\text{volumetric}}$ F/cm ³	C_{specific} F/g _{carbon}	ESR Ω	ESR_{surface} Ω/cm^2	I_{leakage} mA	E_{specific} Wh/kg _{carbon}	P_{specific} W/kg _{carbon}	τ s
CA1	8,64	15,48	6,35	3,16	0,24	0,54	585	3,3
Aerocellulose 1	16,96	54,94	3,25	1,61	0,21	1,91	2065	3,3
Aerocellulose 2	7,12	33,20	1,21	0,60	0,11	1,15	7986	0,5

Figure V-50 shows the behavior of capacitance in dependence of frequency for CA1, Aerocellulose 1, and Aerocellulose 2. For both aerocellulose samples the energy of the capacitor can be withdrawn at frequencies more elevated than those for CA1.

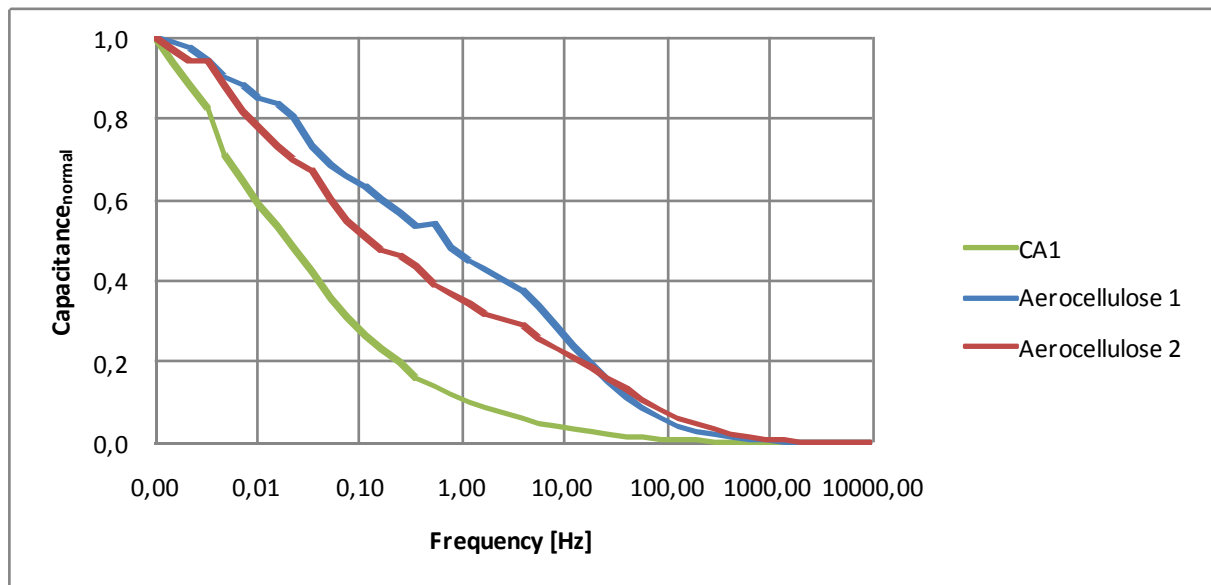


Figure V-50: Normalized capacitance as function of frequency for CA1, Aerocellulose 1, and Aerocellulose 2

Aerocellulose 1 and 2 feature a higher self discharge than CA1, as can be seen in figure V-51. Both aerocellulose samples contain Na residues (of 0.15 and 0.19 wt.-% for Aerocellulose 1 and Aerocellulose 2 respectively), possibly accelerating the self discharge.

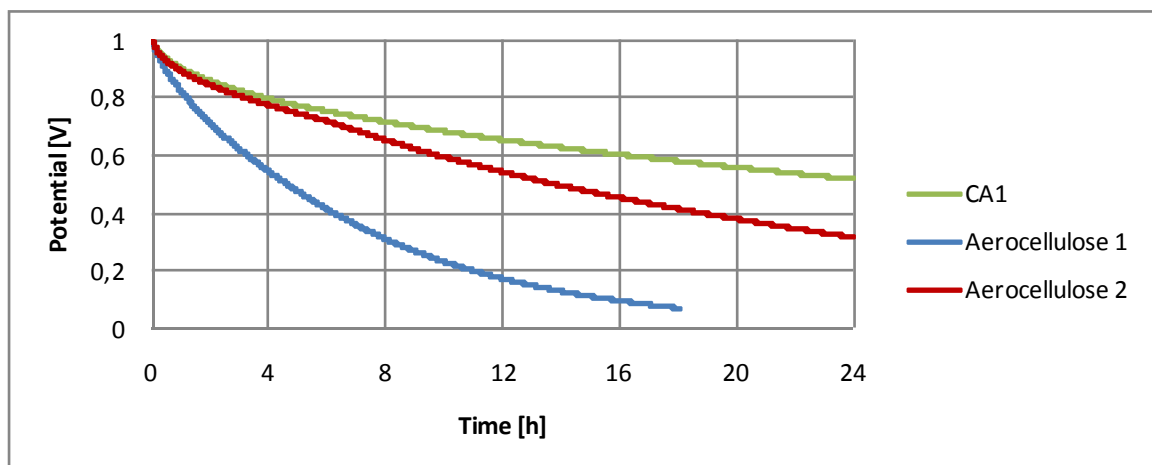


Figure V-51: Self discharge of carbons CA1, Aerocellulose 1, and Aerocellulose 2

In conclusion, carbonized aerocellulose may be an interesting alternative for CAB aerogels, depending on the synthesis conditions. The structure of both aerocellulose samples tested in this work is more interesting for a use as EDLC electrode material than that of pristine CAB CA samples. Thus, aerocellulose samples may show interesting performances in terms of capacitance and resistance, but feature rather high self-discharge rates.

4.4.2. Comparison with a commercially available Activated Carbon

As targeted performances depend inevitably on the test cell assembly used (see paragraph V.1.2), CAB CA1 and activated CAB CA A1050 have been compared to a commercially available activated carbon having been used in EDLC electrode material blends (Maxsorb, s_{BET} of around $2200\text{m}^2/\text{g}$).

Maxsorb features a lower resistance (determined by impedance spectroscopy at 0,11 Hz) and a higher capacitance than CAB CA1, but not than A1050 (see table V-18 and figures V-52 and V-53 for resistance behavior in dependence of frequency and table V-19 and figure V-54 for capacitance values and behavior, respectively). The HFR of Maxsorb is close to that of CAB CA1 (see figure V-52). The loop in the Nyquist plot, corresponding to the effects contact quality between electrode and current collector is much more pronounced than for CAB CA1, as is the distributed resistance. The pronounced distributed resistance for Maxsorb is probably a sign of a high amount of narrow microporosity, whereas the inclined Nyquist plot of CA1 seems to result from a wide pore size distribution.

Table V-18: Resistance in dependence of frequency for CA1, A1050, and Maxsorb

Frequency	9524 Hz		58 Hz		0,11 Hz	
Samples	R Ω	R_{surface} Ω/cm^2	R Ω	R_{surface} Ω/cm^2	R Ω	R_{surface} Ω/cm^2
CA1	0,70	0,35	1,01	0,50	6,35	3,16
A1050	0,56	0,28	0,78	0,39	1,25	0,62
Maxsorb	0,73	0,37	1,18	0,59	1,94	0,96

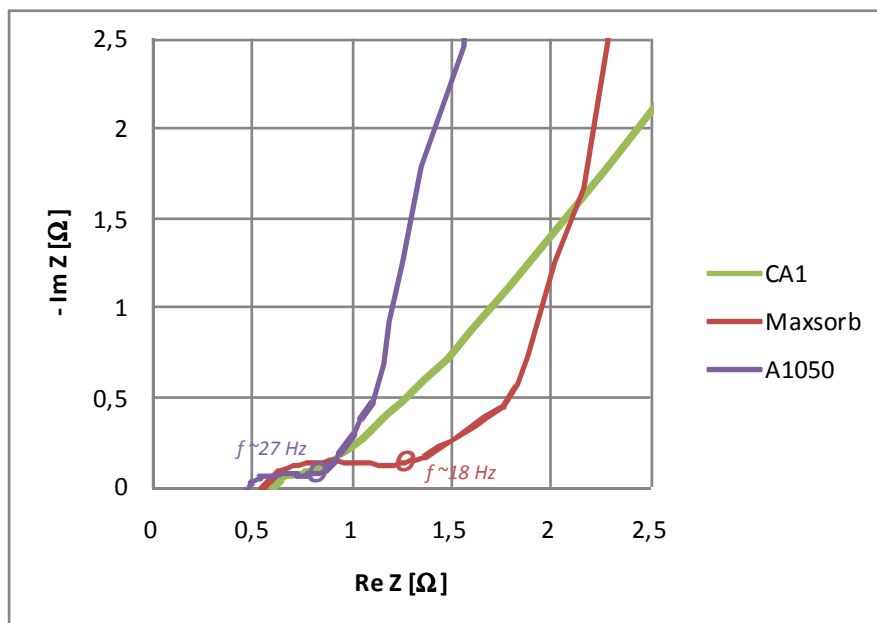


Figure V-52: High frequency region of Nyquist plot for CA1, Maxsorb, and A1050

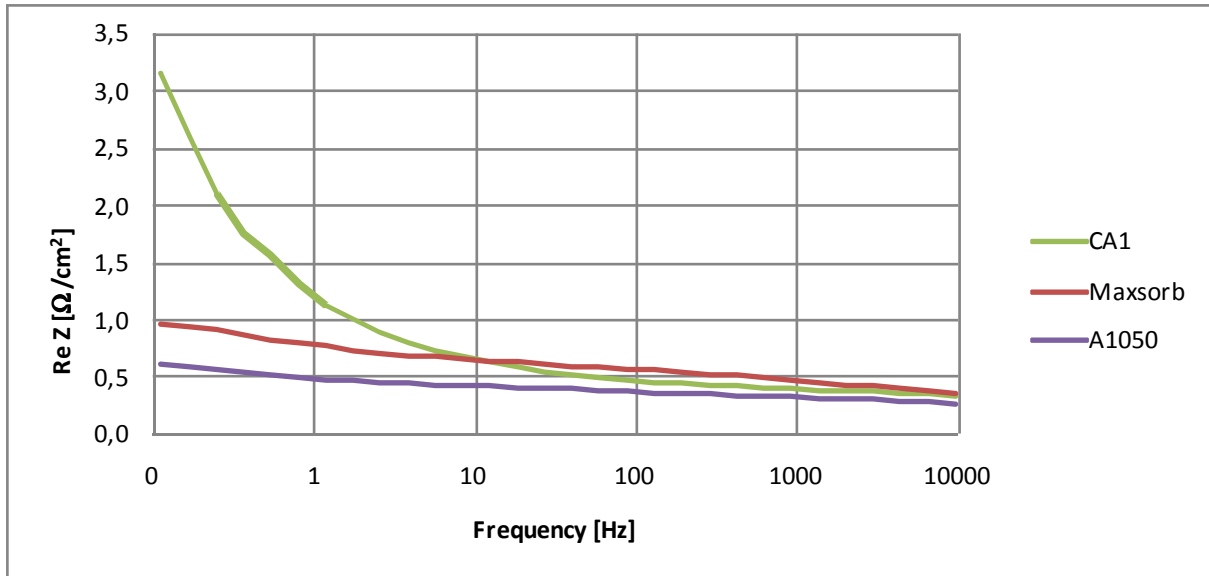


Figure V-53: Resistance as function of frequency for CA1, A1050, and Maxsorb

Table V-19: Characteristic values of CA1, A1050, and Maxsorb

Samples	C _{volume tric} F/cm ³	C _{specific} F/g _{carbon}	ESR Ω	ESR _{surface} Ω/cm ²	I _{leakage} mA	E _{specific} Wh/kg _{carbon}	P _{specific} W/kg _{carbon}	τ s
CA1	8,64	15,48	6,35	3,16	0,24	0,54	585	3,3
A1050	44,92	134,01	1,25	0,62	0,35	4,65	4949	3,4
Maxsorb	55,43	113,74	1,94	0,96	0,81	3,95	2192	6,5

Although Maxsorb's porosity has been said to consist of narrow micropores mainly⁶, its energy can be provided at higher frequencies than for CA1 (but not than for A1050).

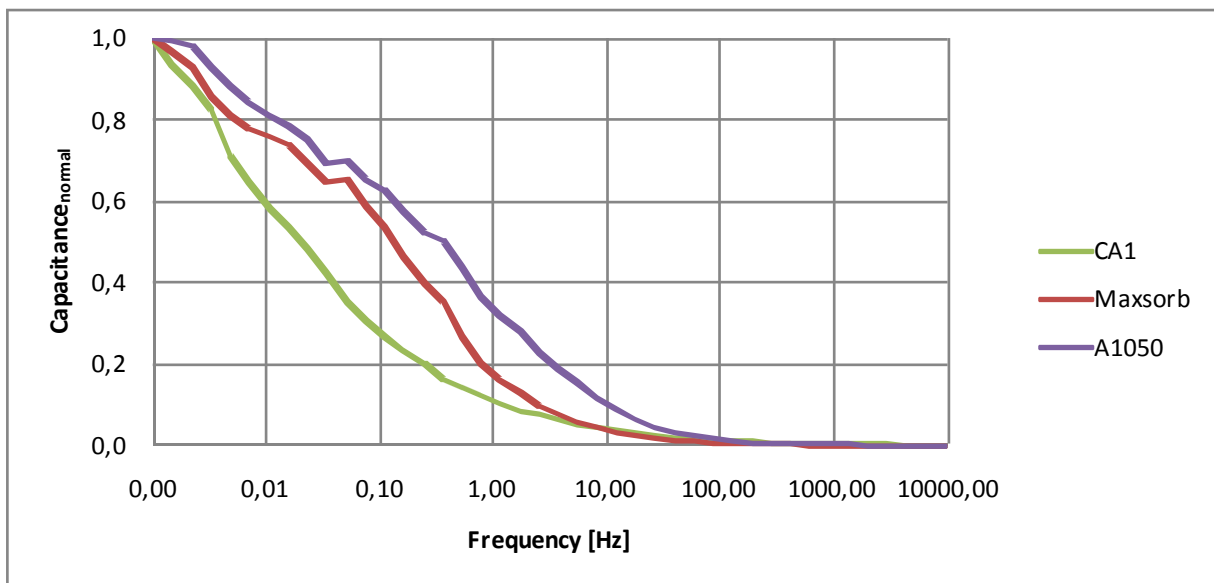


Figure V-54: Normalized capacitance as function of frequency for CA1, A1050, and Maxsorb

⁶ according to TIMCAL having provided Maxsorb used for this work

Capacitance, specific energy and specific power of the CAB CA1 are much lower than for Maxsorb. However, activated CAB CA sample A1050 features not only higher energy and power densities than Maxsorb, but also a lower leakage current and a lower time constant. Nonetheless, Maxsorb possesses the least pronounced self-discharge of all carbons tested in the course of this work (see figure V-55).

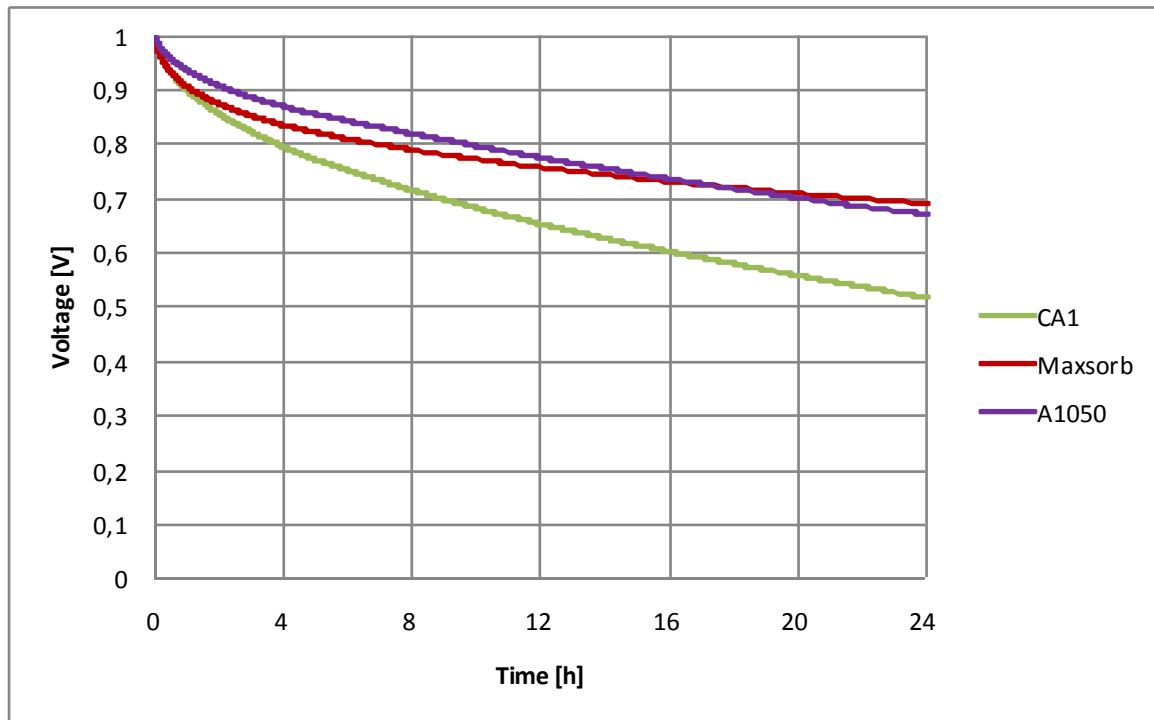


Figure V-55: Self discharge of carbons CA1, A1050, and Maxsorb

In conclusion, compared to Maxsorb, non-activated CAB CA do not seem suitable for the use as EDLC electrode material, primarily due to high micropore volume requirements for this application. However, the performance of activated CAB CA A1050 is better than that of Maxsorb. Therefore, CAB CA remain interesting, notably in terms of low resistance.

5. Conclusion

The performances of different CAB CA, cellulose-based carbon, and commercially available activated carbon if used as EDLC electrode material have been compared.

CAB CA have been found to be largely more interesting for this application than raw cellulose or cellulose acetate having been carbonized in the same conditions, due to its nanostructure. Synthesizing aerogels cellulose or cellulose-acetate based aerogels is thus of interest even if the structure of the organic aerogel is deformed during pyrolysis, as is the case for CAB aerogels. Pyrolyzed CA, but also CAB CA materials seem to have a good electrical conductivity. The synthesis of CAB aerogel/cellulose composites might even increase the conductivity, but the composites' porosity would need to be developed (for example by activation) in order to reach high capacitances. CAB gels do not necessarily have to be dried supercritically, evaporative drying seems to be a good alternative. CAB carbon aerogels and xerogels, however, only possess very low micropore volumes, which may be

significantly increased by activation (see chapter IV). CO₂-activated CAB CA display interesting performances if used as EDLC electrode material, in terms of power and energy capability, as well as in terms of self-discharge (in acidic aqueous electrolyte).

The modification of the surface chemistry of CAB CA alters inevitably their performance if used as EDLC electrode material. An introduction of oxygen surface functionalities may help to improve the capacitance (particularly if treated in H₂O₂) due to different effects the O-containing surface groups may have on the interaction of electrode and the electrolyte, for example by improving the surface wettability. The introduction of nitrogen-containing surface groups, on the other hand, has not been found to contribute necessarily to the symmetric capacitors overall capacitance. However, in order for a symmetric capacitor to show improved performances both the characteristics of positive and negative electrode would need to be increased at the same time [Jur 2003]. Ammonized CAB CA samples have very basic surfaces, whereas other CAB CA having undergone modification of their surface chemistry contain a balanced number of acidic and basic functional groups. As the treatment method does have a notable influence on the functional groups introduced (see chapter IV), it has simultaneously a significant influence on the electrochemical performance. The introduction of oxygen-containing surface functional groups increases the EDLC self-discharge (in acidic aqueous electrolyte) considerably, while an introduction of N-containing functional groups through ammonization does not show detrimental effects.

Cellulose-based alternatives for CAB CA exist. Carbonized aerocellulose samples have shown interesting resistance and capacitance values if used as EDLC electrode material, but their self discharge (in acidic aqueous electrolyte) has been found to be rather elevated and would need to be improved.

In respect of an application as EDLC electrode material, non-treated CAB CA do not possess satisfactory micropore volumes. After activation in CO₂, however, CAB CA may feature specific capacitances, energy and power capabilities even superior to those of carbons conventionally applied in EDLC assemblies, like Maxsorb (see table V-20). Also, ESR and therefore time constant may be better for the activated CAB CA.

Table V-20: Characteristic values of CA1, 10XL, A1050, and Maxsorb

Samples	C_{volumetric} F/cm³	C_{specific} F/g_{carbon}	ESR Ω	ESR_{surface} Ω/cm²	I_{leakage} mA	E_{specific} Wh/kg_{carbon}	P_{specific} W/kg_{carbon}	τ s
CA1	8,64	15,48	6,35	3,16	0,24	0,54	585	3,3
10XL	16,21	23,54	3,24	1,61	0,32	0,82	929	3,2
A1050	44,92	134,01	1,25	0,62	0,35	4,65	4946	3,4
Maxsorb	55,43	113,74	1,94	0,96	0,81	3,95	2192	6,5

As a CAB carbon xerogel has exhibited performances comparable to or even superior to those of CAB CA (sample 10XL), good results should also be achieved by using activated carbon xerogels as EDLC electrode material.

General Conclusion

Present work has aimed at preparing and studying a new type of nanostructured carbonaceous material based on renewable resources. After reviewing possible methods for synthesizing nanostructured carbon material from vegetal biomass, we have chosen to prepare cellulose-acetate-based carbon aerogels. This nanostructured carbon material is obtained by pyrolyzing cellulose-acetate-based organic aerogels, synthesized via sol-gel method (using only non-toxic substances) and subsequent drying typically by supercritical CO₂. Carbon aerogels obtained by pyrolysis of cellulose-acetate-based organic aerogels contain a relatively high amount of heteroatoms (oxygen and nitrogen) due to the nature of the precursor, which distinguishes them from other carbon aerogels. Therefore, cellulose-acetate-based carbon aerogels combine the very interesting structural features of a carbon aerogel with a composition and surface chemistry different from those of conventional carbon aerogels. Thus, cellulose-acetate-based carbon aerogels may be of interest for numerous electrochemical applications. Hence, I have carried out a comprehensive study on possibilities of tailoring the organic and particularly the carbonaceous aerogel structure and surface chemistry of this novel family of nanostructured carbon materials.

The characteristics of any carbon material (such as porous structure) depend obviously on its organic precursor, which is a cellulose-acetate-based organic aerogel in this work. Therefore we have aimed at synthesizing a broad range of structurally different cellulose-acetate-based organic aerogels by varying a selection of basic sol-gel parameters (like precursor and catalyst concentration and catalyst type) and applying different drying methods (drying in supercritical CO₂ or by evaporation in ambient conditions). The influence of the sol-gel parameters and of drying process on the structure of the resulting organic aerogel has been examined. Cellulose-acetate-based aerogels with BET specific surface areas of up to 350 m²/g and porous volumes of up to 5.3 cm³/g (determined using non-intrusive Hg porosimetry) could have been synthesized. Cellulose-acetate-based organic aerogels, however, have been found to be rather dense with specific surface areas of only about half of that of their homologue aerogels.

A carbon's characteristics depend on the organic precursor as well as on the carbonization process. As carbon aerogels are being prepared by pyrolyzing organic aerogels, the pyrolysis conditions are known to participate in determining the resulting carbon aerogels' characteristics. Therefore, in addition to pyrolyzing organic aerogels of different structures, pyrolysis maximum temperature and the type of inert atmosphere have been varied. Effects of pyrolysis at 900 °C, 1000 °C, and 1100 °C and in N₂ and Ar atmosphere have been investigated in this work. In general, by pyrolyzing cellulose-acetate-based organic aerogels, porous and nanostructured carbon materials are generated. A "bubbling" phenomenon occurs during pyrolysis, as the pyrolysis temperature is raised above the cellulose acetate's melting and subsequently above its degradation temperature. The organic aerogels' structure is significantly modified during the pyrolysis process, but has finally not been found to exert an important influence on the resulting carbon aerogels structure, mainly due to "bubbling". In other terms, all carbon aerogels are rather similar and do not conserve the memory of their organic structure having been tailored in the course of the sol-gel process. Nevertheless, it can be underlined that bulk densities generally tend to decrease during pyrolysis (to around 0.25 g/cm³), while porous volumes and accordingly specific surface areas tend to increase (up to about 8 cm³/g and 500 m²/g in certain cases, respectively). However, the fraction of porous volume and surface area created as a result of pyrolysis decreases with increasing pyrolysis maximum temperature. During pyrolysis the aerogels composition is modified as well. The carbon content increases with increasing pyrolysis temperature, the heteroatom content decreases (degradation of oxygen

functionalities), and dehydrogenation and aromatization of the carbon material take place. Nonetheless, the content of heteroatoms remains elevated even after pyrolysis, e.g. at almost 6 wt.% even for pyrolysis at 1100 °C. Furthermore, we have found that the type of inert atmosphere does not seem to have a remarkable influence neither on structure, nor on elemental composition.

As all cellulose-acetate-based aerogels have revealed rather similar structures with only moderate surface areas and similar compositions after pyrolysis, we have investigated different methods to modify the carbon aerogels' structure and composition. Specific surface area and porous volumes, particularly microporous volumes, have been increased considerably by activating cellulose-acetate-based carbon aerogels in CO₂. BET specific surface areas of over 2000 m²/g and BJH porous volumes of almost 1 cm³/g have been obtained for activation at 1050 °C in CO₂ for 2 h. On the contrary, carbon aerogels with a higher density have been prepared by introducing cellulose powder into the cellulose-acetate sol. These cellulose-acetate-based aerogel/cellulose powder composites resist also better to shrinkage during drying in supercritical drying and to deformation during pyrolysis, than cellulose-acetate-based aerogels not containing cellulose. The composition, surface chemistry, and acid/base properties of the cellulose-acetate-based carbon aerogels have been modified by oxidation and introduction of nitrogen-containing surface functional groups. Cellulose-acetate-based carbon aerogels have been oxidized in nitric acid and hydrogen peroxide. Nitrogen-containing functional groups have been introduced by co-heat-treatment of the carbon aerogel with melamine and by ammonization. The structure and surface chemistry of cellulose-acetate-based carbon aerogels, although similar after pyrolysis of different organic aerogels at different temperatures and in different inert atmospheres, may thus be modified significantly and adjusted by means of the different simple chemical/physical methods used in this study.

Finally, the performance of different cellulose-acetate-based aerogel samples if used as EDLC electrode material has been studied in a home-made test cell assembly. Notably, capacitance, resistance, and self discharge have been evaluated for carbon aerogels used as electrode material in a symmetric 2-electrode EDLC with aqueous acidic electrolyte. Cellulose-acetate-based carbon aerogels have revealed better performances than cellulose acetate or cellulose powder pyrolyzed in the same conditions. Thus, synthesizing cellulose-acetate-based aerogels, although their structure undergoes changes during pyrolysis, may be of interest. Compared to evaporation in ambient conditions, drying in supercritical CO₂ has not proven to be necessary or even of advantage in view of an application as EDLC electrode material. Although organic xerogels are much denser than aerogel homologues, their carbonaceous counterparts feature rather similar structures and comparable EDLC performances. However, only activated cellulose-acetate-based carbon aerogels have been found to reach performances comparable to that of Maxsorb, a carbon material having formerly been commercialized as EDLC electrode material.

In conclusion, cellulose-acetate-based carbon aerogels need to undergo a post-treatment in order to develop a high porous volume required for an application as EDLC electrode material. Although this means that cellulose-acetate-based carbon aerogels have to undergo an additional treatment after pyrolysis, the rather complicated and costly step of supercritical drying of the CAB gel can be omitted. As cellulose-acetate-based aerogels containing cellulose powder are quite dense but seem to feature a relatively low electrical resistivity, activation of this type of aerogel might prove to be of interest.

Studies on the electrochemical performance as PEMFC electrode material have shown that the structure of cellulose-acetate-based carbon aerogels is suitable for an application catalyst support in PEMFC [Roo 2009]. For Li/SOCl₂ batteries, on the other hand, cellulose-acetate-base aerogels do not maintain their shape during pyrolysis sufficiently to be used as electrode, even samples containing cellulose. The evaluation of the performance of cellulose-acetate-based carbon aerogels in other applications remains to be examined.

Additionally, cellulose-acetate-based aerogels may not only be used after carbonization, but also in their organic form, for example for an application as thermal insulator.

Résumé en langue française

Introduction

- **Contexte**

La notion de développement durable est aujourd'hui une priorité mondiale, tant économique que politique. Plusieurs axes d'actions sont proposés: la valorisation de la biomasse, l'amélioration de l'efficacité énergétique, la capture des polluants et bien d'autres encore. Cette thèse s'inscrit directement dans cette philosophie. Elle vise à coupler i) valorisation de la biomasse et ii) optimisation de l'efficacité énergétique et ce, en travaillant sur de nouveaux matériaux pour le stockage et la conversion d'énergie par voie électrochimique.

L'énergie électrique peut être stockée et convertie par voie électrochimique, comme par exemple dans i) les piles primaires lithium/chlorure de thionyle, ii) les piles à combustible à membrane échangeuse de protons (PEMFC) ou encore iii) les supercondensateurs. Dans ces trois systèmes, des carbones nanostructurés sont utilisés et jouent un rôle essentiel. Il peut alors apparaître important de les optimiser indépendamment pour chacune de ces applications afin d'augmenter de manière très significative l'efficacité des composants dans lesquels ils sont intégrés.

C'est dans ce contexte que s'inscrit le projet CARBOCELL, projet contractuel ANR auquel est adossée cette thèse. CARBOCELL regroupe des partenaires académiques et industriels dans le but d'élaborer de nouveaux carbones issus de la biomasse et de les adapter aux applications citées ci-dessus. Le consortium de recherche est formé du CEP et du CEMEF es (deux laboratoires de recherche conjoints ARMINES / Mines ParisTech), de TIMCAL (industriel spécialiste des carbones), de la SAFT (industriel notamment spécialisé dans l'application pile primaire Li/SOCl₂), de BatScap (industriel notamment spécialisé dans les applications supercondensateurs), de PAXITECH (industriel spécialisé dans les piles à combustible de type PEMFC) et du LEPMI (laboratoire de l'INPG spécialiste d'électrocatalyse).

Une importante part des carbones actuels est obtenue à partir de cellulose ou d'autres types de matériaux issus de la biomasse. Cependant, leurs caractéristiques sont généralement tributaires du précurseur organique utilisé (i.e. le matériau qui va subir la pyrolyse), et ce notamment en termes de texture. Cette influence est parfaitement illustrée par les deux exemples de carbones obtenus par pyrolyse de cosse de palmier à huile (figure RLF-1) et de cellulose (figure RLF-2). On voit clairement dans ces deux cas représentatifs que la texture initiale est peu modifiée par l'étape de pyrolyse. Ces exemples soulignent ainsi clairement la difficulté d'adapter finement la texture d'un carbone issu de biomasse à une application spécifique. Aussi, synthétiser directement le précurseur organique en vue de l'application visée pourrait théoriquement permettre de mieux contrôler la texture du carbone résultant.

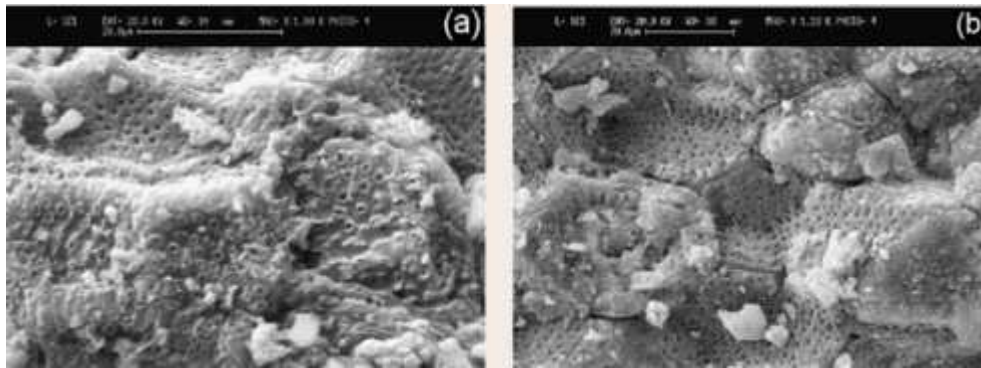


Figure RLF-1: Cosses de palmier à huile (a) avant et (b) après pyrolyse (à 900 °C sous vide pendant 1h) [Jia 2008]

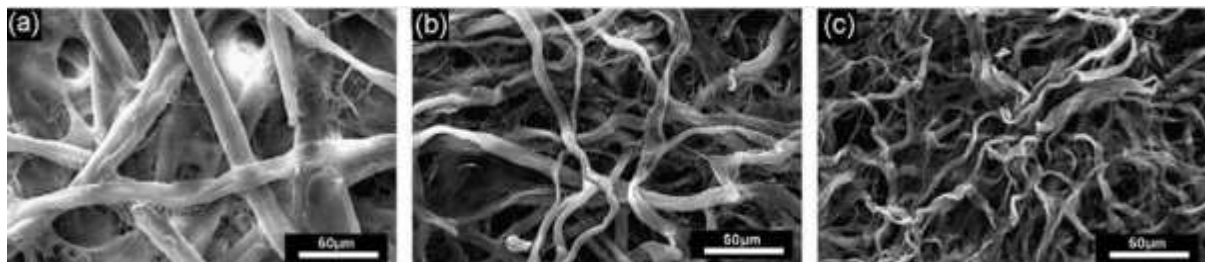


Figure RLF-2: Cellulose (a) naturelle et (b) pyrolysée à 600 °C et (c) 1200 °C [Hae 2009]

- **Objectifs**

Les objectifs de ma thèse concernent (i) l'élaboration de nouveaux carbones nanostructurés à partir d'un précurseur organique de synthèse issu de la biomasse végétale et (ii) la génération d'une large gamme texturale de carbones de chimies de surface différentes en vue de pouvoir les adapter à différentes applications. Il est envisagé que cette large palette de carbones soit le fruit d'une étude étendue de l'influence des paramètres d'élaboration.

- **Rappels bibliographiques**

Les carbones nanostructurés que nous avons choisi d'élaborer sont des aérogels de carbone. Les aérogels, en général, sont préparés selon un procédé de chimie douce, dit procédé sol-gel. Ce procédé permet d'adapter la texture de l'aérogel de carbone par simple variation des paramètres de synthèse du gel. De nombreuses études bibliographiques sur le système chimique de référence à base de résorcinol et de formaldéhyde (aérogels RF), témoignent de cette dépendance marquée.

Afin de créer des aérogels de carbone, trois étapes se succèdent (figure RLF-3):

1. Le gel est synthétisé. On prépare d'abord le sol initial, qui gélifie à l'issue de la transition sol-gel.
2. Le gel est séché en tentant de conserver au mieux sa structure initiale en vue d'obtenir un aérogel (matériau appelé aérogel organique dans ce document).

3. L'aérogel organique subit une pyrolyse afin d'être carbonisé. Le produit final de cette chaîne d'élaboration a été appelé aérogel carbonisé dans ce document.

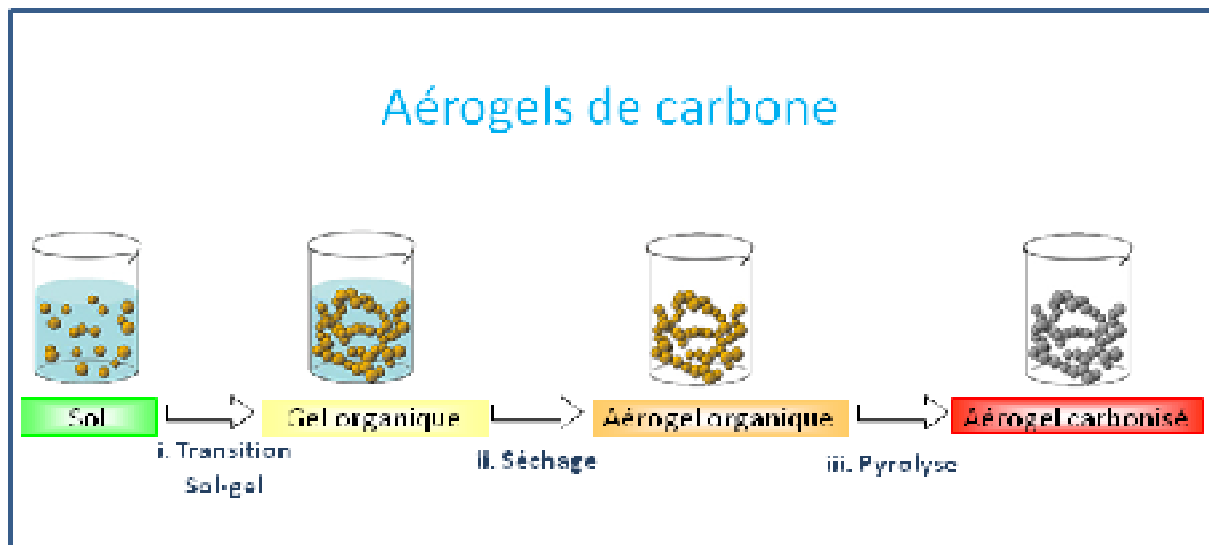


Figure RLF-3: Chaîne d'élaboration d'aérogels de carbonisés

Ce résumé de mon manuscrit de thèse commence par la présentation de mes travaux sur l'élaboration des aérogels organiques qui serviront de précurseurs aux carbones étudiés (i.e. les aérogels de carbone). Ensuite, je présente mes travaux sur la pyrolyse des aérogels organiques, puis sur différentes possibilités de modifier les carbones obtenus. Finalement, je résume les principaux résultats d'évaluation d'une partie de ces carbones comme matériau d'électrode de supercondensateur.

Elaboration des aérogels organiques (Chapitre 2)

- **Système chimique sélectionné**

Le système chimique choisi comme précurseur pour les aérogels carbonisés de cette étude est issu des travaux de F. Fischer [Fis 2006]. Il est à base d'acétate de cellulose.

Dispersé dans l'acétone, l'acétate de cellulose est réticulé par un isocyanate le 4,4'-diisocyanate de diphenylméthylène (MDI). Un catalyseur est employé afin de déclencher les réactions de condensation entre l'acétate de cellulose et le MDI. Plus précisément, le gel cellulosique résultant est réticulé par des liaisons uréthanes qui se forment entre les groupements alcool (R-OH) de l'acétate de cellulose et les groupements d'isocyanate (NCO) du MDI (voir figure RLF-4).

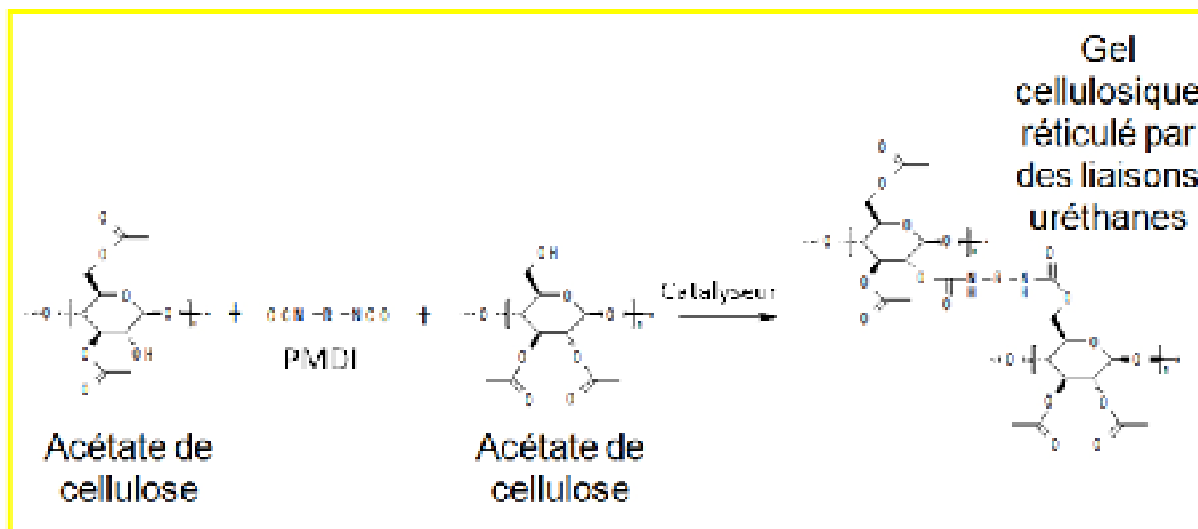


Figure R1F-4: Schéma de réticulation uréthane de l'acétate de cellulose par un isocyanate bifonctionnel

Par rapport aux travaux originels de Florent Fischer, j'ai étendu la gamme de gels synthétisés notamment i) en explorant une plage de concentrations de précurseurs en solution plus importante et ii) en utilisant d'autres catalyseurs. De plus, comme Florent Fischer avait mis en évidence que le dibutyltin dilaurate (noté DD dans ce document) laissait des traces d'étain (Sn) dans les aérogels, traces qui peuvent s'avérer néfastes pour différentes applications électrochimiques, j'ai étudié l'utilisation d'une amine tertiaire le DABCO® TMR (noté DA dans ce document) et de la pyridine (notée P dans ce document) comme catalyseurs alternatifs au DD.

- **Paramètres de l'étude de l'étude paramétrique sol-gel**

Comme la texture des aérogels organiques peut présenter une influence plus ou moins nette sur la texture des aérogels carbonisés, il était important d'élaborer une large gamme d'aérogels organiques. Pour ce faire, j'ai réalisé une étude de sensibilité à la variation des paramètres sol-gel suivants.

- Concentration de précurseur (notée **%CA**), exprimée sous la forme du ratio massique entre l'acétate de cellulose dissous dans l'acétone et l'acétone et variant entre 3 et 15,
- Taux de réticulation (noté **I/CA**), exprimé sous la forme du ratio massique entre l'isocyanate et l'acétate de cellulose et variant entre 0,1 et 1,
- Concentration de catalyseur **I/Cat**, exprimée sous la forme du ratio massique entre l'isocyanate et le catalyseur

et

- Nature du catalyseur en utilisant un sel métallique (dibutyltin dilaurate de formule brute $C_{32}H_{64}O_4Sn$), une amine tertiaire (DABCO TMR de formule brute $C_6H_{12}N_2$) et un composé organique hétérocyclique (pyridine de formule brute C_5H_5N). Le dibutyltin dilaurate agit comme acide de Lewis alors que le DABCO® TMR et la pyridine agissent comme des bases de Lewis. De fait, le dibutyltin dilaurate conduit à un mécanisme réactionnel différent des deux autres catalyseurs étudiés.

- **Influence du mode de séchage**

J'ai ensuite examiné l'influence du mode de séchage sur un gel cellulosique représentatif, en comparant les effets d'un séchage par évaporation, d'un séchage par lyophilisation et d'un séchage au CO₂ supercritique. Comme l'illustre la figure RLF-5, le séchage par lyophilisation ne permet pas de conserver le caractère monolithique du gel, et il a donc été abandonné dans le cadre de ce travail. On peut également s'apercevoir que les gels séchés par évaporation du solvant peuvent garder leur forme monolithique mais subissent une déformation très significative et une densification importante (le gel dans la figure RLF-5 a, par exemple, conservé son diamètre mais son épaisseur a beaucoup diminué). Au vu de ce résultat, une courte étude de sensibilité aux paramètres de séchage évaporatif a été menée afin d'essayer de minimiser ces modifications morphologiques. Enfin, cette figure permet de souligner que le séchage par CO₂ supercritique permet lui de préserver la forme initiale du gel. Pour ces raisons, ce procédé de séchage au CO₂ supercritique a été choisi comme mode de séchage de référence pour cette étude.

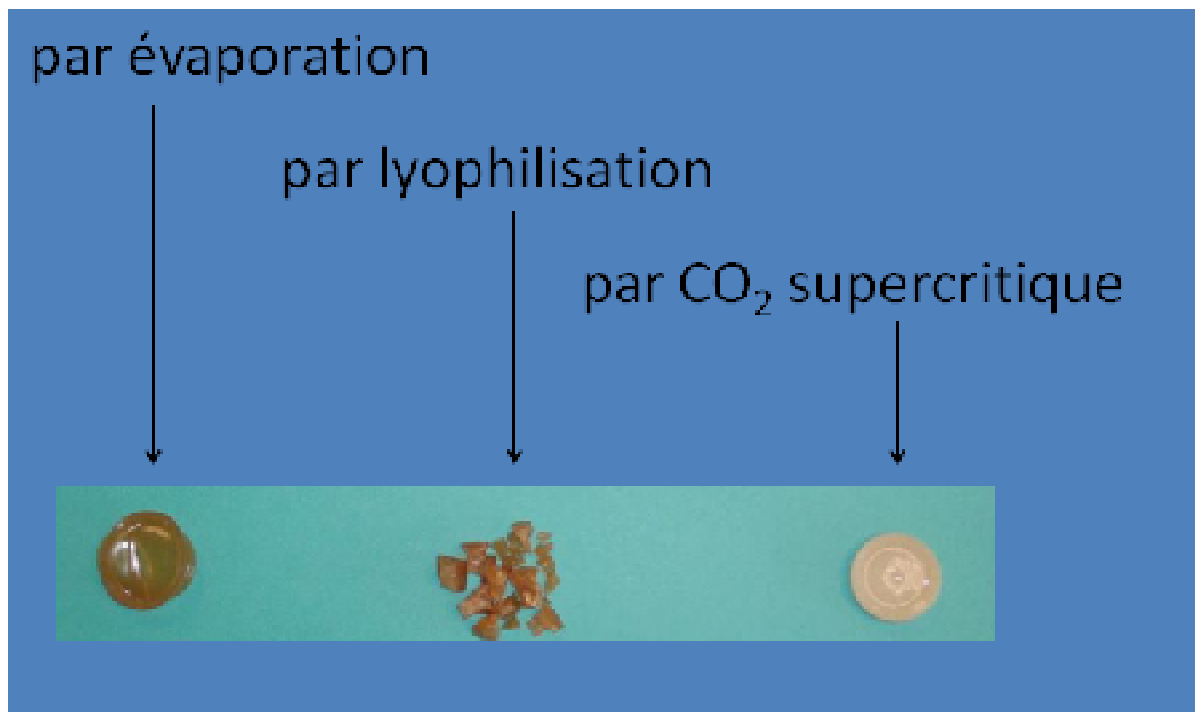


Figure RLF-5: Influence du mode de séchage sur la morphologie d'un gel à base d'acétate de cellulose

Le séchage au CO₂ supercritique pratiqué dans le cadre de ce travail s'effectue en remplaçant le solvant acétone par du CO₂ à l'état supercritique (on rappelle que le CO₂ est utilisé car il agit d'un fluide qui possède une température critique proche de la température ambiante $T_c \approx 31$ °C pour une pression p_c proche de 7,4 MPa). Une fois la totalité de l'acétone substituée par le CO₂ supercritique, une dépressurisation isotherme est réalisée. Ce procédé permet d'extraire le liquide contenu dans la porosité du gel dans des conditions relativement douces qui permettent d'éviter la formation de contraintes capillaires. Le séchage au CO₂ supercritique permet donc théoriquement de conserver aussi bien le caractère monolithique que la texture initiale du réseau solide du gel. Néanmoins, les gels à base d'acétate de cellulose subissent une forte densification pendant le séchage supercritique essentiellement due à une mauvaise affinité chimique entre les gels d'acétate de cellulose et le CO₂ (figure RLF-6).

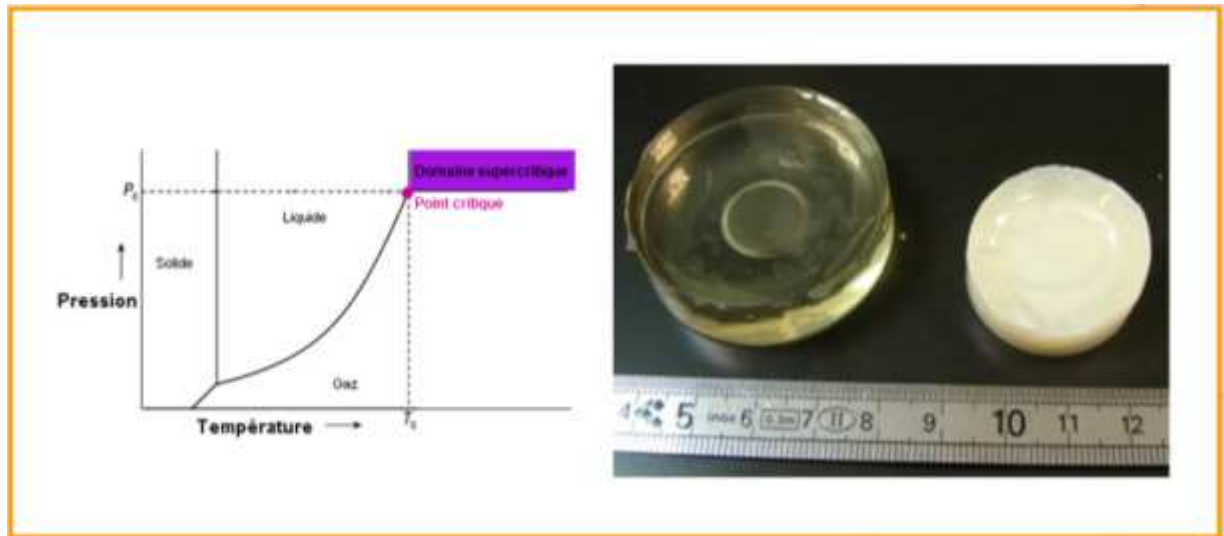


Figure RLF-6: Séchage au CO_2 supercritique des gels à base d'acétate de cellulose. A gauche, visualisation du point critique dans le diagramme p-T; à droite, illustration du retrait du gel dans l'autoclave par comparaison des produits avant et après séchage au CO_2 supercritique

Dans le cadre du séchage par évaporation, une courte étude de sensibilité à la vitesse de séchage a été réalisée (figure RFL-7). On voit sur la figure RFL-8 le gel initial, l'aérogel correspondant et les trois xérogels séchés à des vitesses différentes. Le xérogel XS (en bleu) ici a été séché en quelques heures, le xérogel XM (en rose) en quelques semaines et le xérogel XL (en vert), en quelques mois. Le xérogel obtenu par séchage évaporatif rapide (XS) est clairement le plus déformé et le plus densifié. Néanmoins, les xérogels séchés lentement (XM et XL), même s'ils subissent une déformation apparente moins importante, sont densifiés de manière toute aussi importante. La morphologie (et par voie de conséquence texture) du gel est donc très significativement modifiée. Les xérogels obtenus sont très peu poreux et possèdent une densité apparente très proche de la densité squelettique telle que déterminée par pycnométrie à l'hélium.

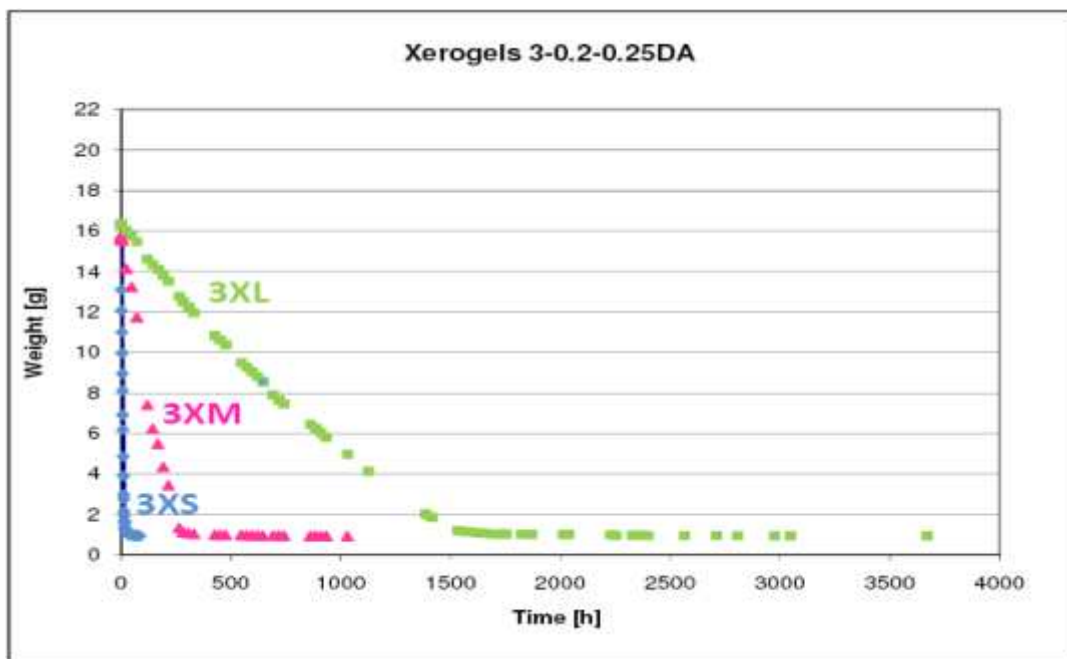


Figure RLF-7: Séchage par évaporation à différentes vitesses



Figure RLF-8: Influence de la vitesse de séchage par évaporation

- **Influence des paramètres sol-gel sélectionnés**

Les paramètres d'élaboration sol-gel ont une influence sur les aérogels résultants, comme l'illustre la figure RLF-9. Cette figure montre une matrice d'aérogels catalysés au DD, obtenue en faisant varier la concentration en acétate de cellulose et le taux de réticulation. La formulation a clairement un impact sur la morphologie (forme et retrait) et l'aspect (coloration, rugosité, ...) de l'aérogel.

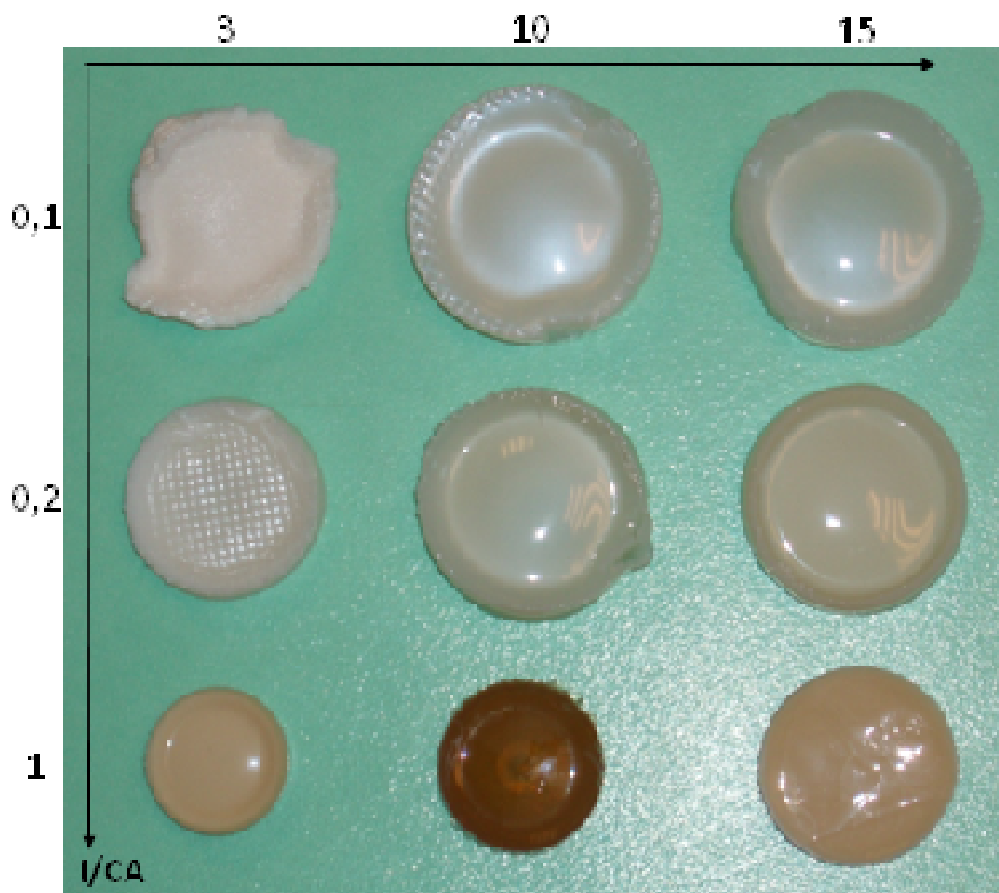


Figure RLF-9: Aérogels à base d'acétate de cellulose obtenus en catalyse DD avec différents %CA et I/CA

Afin d'analyser plus en détail la texture des aérogels obtenus, nous avons employé plusieurs méthodes d'analyse. Nous avons tout d'abord déterminé la densité squelettique par pycnométrie à l'hélium et la densité apparente par pycnométrie au mercure. Ensuite, nous avons employé de la porosimétrie mercure et de l'adsorption d'azote pour évaluer les caractéristiques poreuses (essentiellement volumes poreux spécifiques et taille moyenne des pores mais également distributions de tailles de pores) des aérogels et des xérogels. On rappelle ici que la porosimétrie mercure caractérise plutôt les caractéristiques macro- et mésoporeuses et l'adsorption d'azote caractérise plutôt les caractéristiques méso- et microporeuses, basées sur différentes hypothèses. La surface spécifique a aussi été déterminée par traitement BET des isothermes d'adsorption d'azote. Le tableau RLF-1 illustre un exemple dépendance de la texture des aérogels aux paramètres sol-gel au travers de la gamme de caractéristiques obtenues.

La texture des matériaux organiques à base d'acétate de cellulose élaborés via procédé sol-gel dépend donc de manière importante non seulement du mode de séchage, mais également des paramètres sol-gel (c'est-à-dire, dans le cadre de cette étude, de la concentration en précurseur, du taux de réticulation, du type et de la concentration du catalyseur). Cette étude de sensibilité aux paramètres sol-gel m'a permis d'élaborer des matériaux à base d'acétate de cellulose avec une très grande gamme de textures. La densité squelettique des aéro- et xérogels est d'environ $1,3 \text{ g/cm}^3$. Leur densité apparente varie entre $0,16$ et $1,3 \text{ g/cm}^3$ (une densité apparente très proche la densité squelettique est obtenue pour tous les xérogels). La surface spécifique BET des matériaux organiques à base d'acétate de cellulose varie entre 40 et $350 \text{ m}^2/\text{g}$. Le volume mésoporeux BJH peut être considérable (jusqu'à $1,5 \text{ cm}^3/\text{g}$). Le volume microporeux, cependant, est pratiquement inexistant pour tous les échantillons organiques.

Tableau RLF-1: Gamme de texture des matériaux organiques à base d'acétate de cellulose (aérogels et xérogels)

	Matériaux organiques
ρ_s [g/cm^3]	1,3
ρ_b [g/cm^3]	0,16 – 1,3
V_{BJH} [cm^3/g]	0,03 – 1,85
L_{BJH} [nm]	mésopores (3-60 nm)
S_{BET} [m^2/g]	40 - 350
$V_{\text{t-plot}}$ [cm^3/g]	Quasi nul

Elaboration des aérogels carbonisés (Chapitre 3)

- **Déformations morphologiques**

Les aérogels organiques à base d'acétate de cellulose ont été utilisés en tant que précurseurs pour l'élaboration d'aérogels carbonisés. Pour élaborer une large gamme d'aérogels carbonisés, j'ai carbonisé les aérogels organiques ayant des textures différentes à différentes températures comprises entre 900 et $1100 \text{ }^\circ\text{C}$ sous azote ainsi que sous argon. La pyrolyse des aérogels organiques

a été effectuée à une vitesse de 4 °C/min avec un palier d'une heure à la température maximale du profil.

Tous les aérogels (et xérogels) à base d'acétate de cellulose subissent des déformations importantes pendant la pyrolyse. Ceci est dû au fait qu'il y a un phénomène de fusion avant la dégradation thermique de l'aérogel organique. La dégradation thermique résulte dans une gazéification partielle de l'aérogel et le gaz s'évacue sous forme de bulles déformant ainsi l'aérogel fondu (voir figure RLF-10).



Figure RLF-10: Aérogel à base d'acétate de cellulose et aérogel carbonisé correspondant

Les bulles de gaz induisent de grands macropores dans les aérogels. Les aérogels carbonisés sont donc tous des matériaux macroporeux mais ayant néanmoins des parois nanostructurés. Dans la figure RLF-11 on voit nettement la structure typique d'aérogels carbonisés en «collier de perles». Le MEB permet donc de mettre clairement en évidence les deux principaux réseaux poreux constituant les aérogels carbonisés.

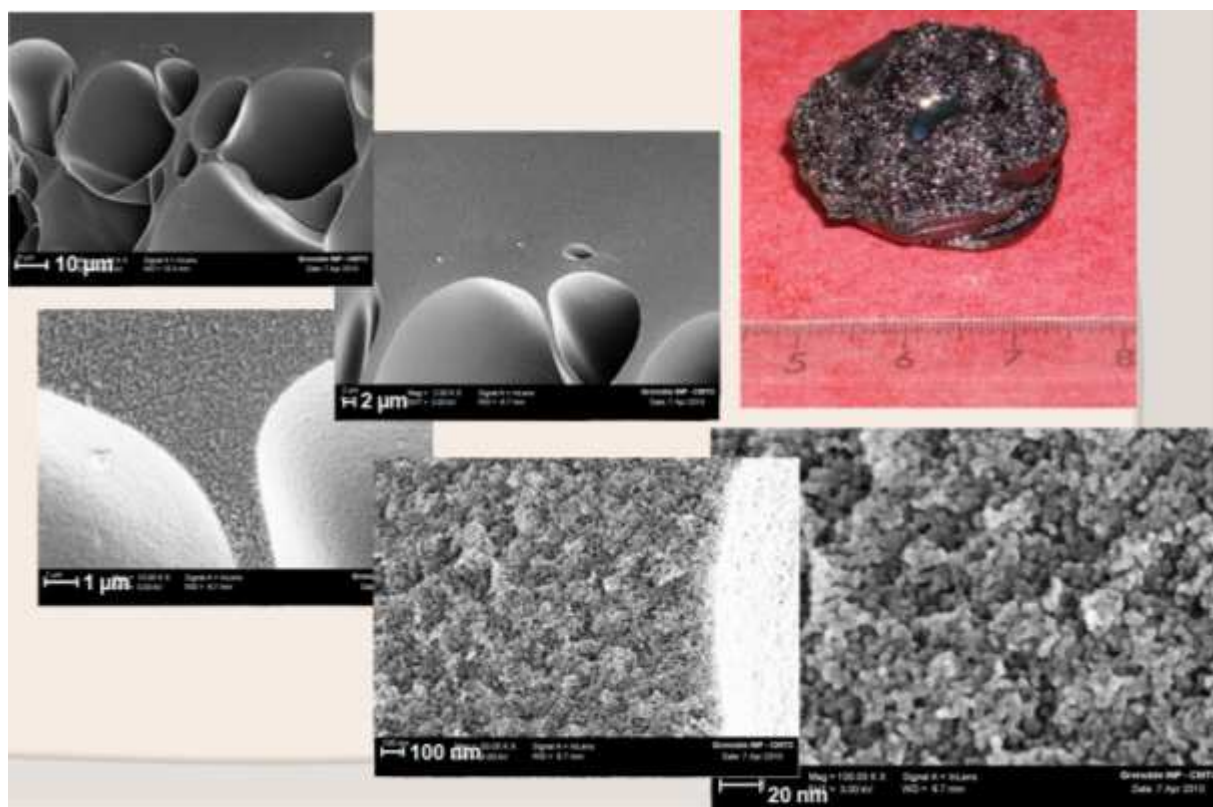


Figure RLF-11: Clichés MEB d'un aérogel carbonisé à base d'acétate de cellulose

- **Caractérisations structurales et chimiques**

La texture des aérogels carbonisés dépend partiellement de l'aérogel organique précurseur et de la température de pyrolyse. Par contre, l'atmosphère inerte ne semble pas avoir d'influence sur la texture finale de l'aérogel carbonisé. La surface spécifique, par exemple, a tendance à diminuer quand la température de pyrolyse augmente, à cause de la diminution du volume microporeux. Cependant, en général, comme l'illustre l'exemple représentatif d'un aérogel présenté dans le tableau RLF-2, on trouve que les surfaces spécifiques augmentent pendant la pyrolyse (i.e. comparaison entre l'aérogel organique et l'aérogel carbonisé). Ce résultat est dû à la création d'un réseau microporeux durant la pyrolyse. On peut aussi observer que la densité apparente diminue généralement pendant la pyrolyse ce qui entraîne une augmentation de la porosité. Bien que la texture des aérogels et xérogels organiques et la température de pyrolyse aient une certaine influence, les gammes de méso- et microporosité ainsi que la variation de la taille moyenne des pores s'avèrent restreintes. De même, les surfaces spécifiques demeurent relativement faibles pour un matériau du type aérogel de carbone. Les volumes mésoporeux BJH sont d'environ 0,25 à 0,45 cm^3/g et les volumes microporeux $V_{t\text{-plot}}$ généralement inférieurs à 0,15 cm^3/g . La taille moyenne des pores se situe autour de 4 nm et les surfaces spécifiques BET restent généralement inférieures à 500 m^2/g .

Tableau RLF-2: Texture des matériaux organiques et carbonisés à base d'acétate de cellulose (aérogels et xérogels)

	Matériaux organiques	Matériaux carbonisés
ρ_s [g/cm ³]	1,3	2,1
ρ_b [g/cm ³]	0,16 – 1,3	0,09 – 1,26
V_{Hg} [cm ³ /g]	0,08-6,04	0,17 – 10,9
V_{BJH} [cm ³ /g]	0,03 – 1,85	~ 0,25 – 0,45
L_{BJH} [nm]	mesopores (3-60 nm)	~ 4
S_{BET} [m ² /g]	40 - 350	160 - 500
$V_{t\text{-plot}}$ [cm ³ /g]	Quasi nul	< 0,15

Un autre effet de la pyrolyse concerne la modification de composition élémentaire (tableau RLF-3). La gazéification résulte dans une perte de masse d'environ 75 %, surtout des groupements oxygénés et hydrogénés. Les aérogels carbonisés contiennent tous environ 90 % massiques de carbone, légèrement plus si la température maximale de pyrolyse est plus élevée. Ceci veut dire que les aérogels carbonisés contiennent encore de l'oxygène ainsi que de l'azote, ce qui en pourrait en faire un matériau carboné relativement original vis-à-vis de l'application visée.

Tableau RLF-3: Composition élémentaire des aérogels organiques à base d'acétate de cellulose et de leurs homologues carbonisés

	Aérogels organiques	Aérogels carbonisés
C [%-massique]	~ 53	~ 90
O [%-massique]	~ 40	~ 5
N [%-massique]	~ 2	~ 3
H [%-massique]	~ 5,5	~ 1

Puisque la morphologie initiale de l'aérogel organique est hautement déformée pendant la pyrolyse, l'influence des différents paramètres examinés (structure initiale de l'aérogel organique, température maximale de pyrolyse, atmosphère inerte de pyrolyse) est relativement peu prononcée et souvent peu évidente

Pour résumer, les aérogels carbonisés à base d'acétate de cellulose possèdent une gamme de textures restreinte et des compositions élémentaires plutôt similaires. Cependant, comme pour tout autre carbone, les aérogels carbonisés peuvent évidemment être modifiés par différents traitements.

Modification de la texture et de la chimie de surface des aérogels carbonisés (Chapitre 4)

Afin d'élargir la gamme de carbones nanostructurés élaborés, nous avons examiné différents moyens pour modifier la structure et la chimie de surface des aérogels carbonisés. Dans le but de modifier les textures, j'ai fait quelques premiers essais d'activation et j'ai élaboré des composites aérogel à base d'acétate de cellulose et de poudre de cellulose. Dans le but de modifier la chimie de surface, nous avons étudié différentes méthodes d'oxydation et d'intégration d'azote dans le réseau.

- **Activation**

L'objectif de l'activation était évidemment d'augmenter la surface spécifique ainsi que le volume poreux. Pour ce faire, nous avons effectué des activations sous CO_2 à 850 °C, 950 °C et 1050 °C pendant 2 heures.

Comme attendu, le degré d'activation (ou *burn-off*) augmente avec la température d'activation. La surface spécifique et les volumes poreux augmentent avec le *burn-off* (figures RLF-12 et RLF 13 respectivement). L'objectif est donc atteint: la surface spécifique et les volumes meso- et microporeux par activation au CO_2 ont significativement augmenté.

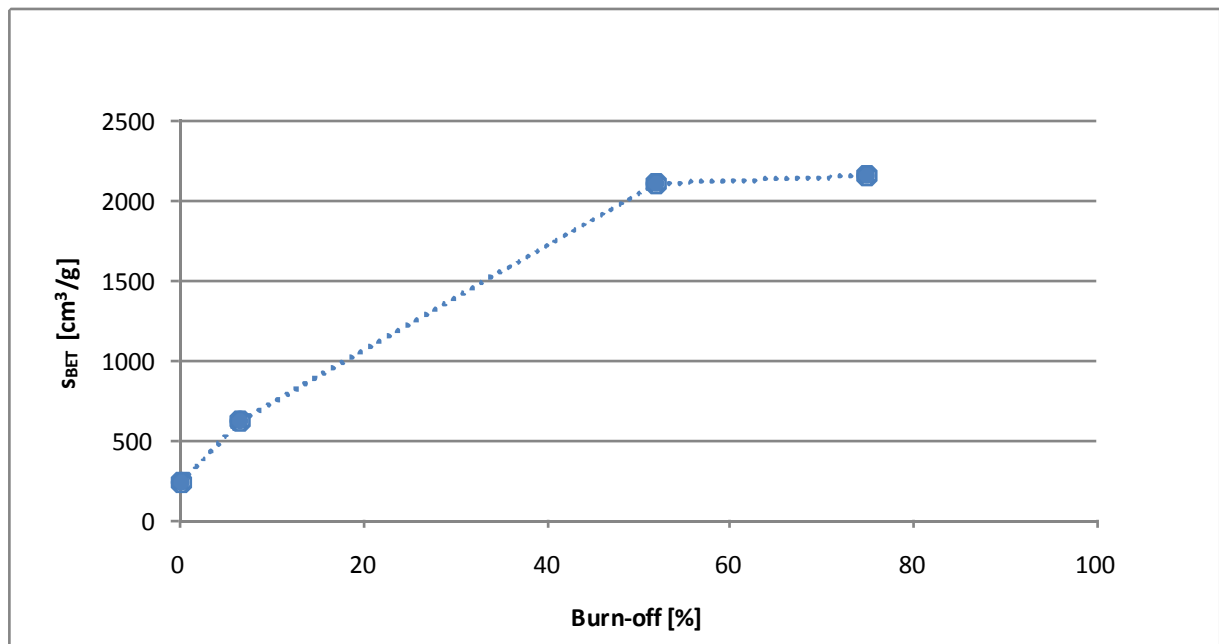


Figure RLF-12: Evolution de la surface spécifique BET d'un aérogel carbonisé avec le burn-off

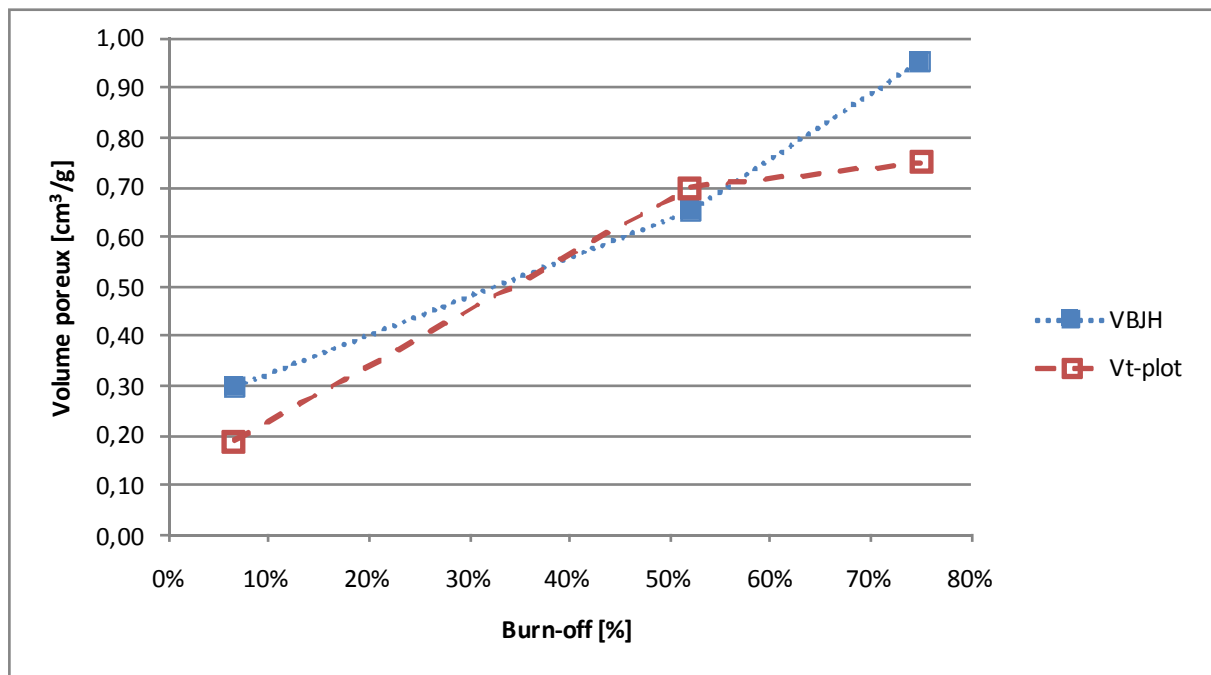


Figure RLF-13: Evolution du volume mésoporeux (V_{BJH}) et microporeux (V_{t-plot}) d'un aérogel carbonisé avec le burn-off

- **Elaboration de composites à base de cellulose**

Une méthode alternative pouvant permettre d'influer sur la texture des aérogels est l'élaboration de précurseurs composites. Cela pourrait notamment permettre de limiter la déformation macroscopique de l'aérogel pendant toute la chaîne d'élaboration, c'est-à-dire le retrait lors du séchage supercritique et le bullage lors de la pyrolyse. Pour cela, de la poudre de cellulose a été introduite dans le sol. L'addition de cellulose a été préférée à l'addition d'acétate de cellulose pour deux raisons: i) la cellulose semble avoir une meilleure affinité chimique avec le CO_2 que l'acétate de cellulose et ii) la cellulose ne subit pas de phénomène de fusion et ne fond donc pas pendant la pyrolyse, contrairement à l'acétate de cellulose.

J'ai réalisé une étude de sensibilité sur les concentrations en cellulose dans le composite (5, 10 et 15 % de la masse d'acétate de cellulose). Comme on peut voir dans la figure RLF-14, le retrait dû au séchage dans le CO_2 supercritique diminue significativement si de la poudre de cellulose est introduite dans le sol initial. Le retrait diminue lorsque les concentrations en poudre de cellulose rajoutée dans le sol à base d'acétate de cellulose augmentent (voir figure RLF-15). Lors de la pyrolyse la forme du gel est mieux conservée, en général, et on n'observe pas de bullage. Néanmoins, les composites se densifient considérablement pendant la pyrolyse et se fissurent (voir figure RLF-16).

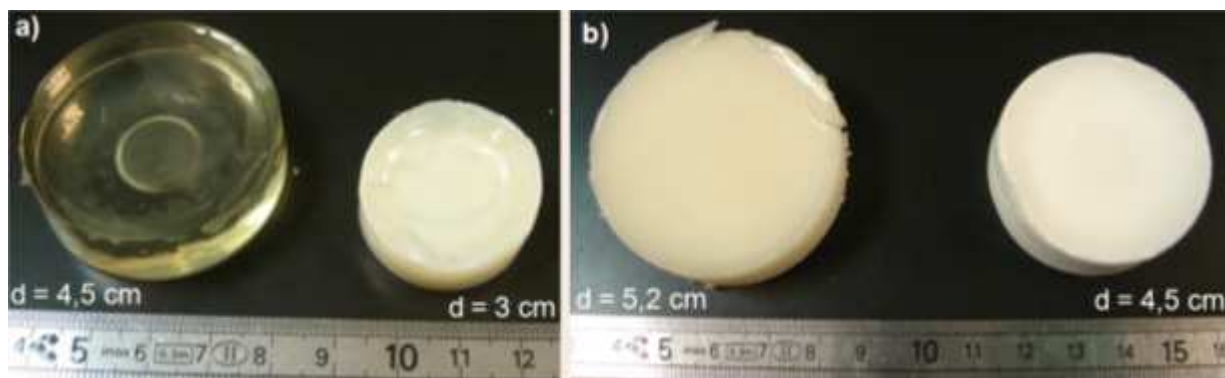


Figure RLF 14: Gels à base d'acétate de cellulose et aérogels correspondants: a) sans poudre de cellulose ajoutée, b) avec 15% massique de poudre de cellulose (par rapport à l'acétate de cellulose)

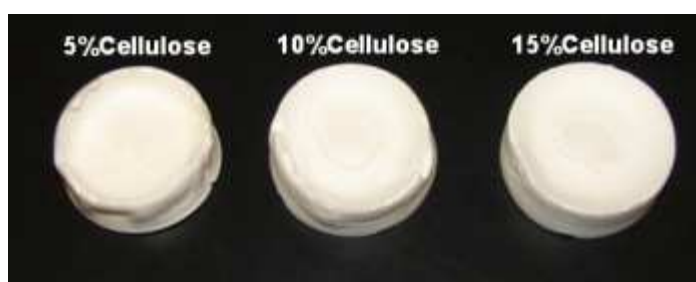


Figure RLF 15: Aérogels composites à base d'acétate de cellulose et poudre de cellulose avec différents contenus en poudre de cellulose (croissants de gauche à droite)

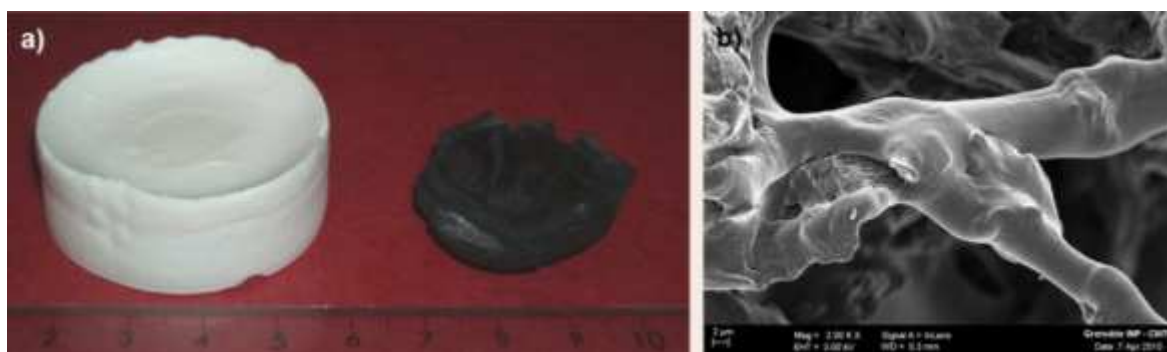


Figure RLF 16: a) Aérogel organique et carbonisé contenant 15% massique de poudre de cellulose et b) cliché MEB du composite carbonisé

- **Modification de la chimie de surface**

Pour modifier la chimie de surface des aérogels carbonisés à base d'acétate de cellulose, nous avons choisi d'étudier différents traitements d'oxydation et d'introduction d'azote visant à modifier la chimie de surface sans pour autant apporter de modifications significatives à la texture. En vue d'introduire des groupements fonctionnels oxygénés différents, nous avons oxydé des poudres d'aérogel carbonisé (appelé CA1 ici) par mise en suspension dans une solution de peroxyde d'hydrogène ainsi que dans une solution d'acide nitrique (figure RLF-17).

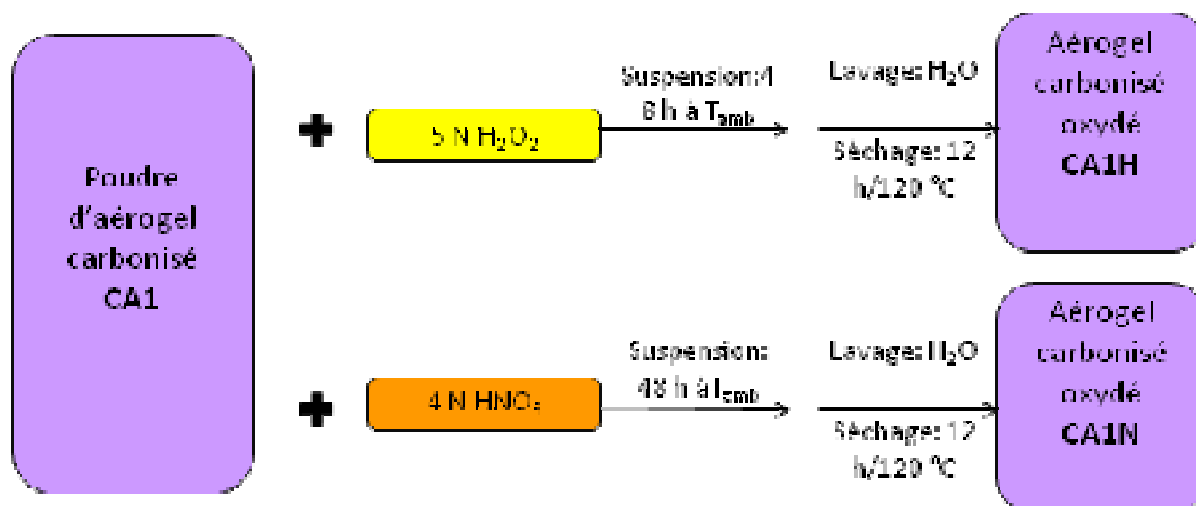


Figure RLF 17: Schéma de principe des 2 voies d'oxydation des aérogels carbonisés à base d'acétate de cellulose

Afin d'introduire différents groupements fonctionnels azotés, de la poudre d'aérogel carbonisé (CA1) a subi un co-traitement thermique avec de la mélamine (CA1) ou a été ammonisé (CA2) (figure RLF-18). De plus, nous avons également oxydé un échantillon à l'acide nitrique que nous avons ammonisé par la suite.

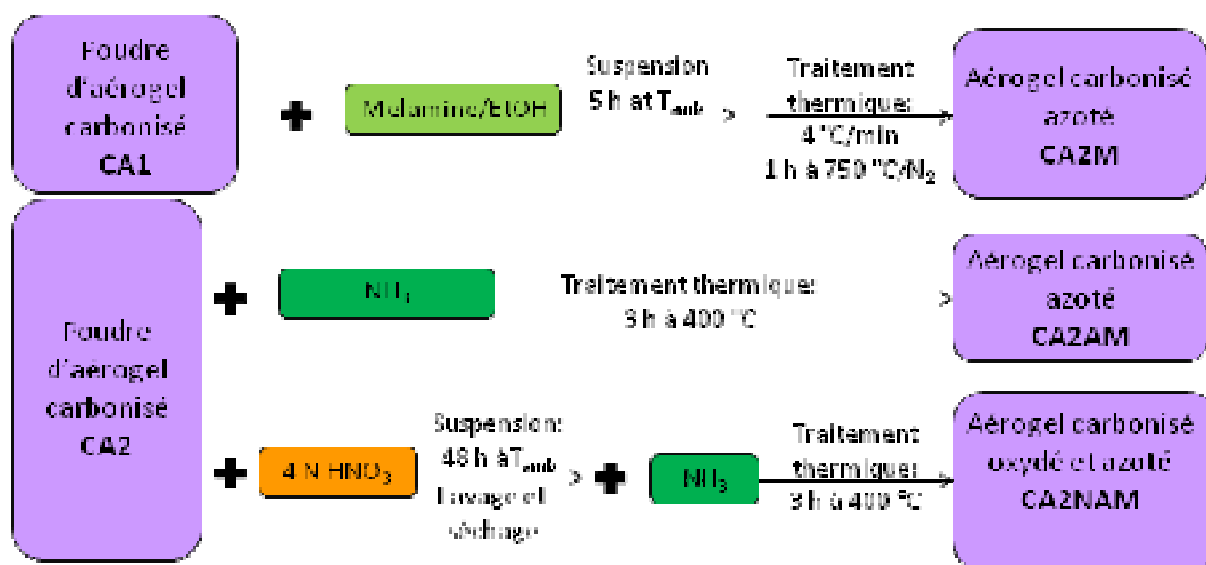


Figure RLF 18: Schéma de principe des voies d'introduction d'azote dans des aérogels carbonisés à base d'acétate de cellulose

Comme nous le supposions, l'oxydation et le co-traitement thermique de l'aérogel avec de la mélamine n'ont pas une influence prononcée sur la texture de l'aérogel carbonisé (analysé par adsorption d'azote). Pour l'ammonisation, en revanche, l'ammoniac agit comme agent d'activation et doubler le volume microporeux et ainsi les surfaces spécifiques (voir tableau RLF-4).

Tableau RLF-4: Texture des aérogels carbonisés modifiés chimiquement

			CA1	CA1H (H ₂ O ₂)	CA1N (HNO ₃)	CA1M (Mélamine)	CA2	CA2AM (NH ₃)	CA2NAM (HNO ₃ /NH ₃)
ρ_s	[g/cm ³]	±0.02	1.92	2.07	2.00	2.00	2.05	2.02	2.03
V_{DUB}	[cm ³ /g]	±0.01	0.07	0.06	0.05	0.06	0.05	0.12	0.12
V_{BdB}	[cm ³ /g]	±0.02	0.23	0.24	0.23	0.23	0.18	0.23	0.22
s_{BET}	[m ² /g]	±10	165	152	121	130	117	280	277
$d_{p,min}$	[nm]	±1	9	8	9	9	8	9	8
$d_{p,max}$	[nm]	±1	14	14	15	15	15	14	14

Comme l'on peut s'en rendre compte en observant la composition élémentaire des carbones précurseurs et des carbones modifiés dans le tableau RLF-5, le traitement avec de l'acide nitrique et du peroxyde d'hydrogène engendre une augmentation nette du contenu final en oxygène. Les carbones traités avec de la mélamine ou ammonisés contiennent plus d'azote. Il faut cependant remarquer que le carbone CA1M, modifié à l'aide de la mélamine, contient également une quantité d'oxygène non-négligeable reliée à la réaction avec l'oxygène ambiant après traitement. Il en résulte que les carbones oxydés CA1H et CA1N, mais aussi l'aérogel carbonisé co-traité avec de la mélamine CA1M contiennent plus de groupements acides que leurs précurseurs et moins de groupements basiques (tels que déterminés par titration de Boehm). Les carbones ammonisés, par contre, sont plus basiques que leurs précurseurs.

Tableau RLF-5: Composition élémentaire des aérogels carbonisés modifiés chimiquement

[%-massique]	%C	%H	%N	%O
CA1	91.1	0.9	3.0	5.1
CA1H (H ₂ O ₂)	86.3	0.9	3.1	9.6
CA1N (HNO ₃)	85.4	0.9	3.4	10.3
CA1M (Mélamine)	87.1	1.1	6.7	5.1
CA2	92.6	0.8	2.9	2.8
CA2AM (NH ₃)	90.5	0.8	4.5	2.8
CA2NAM (HNO ₃ /NH ₃)	89.1	0.9	4.6	3.2

Afin d'identifier le type de groupements fonctionnels introduits dans les aérogels carbonisés, nous avons analysé les différents échantillons par FTIR et XPS. Un exemple de résultat obtenu par FTIR pour les échantillons CA1H et CA1M (comparés avec leur précurseur CA1) est présenté dans la figure RLF-19. L'échantillon CA1H présente plus de groupements carboxyliques et quinone, tandis que CA1M possède plus de groupements d'ester et de lactone que leurs précurseurs respectifs et des groupements fonctionnels d'azote oxydés.

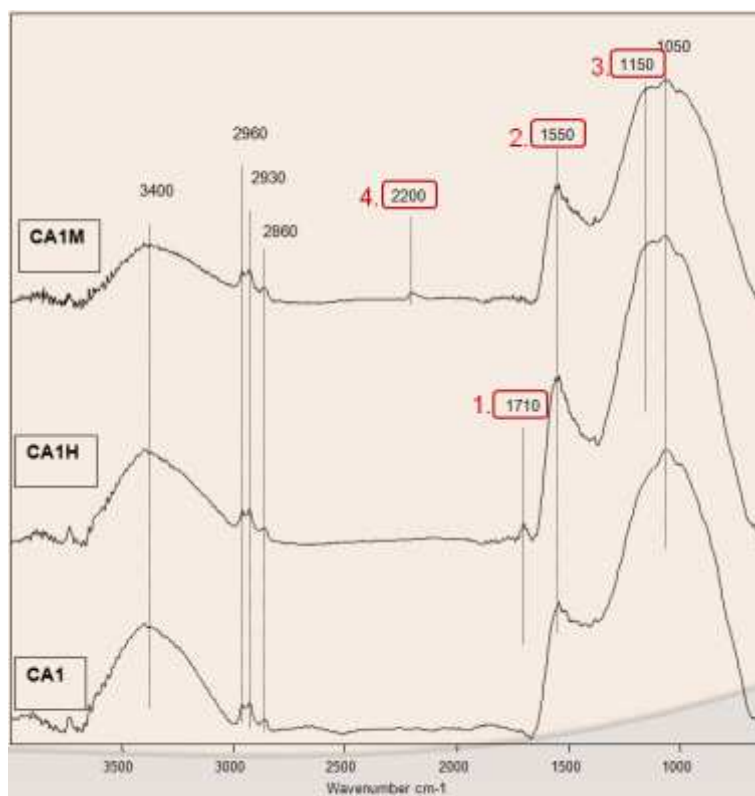


Figure RLF-19: Analyse FTIR de l'aérogel carbonisé CA1 et des aérogels carbonisés modifiés par oxydation CA1H (par H₂O₂) et par introduction d'azote CA1M (co-traitement avec de la mélamine): 1. Groupements carboxyliques, 2. Groupements quinone, 3. Groupements esters et lactones, 4. groupements fonctionnels d'azote oxydés

Pour conclure cette partie, nous avons pu introduire des groupements fonctionnels oxygénés par traitement avec de l'acide nitrique et du peroxyde d'hydrogène et des groupements fonctionnels azotés par traitement avec de la mélamine et par ammonisation. Nous avons trouvé que la nature et la concentration des groupements introduits varient avec la méthode de traitement. Grâce à cette démarche nous avons obtenu une large gamme d'aérogels carbonisés avec des textures assez similaires, mais des chimies de surface différentes.

Analyse des performances des aérogels carbonisés en tant que matériau d'électrode de supercondensateur (Chapitre 5)

Ayant préparé une large gamme d'aérogels carbonisés, nous avons effectué une sélection d'échantillons en tant que matériau d'électrode de supercondensateur. Entre autres, j'ai analysé la performance d'un aérogel carbonisé, d'un xérogel carbonisé et de différents aérogels carbonisés modifiés (activé, oxydé, azoté).

- **Rappels**

Schématiquement, on rappelle que les supercondensateurs stockent de l'énergie électrique dans une double-couche électrochimique en surface d'un carbone nanostructuré sous l'effet de forces

électrostatiques. Le schéma sur la figure RLF-20 rappelle l'impact que la texture et la chimie de surface peuvent avoir sur la performance d'un supercondensateur. En général, la performance d'un supercondensateur en termes de densité d'énergie et de puissance se situe entre les condensateurs conventionnels et les batteries (figure RLF-21).

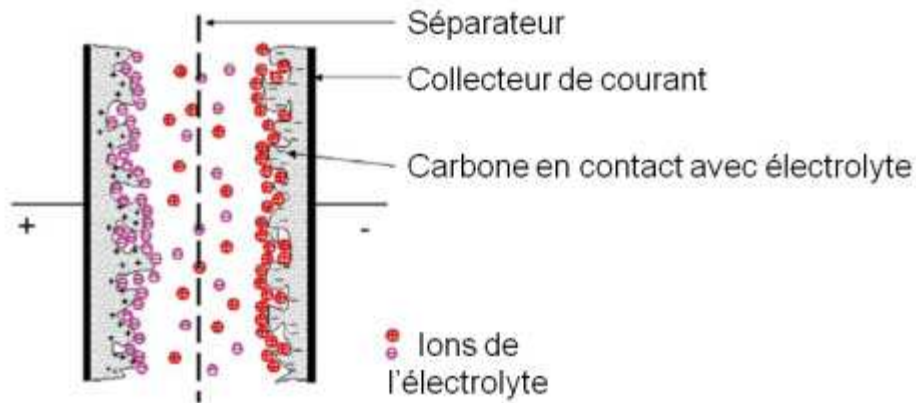


Figure RLF-20: Représentation schématique d'un supercondensateur [Pan 2006]

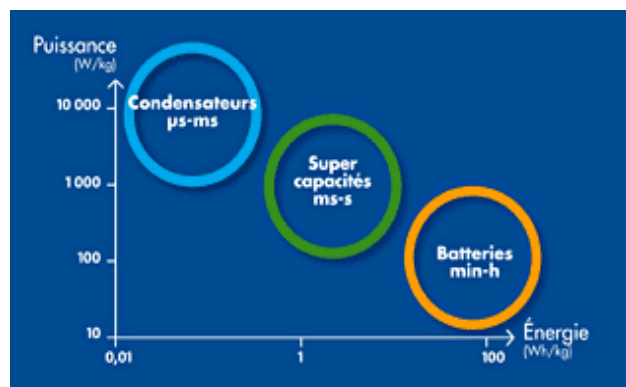


Figure RLF-21: Diagramme de Ragone simplifié pour différents dispositifs de stockage d'énergie [www.batscap.fr]

- **Elaboration des électrodes et protocole de test**

Pour analyser la performance des différents carbones élaborés, j'ai mélangé de la poudre d'aérogel carbonisé avec 10% de PTFE. Puis j'ai réalisé des électrodes d'une épaisseur de 300 μm et d'un diamètre de 16 mm. Sur le schéma RLF-22, on distingue les collecteurs de courant en or que j'ai utilisés, les deux électrodes de carbone, la membrane séparatrice (en microfibrilles de quartz) et l'électrolyte (ici une solution aqueuse d'acide sulfurique).

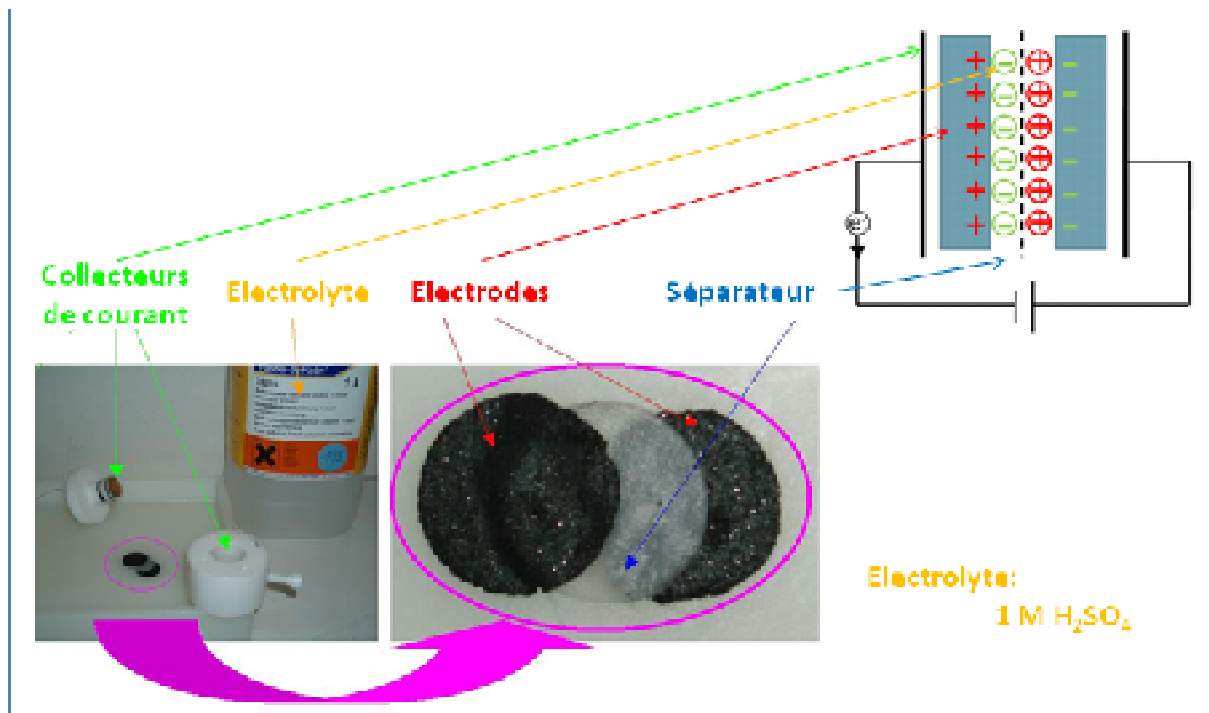


Figure RLF-22: Vue éclatée des électrodes et du séparateur

A l'aide d'un potentiostat nous avons effectué de la voltammétrie cyclique (entre 0 et 1 V à 20 mV/s) et de la spectroscopie d'impédance (à 0,5 V avec une amplitude de 20 mV/s). Grâce à ces deux méthodes j'ai pu déterminer la capacité et la résistance (par spectroscopie d'impédance à 0,11 Hz) de la cellule de supercondensateur contenant des électrodes d'aérogels carbonisés différents. De plus, j'ai observé le degré d'autodécharge pour le supercondensateur chargé à 1 V pendant 24h.

Cela nous a permis de déterminer les trois caractéristiques suivantes de notre supercondensateur de laboratoire:

- l'énergie $E = \frac{1}{2} CV^2$
- la puissance $P = \frac{V^2}{4R}$
- la constante de temps $\tau = RC$

• Principaux échantillons testés

Nous avons évalué la performance d'un aérogel de carbone représentatif CA1 avec une surface spécifique et des volumes méso- et microporeux peu développés. De plus, nous avons étudié les performances d'un xérogel de carbone 10XL possédant un volume mésoporeux plus important mais un très petit volume microporeux, un aérogel activé A1050 de très grande surface spécifique et volume microporeux. Puis nous avons analysé les performances d'un carbone oxydé CA1H (au peroxyde d'hydrogène) et d'un carbone azoté CA1M (co-traitement thermique avec de la mélamine). Puisque les valeurs totales obtenues dépendent de la cellule d'essai ainsi que des méthodes d'analyse et des paramètres utilisés, un carbone activé abondamment commercialisé par le passé

pour les supercondensateurs «Maxsorb». La texture des différents aérogels carbonisés déterminée par adsorption d'azote est reportée dans le tableau RLF-6.

Tableau RLF-6: Texture des aérogels carbonisés analysés en tant que matériau d'électrode de supercondensateur

Echantillon	S_{BET} m^2/g	$V_{mesopores}$ cm^3/g	$V_{\mu pores}$ cm^3/g	d_p nm	Préparation
CA1	165	0,23	0,07	12	10-0.2-0.25DA, 1000°C/N ₂
10XL	142	0,29	0,01	8	10-0.2-0.25DA, Xerogel (evaporation lente), 1000°C/N ₂
A1050	2147	0,94	0,75	4	CA1, activé à 1050°C/CO ₂ /2h
CA1H	152	0,24	0,06	11	CA1, 5N H ₂ O ₂ /48h/T _{amb}
CA1M	130	0,23	0,06	12	CA1, co-traitement thermique avec mélamine at 750°C/N ₂
Maxsorb	2200	-	-	-	carboné activé industriel

• Résultats

Les performances de l'aérogel carbonisé à base d'acétate de cellulose non-traité CA1 sont peu avantageuses. La capacité est assez faible et la résistance élevée (voir tableau RLF-7). Même le xérogel 10XL, possédant une surface spécifique comparable à celle de l'aérogel représentatif CA1, présente des performances plus avantageuses en termes de capacité et résistance. L'aérogel carbonisé activé A1050 ne présente pas seulement la plus grande capacité spécifique mais aussi la plus petite résistance parmi les carbones étudiés et en conséquence la plus grande densité d'énergie et puissance. Même le carbone industriel Maxsorb, qui a une surface spécifique comparable, se trouve être moins performant que lui sur tous les points, excepté en termes de capacité volumique. Par modification de la chimie de surface, une amélioration des performances est possible, dépendant clairement des groupements chimiques introduits. L'introduction des groupements fonctionnels oxydés par H₂O₂ conduit à de bien meilleurs résultats en termes de capacité et de résistance que l'introduction de groupements par co-traitement avec de la mélamine, et ce alors que les caractéristiques texturales des deux carbones sont comparables.

Tableau RLF-7: Performance des matériaux carbonisés à base d'acétate de cellulose en tant que matériau d'électrode de supercondensateur

Echantillon	C_{vol} F/cm^3	$C_{spécifique}$ F/g_c	ESR Ω	$E_{spécifique}$ Wh/kg_c	$P_{spécifique}$ W/kg_c	τ s
CA1	8,64	15,48	6,35	0,54	585	3,3
10XL	16,21	23,54	3,24	0,82	929	3,2
A1050	44,92	134,01	1,25	4,65	4946	3,4
CA1H	41,20	67,02	1,42	2,33	2374	3,5
CA1M	10,11	17,59	4,28	0,61	843	2,6
Maxsorb	55,43	113,74	1,94	3,95	2192	6,5

En résumé, on peut retenir que :

- les aérogels carbonés bruts possèdent une porosité insuffisante pour être utilisés comme électrode de supercondensateur,
- un séchage supercritique n'est pas indispensable pour cette application,
- l'introduction des groupements fonctionnels peut améliorer la capacité et résistance des matériaux carbonés,
- l'aérogel activé possède aussi bien une densité d'énergie qu'une puissance intéressante.

Cependant, même si les performances en termes de capacité et résistance sont améliorées par modification de la chimie de surface, l'autodécharge augmente de manière importante (figure RLF-23) probablement du fait de la concentration significative d'hétéroatomes. Par activation au CO₂, par contre, l'autodécharge diminue. Ceci est probablement dû à l'effet de « nettoyage de la surface » par traitement à une température au-dessus de la température de pyrolyse. Il semblerait donc que le carbone Maxsorb contienne lui aussi soit des hétéroatomes, soit de l'hydrogène, soit des impuretés.

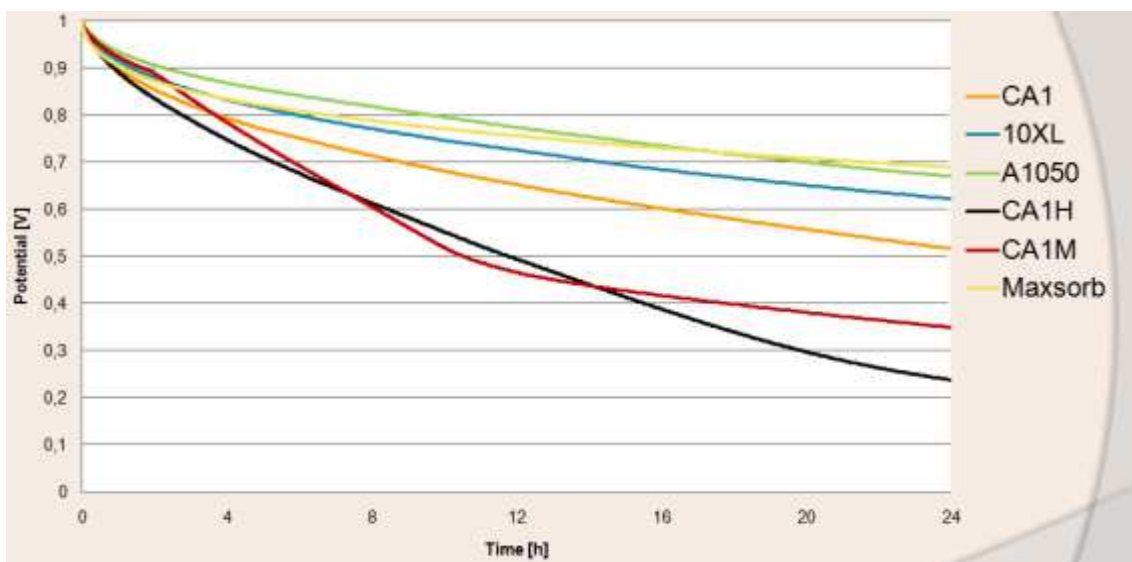


Figure RLF-23: Autodécharge des matériaux carbonés à base d'acétate de cellulose

Conclusion et perspectives

Dans le cadre de ces travaux de thèse, je suis parvenue à élaborer des aérogels organiques aux textures très différentes. Par pyrolyse de ces matériaux, nous avons obtenu des aérogels carbonés à base d'acétate de cellulose. La composition élémentaire de ces aérogels carbonés est plutôt similaire mais relativement originale grâce à un contenu non-négligeable d'oxygène et d'azote. La gamme de textures des aérogels carbonés est assez restreinte. Néanmoins, une augmentation significative de la surface spécifique et des volumes poreux est possible par simple activation au CO₂. Par traitement avec différents agents chimiques, une grande variété de groupements fonctionnels de surface peut être introduite dans ces structures carbonées. Pour l'application en tant que matériau d'électrode de supercondensateur, les aérogels carbonés à base d'acétate de cellulose non-activés s'avèrent, malheureusement, peu performants.

Il serait intéressant dans un premier temps de poursuivre ces études en laissant de côté l'application en tant que matériau d'électrode de supercondensateur, et en se tournant vers d'autres applications. Les aérogels organiques à base d'acétate de cellulose pourraient par exemple être évalués pour l'isolation thermique et les aérogels carbonisés pour une application en tant que matériau d'électrode de piles primaires à combustible à membrane échangeuse de protons.

Dans un deuxième temps la gamme de textures des matériaux carbonisés à base d'acétate de cellulose pourrait encore être élargie i) en faisant varier différents paramètres sol-gel et de pyrolyse (tels que la nature du solvant de l'acétate de cellulose ou la température maximale de pyrolyse), ii) en faisant varier des conditions d'activation (soit la température ou la durée d'activation, soit la nature de l'agent d'activation) ou encore iii) en étudiant différentes possibilités d'élaboration de matériaux composites à base d'aérogel d'acétate de cellulose (par exemple, directement par dispersion de fibres de carbone dans le sol). Parallèlement le procédé d'élaboration de matériaux carbonisés à base d'acétate de cellulose pourrait encore être simplifié sans pour autant dégrader les caractéristiques d'usage des carbones en optimisant le séchage subcritique des gels.

References

- [Aal 2009] Aaltonen O., Jauhiainen O., 2009, **The preparation of lignocellulosic aerogels from ionic liquid solutions**, Carbohydrate Polymers 75, 125-129.
- [Alc 2009] Alcañiz-Monge J., Lozano-Castelló D., Cazorla-Amorós D., Linares-Solano A., 2009, **Fundamentals of methane adsorption in microporous carbons**, Microporous and Mesoporous Materials 124, 110-116.
- [Alt 1986] Altena F.W., Shroder J.S, Van de Huls R., Smolders C.A, 1986, **Thermoreversible gelation of cellulose acetate solutions studied by differential scanning calorimetry**, Journal of polymer science part B: Polymer physics 24, 1725-1735.
- [Anb 1990] Anbergen U., Oppermann W., 1990, **Elasticity and swelling behaviour of chemically crosslinked cellulose ethers in aqueous systems**, Polymer 31, 1854-1858.
- [Ani 2006] Ania C.O., Pernak J., Stefaniak F., Raymundo-Piñero E., Béguin F., 2006, **Solvent-free ionic liquids as in situ probes for assessing the effect of ion size on the performance of electrical double layer capacitors**, Carbon 44, 3113-3148.
- [Ant 2009] Antolini E., 2009, **Carbon supports for low-temperature fuel cell catalysts**, Applied Catalysis B: Environmental 88, 1-24.
- [Ari 2007] Ariunaa A., Li B., Li W., Purevsuren B., Munkhjargal S., Liu F., Bai Z., Wang G., 2007, **Coal pyrolysis under synthesis gas, hydrogen and nitrogen**, Journal of Fuel Chemistry and Technology 35(1), 1-4.
- [Aue 1998] Auer E., Freund A., Pietsch J., Tacke T., 1998, **Carbons as supports for industrial precious metal catalysts**, Applied Catalysis A: General 173, 259-271.
- [Aza 2003] Azaïs P., 2003, **Recherche des causes du vieillissement de supercondensateurs à électrolyte organique à base de carbones activés**, PhD thesis, Université d'Orléans, France.
- [Aza 2007] Azaïs P., Duclaux L., Florian P., Massiot D., Lillo-Rodenas M.-A., Linares-Solano A., Peres J.-P., Jehoulet C., Béguin F., 2007, **Causes of supercapacitors ageing in organic electrolyte**, Journal of Power Sources 171, 1046-1053.
- [Bai 2006] Bai Y.X., Li Y-F., 2006, **Preparation and characterization of crosslinked porous cellulose beads**, Carbohydrate polymers 64, 402-407.
- [Bar 1951] Barret E.P., Joyner L.G., Halenda P.H., 1951, **The determination of pore volume and area distributions in porous substances. I. computations from nitrogen isotherms**, Journal of the American Chemical Society 73, 373-380.
- [Bar 2001] Bard A.J., Faulkner L.R., 2001, **Electrochemical Method: Fundamentals and Applications**, 2nd Edition, Wiley, New York.

- [BeF 2006] Béguin F., Friebe M., Jurewicz K., Vix-Guterl C., Dentzer J., Frackowiak E., 2006, **State of hydrogen electrochemically stored using nanoporous carbons as negative electrode materials in an aqueous medium**, Carbon 44, 2392-2398.
- [BeK 2006] Béguin F., Kierzek K., Friebe M., Jankowska A., Machnikowski J., Jurewicz K., Frackowiak E., 2006, **Effect of various porous nanotextures on the reversible electrochemical sorption of hydrogen in activated carbons**, Electrochimica Acta 51, 2161-2167.
- [Bie 1987] Biermann C. J., Narayan R., 1987, **Crosslinking of Cellulose Acetate with Phosphorus Pentoxide**, Journal of Polymer Science part C: Polymer Letters 25, 89-92.
- [Bie 1998] Biesmans G., Mertens A., Duffours L., Woignier T., Phalippou J., 1998, **Polyurethane based organic aerogels and their transformation into carbon aerogels**, Journal of Non-Crystalline Solids 225, 64-68.
- [Bim 1998] Bimer J., Salbut P.D., Berlozecki S., Boudou J.-P., Broniek E., Siemieniowska T., **Modified active carbons from precursors enriched with nitrogen functions: Sulfur removal capabilities**, Fuel 77, 519-525.
- [Bis 2003] Bisson A., Rigacci A., Lecomte D., Rodier E., Achard P., 2003, **Drying of silica gels to obtain aerogels: Phenomenology and basic techniques**, Drying Technology 21, 593-628.
- [Bla 1999] Blank W.J., He Z.A., Hessel E.T., 1999, **Catalysis of the isocyanate-hydroxyl reaction by non-tin catalysts**, Progress in Organic coatings 35, 19-29.
- [Ble 2008] Bleda-Martínez M.J., Pérez J.M., Linares-Solano A., Morallón E., Cazorla-Amorós D., 2008, **Effect of surface chemistry on electrochemical storage of hydrogen in porous carbon materials**, Carbon 46, 1053-1059.
- [Boc 1998] Bock V., Emmerling A., Fricke J., 1998, **Influence of monomer and catalyst concentration on RF and carbon aerogel structure**, Journal of Non-Crystalline Solids 225, 69-73.
- [Boe 1966] de Boer J.H., Lippens B.C., Linsen B.G., Broekhoff J.C.P., van den Heuvel A., Osinga Th.J., 1966, **Thet-curve of mulitmolecular N₂ adsorption**, Journal of Colloid and Interface Science 21, 405-414.
- [Bom 1995] van Bommel M.J., Haan A.B. de, 1995, **Drying of silica aerogel with supercritical carbon dioxide**, Journal of Non-Crystalline Solids 186, 78-82.
- [Bra 1981] van Brakel J., Modry S., Svata M., 1981, **Mercury porosimetry: State of the art**, Powder Technology 29, 1-12.
- [Bra 1993] Bradley R.H., Beamson G., Ling X., Sutherland I., 1993, **Surface nitrogen chemistry of PAN carbon fibres**, Applied Surface Science 72, 273-276.

- [Bri 1990] Bridgwater A.V., 1990, **Biomass for energy and Industry: Biomass pyrolysis technologies**, In: Biomass for pyrolysis technologies, Elsevier Applied Science, London.
- [Bri 1990] Brinker C.J., Scherer G.W., 1990, **Sol-gel Science: The Physics and Chemistry of Sol-Gel Processing**, Academic Press, San Diego.
- [Bru 1938] Brunauer S., Emmett P.H. and Teller E., 1938, **Adsorption of gases in multimolecular layers**, Journal of the American Chemical Society 60, 309-319.
- [Bud 2010] Budtova T., Egal M., Gavillon R., Gericke M., Heinze T., Liebert T., Roy C., Schluffer K., Navard P., 2010, **Comparison of Solution-State Properties of Cellulose Dissolved in NaOH/Water and in Ionic Liquid (EMIMAc)**, in: Cellulose Solvents: For Analysis, Shaping, and Chemical Modification, Chapter 10, 179-196.
- [Cai 2008] Cai J., Kimura Z., Wada M., Kuga S., Zhang L., 2008, **Cellulose Aerogels from Aqueous Alkali Hydroxide-Urea Solution**, ChemSusChem 1, 129-139.
- [Car 2001] Carmier D., Vix-Guterl C., Lahaye J., 2001, **Porosity of the cathode during the discharge of SOCl₂/Li batteries. II. Model cathodes**, Carbon 39, 2187-2193.
- [Car 2002] Carmier D., Vix-Guterl C., Lahaye J., 2002, **Porosity of the cathode during the discharge of SOCl₂/Li batteries. Influence of the porous morphology of the carbons used**, Journal of Power Sources 103, 237-244.
- [Che 1998] Chelbli C., Cartillier L., 1998, **Cross-linked cellulose as tablet excipient: a binding/disintegrating agent**, International Journal of Pharmaceutics 171, 101-110.
- [Che 2006] Chen C.C., Wang C.-C., 2006, **Crosslinking of cotton cellulose with succinic acid in the presence of titanium dioxide nano-catalyst under UV irradiation**, Journal of Sol-Gel Science and Technology 40, 31-38.
- [Cli 2005] Clipper controls, 2005, **Dielectric Constants of Materials**, http://clippercontrols.com/info/dielectric_constants.html (17.April 2008).
- [Con 1999] Conway B.E., 1999, **Electrochemical Supercapacitors: Scientific Fundamentals and Technological Applications**, Kluwer Academic, New York.
- [Cou 2007] Couhert C., 2007, **Pyrolyse flash à haute température de la biomasse ligno-cellulosique et de ses composés – production de gaz de synthèse**, PhD thesis, Ecole des Mines de Paris, France.
- [Cuc 1983] Cuculo J.A., Hudson S.M., 1983, **Preparation of cellulose films or fibers from cellulose solutions**, US Patent 4 367 191.
- [CYD 2006] Chmiola J., Yushin G., Dash R., Gogotsi Y., 2006, **Effect of pore size and surface area of carbide derived carbons on specific capacitance**, Journal of Power Sources 158, 765-772.

- [CYG 2006] Chmiola J. Yushin G., Gogotsi Y., Portet C., Simon P., Taberna P.L., 2006, **Anomalous Increase in Carbon Capacitance at Pore Sizes Less Than 1 Nanometer**, Science 313, 1760-1763.
- [Déb 2007] Débart A., Bao J., Armstrong G., Bruce P.G., 2007, **An O₂ cathode for rechargeable lithium batteries: The effect of a catalyst**, Journal of Power Sources 174, 1177-1182.
- [Déb 2008] Débart A., Paterson A.J., Bao J., Bruce P.G., 2008, **α -MnO₂ Nanowires: A Catalyst for the O₂ Electrode in Rechargeable Lithium Batteries**, Angewandte Chemie International Edition 47, 4521-4524.
- [DeG 1979] De Gennes P.G, 1979, **Scaling concepts in polymer physics**, Cornell University Press, Ithaca New York.
- [Den 2009] Deng M., Zhou Q., Du A., Van Kasteren J., Wang Y., 2009, **Preparation of nanoporous cellulose foams from cellulose-ionic liquid solutions**, Materials Letters 63, 1851-1854.
- [Des 1998] Desbrières J., Hirrien M., Rinaudo M., 1998, **A calorimetric study of methylcellulose gelation**, Carbohydrate polymers 37, 145-152.
- [Dic 2006] Dicks A.L., 2006, **The role of carbon in fuel cells**, Journal of Power Sources 156, 128-141.
- [Don 1998] Donnet J.-B., Wang T. K., Rebouillat S., Peng J. C. M., 1998, **Carbon Fibers**, Marcel Dekker, Inc., New York.
- [Dub 1960] Dubinin M.M., 1960, **The Potential Theory of Adsorption of Gases and Vapors for adsorbents with Energetically Non-uniform Surfaces**, Chemical Reviews 60, 235-241.
- [Duf 1996] Duffours L., Woignier T., Phalippou J., 1996, **Irreversible volume shrinkage of silica aerogels under isostatic pressure**, Journal of Non-Crystalline Solids 194 , 283-290.
- [Dul 2006] Dulong V., Mocanu G., Picton L., Le Cerf D., 2006, **Hydrogels amphiphiles à base de polysaccharides**, Matériaux2006 (14-17 November 2006), Dijon, France.
- [Ega 2006] Egal M., 2006, **Structure and properties of cellulose/NaOH aqueous solutions, gels and regenerated objects**, PhD thesis, Ecole des Mines de Paris, France.
- [Esp 1996] Esposito F., Del Nobile M.A., Mensitieri G., Nicolais L., 1996, **Water sorption in cellulose-based hydrogels**, Journal of Applied Polymer Science 60, 2403-2407.
- [Ess 1989] Essig M., Richards G.N., Schenck E., 1989, **Mechanism of formation of the major volatile products from pyrolysis of cellulose** (p. 841), Wiley, New York.
- [Fan 2006] Fang B., Binder L., 2006, **A modified activated carbon aerogel for high-energy storage in electric double layer capacitors**, Journal of Power Sources 163, 616-622.

- [Fan 2007] Fang B., Binder L., 2007, **Enhanced surface hydrophobisation for improved performance of carbon aerogel electrochemical capacitor**, *Electrochimica Acta* 52, 6916-6921.
- [Fey 2002] Fey G. T.-K., Kao Y.-C., 2002, **Synthesis and characterization of pyrolyzed sugar carbons under nitrogen or argon atmospheres as anode materials for lithium-ion batteries**, *Materials Chemistry and Physics* 73, 37-46.
- [Fin 2001] Fink H.P., Weigel P., Purz H.J., Ganster J., 2001, **Structure formation of regenerated cellulose materials from NMMO solutions**, *Progress in Polymer Science* 26, 1473-1524.
- [FiR 2006] Fischer F., Rigacci A., R. Pirard, Berthon-Fabry S., Achard P., 2006, **Cellulose-based aerogels**, *Polymer* 47, 7636-7645.
- [FiR 2007] Fischer F., Rigacci A., Berthon-Fabry S., Simon B., Achard P., 2007, **Macroporous nanostructured carbons from cellulosic aerogels**, XIVth International Sol-Gel conference (2-7 September 2007), Montpellier, France.
- [Fis 2006] Fischer F., 2006, **Synthèse et étude de matériaux nanostructurés à base d'acétate de cellulose pour applications énergétiques**, PhD thesis, Ecole des Mines de Paris, France.
- [Fit 1995] Fitzer E., Kochling K.-H., Boehm H.P., Marsh H., 1995, **Recommended terminology for the description of carbon as a solid**, *Pure and Applied Chemistry* 67, 473-506.
- [Fra 2001] Frackowiak E., Béguin F., 2001, **Carbon materials for the electrochemical storage of energy in capacitors**, *Carbon* 39, 937-950.
- [Fra 2006] Frackowiak E., Lota G., Machnikowski J., Vix-Guterl C., Béguin F., 2006, **Optimisation of supercapacitors using carbons with controlled nanotexture and nitrogen content**, *Electrochimica Acta* 51, 2209-2214.
- [Fra 2007] Frackowiak E., 2007, **Carbon materials for supercapacitor application**, *Physical Chemistry Chemical Physics* 9, 1774-1785.
- [Fre 1996] Frey M.W., Cuculo J.A., Khan S.A., 1996, **Rheology and gelation of cellulose/ammonia/ammonium thiocyanate solutions**, *Journal of Polymer Science Part B: Polymer Physics* 34, 2375-2381.
- [FuL 2010] Fu Z., Li W., Zhang W., Sun F., Zhou Z., Xiang X., 2010, **Preparation and activity of carbon supported porous platinum as electrocatalyst for methanol oxidation**, *International Journal of Hydrogen Energy*, Article in press.
- [Gad 2005] Gadiou R., Saadallah S., Piquero T., David P., Parmentier J., Vix-Guterl C., 2005, **The influence of textural properties on the adsorption of hydrogen on ordered nanostructured carbons**, *Microporous and Mesoporous Materials* 79, 121-128.

- [Gam 2001] Gamby J., Taberna P.L., Simon P., Fauvarque J.F., Chesneau M., 2001, **Studies and characterisations of various activated carbons used for carbon/carbon supercapacitors**, Journal of Power Sources 101, 109-116.
- [Gam 2007] Gamry Instruments, **Basics of Electrochemical Impedance Spectroscopy**, http://www.gamry.com/App_Notes/EIS_Primer/EIS_Primer_2007.pdf (July 5th 2010).
- [Gao 2001] Gao J., Haidar G., Lu X., Hu Z., 2001, **Self-association of Hydroxypropylcellulose in water**, Macromolecules 34, 2242-2247.
- [Gav 2007] Gavillon R., 2007, **Préparation et caractérisation de matériaux cellulose ultra poreux**, PhD thesis, Ecole des Mines de Paris, France.
- [Gav 2008] Gavillon R., Budtova T., 2008, **Aerocellulose: New Highly Porous Cellulose Prepared from Cellulose-NaOH Aqueous Solutions**, Biomacromolecules 9, 269-277.
- [Glo 2001] Glora M., Wiener M., Petričević R., Pröbstle H., Fricke J., 2001, **Integration of carbon aerogels in PEM fuel cells**, Journal of Non-Crystalline Solids 285, 283-287.
- [Gor 2009] Gorgulho H.F., Gonçalves F., Pereira M.F.R., Figueiredo J.L., 2009, **Synthesis and characterization of nitrogen-doped carbon xerogels**, Carbon 47, 2032-2039.
- [Gre 1976] Gregg S.J., Sing K.S.W., 1976, **Adsorption, Surface Area and Porosity**, 2nd Edition, Academic Press, New York.
- [Gre 1982] Gregg S.J., Sing K.S.W., 1982, **Adsorption, Surface Area and Porosity**, Academic Press, New York.
- [Grz 2010] Grzyb B., Hildenbrand C., Berthon-Fabry S., Bégin D., Job N., Rigacci A., Achard P., 2010, **Functionalisation and chemical characterization of cellulose-derived carbon aerogels**, Carbon 48, 2297-2307.
- [Gui 2007] Guilminot E., Fischer F., Chatenet M., Rigacci A., Berthon-Fabry S., Achard P., Chainet E., 2007, **Use of cellulose-based carbon aerogels as catalyst support for PEM fuel cell electrodes: Electrochemical characterization**, Journal of Power Sources 166, 104-111.
- [Gui 2008] Guilminot E., Gavillon R., Chatenet M., Berthon-Fabry S., Rigacci A., Budtova T., 2008, **New nanostructured carbons based on porous cellulose: Elaboration, pyrolysis and use as platinum nanoparticles substrate for oxygen reduction electrocatalysis**, Journal of Power Sources 185, 717-726.
- [Guo 2003] Guo J., Lua A.C., 2003, **Textural and chemical properties of adsorbent prepared from palm shell by phosphoric acid activation**, Materials Chemistry and Physics 80, 114-119.
- [Guo 2005] Guo J., Xu W.S., Chen Y.L., Lua A.C., 2005, **Adsorption of NH₃ onto activated carbon prepared from palm shells impregnated with H₂SO₄**, Journal of Colloid and Interface Science 281, 285-290.

- [Hae 2009] Haensel T., Comouth A., Lorenz P., Ahmed S. I.-U., Krischok S., Zydziak N., Kauffmann A., Schaefer J.A., 2009, **Pyrolysis of cellulose and lignin**, Applied Surface Science 255, 8183-8189.
- [Hal 2010] Halama A., Szubsda B., Pasciak G., 2010, **Carbon aerogels as electrode material for electrical double layer supercapacitors: Synthesis and properties**, Electrochimica Acta, Article in press.
- [Han 1996] Hanzawa Y., Kaneko K., Pekala R.W., Dresselhaus M.S., 1996, **Activated Carbon Aerogels**, Langmuir 12, 6167-6169.
- [Haq 1993] Haque A., Morris E.R., 1993, **Thermogelation of methylcellulose. Part I: Molecular structures and processes**, Carbohydrates Polymers 22, 161-173.
- [Has 1963] Hassler J.W., 1963, **Activated Carbon**, Chemical Publishing Co., Inc., New York.
- [Hat 1998] Hattori M., Koga T., Shimaya Y., Saito M., 1998, **Aqueous Calcium Thiocyanate Solution as a Cellulose Solvent. Structure and Interactions with Cellulose**, Polymer Journal 30, 43-48.
- [Her 2004] Hernadi K., Gaspar A., Seo J.W., Hammida M., Demortier A., Forró L., Nagy J.B., Kiricsi I., 2004, **Catalytic carbon nanotube and fullerene synthesis under reduced pressure in batch reactor**, Carbon 42, 1599-1607.
- [Hin 1993] Hinterholzer P., 1993, **Cellulose solution in water and NMMO**, US Patent 5 189 152.
- [Hoe 2008] Hoepfner S., Ratke L., Milow B., 2008, **Synthesis and characterization of nanofibrillar cellulose aerogels**, Cellulose 15, 121-129.
- [Hou 1996] Houghton R.P., Mulvaney A.W., 1996, **Mechanism of tin(IV)-catalysed urethane formation**, Journal of Organometallic Chemistry 518, 21-27.
- [Hsi 2002] Hsieh C.-T., Teng H., 2002, **Influence of oxygen treatment on electric double-layer capacitance of activated carbon fabrics**, Carbon 40, 667-674.
- [Hüs 1998] Hüsing N., Schubert U., 1998, **Aerogels: Airy Materials: Chemistry, Structure, and Properties**, Angewandte Chemie International Edition 37, 22-45.
- [Hul 2005] Hulicova D., Yamashita J., Soneda Y., Hatori H., Kodama M., 2005, **Supercapacitors Prepared from Melamine-Based Carbon**, Chemistry of Materials 17, 1241-1247.
- [Hul 2006] Hulicova D., Kodama M., Hatori H., 2006, **Electrochemical Performance of Nitrogen-Enriched Carbons in Aqueous and Non-Aqueous Supercapacitors**, Chemistry of Materials 18, 2318-2326.
- [Hwa 2004] Hwang S.-W., Hyun S.-H., 2004, **Capacitance control of carbon aerogel electrodes**, Journal of Non-Crystalline Solids 347, 238-245.
- [Ina 2002] Inagaki M., Radovic L.R., 2002, **Nanocarbons**, Carbon 40, 2279-2282.

- [Ina 2009] Inagaki M., 2009, **Pores in carbon materials - importance of their control**, New Carbon Materials 24, 193-232.
- [InK 2004] Inagaki M., Kaneko K., Nishizawa T., 2004, **Nanocarbons: recent research in Japan**, Carbon 42, 1401-1417.
- [InN 2004] Inagaki M., Nishikawa T., Sakuratani K., Katakura T., Konno H., Morozumi E., 2004, **Carbonization of kenaf to prepare highly-microporous carbons**, Carbon 42, 890-893.
- [Inn 2006] Innerlohniger J., Weber H.K., Kraft G., 2006, **Aerocellulose: Aerogels and Aerogel-like Materials made from Cellulose**, Macromolecular Symposia 244, 126-135.
- [Ish 2004] Ishida O., Kim D.-Y., Kuga S., Nishiyama Y., Malcolm Brown Jr. R., 2004, **Microfibrillar carbon from native cellulose**, Cellulose 11, 475-480.
- [Ism 2005] Ismadji S., Sudaryanto Y., Hartono S.B., Setiawan L.E.K., Ayucitra A., 2005, **Activated carbon from char obtained from vacuum pyrolysis of teak sawdust: pore structure development and characterization**, Bioresource Technology 96, 1364-1369.
- [Ita 2007] Itagaki M., Suzuki S., Shitanda I., Watanabe K., Nakazawa H., 2007, **Impedance analysis on electric double layer capacitor with transmission line model**, Journal of Power Sources 164, 415-424.
- [IUP 1997] IUPAC, 1997, **Compendium of Chemical Terminology**, Blackwell Scientific Publications, Oxford.
- [Jan 1994] Jansen R.J.J., van Bekkum H., 1994, **Amination and ammoxidation of activated carbons**, Carbon 32, 1507-1516.
- [Jia 2008] Jia Q., Lua A. C., 2008, **Effects of pyrolysis conditions on the physical characteristics of oil-palm-shell activated carbons used in aqueous phase phenol adsorption**, Journal of Analytical and Applied Pyrolysis 83, 175-179.
- [Jin 2004] Jin H., Nishiyama Y., Wada M., Kuga S., 2004, **Nanofibrillar cellulose aerogels**, Colloids and surfaces A 240, 63-67.
- [Job 2006] Job N., Sabatier F., Pirard J.-P., Crine M., Léonard A., 2006, **Towards the production of carbon xerogel monoliths by optimizing convective drying conditions**, Carbon 44, 2534-2542.
- [Job 2009] Job N., Berthon-Fabry S., Chatenet M., Marie J., Brigaudet M., Pirard J.-P., 2009, **Nanostructured Carbons as Platinum Catalyst Supports for Proton Exchange Membrane Fuel Cell Electrodes**, Topics in Catalysis 52, 2117-2122.
- [Job 2010] Job N., Lambert S., Chatenet M., Gommès C.J., Maillard F., Berthon-Fabry S., Regalbuto J.R., Pirard J.-P., 2010, **Preparation of highly loaded Pt/carbon xerogel catalysts for Proton Exchange Membrane fuel cells by the Strong Electrostatic Adsorption method**, Catalysis Today 150, 119-127.

- [JoH 2005] Job N., Heinrichs B., Ferauche F., Noville F., Marien J., Pirard J.-P., 2005, **Hydrodechlorination of 1,2-dichloroethane on Pd-Ag catalysts supported on tailored texture carbon xerogels**, *Catalysis Today* 102-103, 234-241.
- [Joo 2001] Joo S.H., Jun S., Ryoo R., 2001, **Synthesis of ordered mesoporous carbon sieves CMK-1**, *Microporous and Mesoporous Materials* 44-45, 153-158.
- [Jor 2008] Jordá-Beneyto M., Lozano-Castelló D., Suárez-García F., Cazorla-Amorós D., **Linares-Solano A., 2008, Advanced activated carbon monoliths and activated carbons for hydrogen storage**, *Microporous and Mesoporous Materials* 112, 235-242.
- [JoT 2005] Job N., Théry A., Pirard R., Marien J., Kocon L., Rouzaud J.-N., Béguin F., Pirard J.-P., 2005, **Carbon aerogels, cryogels and xerogels: Influence of the drying method on the textural properties of porous carbon materials**, *Carbon* 43, 2481-2494.
- [Jur 2003] Jurewicz K., Babel K., Ziólkowski A., Wachowska H., 2003, **Amoxidation of active carbons for improvement of supercapacitor characteristics**, *Electrochimica Acta* 48, 1491-1498.
- [Jur 2006] Jurewicz K., Babel K., Pietrzak R., Delpeux S., Wachowska H., 2006, **Capacitance properties of multi-walled carbon nanotubes modified by activation and amoxidation**, *Carbon* 44, 2368-2375.
- [Kal 2001] Kaluža L., Zdražil M., 2001, **Carbon-supported Mo catalysts prepared by a new impregnation method using a MoO₃/water slurry: saturated loading, hydrosulfurization activity and promotion by Co**, *Carbon* 39, 2023-2034.
- [Kam 1996] Kamath M., Mandal B. K., 1996, **Crosslinked copolymers of cyanoethylated cellulose**, *European Polymer Journal* 32, 285-288.
- [Kap 1999] Kapteijn F., Moulijn J.A., Matzner S., Boehm H.P., 1999, **The development of nitrogen functionality in model chars during gasification in CO₂ and O₂**, *Carbon* 37, 1143-1150.
- [Kas 2009] Kaskhedikar N.A., Maier J., 2009, **Lithium Storage in Carbon Nanostructures**, *Advanced Materials* 21, 2664-2680.
- [Kat 2004] Kato N., Gehrke S. H., 2004, **Microporous, fast response cellulose ether hydrogel prepared by freeze-drying**, *Colloids and Surfaces B: Biointerfaces* 38, 191-196.
- [Kav 1998] Kavanagh G.M., Ross-Murphy S.B., 1998, **Rheological characterisation of polymer gels**, *Progress in Polymer Science* 23, 533-562.
- [Kho 2005] Khomenko V., Frackowiak E., Béguin F., 2005, **Determination of the specific capacitance of conducting polymer/nanotubes composite electrodes using different cell configurations**, *Electrochimica Acta* 50, 2499-2506.
- [Kho 2006] Khomenko V., Raymundo-Piñero E., Béguin F., 2006, **Optimisation of an asymmetric manganese oxide/activated carbon capacitor working at 2 V in aqueous medium**, *Journal of Power Sources* 153, 183-190.

- [Kho 2008] Khomenko V., Raymundo-Piñero E., Béguin F., 2008, **High-energy density graphite/AC capacitor in organic electrolyte**, Journal of Power Sources 177, 643-651.
- [Kie 2004] Kierzek K., Frackowiak E., Lota G., Gryglewicz G., Machnikowski J., 2004, **Electrochemical capacitors based on highly porous carbons prepared by KOH activation**, Electrochimica Acta 49, 515-523.
- [Kim 2002] Kim M. I., Yun C. H., Kim Y. J., Park C. R., Inagaki M., 2002, **Changes in pore properties of phenol formaldehyde-based carbon with carbonisation and oxidation conditions**, Carbon 40, 2003-2012.
- [Kim 2004] Kim C., Choi Y.-O., Lee W.-J., Yang K.-S., 2004, **Supercapacitor performances of activated carbon fiber webs prepared by electrospinning of PMDA-ODA poly(amic acid) solutions**, Electrochimica Acta 50, 883-887.
- [Kim 2005] Kim C., 2005, **Electrochemical characterization of electrospun activated carbon nanofibres as an electrode in supercapacitors**, Journal of Power Sources 142, 328-388.
- [Kin 1988] Kinoshita K., 1988, **Carbon - Electrochemical and Physicochemical Properties**, Wiley, New York.
- [Kis 1931] Kistler S.S., 1931, **Coherent expanded aerogels and jellies**, Nature 127, 741.
- [Koc 2005] Kocon L., Phalippou J., 2005, **Aérogels. Aspect matériau**, AF3610, Techniques de l'Ingénieur, Paris.
- [Kos 2008] Kosan B., Michels C., Meister F., 2008, **Dissolution and forming of cellulose with ionic liquids**, Cellulose 15, 59-66.
- [Köt 2000] Kötz R., Carlen M., 2000, **Principles and applications of electrochemical capacitors**, Electrochimica Acta 45, 2483-2498.
- [Köt 2006] Kötz R., Hahn M., Gallay R., 2006, **Temperature behaviour and impedance fundamentals of supercapacitors**, Journal of Power Sources 154, 550-555.
- [Kra 2000] Kratzert M., 2000, **Herstellung von Kunststoffen: Polyaddition**, FU Berlin, Didaktik der Chemie, <http://www.chemie.fu-berlin.de/chemistry/kunststoffe/index.htm> (August 25 2008).
- [Kug 1980] Kuga S., 1980, **The porous structure of cellulose gel regenerated from calcium thiocyanate solution**, Journal of Colloid and Interface Science 77, 413-417.
- [Kun 2001] Kundu P.P., Kundu M., 2001, **Effect of salt and surfactant and their doses on the gelation of extremely dilute solutions of methyl cellulose**, Polymer 42, 2015-2020.
- [Kun 2010] Kunowsky M., Marco-Lozar J.P., Cazorla-Amorós D., Linares-Solano A., 2010, **Scale-up activation of carbon fibres for hydrogen storage**, International Journal of Hydrogen Energy 35, 2393-2402.

- [Lah 1999] Lahaye J., Nans, G., Bagreev A., Strelko V., 1999, **Porous structure and surface chemistry of nitrogen containing carbons from polymers**, Carbon 37, 585-590.
- [Lan 1999] Lang H., Loth F., 1999, **Poröse Cellulose-Matrix in Form von Schwämmen und Tüchern und Verfahren zur Herstellung durch Koagulation von Lösungen eines instabilen Cellulosederivates**, DE Patent 199 10 105 A 1.
- [Las 1999] Laszlo K., Bota A., Nagy L.G., Cabasso I., 1999, **Porous carbon from polymer waste materials**, Colloids and Surfaces A: Physicochemical and Engineering Aspects 151, 311-320.
- [Las 2001] Lassègues J.-C., 2001, **Supercondensateurs**, Techniques de l'Ingénieur, D 3334, Paris.
- [Lás 2001] László K., Tombácz E., Josepovits K., 2001, **Effect of activation on the surface chemistry of carbons from polymer precursors**, Carbon 39, 1217-1228.
- [Lee 2005] Lee W.H., Park J.S., Sok J.H., Reucroft P.J., 2005, **Effects of pore structure and surface state on the adsorption properties of nano-porous carbon materials in low and high relative pressures**, Applied Surface Science 246, 77-81.
- [Lee 2010] Lee Y.J., Jung J.C., Yi J., Baek S.-H., Yoon J.R., Song I.K., 2010, **Preparation of carbon aerogel in ambient conditions for electrical double-layer capacitor**, Current Applied Physics 10, 682-686.
- [Lie 2009] Liebner F., Haimer E., Loidl D., Tschegg S., Neouze M.-A., Rosenau T., Wendland M., 2009, **Cellulosic aerogels as ultra-lightweight materials. Part2: Synthesis and properties**, Holzforschung 63, 3-11.
- [Lil 2005] Lillo-Ródenas M.-A., Cazorla-Amorós D., Linares-Solano A., 2005, **Behaviour of activated carbons with different pore size distributions and surface oxygen groups for benzene and toluene adsorption at low concentrations**, Carbon 43, 1785-1767.
- [LiT 2001] Li L., Thangamathesvaran P.M., Yue C.Y., Tam K.C., Hu X., Lam Y.C., 2001, **Gel network structure of methylcellulose in water**, Langmuir 17, 8062-8068.
- [LiW 2006] Li J., Wang X., Huang Q., Gamboa S., Sebastian P.J., 2006, **Studies on preparation and performances of carbon aerogel electrodes for the application of supercapacitor**, Journal of Power Sources 158, 784-788.
- [LiW 2008] Li J., Wang X., Wang Y., Huang Q., Dai C., Gamboa S., Sebastian P.J., 2008, **Structure and electrochemical properties of carbon aerogels synthesized at ambient temperatures as supercapacitors**, Journal of Non-Crystalline Solids 354, 19-24.
- [LoQ 2002] Lozano-Castelló D., Cazorla-Amorós D., Linares-Solano A., Quinn D.F., 2002, **Influence of pore size distribution on methane storage at relatively low pressure: preparation of activated carbon with optimum pore size**, Carbon 40, 989-1002.
- [Lot 2007] Lota G., Lota K., Frackowiak E., 2007, **Nanotubes based composites rich in nitrogen for supercapacitor application**, Electrochemistry Communications 9, 1828-1832.

- [Loz 2002] Lozano-Castelló D., Cazorla-Amorós D., Linares-Solano A., 2002, **Can highly activated carbons be prepared with a homogeneous micropore size distribution?**, Fuel Processing Technology 77-78, 325-330.
- [Lub 1979] Luby P., Kuniak T., Fanter C., 1979, **Crosslinking statistics, 3. Relation between relative reactivity and accessibility of cellulose hydroxyl groups**, Die Makromolekulare Chemie 180, 2379-2386.
- [LuC 1995] Lu X., Caps R., Fricke J., Alviso C.T., Pekala R.W., 1995, **Correlation between structure and thermal conductivity of organic aerogels**, Journal of Non-Crystalline Solids 188, 226-234.
- [Mac 2005] Machnikowski J., Grzyb B., Machnikowska H., Weber J.V., 2005, **Surface chemistry of porous carbons from N-polymers and their blends with pitch**, Microporous and Mesoporous Materials 82, 113-120.
- [Man 2001] Mangun C.L., DeBarr J.A., Economy J., 2001, **Adsorption of sulfur dioxide on ammonia-treated activated carbon fibers**, Carbon 39, 1689-96.
- [Mao 2006] Mao Y., Zhou J., Cai J., Zhang L., 2006, **Effects of coagulants on porous structure of membranes prepared from cellulose in NaOH/urea aqueous solution**, Journal of Membrane Science 279, 246-255.
- [Mar 2000] Marin M., Ren, F., 2000, **Lyophilisation**, F3240, Techniques de l'ingénieur, Paris.
- [Mar 2004] Marie J., Berthon-Fabry S., Achard P., Chatenet M., Pradourat A., Chainet E., 2004, **Highly dispersed platinum on carbon aerogels as supported catalysts for PEM fuel cell-electrodes: comparison of two different synthesis paths**, Journal of Non-crystalline Solids 350, 88-96.
- [Mar 2005] Maroto-Valer M.M., Tang Z., Zhang Y., 2005, **CO₂ capture by activated and impregnated anthracites**, Fuel Processing Technology 86, 1487-1502.
- [Mar 2006] Marsh H., Rodríguez-Reinoso F., 2006, **Activated Carbon**, Elsevier Science Ltd., Oxford.
- [Mar 2009] Marie J., Chenitz R., Chatenet M., Berthon-Fabry S., Cornet N., Achard P., 2009, **Highly porous PEM fuel cell cathodes based on low density carbon aerogels as Pt-support: Experimental study of the mass-transport losses**, Journal of Power Sources 190, 423-434.
- [Mas 2006] Masmoudi Y., Rigacci A., Ilbizian P., Cauneau F., Achard P., 2006, **Diffusion During the Supercritical Drying of Silica Gels**, Drying Technology 24, 1121-1125.
- [Mer 2006] Mermoud F., Salvador S., Von de Steene L., Golfier F., 2006, **Influence of the pyrolysis heating rate on the steam gasification rate of large wood char particles**, Fuel 85, 1473-1482.

- [Mil 1996] Milosavljevic I., Oja V., Suuberg E.M., 1996, **Thermal Effects in Cellulose Pyrolysis: Relationship to Char Formation Processes**, Industrial & Engineering Chemistry Research 35, 653-662.
- [Mir 2009] Mirzaeian M., Hall P.J., 2009, **Preparation of controlled porosity carbon aerogels for energy storage in rechargeable lithium oxygen batteries**, Electrochimica Acta 54, 7444-7451.
- [Moh 2006] Mohan D., Pittman Jr. C. U., Steele P. H., 2006, **Pyrolysis of Wood/Biomass for Bio-oil: A critical review**, Energy & Fuels 20, 848-889.
- [Mol 1996] Molina-Sabio M., González M. T., Rodríguez-Reinoso F., Sepúlveda-Escribano A., 1996, **Effect of steam and carbon dioxide activation in the micropore size distribution of activated carbon**, Carbon 34, 505-509.
- [Mon 2002] Montilla F., Morallón E., Vázquez J.L., Alcañiz-Monge J., Cazorla-Amorós D., Linares-Solano A., 2002, **Carbon-ceramic composites from coal-tar pitch and clays: application as electrocatalyst support**, Carbon 40, 2193-2200.
- [Mor 2000] Moreau L., 2000, **Etude de carbones actifs microporeux de très haute surface spécifique pour supercondensateur à électrolyte organique**, PhD thesis, Université Pierre et Marie Curie (Paris VI), France.
- [Mor 2005] Moreno-Castilla, Maldonado-Hódar F.J., 2005, **Carbon aerogels for catalysis applications: An overview**, Carbon 43, 455-465.
- [Mor 2006] Moreno M., 2006, **Synthèse en phase gazeuse de nanoparticules de carbone par plasma hors équilibre**, PhD thesis, Ecole des Mines de Paris, France.
- [Mos 1963] Mosher R.A., 1963, **Nonyl pyridine catalyst for polyurethane reaction**, US Patent 3 075 951.
- [Muñ 1998] Muñoz J., Herrero J.E., Fuertes A.B., 1998, **Treatments to enhance the SO₂ capture by activated carbon fibres**, Applied Catalysis B: Environmental 18, 171-179.
- [NgV 2009] Ng S.H., Vix-Guterl C., Bernardo P., Tran N., Ufheil J., Buqa H., Dentzer J., Gadiou R., Spahr M.E., Goers D., Novák P., 2009, **Correlations between surface properties of graphite and the first cycle specific charge loss in lithium-ion batteries**, Carbon 47, 705-712.
- [Oku 2004] Okuno H., Grivei E., Fabry F., Gruenberger T.M., Gonzalez-Aguilar J., Palnichenko A., Fulcheri L., Probst N., Charlier J.-C., 2004, **Synthesis of carbon nanotubes and nano-necklaces by thermal plasma process**, Carbon 42, 2543-2549.
- [Oli 2009] Olivares-Marín M., Fernández J.A., Lázaro M.J., Fernández-González C., Macías-García A., Gómez-Serrano V., Stoeckli F., Centeno T.A., 2009, **Cherry stones as precursor of activated carbons for supercapacitors**, Materials Chemistry and Physics 114, 323-327.

- [Ona 2003] Onay O., Kockar O.M., 2003, **Slow, fast and flash pyrolysis of rapeseed**, Renewable Energy 28, 2417-2433.
- [Oua 2009] Ouajai S., Shanks R.A., 2009, **Biocomposites of Cellulose Acetate Butyrate with Modified Hemp Cellulose Fibres**, Macromolecular Materials and Engineering 294, 213-221.
- [Paj 1989] Pajonk G.M., 1989, **Drying methods preserving the textural properties of gels**, Revue de Physique Appliquée 4, Colloque C4.
- [Pan 2006] Pandolfo A.G., Hollenkamp A.F., 2006, **Carbon properties and their role in supercapacitors**, Journal of Power Sources 157, 11-27.
- [Pas 2002] J. Pastor-Villegas, C.J. Durán-Valle, 2002, **Pore structure of activated carbons prepared by carbon dioxide and steam activation at different temperatures from extracted rockrose**, Carbon 40, 397-402.
- [Pek 1989] Pekala R.W., 1989, **Organic aerogels from the polycondensation of resorcinol with formaldehyde**, Journal of Materials Science 24, 3221-3227.
- [Pek 1998] Pekala R.W., Farmer J.C., Alviso C.T., Tran T.D., Mayer S.T., Miller J.M., Dunn B., 1998, **Carbon aerogels for electrochemical applications**, Journal of Non-Crystalline Solids 225, 74-80.
- [Pel 1995] Pels J.R., Kapteijn F., Moulijn J.A., Zhu Q., Thomas K.M., 1995, **Evolution of nitrogen functionalities in carbonaceous materials during pyrolysis**, Carbon 33, 1641-1653.
- [Pér 2008] Pérez-Cadenas M., Moreno-Castilla C., Carrasco-Marín F., Pérez-Cadenas M., 2009, **Surface Chemistry, Porous Texture, and Morphology of N-Doped Carbon Xerogels**, Langmuir 25, 466-470.
- [Pet 2001] Petričević R., Glora M., Fricke J., 2001, **Planar fibre reinforced carbon aerogels for application in PEM fuel cells**, Carbon 39, 857-867.
- [Pev 2008] Pevida C., Drage T.C., Snape C.E., 2008, **Silica-templated melamine-formaldehyde resin derived adsorbents for CO₂ capture**, Carbon 46, 1464-1474.
- [Pha 2004] Phalippou J., Kocon L., 2004, **Elaboration des gels et des Aérogels**, J2230, Techniques de l'ingénieur, Paris.
- [Pha 2006] Phan N. H., Rio S., Faur C., Le Coq L., Le Cloirec P., Nguyen T. H., 2006, **Production of fibrous activated carbons from natural cellulose (jute, cocnut) fibers for water treatment applications**, Carbon 44, 2569-2577.
- [Pie 1967] Pierce A.G. (Jr.), Frick J.G. (Jr.), 1967, **Crosslinking cotton with formaldehyde in phosphoric acid**, Journal of Applied Polymer Science 11, 2577-2585.
- [Pim 2003] Pimenov V.G., Drozhzhin V.S., Sakharov A. M., 2003, **Ultra-low density microcellular aerogels based on cellulose acetate**, Polymer Science. Series B 45, 4-6.

- [Pir 2000] Pirard R., 2000, **Etude de la texture des matériaux hyper poreux par porosimétrie au mercure**, PhD thesis, Université de Liège, Belgium.
- [Pir 2003] Pirard, R., Rigacci, A., Maréchal, J.C., Quenard, D., Chevalier, B., Achard, P., Pirard, J.P., 2003, **Characterization of hyperporous polyurethane-based gels by non-intrusive mercury porosimetry**, Polymer 44, 4881-4887.
- [Pla 2009] Plaza M.G., Pevida C., Arias B., Feroso J., Casal M.D., Martín C.F., Rubiera F., Pis J.J., 2009, **Development of low-cost biomass-based adsorbents for postcombustion CO₂ capture**, Fuel 88, 2442-2447.
- [Pol 2002] Polarz S., Smarsly B., 2002, **Nanoporous Materials**, Journal of Nanoscience and Nanotechnology 2, 6, 581-612.
- [Pra 2008] Prahas D., Kartika Y., Indraswati N., Ismadji S., 2008, **Activated carbon from jackfruit peel waste by H₃PO₄ chemical activation: Pore structure and surface chemistry characterization**, Chemical Engineering Journal 140, 32-42.
- [Prö 2002] Pröbstle H., Schmitt C., Fricke J., 2002, **Button cell supercapacitors with monolithic carbon aerogels**, Journal of Power Sources 105, 189-194.
- [RaK 2006] Raymundo-Piñero E., Kierzek K., Machnikowski J., Béguin F., 2006, **Relationship between the nanoporous texture of activated carbons and their capacitance properties in different electrolytes**, Carbon 44, 2498-2507.
- [RaL 2006] Raymundo-Piñero E., Leroux F., Béguin F., 2006, **A high performance carbon for supercapacitors obtained by carbonisation of a seaweed biopolymer**, Advanced Materials 18, 1877-1882.
- [Rat 1997] Ratner B.D., Castner D.G., 1997, **Electron Spectroscopy for Chemical Analysis**, In: Surface analysis: the principal techniques (43-98), Wiley, New York.
- [Ray 2000] Raymundo-Piñero E., Cazorla-Amorós D., Salinas-Martinez de Lecea C., Linares-Solano A., 2000, **Factors controlling the SO₂ removal by porous carbons: relevance of the SO₂ oxidation step**, Carbon 38, 335-344.
- [Rei 1998] Reichenauer G., Emmerling A., Fricke J., Pekala R.W., 1998, **Microporosity in carbon aerogels**, Journal of Non-Crystalline Solids 225, 210-214.
- [Reu 1986] Reuvers A.J., Altena F.W., Smolders C.A., 1986, **Demixing and gelation behavior of ternary cellulose acetate solutions**, Journal of Polymer Science Part B: Polymer Physics 24, 793-804.
- [Ric 1990] Richter E., 1990, **Carbon catalysts for pollution control**, Catalysis Today 7, 93-112.
- [Rig 1998] Rigacci A., 1998, **Elaboration d'aérogels de silice monolithiques et étude des relations entre leur structure et leur conductivité thermique équivalente**, PhD thesis, Ecole des Mines de Paris, France.

- [Rig 2004] Rigacci A., Marechal J.-C., Repoux M., Moreno M., Achard P., 2004, **Preparation of polyurethane-based aerogels and xerogels for thermal superinsulation**, Journal of Non-Crystalline Solids 350, 372-378.
- [Rig 2007] Rigacci A., Marechal J.-C., Maury D., Repoux M., Achard P., 2007, **Elaboration and characterisation of polyurethane cryogels**, XIVth International Sol-Gel Conference (2-7 September 2007), Montpellier, France.
- [Riv 2004] Rivera-Armenta J.L., Heinze Th., Mendoza-Martinez A.M, 2004, **New polyurethane foams modified with cellulose derivatives**, European Polymer Journal 41, 2803-2812.
- [Rod 1992] Rodríguez-Reinoso F., Molina-Sabio M., 1992, **Activated carbons from lignocellulosic materials by chemical and/or physical activation: an overview**, Carbon 30, 1111-1118.
- [Rod 1995] Rodríguez-Reinoso F., Molina-Sabio M., González M.T., 1995, **The use of steam and CO₂ as activating agents in the preparation of activated carbons**, Carbon 33, 15-23.
- [Roo 2009] Rooke J., Hildenbrand C., Berthon-Fabry S., Sescousse R., Budtova T., Chatenet M., Maillard F., 2009, **Elaboration and characterizations of platinum nanoparticles supported on cellulose-based carbon aerogel**, Carbon 2009 (14-19 June 2009), Biarritz, France.
- [Rou 1994] Rouquérol J., Avnir D., Fairbridge C.W., Everett D.H., Haynes J.H., Pericone N., Ramsay J.D.F., Sing K.S.W., Unger K.K., 1994, **Recommendation for the characterization of porous solids**, Pure and Applied Chemistry 66, 1739-1758.
- [Row 1966] Rowland S.P., Post A.W., 1966, **A measure of effective crosslinks in formaldehyde-modified cotton celluloses**, Journal of Applied Polymer Science 10, 1751-1761.
- [Roy 2002] Roy C., 2002, **Etude de mélanges de cellulose dans des solutions aqueuses de soude**, PhD thesis, Ecole des Mines de Paris, France.
- [Sal 1998] Saliger R., Fischer U., Herta C., Fricke J., 1998, **High surface area carbon aerogels for supercapacitors**, Journal of Non-Crystalline Solids 225, 81-85.
- [San 2005] Sannino A., Nicolais B., 2005, **Concurrent effect of microporosity and chemical structure on the equilibrium sorption properties of cellulose-based hydrogels**, Polymer 46, 4676-4685.
- [Sar 1995] Sarkar N., 1995, **Kinetics of thermal gelation of methylcellulose and hydroxypropylmethylcellulose in aqueous solutions**, Carbohydrate Polymers 26, 195-203.
- [Sch 1994] Scherer G.W., 1994, **Stress in aerogel during depressurization of autoclave: I. Theory**, Journal of Sol-Gel Science and Technology 3, 127-139.
- [ScN 1994] Schwetlick K., Noack R., Stebner F., 1994, **Three fundamental mechanisms of base-catalysed reactions of isocyanates with hydrogen-acidic compounds**, Perkin Transactions. 2 3, 599-608.

- [Sch 1995] Schaefer D.W., Pekala R., Beaucage G., 1995, **Origin of porosity in resorcinol-formaldehyde aerogels**, Journal of Non-Crystalline Solids 186, 159-167.
- [Sch 2001] Schmitt C., Pröbstle H., Fricke J., 2001, **Carbon cloth-reinforced and activated aerogel films for supercapacitors**, Journal of Non-Crystalline Solids 285, 277-282.
- [Sch 2007] Schröder E., Thomauske K., Weber C., Hornung A., Tumiatti V., 2007, **Experiments on the generation of activated carbon from biomass**, Journal of Analytical and Applied Pyrolysis 79, 106-111.
- [ScP 1995] Schaefer D.W., Pekala R., Beaucage G., 1995, **Origin of porosity in resorcinol-formaldehyde aerogels**, Journal of Non-Crystalline Solids 186, 159-167.
- [ScS 1995] Scherer G.W., Smith D.M., Stein D., 1995, **Deformation of aerogels during characterization**, Journal of Non-Crystalline Solids 186, 309-315.
- [Seg 2010] Segalini J., Daffos B., Taberna P.L., Gogotsi Y., Simon P., 2010, **Qualitative Electrochemical Impedance Spectroscopy study of ion transport into sub-nanometer carbon pores in Electrochemical Double Layer Capacitor electrodes**, Electrochimica Acta, Article in press.
- [Ser 2008] Seredych M., Hulicova-Jurcakova D., Lu G.Q., Bandosz T.J., 2008, **Surface functional groups of carbons and the effects of their chemical character, density and accessibility to ions on electrochemical performance**, Carbon 46, 1475-1488.
- [Ses 2009] Sescousse R., Budtova T., 2009, **Influence of processing parameters on regeneration kinetics and morphology of porous cellulose from cellulose-NaOH-water solutions**, Cellulose 16, 417-426.
- [Sha 2008] Shan X.-m., Zhu S.-q., Zhang W.-h., 2008, **Effect of surface modification of activated carbon on its adsorption capacity for NH₃**, Journal of China University of Mining & Technology 18, 0261-0265.
- [Shi 1984] Shinn J.H., 1984, **From coal to single-stage and two-stage products: A reactive model of coal structure**, Fuel 63, 1187-1196.
- [Sig 2010] <http://www.sigmaldrich.com>
- [Sil 2004] Silva A.L., Bordado J.C., 2004, **Recent Developments in Polyurethane Catalysis: Catalytic Mechanisms Review**, Catalysis Reviews 46, 31-51.
- [Sim 2005] Simon B., Hilaire M., Jehoulet C., Cousseau J.-F., 2005, **Electrochemical cell having a carbon aerogel cathode**, US Patent 2005/0287421 A1.
- [Sin 1982] Sing K.S.W., 1982, **Reporting physisorption data for gas/solid systems with special reference to the determination of surface area and porosity**, Pure and Applied Chemistry 54, 2201-2218.
- [Sta 2006] Starck J., Burg P., Muller S., Bimer J., Furdin G., Fioux P., Vix-Guterl C., Begin D., Faure P., Azambre B., 2006, **The influence of demineralisation and amoxidation on the**

- adsorption properties of an activated carbon prepared from Polish lignite**, Carbon 44, 2549-2557.
- [Ste 2005] Steel K. M., Koros W. J., 2005, **An investigation of the effects of pyrolysis parameters on gas separation properties of carbon materials**, Carbon 43, 1843-1856.
- [StG 2006] Ströbel R., Garche J., Moseley P.T., Jörissen L., Wolf G., 2006, **Hydrogen storage by carbon materials**, Journal of Power Sources 159, 781-801.
- [Str 2006] Ströck M., 2006, **Eight allotropes of carbon**, [http://en.wikipedia.org/wiki/File:Eight Allotropes of Carbon.png](http://en.wikipedia.org/wiki/File:Eight_Allotropes_of_Carbon.png) (May 14th 2010).
- [Sub 2000] Subrayan R.P., Zhang S., Jones F.N., Swarum V., Yezrielev, A.I., 2000, **Reactions of phenolic ester alcohol with aliphatic isocyanates - transcarbamoylation of phenolic to aliphatic urethane: A 13C-NMR study**, Journal of Applied Polymer Science 77, 2212-2228.
- [Sug 2005] Sugimoto W., Iwata H., Yokoshima, K., Murakami Y., Takasu Y., 2005, **Proton and Electron Conductivity in Hydrous Ruthenium Oxides Evaluated by Electrochemical Impedance Spectroscopy: The Origin of Large Capacitance**, Journal of Physical Chemistry B 109, 7330-7338.
- [SuL 2007] Su J., Lua A.C., 2007, **Effects of carbonisation atmosphere on the structural characteristics and transport properties of carbon membranes prepared from Kapton® polyimide**, Journal of Membrane Science 305, 263-270.
- [Swi 2004] Swiatkowski A., Pakula M., Biniak S., Walczyk M., 2004, **Influence of the surface chemistry of modified activated carbon on its electrochemical behaviour in the presence of lead(II) ions**, Carbon 42, 3057-3069.
- [Tab 2003] Taberna P.L., Simon P., Fauvarque J.F., 2003, **Electrochemical Characteristics and Impedance Spectroscopy Studies of Carbon-Carbon Supercapacitors**, Journal of The Electrochemical Society 150, A292-A300.
- [Tab 2006] Taberna P.L., Simon P., 2006, **The role of interfaces on supercapacitor performances**, ESSCAP'06 (2-3 November 2006), Lausanne, Switzerland.
- [Tak 1999] Takeuchi Y., Hino M., Yoshimura Y., Otowa T., Izuhara H., Nojima T, 1999, **Removal of single component chlorinated hydrocarbon vapour by activated carbon of very high surface area**, Separation and Purification Technology 15, 79-90.
- [Tak 2001] Takahashi M., Shimazaki M., Yamamoto J., 2001, **Thermoreversible gelation and phase separation in aqueous methyl cellulose solutions**, Journal of Polymer Science Part B: Polymer Physics 39, 91-100.
- [Tam 1998] Tamon H., Ishizaka H., 1998, **Porous characterization of carbon**, Carbon 36, 1397-1998.
- [Tan 1981] Tanaka T., 1981, **Gels**, Scientific American 244, 124-138.

- [Tan 2001] Tan C., Fung B. M., Newman J. K., Vu C., 2001, **Organic aerogels with very high impact strength**, *Advanced materials* 13, 644-646.
- [Tay 2009] Tay T., Ucar S., Karagöz S., 2009, **Preparation and characterization of activated carbon from waste biomass**, *Journal of Hazardous Materials* 165, 481-485.
- [Tew 1985] Tewari P.H., Hunt A.J., Lofftus K.D., 1985, **Ambient-temperature supercritical drying of transparent silica aerogels**, *Materials Letters* 3, 363-367.
- [Tex2004] Texier-Mandoki N., Dentzer J., Piquero T., Saadallah S., David P., Vix-Guterl C., 2004, **Hydrogen storage in activated carbon materials: Role of the nanoporous texture**, *Carbon* 42, 2744-2747.
- [Thi 1993] Thiele L., Becker R., 1993, **Catalytic Mechanisms of polyurethane formation**, In: *Advances in Urethane Science & Technology - Volume XII*, 59-85, Technomic Publishing Company, Inc., Lancaster.
- [Tsi 2009] Tsiptsias C., Michailof C., Stauroopoulos G., Panayiotou C., 2009, **Chitin and carbon aerogels from chitin alcogels**, *Carbohydrate Polymers* 76, 535-540.
- [ViD 2001] Vix-Guterl C., Dentzer J., Ehrburger P., Méténier K., Bonnamy S., Béguin F., 2001, **Surface properties and mixrotecture of catalytic multi-walled carbon nanotubes**, *Carbon* 39, 318-320.
- [Vix2004] Vix-Guterl C., Saadallah S., Jurewicz K., Frackowiak E., Reda M., Parmentier J., Patarin J., Béguin F., 2004, **Supercapacitor electrodes from new ordered porous carbon materials obtained by a templating procedure**, *Materials Science and Engineering B108*, 148-155.
- [Vix2005] Vix-Guterl C., Frackowiak E., Jurewicz K., Friebe M., Parmentier J., Béguin F., 2005, **Electrochemical energy storage in ordered porous carbon materials**, *Carbon* 43, 1293-1302.
- [Wad 2006] Wade T.L., 2006, **High Power Carbon-Based Supercapacitors**, PhD thesis, School of Chemistry, The University of Melbourne, Australia.
- [Wan 2004] Wang Z.-M., Yamashita N, Wang Z.-X., Hoshinoo K., Kanoh H., 2004, **Air oxidation effects on microporosity, surface property, and CH₄ adsorptivity of pitch-based activated carbon fibers**, *Journal of Colloid and Interface Science* 276, 143-150.
- [Was 1921] Washburn E.W., 1921, **The dynamics of capillary flow**, *Physical Review* 17, 273-278.
- [Wea 1978] Weatherwax R. C., Caufield D.F., 1978, **The pore structure of papers wet stiffened by formaldehyde crosslinking**, *Journal of Colloid and Interface Science* 67, 498-505.
- [Weg 2001] Wegener F., Brandt M., Duda L., Hofmann, J., Kleszczewski B., Koch D., Kumpf R.-J., Orzesek H., Pirkl H.-G., Sic C., Steinlein C., Weisbeck M., 2001, **Trends in industrial catalysis in the polyurethane industry**, *Applied Catalysis A: General* 21, 303-335.

- [Wer 1980] Werbowyj R.S., Derek G.G., 1980, **Ordered phase formation in concentrated Hydroxypropylcellulose solutions**, *Macromolecules* 13, 69-73.
- [Wil 1996] Williams P.T., Besler S., 1996, **The influence of temperature and heating rate on the slow pyrolysis of biomass**, *Renewable Energy* 7, 233-250.
- [Wil 2006] Williams P.T., Reed A.R., 2006, **Development of activated carbon pore structure via physical and chemical activation of biomass fibre waste**, *Biomass and Bioenergy* 30, 144-152.
- [Win 2004] Winter M., Brodd R.J., 2004, **What are Batteries, Fuel Cells, and Supercapacitors?**, *Chemical Reviews* 104, 4245-4269.
- [Woi 1994] Woignier T., Scherer G.W., 1994, **Stress in aerogel during depressurization of autoclave: II. Silica gels**, *Journal of Sol-Gel Science and Technology* 3, 141-150.
- [YaC 1991] Yang C.Q., Andrews B.A.K., 1991, **Infrared spectroscopic studies of the nonformaldehyde durable press finishing of cotton fabrics by use of polycarboxylic acids**, *Journal of Applied Polymer Science* 43, 1609-1616.
- [YaC 1993] Yang C.Q., 1993, **Infrared spectroscopic studies of the effects of the catalyst on the ester Crosslinking of cellulose by polycarboxylic acids**, *Journal of Applied Polymer Science* 50, 2047-2053.
- [YaC 2002] Yang C.Q., Hu C., Lickfield G.C., 2002, **Crosslinking cotton with poly(itaconic acid) and in situ polymerisation of itaconic acid: fabric mechanical strength retention**, *Journal of Applied Polymer Science* 87, 2023-2030.
- [Yam 2003] Yamashita J., Ojima T., Shioya M., Hatori H., Yamada Y., 2003, **Organic and carbon aerogels derived from poly(vinyl chloride)**, *Carbon* 41, 285-294.
- [Yan 1996] Yang G., Zhang L., 1996, **Regenerated cellulose microporous membranes by mixing cellulose cuoxam with a water soluble polymer**, *Journal of Membrane Science* 114, 149-155.
- [Yan 1999] Yang G., Zhang L., Feng H., 1999, **Role of polyethylene glycol in formation and structure of regenerated cellulose microporous membrane**, *Journal of Membrane Science* 161, 31-40.
- [Yan 2000] Yang G., Zhang L. Yonggang L., 2000, **Structure and microporous formation of cellulose/silk fibroin blend membranes I. Effect of coagulants**, *Journal of Membrane Science* 177, 153-161.
- [YaX 2002] Yang G., Xiong X., Zhang L., 2002, **Microporous formation of blend membranes from cellulose/konjac glucomannan in NaOH/thiourea aqueous solution**, *Journal of Membrane Science* 201, 161-173.
- [Yoo 2010] Yoon S., Lee C.W., Oh S.M., 2010, **Characterization of equivalent series resistance of electric double-layer capacitor electrodes using transient analysis**, *Journal of Power Sources* 195, 4391-4399.

- [Yür 2009] Yürüm Y., Taralp A., Veziroglu T.N., 2009, **Storage of hydrogen in nanostructured carbon materials**, International Journal of Hydrogen Energy 34, 3784-3798.
- [Zaw 1989] Zawadzki J., 1989, **IR Spectroscopy in Carbon Surface Chemistry**, In: Chemistry and physics of carbon (pp. 149-380), Marcel Dekker, New York.
- [Zaw 2003] Zawadzki J., Wisniewski M., 2003, **In situ characterization of interaction of ammonia with carbon surface in oxygen atmosphere**, Carbon 41, 2257-2267.
- [Zhe 1995] Zheng J.P., Jow T.R., 1995, **A new charge storage mechanism for electrochemical capacitors**, Journal of the Electrochemical Society 142, L6-L8.
- [Zhe 2002] Zheng X., Zhang S., Xu J., Wei K., 2002, **Effect of thermal and oxidative treatments of activated carbon on its surface structure and suitability as a support for barium-promoted ruthenium in ammonia synthesis catalysis**, Carbon 40, 2597-2603.
- [Zho 1995] Zhou Y.J., Luner P., Caluwe P., 1995, **Mechanism of Crosslinking of papers with polyfunctional carboxylic acids**, Journal of Applied Polymer Science 58, 1523-1534.
- [Zho 2002] Zhou J., Zhang L., Cai J., Shu H., 2002, **Cellulose microporous membranes prepared from NaOH/urea aqueous solution**, Journal of Membrane Science 210, 77-90.
- [Zho 2003] Zhou H., Zhu S., Hibino M., Honma I., 2003, **Electrochemical capacitance of self-ordered mesoporous carbon**, Journal of Power Sources 122, 219-223.
- [Zho 2008] Zhou S., Li X., Wang Z., Guo H., Peng W., 2008, **Comparison of capacitive behavior of activated carbons with different pore structures in aqueous and non-aqueous systems**, Journal of Central South University of Technology 15, 674-678.
- [Zhu 2006] Zhu Y., Hu H., Li W.-C., Zhang X., 2006, **Cresol-formaldehyde based carbon aerogel as electrode material for electrochemical capacitor**, Journal of Power Sources 162, 738-742.
- [Zub 2009] Zubizarreta L., Arenillas A., Pis J.J., 2009, **Carbon materials for H₂ storage**, International Journal of Hydrogen Energy 34, 4575-4581.
- [Zug 2004] Zugenmaier P., 2004, **4 Characteristics of cellulose acetates – 4.1. Characterization and physical properties of cellulose acetates**, In: Cellulose acetates: properties and applications, Wiley, Macromolecular symposia 208, 103-113.

Personal references

Article in international journal

Grzyb B., Hildenbrand C., Berthon-Fabry, Bégin D., Job N., Rigacci A., Achard P., 2010, **Functionalisation and chemical characterisation of cellulose derived carbon aerogels**, Carbon 48, 2297–2307.

National conferences

Rooke J., Chatenet M., Maillard F., Hildenbrand C., Berthon-Fabry S., 2008, **Synthèse et caractérisation de nanoparticules de platine supportée sur aérocellulose pyrolysée**, GDR PACTE (30 September-2 October 2008), Grenoble, France. (Poster)

Hildenbrand C., Berthon-Fabry S., Rigacci A., Achard P., 2009, **Influence of sol-gel parameters on cellulose-acetate aerogels and their carbon counterparts**, Journée Industrielle Nanomines (22 January 2009) Paris, France. (Poster)

International conferences

Hildenbrand C., Rigacci A., Berthon-Fabry S., Simon B., Achard P., 2007, **Influence of sol-gel parameters on cellulose-acetate aerogels and their carbon counterparts**, XIV International Sol-Gel conference (2-7 September 2007), Montpellier, France. (Poster)

Hildenbrand C., Grzyb B., Berthon-Fabry S., Job N., Rigacci A., Achard P., 2009, **EDLC electrodes from cellulose-based carbon aerogels: influence of the carbon's surface chemistry**, Carbon 2009 (15-19 June 2009), Biarritz, France. (Oral)

Rooke J., Hildenbrand C., Berthon-Fabry S., Sescousse R., Budtova T., Chatenet M., Maillard F., 2009, **Elaboration and characterizations of platinum nanoparticles supported on cellulose-based carbon aerogel**, Carbon 2009 (15-19 June 2009), Biarritz, France. (Poster)

Gavillon R., Hildenbrand C., Fischer F., Sescousse R., Rigacci A., Berthon-Fabry S., Budtova T., 2009, **Preparation, properties and applications of novel cellulose and cellulose acetate aerogels**, Biofoams 2009 (26-28 October 2009), Niagara Falls, Canada. (Oral)

Titre

RESUME: Les carbones nanostructures sont très largement utilisés dans les systèmes de stockage et conversion d'énergie par voie électrochimique, par exemple en tant que matériau d'électrode de pile à combustible et de batterie ou encore de supercondensateur. La structure du carbone ainsi que sa chimie de surface sont des paramètres primordiaux et doivent être adaptés aux différentes spécificités de chacune de ces applications. Dans ce cadre général, cette thèse a pour but de développer une nouvelle famille de carbones nanostructurés, les aérogels de carbone cellulosiques. Ces derniers sont obtenus par pyrolyse d'aérogels organiques élaborés à base d'acétate de cellulose. Pour ce faire, nous avons fait varier les paramètres de synthèse sol-gel ainsi que les conditions de séchage et de pyrolyse (principalement la composition du sol, la nature du catalyseur, la température et l'atmosphère de pyrolyse) afin de générer une vaste palette de structures. Dans un second temps, ces aérogels ont subi différents post-traitements visant à modifier leur chimie de surface et ce, par introduction de groupements fonctionnels oxygénés et azotés. Finalement, les performances de ces nouveaux aérogels de carbone ont été analysées sous la forme de matériaux d'électrode de supercondensateur.

Mots clés: synthèse sol-gel, aérogel, aérogel organique, aérogel de carbone, acétate de cellulose, supercondensateur

Title

ABSTRACT : Nanostructured carbons are widely used in electrochemical energy storage and conversion devices, e.g. as electrode material for fuel cells, batteries, or still EDLCs (Electric Double Layer Capacitor). The carbon structure and surface chemistry are crucial parameters and consequently need to be adjusted to the specific application's requirements. This PhD thesis has aimed at developing a new family of nanostructured carbons, aerogels from renewable organic sol-gel precursors, i.e. pyrolyzed cellulose-acetate-based aerogels. Sol-gel synthesis parameters of the organic aerogel, drying conditions, as well as pyrolysis parameters (particularly the influence of the sol composition, the type of catalyst used in the sol-gel synthesis step, pyrolysis temperature, and atmosphere) have been varied systematically in order to generate a broad range of structurally different cellulose-acetate-based carbonaceous aerogels. Further, cellulose-acetate-based carbon aerogels have been exposed to different post-treatments (e.g. introduction of oxygen and nitrogen-containing surface functional groups) to create cellulose-acetate-based carbon aerogels with different surface chemistries. Finally, the performance of these cellulose-acetate-based carbon aerogels has been analyzed as EDLC electrode material.

Keywords: sol-gel synthesis, aerogel, organic aerogel, carbon aerogel, cellulose acetate, EDLC